11. Status of Higgs Boson Physics

Revised August 2023 by M. Carena (FNAL; Chicago U.; Chicago U., Kavli Inst.), C. Grojean (DESY, Hamburg; Physik, Humboldt U.), M. Kado (MPI Munich) and V. Sharma (UC San Diego).

11.1 Introduction . . . 1
11.2 The Standard Model and the mechanism of electroweak symmetry breaking . . . 3
11.2.1 The SM Higgs boson mass, couplings and quantum numbers . . . 5
11.2.2 The SM custodial symmetry . . . 5
11.2.3 Stability of the Higgs potential . . . 6
11.2.4 Higgs boson production and decay mechanisms . . . 6
11.3 The experimental profile of the Higgs boson . . . 15
11.3.1 The principal decay channels of the Higgs boson . . . 15
11.3.2 The Higgs boson decay to vector bosons . . . 16
11.3.3 Measurement of the Higgs boson mass . . . 18
11.3.4 Higgs decays to third generation fermions ($b\bar{b}$ and $\tau^+\tau^-$) . . . 20
11.3.5 Higgs boson production in association with top quarks . . . 23
11.3.6 Combining the main channels . . . 26
11.3.7 Probing the Higgs boson coupling to the second generation . . . 29
11.3.8 Searches for rare decays of the Higgs boson . . . 31
11.3.9 Higgs boson pair production and self-coupling . . . 36
11.3.10 Beyond the main Higgs boson production modes . . . 39
11.3.11 First results on the main production and decay channels at 13.6 TeV . . . 40
11.4 Main quantum numbers and width of the Higgs boson . . . 40
11.4.1 Main quantum numbers J^{PC} . . . 40
11.4.2 Off-shell couplings of the Higgs boson . . . 47
11.4.3 The Higgs boson width . . . 48
11.5 Probing the coupling properties of the Higgs boson . . . 50
11.5.1 Probing coupling properties . . . 52
11.5.2 Effective Lagrangian framework . . . 60
11.6 New physics models of EWSB in the light of the Higgs boson discovery . . . 63
11.6.1 Higgs bosons in the minimal supersymmetric standard model (MSSM) . . . 65
11.6.2 Supersymmetry with singlet extensions . . . 69
11.6.3 Supersymmetry with extended gauge sectors . . . 71
11.6.4 Effects of CP violation . . . 72
11.6.5 Non-supersymmetric extensions of the Higgs sector . . . 73
11.6.6 Composite Higgs models . . . 78
11.6.7 Searches for signatures of extended Higgs sectors . . . 84
11.7 Summary and outlook . . . 94

11.1 Introduction

Understanding how the masses of the known elementary particles are generated has been one of the fundamental endeavours in particle physics for several decades. The chiral nature of the weak interactions forbids an intrinsic mass terms for the quarks and leptons at high energy, and their masses can only appear as emergent quantities after the spontaneous symmetry of the electroweak

symmetry. The discovery in 2012 by the ATLAS [1] and the CMS [2] collaborations of a new resonance with a mass of approximately 125 GeV and the subsequent studies of its properties with the full data set from Run 1, from 2009 to 2012, with a centre-of-mass energy of 7 TeV and 8 TeV, conclusively provided a first sketch of the Electroweak Symmetry Breaking (EWSB) mechanism. The much larger dataset collected during the LHC Run 2, from 2015 to 2018, with a higher centre-of-mass energy of 13 TeV, demonstrated the compatibility of the measured resonance with the Higgs boson of the Standard Model (SM) [3] and strongly challenged other contenders. The LHC started its Run 3 in 2022 and this data taking phase is expected to comprise of four years of operations until 2026. By then the LHC is expected to deliver proton-proton collision data corresponding to an integrated luminosity of approximately $250\,\text{fb}^{-1}$ per experiment.

In the SM, the electroweak interactions are described by a gauge field theory invariant under the $\text{SU}(2)_L \times \text{U}(1)_Y$ symmetry group. The mechanism of EWSB [4] provides a general framework to keep untouched the structure of these gauge interactions at high energies and still generate the observed masses of the W and Z gauge bosons as well as those of the quarks and charged leptons. The EWSB mechanism posits a self-interacting complex EW doublet scalar field, whose CP-even neutral component acquires a vacuum expectation value (VEV) $v \approx 246\,\text{GeV}$, which sets the scale of the symmetry breaking. Three massless Goldstone bosons are generated and are absorbed to give masses to the W and Z gauge bosons. The remaining component of the complex doublet becomes the Higgs boson – a new, and so far unique, fundamental scalar particle. The masses of all fermions are also a consequence of EWSB since the Higgs doublet is postulated to couple to the fermions through Yukawa interactions in a way consistent with all the gauge symmetries of the SM.

The initial measurements during the LHC Run 1 were accessible mainly through production and decay channels related to the couplings of the Higgs boson to the vector gauge bosons. The outstanding performance of the LHC Run 2, made it possible for the ATLAS and CMS experiments to independently and unambiguously establish the couplings of the Higgs boson to the charged fermions of the third generation (the top quark, the bottom quark, and the tau lepton). In all observed production and decay modes measured so far, the rates and differential measurements are found to be consistent, within experimental and theoretical uncertainties, with the SM predictions. In high mass resolution decay channels, such as the ones with four leptons (electrons or muons) or diphoton final states, the mass of the Higgs boson has been measured at the permill precision level. And, from the search for Higgs boson decays to muons, there are tentalising experimental evidences for Yukawa interactions of the Higgs boson to the second generation of fermions. Nevertheless, several Higgs boson decay channels are very challenging experimentally at the LHC. The couplings of the Higgs boson to the first generation of fermions, at the level expected in the Standard Model, remain so far out of reach at the LHC.

Within the current precision, a more complex Higgs sector with additional states, although significantly constrained, is not ruled out. Nor has it been established whether the Higgs boson is an elementary particle or whether it has an internal structure like any other scalar particle observed before it. Therefore, Higgs physics remains a vivid and intense field of research on the experimental and theoretical fronts.

Without the Higgs boson, the calculability of the SM would have been spoiled. In particular, perturbative unitarity [5] would be lost at high energies since the longitudinal W/Z boson scattering amplitude would grow with the centre-of-mass energy. In addition, the radiative corrections to the gauge boson self-energies would exhibit dangerous logarithmic divergences that would be difficult to reconcile with EW precision data. With the discovery of the Higgs boson, the SM is a spontaneously broken gauge theory and, as such, it could a priori be consistently extrapolated well above the masses of the W and Z bosons. Hence, formally there is no need for new physics at the EW scale.

However, as the SM Higgs boson is a scalar particle, it has sensitivity to possible new physics scales. Quite generally, the Higgs boson mass is affected by the presence of heavy particles and it receives large quantum corrections which destabilise the weak scale barring a large fine-tuning of unrelated parameters. This is known as the Higgs naturalness or hierarchy problem [6], and it has been the prime argument for expecting new physics right at the TeV scale. To remedy to his unsatisfactory feature, theoretically motivated paradigms have been explored for several decades, such as a new fermion-boson symmetry called supersymmetry (SUSY) [7] (for recent reviews, see Refs. [8, 9]), or the existence of strong interactions at a scale of the order of a TeV from which the Higgs boson would emerge as a composite state [10] (see Refs. [11, 12] for recent reviews). Alternatively, new agents stabilising the weak scale could also be light but elusive, like in models of neutral naturalness [13,14]. And it was recently appreciated [15,16] that the cosmological evolution of the Universe could drive the Higgs boson mass to a value much smaller than the cutoff of the theory, alleviating the hierarchy problem without the need for TeV scale new physics, even though there might still be interesting and spectacular signatures [15, 17]. This new approach spurs a change in perspective invoking our Universe as part of a multiverse that should be treated as a quantum statistical system [18].

The Higgs boson is special and, in the eleven years since its discovery, it became a powerful tool to explore the manifestations of the SM and to probe the physics landscape beyond it.

This review is organised as follows. Section 11.2 is a theoretical introduction to the SM Higgs boson, its properties, production mechanisms and decay rates. The experimental measurements are described in Section 11.3. In Section 11.3.6, the combination of the main Higgs boson production and decay channels is presented. In Section 11.4, measurements of the main quantum numbers and CP properties of the Higgs boson are reported and the bounds on its total width are discussed. In Section 11.5, a general theoretical framework to describe the deviations of the Higgs boson couplings from the SM predictions is introduced and the experimental measurements of these Higgs couplings are reviewed. Measurements of differential cross sections are also outlined. Section 11.6 presents, in detail, some interesting models with an extended Higgs sector, addressing the hierarchy problem or not, and considers their experimental signatures. Section 11.7 provides a short summary and a brief outlook.

11.2 The Standard Model and the mechanism of electroweak symmetry breaking

In the SM [3], electroweak symmetry breaking [4] is responsible for generating a mass for the W and Z gauge bosons rendering the weak interactions short ranged. The SM scalar potential reads:

$$V(\Phi) = m^2 \Phi^\dagger \Phi + \lambda (\Phi^\dagger \Phi)^2 \tag{11.1}$$

with the Higgs field Φ being a self-interacting $\mathrm{SU}(2)_L$ complex doublet (four real degrees of freedom) with weak hypercharge $Y{=}1$ (the hypercharge is normalised such that $Q = T_{3L} + Y/2$, Q being the electric charge and T_{3L} the eigenvalue of the diagonal generator of $\mathrm{SU}(2)_L$):

$$\Phi = \frac{1}{\sqrt{2}} \begin{pmatrix} \sqrt{2}\phi^+ \\ \phi^0 + i a^0 \end{pmatrix}, \tag{11.2}$$

where ϕ^0 and a^0 are the CP-even and CP-odd neutral components, and ϕ^+ is the complex charged component of the Higgs doublet, respectively. $V(\Phi)$ is the most general renormalisable scalar potential invariant under $\mathrm{SU}(2)_L \times \mathrm{U}(1)_Y$. If the quadratic term is negative, the neutral component of the scalar doublet acquires a non-zero (real) vacuum expectation value (VEV)

$$\langle \Phi \rangle = \frac{1}{\sqrt{2}} \begin{pmatrix} 0 \\ v \end{pmatrix}, \tag{11.3}$$

with $\phi^0 = H + \langle\phi^0\rangle$ and $\langle\phi^0\rangle \equiv v$, inducing the spontaneous breaking of the SM gauge symmetry $\mathrm{SU}(3)_C \times \mathrm{SU}(2)_L \times \mathrm{U}(1)_Y$ into $\mathrm{SU}(3)_C \times \mathrm{U}(1)_{\rm em}$. The global minimum of the theory defines the ground state, and spontaneous symmetry breaking implies that there is a (global and/or local) symmetry of the system that is not respected by the ground state. From the four generators of the $\mathrm{SU}(2)_L \times \mathrm{U}(1)_Y$ SM gauge group, three are spontaneously broken, i.e., they do not leave the ground state invariant. This breaking implies the existence of three massless Goldstone bosons identified with three of the four Higgs field degrees of freedom. The Higgs field couples to the W_μ and B_μ gauge fields associated with the $\mathrm{SU}(2)_L \times \mathrm{U}(1)_Y$ local symmetry through the covariant derivative appearing in the kinetic term of the Higgs Lagrangian,

$$\mathcal{L}_{\rm Higgs} = (D_\mu \Phi)^\dagger (D^\mu \Phi) - V(\Phi)\,, \tag{11.4}$$

where $D_\mu \Phi = (\partial_\mu + ig\sigma^a W^a_\mu/2 + ig' Y B_\mu/2)\Phi$, g and g' are the $\mathrm{SU}(2)_L$ and $\mathrm{U}(1)_Y$ gauge couplings, respectively, and $\sigma^a, a = 1,2,3$ are the usual Pauli matrices. As a result, the neutral and the two charged massless Goldstone degrees of freedom mix with the gauge fields corresponding to the broken generators of $\mathrm{SU}(2)_L \times \mathrm{U}(1)_Y$ and become, in the unitarity gauge, the longitudinal components of the Z and W physical gauge bosons, respectively. The Z and W gauge bosons acquire masses,

$$m_W^2 = \frac{g^2 v^2}{4}\,, \quad m_Z^2 = \frac{(g'^2 + g^2)v^2}{4}. \tag{11.5}$$

The fourth generator remains unbroken since it is the one associated to the conserved $\mathrm{U}(1)_{\rm em}$ gauge symmetry, and its corresponding gauge field, the photon, remains massless. Similarly, the eight color gauge bosons, the gluons, corresponding to the conserved $\mathrm{SU}(3)_C$ gauge symmetry with 8 unbroken generators, also remain massless (though confined inside hadrons and mesons as the result of the asymptotic freedom behaviour of Quantum ChromoDynamics (QCD)). Hence, from the initial four degrees of freedom of the Higgs field, two are absorbed by the $W^\pm$ gauge bosons, one by the Z gauge boson, and there is one remaining degree of freedom, H, that is the physical Higgs boson — a new scalar particle first imagined by P. Higgs [4]. The Higgs boson is neutral under the electromagnetic interactions and transforms as a singlet under $\mathrm{SU}(3)_C$ and hence does not couple at tree level to the massless photons and gluons.

The fermions of the SM acquire a mass through renormalisable and gauge invariant interactions between the Higgs field and the fermions: the Yukawa interactions,

$$\mathcal{L}_{\rm Yukawa} = -\hat{h}_{d_{ij}} \bar{q}_{L_i} \Phi\, d_{R_j} - \hat{h}_{u_{ij}} \bar{q}_{L_i} \tilde{\Phi} u_{R_j} - \hat{h}_{l_{ij}} \bar{l}_{L_i} \Phi\, e_{R_j} + h.c., \tag{11.6}$$

which respect the symmetries of the SM but generate fermion masses once EWSB occurs. In the Lagrangian above, $\tilde{\Phi} = i\sigma_2 \Phi^*$ and q_L (l_L) and u_R, d_R (e_R) are the quark (lepton) $\mathrm{SU}(2)_L$ doublets and singlets, respectively, while in each term, $\hat{h}_{f_{ij}}$, $f = u, d, l$ is parametrised by a 3×3 matrix in family space. The mass term for neutrinos is omitted, but could be added in an analogous manner to the up-type quarks when right-handed neutrinos are supplementing the SM particle content (neutrinos can also acquire Majorana masses via non-renormalisable dimension-5 interactions with the Higgs field [19]). Once the Higgs field acquires a VEV, and after rotation to the fermion mass eigenstate basis that also diagonalises the Higgs-fermion interactions, $\hat{h}_{f_{ij}} \to h_{f_i}\delta_{ij}$ (the diagonal Yukawa coupling h_{f_i} is often denoted as y_{f_i}), all fermions acquire a mass given by $m_{f_i} = h_{f_i} v/\sqrt{2}$. The indices $i, j = 1, 2, 3$ refer to the three families in the up-quark, down-quark or charged lepton sectors. Remarkably, if the Yukawa interactions Eq. (11.6) are indeed fully responsible for the fermion masses, the Higgs interactions do not mediate flavour changing neutral currents at tree-level. It should be further noted that the EWSB mechanism provides no additional insight on possible underlying reasons for the large variety of mass values of the fermions, often referred to as

the flavour hierarchy. The fermion masses, accounting for a large number of the free parameters of the SM, are simply translated into Yukawa couplings.

11.2.1 *The SM Higgs boson mass, couplings and quantum numbers*

The SM Higgs boson is a CP-even scalar of spin 0. Its mass is given by $m_H = \sqrt{2\lambda}\, v$, where λ is the self-coupling parameter in $V(\Phi)$. The expectation value of the Higgs field, $v = (\sqrt{2}G_F)^{-1/2} \approx 246\,\text{GeV}$, is fixed by the Fermi coupling G_F, which is determined with a precision of 0.6 ppm from muon decay measurements [20]. The quartic coupling λ is a free parameter in the SM, and hence, there is no a priori prediction for the Higgs mass. Moreover the sign of the quadratic coupling, $m^2 = -\lambda v^2$, in the Higgs field potential $V(\Phi)$ has to be negative for the EW symmetry breaking to take place, but there is no a priori understanding of what decides of this sign. The experimentally measured Higgs boson mass, $m_H \simeq 125\,\text{GeV}$ [20], implies that $\lambda \simeq 0.13$ and $|m| \simeq 88.4\,\text{GeV}$.

The Higgs boson couplings to the fundamental particles are set by their masses. This is a new type of interaction; very weak for light particles, such as up and down quarks, and electrons, but strong for heavy particles such as the W and Z bosons and the top quark. More precisely, the SM Higgs couplings to fundamental fermions are linearly proportional to the fermion masses, whereas the couplings to bosons are proportional to the square of the boson masses. The SM Higgs boson couplings to gauge bosons and fermions, as well as the Higgs boson self coupling, are summarised in the following Lagrangian:

$$\mathcal{L} = -g_{Hf\bar{f}}\bar{f}fH + \frac{g_{HHH}}{6}H^3 + \frac{g_{HHHH}}{24}H^4 + \delta_V V_\mu V^\mu \left(g_{HVV}H + \frac{g_{HHVV}}{2}H^2\right) \tag{11.7}$$

with

$$g_{Hf\bar{f}} = \frac{m_f}{v},\ g_{HVV} = \frac{2m_V^2}{v},\ g_{HHVV} = \frac{2m_V^2}{v^2},\ g_{HHH} = \frac{3m_H^2}{v},\ g_{HHHH} = \frac{3m_H^2}{v^2}, \tag{11.8}$$

where $V = W^\pm$ or Z and $\delta_W = 1, \delta_Z = 1/2$. As a result, the dominant mechanisms for Higgs boson production and decay involve the coupling of H to W, Z and/or the third generation quarks and leptons. The Higgs boson coupling to gluons [21, 22] is induced at leading order by a one-loop process in which H couples to a virtual $t\bar{t}$ pair (with minor contributions from the other lighter quarks). Likewise, the Higgs boson coupling to photons is also generated via loops, although in this case the one-loop graph with a virtual W^+W^- pair provides the dominant contribution [23] and it is interfering destructively with the smaller contribution involving a virtual $t\bar{t}$ pair (as such, the Higgs coupling to photons is sensitive to the relative phase of the interactions between bosons and fermions).

11.2.2 *The SM custodial symmetry*

The SM Higgs Lagrangian, $\mathcal{L}_{\text{Higgs}} + \mathcal{L}_{\text{Yukawa}}$ of Eq. (11.4) and Eq. (11.6), is, by construction, $\text{SU}(2)_L \times \text{U}(1)_Y$ gauge invariant, but it also has an approximate global symmetry. In the limit $g' \to 0$ and $h_f \to 0$, a global $\text{SU}(2)_R$ symmetry emerges. This symmetry is preserved for non-vanishing Yukawa couplings provided $\hat{h}_u = \hat{h}_d$. Once the Higgs field acquires a VEV, both the $\text{SU}(2)_L$ and $\text{SU}(2)_R$ symmetry groups are broken but the diagonal subgroup $\text{SU}(2)_{L+R}$ remains unbroken and it is this subgroup that defines the custodial symmetry of the SM [24].

In the limit $g' \to 0$, the $W^\pm$ and Z gauge bosons have equal mass and form a triplet of the $\text{SU}(2)_{L+R}$ unbroken global symmetry. Using the expressions for the W and Z gauge boson masses in term of the gauge couplings, one obtains at tree level

$$\frac{m_W^2}{m_Z^2} = \frac{g^2}{g'^2 + g^2} \equiv \cos^2\theta_W \quad \text{i.e.} \quad \rho \equiv \frac{m_W^2}{m_Z^2 \cos^2\theta_W} = 1. \tag{11.9}$$

The custodial symmetry protects the above relation from large radiative corrections. All corrections to the ρ parameter are therefore proportional to terms that break the custodial symmetry. For instance, radiative corrections involving the Higgs boson are proportional to $\sin^2\theta_W$, $\delta\rho = -11 G_F m_Z^2 \sin^2\theta_W \log(m_H^2/m_Z^2)/(24\sqrt{2}\pi^2)$, and vanish in the limit $g' \to 0$. Since $m_t \neq m_b$, there are also relevant radiative corrections generated by massive fermions. They are proportional to $m_t^2 + m_b^2 - 2(m_t^2 m_b^2)\log(m_t^2/m_b^2)/(m_t^2 - m_b^2)$ and would indeed vanish for $m_t = m_b$ [25].

11.2.3 *Stability of the Higgs potential*

The discovery of the Higgs boson with $m_H \approx 125\,\text{GeV}$ has far reaching consequences within the SM framework. In particular, the precise value of m_H determines the value of the quartic coupling λ at the electroweak scale and makes it possible to study its behavior up to high energy scales. A larger value of m_H would have implied that the self coupling λ would become non-perturbative at some scale Λ that could be well below the Planck scale [26].

However, for the value of Higgs boson mass experimentally measured, the EW vacuum of the Higgs potential is most likely metastable [27]. The high-energy evolution of λ shows that it becomes negative at energies $\Lambda = \mathcal{O}(10^{11})\,\text{GeV}$ (even though λ could remain positive till higher energy, maybe all the way to the Planck scale, if the top quark mass exceeds its current measured value by 3σ). When this occurs, the SM Higgs potential develops an instability and the long term existence of the EW vacuum is challenged. This behaviour may call for new physics at an intermediate scale before the instability develops, i.e., below M_{Planck}, even though new physics at M_{Planck} could influence the stability of the EW vacuum and possibly modify this conclusion [28]. The consequences of the instability of the EW vacuum on high-scale inflation have been discussed in Ref. [29]. It was also noticed that Higgs field fluctuations during inflation could seed the formation of primordial black holes, possibly making up the Dark Matter relic abundance [30] or they could produce a stochastic background of gravitational waves with characteristic structures [31], offering a probe of the EW vacuum near criticality.

The lifetime of the EW metastable vacuum is determined by the rate of quantum tunnelling from this vacuum into the true vacuum of the theory (for the most recent computation of the EW vacuum lifetime within the SM, see Ref. [32]). Within the SM, the running of the Higgs self coupling slows down at high energies with a cancellation of its β-function at energies just one to two orders of magnitude below the Planck scale [33]. This slow evolution of the quartic coupling is responsible for saving the EW vacuum from premature collapse. It might also help the Higgs boson to play the role of an inflaton [34] (see, however, Ref. [35] for potential issues with this Higgs-boson-as-an-inflaton idea).

11.2.4 *Higgs boson production and decay mechanisms*

Comprehensive reviews of the SM Higgs boson properties and phenomenology, with an emphasis on the impact of loop corrections to the Higgs boson decay rates and cross sections, can be found in Refs. [36–40]. The main results are summarised here.

11.2.4.1 *Production mechanisms at hadron colliders*

The main production mechanisms at the Tevatron collider and the LHC are gluon fusion (ggF), weak-boson fusion (VBF), associated production with a gauge boson (VH), and associated production with a $t\bar{t}$ pair ($t\bar{t}H$) or with a single top quark (tHq). Figure 11.1 depicts representative diagrams for these dominant Higgs boson production processes.

The state-of-the-art of the theoretical calculations in the main different production channels is summarised in Table 11.1.

The cross sections for the production of a SM Higgs boson as a function of $\sqrt{s}$, the center of mass energy, for pp collisions, including bands indicating the theoretical uncertainties, are summarised

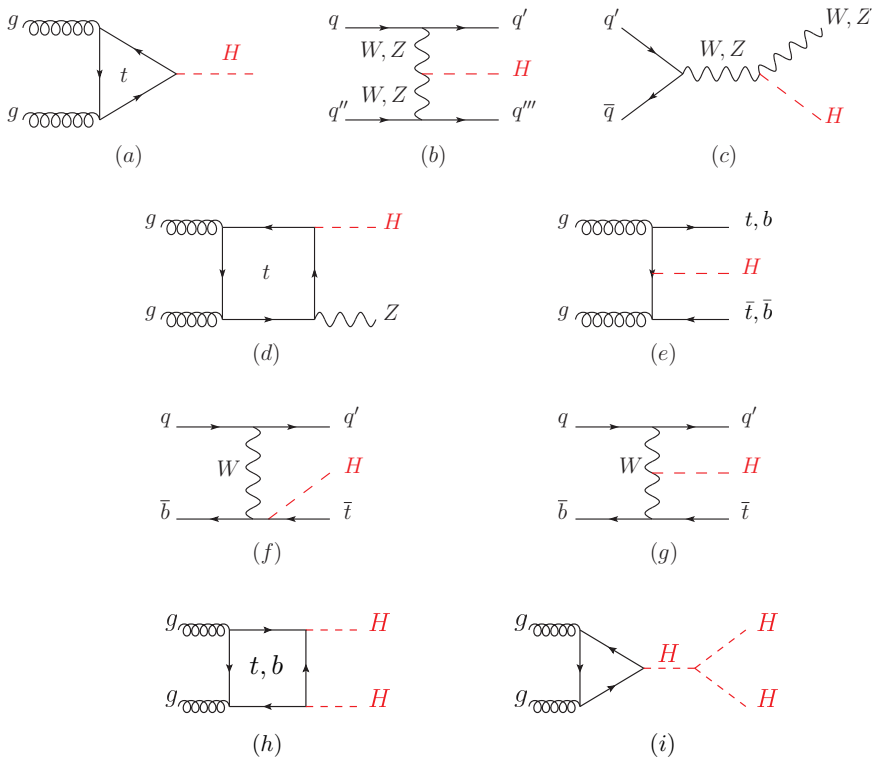

Figure 11.1: Main leading order Feynman diagrams contributing to the single Higgs boson production in (a) gluon fusion, (b) Vector-boson fusion, (c) Higgs-strahlung (or associated production with a gauge boson at tree level from a quark-quark interaction), (d) associated production with a gauge boson (at loop level from a gluon-gluon interaction), (e) associated production with a pair of top/bottom quarks, (f-g) production in association with a single top quark, and double Higgs production through (h) a top- and bottom-quark loop, (i) the self coupling of the Higgs boson.

in Fig. 11.2 (left) [43]. A detailed discussion, including uncertainties in the theoretical calculations due to missing higher-order effects and experimental uncertainties on the determination of SM parameters involved in the calculations, can be found in Refs. [37–40]. These references also contain state-of-the-art discussions on the impact of PDF uncertainties, QCD scale uncertainties and uncertainties due to different procedures for including higher-order corrections matched to parton shower simulations, as well as uncertainties due to hadronisation and parton-shower events.

Table 11.2 summarises the Higgs boson production cross sections and relative uncertainties for a Higgs boson mass of 125 GeV, for $\sqrt{s} = 7$, 8, 13, 13.6 and 14 TeV.

i. *Gluon fusion production mechanism*

At high-energy hadron colliders, the Higgs boson production mechanism with the largest cross section is the gluon-fusion process, $gg \to H + X$, mediated by the exchange of a virtual, heavy top quark [45]. Contributions from lighter quarks propagating in the loop are suppressed proportionally to m_q^2. QCD radiative corrections to the gluon-fusion process are very important and have been studied in detail. Including the full dependence on the (top, bottom, charm) quark and Higgs boson masses, the cross section has been calculated at the next-to-leading order (NLO) in α_s [46,47]. To a very good approximation, the leading top-quark contribution can be evaluated in the limit $m_t \to \infty$ by matching the SM to an effective theory. The gluon-fusion amplitude is then evaluated from an

Table 11.1: State-of-the-art of the theoretical calculations in the main Higgs boson production channels in the SM, and, when publicly available, the major MC tools used in the simulations. Furthermore, all the Higgs-boson production modes have been interfaced with parton-shower event generators at NLO QCD like `Poweg-Box, MG5_aMC@NLO or Sherpa` (the entries "—" indicate cases when the results are implemented in codes that are not yet public). For ggF and VH NNLO matched simulations now also exist. Differential NNLO QCD results exist for $t\bar{t}H$ [41] (though the exact 2-loop virtual corrections are still missing) and have been implemented in `MATRIX` [42].

ggF	VBF	VH	$t\bar{t}H$
Inclusive:	Inclusive:	Inclusive:	Inclusive:
N3LO QCD + NLO EW	N3LO QCD	N3LO QCD	NNLO QCD
`(iHixs)`	`proVBFH`	`(n3loxs)`	—
N3LO QCD		NNLO QCD	
`ggHiggs`		`(VH@NNLO)`	
Differential:	Differential:	Differential:	Differential:
NNLO+N3LL QCD	NNLO QCD	NNLO QCD	NLO QCD+EW
`(Radish+NNLOJET)`	—	—	`(MG5_aMC@NLO)`
N3LO+N3LL′ QCD	NLO QCD + EW	NLO QCD + EW	
`(TROLL)`	`(HAWK)`	`(HAWK)`	

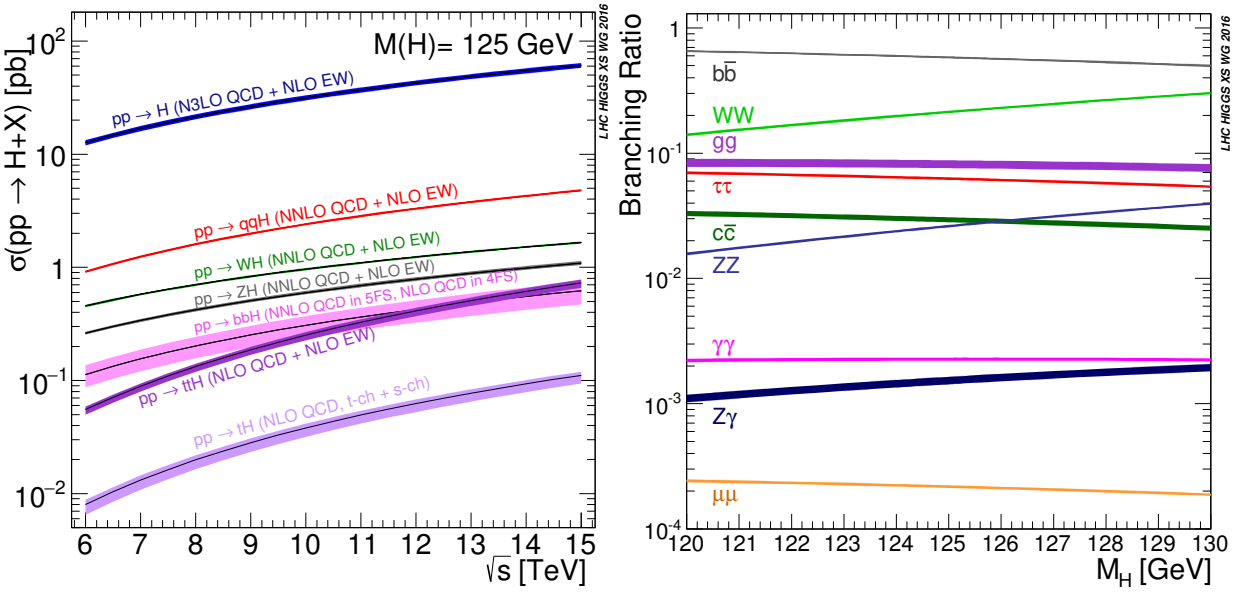

Figure 11.2: (Left) The SM Higgs boson production cross sections as a function of the center of mass energy, $\sqrt{s}$, for pp collisions [43]. The VBF process is indicated here as qqH. (Right) The branching ratios for the main decays of the SM Higgs boson near $m_H = 125\,\text{GeV}$ [39, 40]. The theoretical uncertainties are indicated as bands.

effective Lagrangian containing a local $HG^a_{\mu\nu}G^{a\,\mu\nu}$ operator [21, 22]. In this approximation, the cross section is known at next-to-next-to-next-to-leading order in α_s expansion (N3LO QCD) [48]. The validity of the effective theory with infinite m_t is greatly enhanced by rescaling the result by the exact LO result: $\sigma = (\sigma^{\text{LO}}_{m_t}/\sigma^{\text{LO}}_{m_t=\infty}) \times \sigma_{m_t=\infty}$ [40]. The large top-quark mass approximation, after

Table 11.2: The SM Higgs boson production cross sections for $m_H = 125\,\text{GeV}$ in pp collisions ($p\bar{p}$ collisions at $\sqrt{s} = 1.96\,\text{TeV}$ for the Tevatron), as a function of the center of mass energy, $\sqrt{s}$. The predictions for the LHC energies are taken from Refs. [37–40, 43], the ones for the Tevatron energy are the ones used in Ref. [44]. The predictions for the ggF channel at the LHC include the latest N3LO QCD + NLO EW results. The uncertainties are estimated assuming no correlation between α_S and PDF uncertainties. The uncertainties on the total cross sections are dominated by the ones on the gluon fusion process.

$\sqrt{s}$ (TeV)	Production cross section (in pb) for $m_H = 125\,\text{GeV}$					
	ggF	VBF	WH	ZH	$t\bar{t}H$	total
1.96	$0.95^{+17\%}_{-17\%}$	$0.065^{+8\%}_{-7\%}$	$0.13^{+8\%}_{-8\%}$	$0.079^{+8\%}_{-8\%}$	$0.004^{+10\%}_{-10\%}$	$1.23^{+15\%}_{-15\%}$
7	$16.9^{+5.5\%}_{-7.6\%}$	$1.24^{+2.2\%}_{-2.2\%}$	$0.58^{+2.2\%}_{-2.3\%}$	$0.34^{+3.1\%}_{-3.0\%}$	$0.09^{+5.6\%}_{-10.2\%}$	$19.1^{+5\%}_{-7\%}$
8	$21.4^{+5.4\%}_{-7.6\%}$	$1.60^{+2.1\%}_{-2.1\%}$	$0.70^{+2.1\%}_{-2.2\%}$	$0.42^{+3.4\%}_{-2.9\%}$	$0.13^{+5.9\%}_{-10.1\%}$	$24.2^{+5\%}_{-7\%}$
13	$48.6^{+5.6\%}_{-7.4\%}$	$3.78^{+2.1\%}_{-2.1\%}$	$1.37^{+2.0\%}_{-2.0\%}$	$0.88^{+4.1\%}_{-3.5\%}$	$0.50^{+6.8\%}_{-9.9\%}$	$55.1^{+5\%}_{-7\%}$
13.6	$52.2^{+5.6\%}_{-7.4\%}$	$4.1^{+2.1\%}_{-1.5\%}$	$1.46^{+1.8\%}_{-1.9\%}$	$0.95^{+4.0\%}_{-3.6\%}$	$0.57^{+6.9\%}_{-9.9\%}$	$59.2^{+5\%}_{-7\%}$
14	$54.7^{+5.6\%}_{-7.4\%}$	$4.28^{+2.1\%}_{-2.1\%}$	$1.51^{+1.8\%}_{-1.9\%}$	$0.99^{+4.1\%}_{-3.7\%}$	$0.61^{+6.9\%}_{-9.8\%}$	$62.1^{+5\%}_{-7\%}$

this rescaling of the cross section, yields a next-to-next-to-leading order (NNLO) QCD result that has been established to be at the percent level accuracy [49]. Further progress was made to include full top mass dependence at NNLO QCD [50]. And the bottom and light quark contributions to the Higgs production have been reassessed in Refs. [51–53].

The LO contribution and NLO QCD corrections [54] amount to about 80% of the total N3LO QCD cross section. The NNLO QCD corrections [55] further enhance the cross section by approximately 30% of the LO plus NLO result (at $\mu_f = \mu_r = m_H/2$). Electroweak radiative corrections have been computed at NLO and increase the LO cross section by about 5% for $m_H \simeq 125\,\text{GeV}$ [56]. Mixed QCD-EW corrections are now being investigated with encouraging results on the computation of the exact 3-loop amplitude [57] complementing the results obtained in either limit of heavy [58] or massless [59] gauge bosons. The mixed QCD-EW corrections still have to be evaluated at large p_T.

At N3LO QCD, the perturbation series is rather stable with a mere enhancement of 3% of the total cross section, with a central value quite insensitive to threshold resummation effects with the scale choice mentioned above ($\mu_f = \mu_r = m_H/2$) [40, 48, 60, 61]. At the LHC with a center-of-mass energy of 13 TeV, the most up-to-date value for the production cross section of a 125 GeV Higgs boson amounts to [40]

$$\sigma_{\text{ggF}}^{\text{N3LO}} = 48.6\,^{+2.2\,(4.6\%)}_{-3.3\,(6.7\%)}\,(\text{theory}) \pm 1.6\,(3.2\%)\,(\text{PDF} + \alpha_s)\,\text{pb}. \tag{11.10}$$

This cross-section was first computed in terms of an expansion around the production threshold of the Higgs boson. This approximation was overcome in Ref. [61]. The PDF uncertainty of order 1-2% quoted above has been questioned as the first global analysis of PDFs at approximate N3LO

QCD was presented, suggesting an unexpected decrease of the cross-section central value by more than 5% [62].

Besides considering the inclusive Higgs boson production cross section at the LHC, it is important to study differential distributions in order to probe the properties of the Higgs boson in a detailed way. The Higgs boson rapidity distribution has been computed at the N3LO QCD order in Ref. [63]. And fully differential N3LO QCD predictions for Higgs production in gluon fusion have been obtained by combining N3LO QCD predictions for Higgs rapidity distribution with NNLO QCD predictions for H+jet [64]. A more exclusive account of Higgs boson production is also required because experimental analyses often impose cuts on the final states in order to improve the signal-to-background ratio. Using soft-collinear effective theory, large fiducial power corrections induced by fiducial cuts have been resummed at N3LO+N3LL$'$ QCD accuracy, i.e. at next-to-next-to-next-leading-log, incorporating the complete $\mathcal{O}(\alpha_s^3)$ singular structure for $q_T \to 0$ allowing one to consistently match to N3LO QCD [65]. This is the most accurate result that can be directly compared with fiducial measurements. Different fiducial cuts are explored to suppress these fiducial effects. In addition, progress has been made to improve the calculation of the Higgs boson production cross section with a jet veto (the "0-jet bin" or in the presence of a veto bounding the transverse momentum of the hardest accompanying jet) [66], reaching NNLL accuracy matched to N3LO QCD. These accurate predictions for the jet-veto cross section are required, e.g., to suppress the $t\bar{t}$ background in the $H \to WW$ channel [67].

ii. *Vector boson fusion production mechanism*

The SM Higgs boson production mode with the second-largest cross section at the LHC is vector boson fusion. At the Tevatron collider, VBF also occurred, but for $m_H = 125\,\text{GeV}$ had a smaller cross section than Higgs boson production in association with a W or Z boson. Higgs boson production via VBF, $qq \to qqH$, proceeds by the scattering of two (anti-)quarks, mediated by t- or u-channel exchange of a W or Z boson, with the Higgs boson radiated off the weak-boson propagator. The scattered quarks give rise to two hard jets in the forward and backward regions of the detector with a large rapidity gap [68]. Because of the color-singlet nature of the weak-gauge boson exchange, gluon radiation from the central-rapidity regions is strongly suppressed. These characteristic features of VBF processes can be exploited to distinguish them from overwhelming QCD backgrounds, including gluon-fusion induced Higgs boson + 2 jet production, and from s-channel WH or ZH production with a hadronically decaying weak gauge boson. After the application of specific selection cuts, the VBF channel provides a clean environment, not only for the Higgs boson searches originally performed, but also for the subsequent determination of Higgs boson couplings at the LHC.

The cross-section is known at N3LO QCD at the inclusive level [69] and at NNLO enforcing the VBF cuts [70] with a residual uncertainty of the order of few permill. However, this result is obtained in the DIS/factorized approximation [71] where the fusing gauge bosons are emitted from the two quark legs independently. While, the exact NNLO QCD VBF calculation will remain out-of-reach in the near future, the leading non-factorisable contributions with two forward jets have been estimated [72] and the impact of non-factorizable effects have been studied in Ref. [73]. They give some corrections, also of the order of few permill, to inclusive quantities, but they are an order of magnitude larger for differential observables. Overall, the residual uncertainty is of the order of a few percent but is quite sensitive to the tagging jet cuts and jet radius modelling [74]. Extensive studies on VBF at fixed order and with parton shower matched computations can be found in Ref. [75]. In addition, EW corrections have been included and the VBF process is known at NLO QCD+EW order for some time [76, 77].

iii. *WH and ZH associated production mechanism*

The next most relevant Higgs boson production mechanisms are associated production with W and Z gauge bosons. The cross sections for the associated production processes, $pp \to VH + X$, with $V = W^{\pm}, Z$ receive contributions at NLO QCD given by NLO QCD corrections to the Drell–Yan cross section [78,79] and from NLO EW corrections. The latter, unlike the QCD corrections, do not respect the factorisation into Drell–Yan production since there are irreducible box contributions already at one loop [76,80]. At NNLO QCD, the Drell–Yan-like corrections to WH production also give the bulk of the corrections to ZH production [81]. For ZH production there are, however, gluon-gluon induced contributions that do not involve a virtual Z gauge boson but are such that the Z gauge boson and H boson couple to gluons via top-quark loops [82], see diagram (d) in Fig. 11.1. NLO QCD virtual corrections to the partonic cross section for $gg \to ZH$, in the high-energy and large top mass limits are available in Refs. [83]. In addition, WH and ZH production receive non Drell–Yan-like corrections in the $q\bar{q}'$ and $q\bar{q}$ initiated channels, respectively, at the NNLO level in QCD, where the Higgs boson is radiated off top-quark loops [84]. The full QCD corrections up to NNLO order, the NLO EW corrections and the NLO corrections to the gluon-gluon channel are available in `VH@NNLO` [85]. NNLO QCD corrections to $pp \to WH$+jet are important for signal modelling. NLO corrections to cross section inclusive in the number of jets show excellent convergence while NNLO QCD corrections to exclusive single jet cross section are much more significant [86].

As neither the Higgs boson nor the weak gauge bosons are stable particles, their decays also have to be taken into account. Providing full kinematical information for the decay products can furthermore help in the suppression of large QCD backgrounds. Differential distributions for the processes $pp \to WH \to \bar{\nu}_\ell \ell H$ and $pp \to ZH \to \ell^+\ell^- H/\nu_\ell \bar{\nu}_\ell H$, including NLO QCD and EW corrections, have been presented in Ref. [87]. The NNLO QCD corrections to differential observables for WH production at the LHC, including the leptonic decays of the W boson and the decay of the Higgs boson into a $b\bar{b}$ pair, are presented in Ref. [88]. Calculations at the same level, including also the ZH process have been performed [89]. The WH production mode has also been matched to a parton shower at NNLO QCD accuracy [90]. Full NNLO QCD results for both the production and decay are available [91] and show a large impact of radiation from the final-state bottoms. The WH and ZH production modes, especially in the boosted regime, provide a relatively clean environment for studying the decay of the Higgs boson into bottom quarks [92]. Bottom mass effects have been computed at NNLO [93,94] and tend to increase the rates by 6-7%.

The inclusive cross section for associated Higgs boson production with a massive gauge boson is recently known up to N3LO QCD too [95].

iv. *Higgs boson production in association with $t\bar{t}$*

Higgs boson radiation off top quarks, $pp \to t\bar{t}H$, provides a direct probe of the top-Higgs Yukawa coupling. The LO cross section for this production process was computed in Ref. [96]. Later, the NLO QCD [97] and NLO EW corrections [98] were evaluated yielding a moderate increase in the total cross section of at most 20%, but significantly reducing the scale dependence of the inclusive cross section. The EW corrections can be enhanced by large electroweak Sudakov logarithms in particular in the boosted regime often used in the phenomenological analyses [99]. The resummation of soft gluon contributions close to the partonic kinematical threshold are considered in Refs. [100] to reach a result at NLO+NNLL QCD order. Full off-shell calculations with decaying top quarks are computed at NLO QCD [101] and NLO QCD + EW [102] order, respectively. The fixed-order NLO QCD calculation has been interfaced with the standard parton shower Monte-Carlo generators

in Refs. [103], allowing an accurate description of the $t\bar{t}H$ signal, from the energy scale of the hard scattering to the hadronisation energy scale. These programs provide the most flexible tools to date for the computation of differential distributions, including experimental selection cuts and vetoes on the final-state particles and their decay products. The exploitation of this $t\bar{t}H$ channel requires, however, a proper description of the background, in particular $t\bar{t}b\bar{b}$, which exhibits a huge k-factor[1] enhancement from shower effects, see Ref. [40] for a detailed discussion. While the $H \to b\bar{b}$ decay mode was first considered, the focus has been broadened and other modes have been studied too, in particular the multilepton channel and other backgrounds such as $t\bar{t}W$ and $t\bar{t}Z$ have become relevant and intensively analyzed.

The total theoretical uncertainties, estimated by combining the ones from factorisation and renormalisation scales, strong gauge coupling, and parton distributions, amount to 10–15% of the corresponding inclusive cross section. To match the experimental precision envisioned at the end of HL-LHC, NNLO QCD predictions are required. Using the q_T subtraction formalism for $t\bar{t}H$ production, Ref. [104] presented the first quantitative results at NNLO. The calculation is accurate at NLO in QCD and agrees with the results obtained using the conventional subtraction methods. The NNLO corrections are computed for the flavour off-diagonal partonic channels but their contribution turn out to be at the permill level. The results for the diagonal channels have been obtained in Ref. [41]. The two-loop amplitudes are not yet known, but they have been reliably evaluated by using a soft Higgs boson approximation. At the 13 TeV centre-of-mass energy, the NNLO corrections increase the NLO result for the total cross section by about 4% and lead to a significant reduction of perturbative uncertainties. Also recently, the fragmentation and splitting functions for the production of a Higgs boson have been computed at order $y_t^2\alpha_s$ and they can be used to compute differential cross sections with arbitrary top-quark and Higgs-boson masses directly from the results in the massless limit [105].

v. *Other single Higgs boson production mechanisms at the LHC*

The Higgs boson production in association with a single top quark, though subdominant, can bring valuable information, in particular regarding the sign of the top Yukawa coupling. This is due to an almost totally destructive interference between two large contributions, one where the Higgs boson couples to a space-like W boson and the other where it couples to the top quark. This process has been computed at NLO QCD in a five-flavour scheme [106] and amounts to about 90 fb at $\sqrt{s} = 14$ TeV (with the opposite sign of the top Yukawa coupling, the cross section increases by one order of magnitude while the cross section for associated production with a pair of top quarks is unaffected). Recently, the tHj (and tZj) process has been computed at NLO QCD+EW accuracy [107]. The NLO EW correction is found to be within the NLO QCD theory uncertainties if the 4 vs 5 flavour scheme uncertainty is taken into account. The EW corrections reduce the total cross section by 3-4%.

The Higgs boson production in association with a pair of bottom quarks ($b\bar{b}H$) has been computed at the N3LO QCD order in the 5-flavour scheme [108], while the production with one/two b-jets, defined by specific kinematic cuts, is known respectively at NLO QCD in the 4-flavour scheme and at NNLO QCD in the 5-flavour scheme [109–111]. The coupling of the Higgs boson to a b-quark is suppressed in the SM by the bottom-quark mass over the Higgs VEV, m_b/v, implying that associated production of a SM Higgs boson with b-quarks is small at the LHC. Yet, at high energy, large logarithms are present and need to be resummed, leading to an enhancement of the inclusive cross section. At $\sqrt{s} = 14$ TeV, the $b\bar{b}H$ cross section can be as large as 550 fb, still two orders of magnitude below the ggF production cross section. Furthermore, the overwhelming ZH and

[1] the k-factor is defined as the ratio of a physical quantity with and without radiative corrections included.

VBF backgrounds (at the inclusive but also differential levels) make it challenging to extract genuine bottom Yukawa signal in a traditional cut-based analysis [112] but innovative machine-learning techniques are a promising avenue to obtain information complementary to the ones extracted from $gg \to h \to b\bar{b}$, in particular for what concerns the phase of the bottom Yukawa coupling [113]. In a two Higgs doublet model or a SUSY model, which will be discussed in Section 11.6, this coupling is proportional to the ratio of neutral Higgs boson vacuum expectation values, $\tan\beta$, and can be significantly enhanced for large values of this ratio. Consequently, the $b\bar{b}H$ mode can even become the dominant production process for the Higgs boson, unlike in the SM.

The Higgs boson production in association with charm quarks is also known at NNLO QCD and its cross section is approximately 85 fb at $\sqrt{s} = 13$ TeV [40].

vi. *Double Higgs boson production at the LHC*

The main interest in the double Higgs boson production is that it can provide invaluable information on the Higgs potential. In particular, it gives access to the Higgs trilinear self coupling. The dominant production is via gluon fusion $gg \to HH$ (slightly more than 31 fb at 13 TeV) and it accounts for more than 90% of the total inclusive cross-section, the sub-leading production mechanisms are VBF $HHjj$ (around 1.7 fb at 13 TeV), HHW (0.50 fb), HHZ (0.36 fb) and $t\bar{t}HH$ (0.8 fb). The fixed order QCD corrections, computed in the infinite top mass limit, are large, typically doubling the cross section from LO to NLO QCD [114], further enhancing it by 20% and reducing the scale uncertainty by a factor 2-3 from NLO to NNLO QCD [115], with a milder increase of order 3% at N3LO [116] to finally reach at 13 TeV

$$\sigma(gg \to HH)^{\rm N3LO}_{\rm ggF, m_t \to \infty} = 31.31\,^{+0.66\%}_{-2.8\%}\ {\rm fb}. \tag{11.11}$$

Recently, the complete NLO corrections with all top quark mass effects also became available numerically [117], intriguingly revealing a k-factor much less flat than predicted in the large top mass approximations. The non-trivial dependence of the results on the renormalisation scheme and scale for the top quark mass questions the assessment of the scale uncertainty and would warrant a proper NNLO computation that will however remain out of reach for quite some time. At the differential level, the destructive interference between the box and the triangle contributions complicates the predictions made in the infinite top mass limit for both the HH invariant mass and the leading Higgs boson p_T distributions. With an inclusive cross section of about 35 fb at $\sqrt{s} = 13$ TeV and a difficult signal vs background discrimination, the double Higgs boson production remains a challenging channel to probe and will greatly benefit from the high-luminosity run of the LHC and the combination of various decay modes [118]. The double Higgs channel is definitively a prime target on the Higgs physics agenda and the forthcoming analyses will greatly benefit from the solidification of the fixed order predictions and the detailed uncertainty budget estimate that is underway [119].

11.2.4.2 *Production mechanisms at e^+e^- colliders*

The dominant Higgs boson production cross sections at an e^+e^- collider are from the Higgs-strahlung process [21,120], $e^+e^- \to ZH$, and the WW fusion process [121], $e^+e^- \to \bar{\nu}_e\nu_e W^*W^* \to \bar{\nu}_e\nu_e H$. The cross-section for the Higgs-strahlung process scales as the inverse of the collision centre-of-mass squared energy, s, and is predominant at low energies, while the cross-section for the WW fusion process scales as $\ln(s/m_H^2)$ and dominates at high energies [122]. The ZZ fusion mechanism, $e^+e^- \to e^+e^- Z^*Z^* \to e^+e^- H$, also contributes to the Higgs boson production, with a cross-section suppressed by an order of magnitude with respect to that of WW fusion. The process $e^+e^- \to t\bar{t}H$ [123] becomes important for $\sqrt{s} \geq 500$ GeV. For a more detailed discussion of Higgs

boson production properties at lepton colliders, see for example Refs. [124]. Interesting progress has been made recently [125] to accurately account for beamstrahlung and initial state radiation using the factorisation approach primarily developed for hadron colliders and this method is being implemented in Monte Carlo event generators. Further information about Higgs physics at an e^+e^- collider can be found in Ref. [126].

11.2.4.3 *SM Higgs boson branching ratios and total width*

For the understanding and interpretation of the experimental results, the computation of all relevant Higgs boson decay widths is essential, including an estimate of their uncertainties and, when appropriate, the effects of Higgs boson decays into off-shell particles with successive decays into lighter SM ones. A Higgs boson mass of about 125 GeV allows to explore the Higgs boson couplings to many SM particles. In particular the dominant decay modes are $H \to b\bar{b}$ and $H \to WW^*$, followed by $H \to gg$, $H \to \tau^+\tau^-$, $H \to c\bar{c}$ and $H \to ZZ^*$. With much smaller rates follow the Higgs boson decays into $H \to \gamma\gamma$, $H \to \gamma Z$ and $H \to \mu^+\mu^-$. Since the decays into gluons, diphotons and $Z\gamma$ are loop induced, they provide indirect information on the Higgs boson couplings to WW, ZZ and $t\bar{t}$ in different combinations. The uncertainties in the branching ratios include the missing higher-order corrections in the theoretical calculations as well as the errors in the SM input parameters, in particular fermion masses and the QCD gauge coupling, involved in the decay. In the following the state-of-the-art of the theoretical calculations compiled by the LHC Higgs Working Group [43] will be discussed and the reader is referred to Refs. [37–40, 127] for detail.

The evaluation of the radiative corrections to the fermionic decays of the SM Higgs boson are implemented in HDECAY [128] at different levels of accuracy. The computations of the $H \to b\bar{b}$ and $H \to c\bar{c}$ decays include the complete massless QCD corrections up to N4LO, with a corresponding scale dependence of about 0.1% [129]. Both the electroweak corrections to $H \to b\bar{b}$, $c\bar{c}$ as well as $H \to \tau^+\tau^-$ are known at NLO [130] providing predictions with an overall accuracy of about 1–2% for $m_H \simeq 125\,\text{GeV}$.

The loop induced decays of the SM Higgs boson are known fully at NLO and partially beyond that approximation. For $H \to gg$, the QCD corrections are known up to N3LO in the limit of heavy top quarks [47, 131] and the uncertainty from the scale dependence is about 3%. For the $H \to \gamma\gamma$, the full NLO QCD corrections are available [47, 132] and the three-loop QCD corrections have also been evaluated [133]. The NLO electroweak corrections to $H \to gg$ and $H \to \gamma\gamma$ have been computed in Ref. [134]. All these corrections are implemented in HDECAY [128]. For $m_H \simeq 125\,\text{GeV}$, the overall impact of known QCD and EW radiative effects turns out to be well below 1%. In addition, the contribution of the $H \to \gamma e^+e^-$ decay via virtual photon conversion has been computed in Ref. [135]. The partial decay width $H \to Z\gamma$ is only implemented at LO in HDECAY, including the virtual W, top-, bottom-, and τ-loop contributions. The QCD corrections have been calculated and are at the percent level [136]. The theoretical uncertainty due to unknown electroweak corrections is estimated to be less than 5%, an accuracy that will be hard to achieve in the measurement of this process at the LHC.

The decays $H \to WW/ZZ \to 4f$ can be simulated with the `Prophecy4f` Monte-Carlo generator [137] that includes complete NLO QCD and EW corrections for Higgs decays into any possible four-fermion final state. All calculations are consistently performed with off-shell gauge bosons, without any on-shell approximation. For the SM Higgs boson, the missing higher-order corrections are estimated to be roughly 0.5%. Such uncertainties will have to be combined with the parametric uncertainties, in particular those associated to the bottom-quark mass and the strong gauge coupling, to arrive at the full theory uncertainty. A detailed treatment of the differential distributions for a Higgs boson decay into four charged leptons in the final state is discussed in Refs. [39, 138].

The total width of a 125 GeV SM Higgs boson is $\Gamma_H = 4.07 \times 10^{-3}\,\text{GeV}$, with a relative uncer-

Table 11.3: The branching ratios and the relative uncertainty for a SM Higgs boson with $m_H = 125\,\text{GeV}$ [39, 40].

Decay channel	Branching ratio	Rel. uncertainty
$H \to \gamma\gamma$	2.27×10^{-3}	2.1%
$H \to ZZ$	2.62×10^{-2}	$\pm$1.5%
$H \to W^+W^-$	2.14×10^{-1}	$\pm$1.5%
$H \to \tau^+\tau^-$	6.27×10^{-2}	$\pm$1.6%
$H \to b\bar{b}$	5.82×10^{-1}	$^{+1.2\%}_{-1.3\%}$
$H \to c\bar{c}$	2.89×10^{-2}	$^{+5.5\%}_{-2.0\%}$
$H \to Z\gamma$	1.53×10^{-3}	$\pm$5.8%
$H \to \mu^+\mu^-$	2.18×10^{-4}	$\pm$1.7%

tainty of $^{+4.0\%}_{-3.9\%}$. The branching ratios for the most relevant decay modes of the SM Higgs boson as a function of m_H, including the most recent theoretical uncertainties, are shown in Fig. 11.2 (right) and listed for $m_H = 125\,\text{GeV}$ in Table 11.3. Further details of these calculations can be found in the reviews [37–40] and references therein.

11.3 The experimental profile of the Higgs boson

The observation [1, 2] at the LHC of a narrow resonance with a mass of about 125 GeV was an important landmark in the decades-long direct search [44, 139] for the SM Higgs boson. This observation is being followed by a detailed exploration of properties of the Higgs boson at the different runs of the LHC at $\sqrt{s}$ = 7, 8,13 and 13.6 TeV.

The dataset at $\sqrt{s}$ =13 TeV collected during the Run-2 phase of the LHC operation is the largest analysed dataset so far and corresponds to an integrated luminosity of about 160 fb^{-1} delivered to the ATLAS and CMS experiments, see Table 11.4 [140]. The datasets effectively useful for analysis need to take into account the data-taking efficiency with fully operational detectors and the data quality efficiency. The typical total inefficiency for both ATLAS and CMS is approximately 10%, where approximately half is due to the data aquisition inefficiency and the other half from data quality requirements.

In this section, most of the references for the Run-1 measurements that have been updated with the data delivered in Run 2 are given in the previous version of this review [141] and are not repeated herein.

11.3.1 *The principal decay channels of the Higgs boson*

For a given m_H, the sensitivity of a channel depends on the production cross section of the Higgs boson, its decay branching fraction, the reconstructed mass resolution, the selection efficiency and the level of background in the final state. It is defined typically as the expected significance for the observation of a given process or in terms of expected upper limit at 95% Confidence Level (CL). At the LHC, for a Higgs boson with a mass close to 125 GeV, five decay channels play an important role. In the $H \to \gamma\gamma$ and $H \to ZZ^* \to 4\ell$ channels, all final state particles can be very precisely measured and the reconstructed m_H resolution is excellent (typically 1-2%). The $H \to W^\pm W^{\mp(*)} \to \ell^+\nu_\ell\ell'^-\bar{\nu}_{\ell'}$ channel has a relatively large branching fraction. However, the

Table 11.4: The LHC pp collision centre-of-mass energies and approximate collision samples delivered to ATLAS & CMS experiments.

Year	$\sqrt{s}$ (TeV)	$\int$ L.dt (fb^{-1})	Period
2010	7.0	0.04	Run 1
2011	7.0	6	Run 1
2012	8.0	23	Run 1
2015	13.0	4	Run 2
2016	13.0	39	Run 2
2017	13.0	51	Run 2
2018	13.0	61	Run 2
2022	13.6	39	Run 3
2023	13.6	32	Run 3

presence of neutrinos, which are not reconstructed in the final state, means that the m_H resolution, obtained through observables sensitive to the Higgs boson mass such as the transverse mass, is poor (approximately 20%). The $H \to b\bar{b}$ and the $H \to \tau^+\tau^-$ (with the tau subsequently decaying to electrons or muons and two neutrinos $\tau \to \ell\nu\bar{\nu}$ or to hadrons and one neutrino $\tau \to$ hadrons ν) channels suffer from large backgrounds and lead to an intermediate mass resolution of about 10% and 15% respectively.

With the increase in the size of datasets, measurements in the most sensitive channels are now carried out differentially or in exclusive modes depending on specific production characteristics. These measurements are discussed in Section 11.5.1.5.

The candidate events in each Higgs boson decay channel are split into several mutually exclusive categories (or event tags) based on the specific topological, kinematic or other features present in the event. The categorization of events increases the sensitivity of the overall analysis and allows a separation of different Higgs boson production processes. Most categories are dominated by signal from one Higgs boson decay mode but contain an admixture of various Higgs boson production processes. For example, a typical VBF selection requires Higgs boson candidates to be accompanied by two energetic jets (≥ 30 GeV) with a large dijet mass (≥ 400 GeV) and separated by a large pseudo-rapidity ($\Delta\eta_{jj} \geq 3.5$) [142]. While such a category is enriched in Higgs bosons produced via VBF, the contamination from the ggF or VH production mechanisms can be significant. Hence, a measurement of the signal rate in the VBF category is not equivalent to a measurement of VBF production cross section since one cannot resolve the contamination from ggF. Simulations are used to determine the relative contributions of the various Higgs boson production modes in each of the specific categories.

11.3.2 *The Higgs boson decay to vector bosons*

11.3.2.1 $H \to \gamma\gamma$

In the diphoton channel, the measurement of a narrow peak over a smoothly falling background in the invariant mass distribution of two high p_T photons is performed. The background in this channel is conspicuous and stems from prompt $\gamma\gamma$ processes for the irreducible backgrounds, and the γ+jet and dijet processes for the reducible backgrounds where one jet fragments typically into a leading π^0. In order to optimise search sensitivity and also to separate the various Higgs boson production modes, ATLAS and CMS split events into several mutually exclusive categories. Diphoton events containing high p_T muons or electrons, or missing energy (E_T^{miss}) consistent with the decay of a W or Z boson, are tagged in the VH production category. Diphoton events containing energetic dijets with a large mass and pseudo-rapidity difference are assigned to the VBF production

category, and events with two jets compatible with the hadronic decay of a W or a Z are considered in the VH category. . While the leptonic VH category is relatively pure, the VBF category has significant contamination from the gluon fusion process. Finally more complex topologies aiming at selecting events from the $t\bar{t}H$ productiuon mode in the semi-leptonic and fully hadronic top decays are also considered and discussed in more detail in Section 11.3.5.1 Events are also further categorised according to their expected $m_{\gamma\gamma}$ resolution and signal-to-background ratio. Categories with good m_H resolution and larger signal-to-background ratio contribute most to the sensitivity of the search.

Both ATLAS and CMS have studied in detail the calibration of the energy response of photons, in particular using $Z \to e^+e^-$, $Z \to \mu^+\mu^-\gamma$ and the response of muons in the calorimeter (for ATLAS) from $Z \to \mu^+\mu^-$ events. This information is used to correct the simulated signal mass line-shapes. In each category, parametric signal models are adjusted to these line-shapes to provide a functional form for the signal. Simple functional forms of the backgrounds are determined by a fit to the $m_{\gamma\gamma}$ distribution in each category (typically exponential, Bernstein polynomials, Laurent series or power laws). All categories are fitted simultaneously to determine the signal yield at a given Higgs boson mass hypothesis.

The results are expressed in terms of signal strength, which can be defined as $\mu = (\sigma \cdot \mathrm{BR})_{\mathrm{obs}}/(\sigma \cdot \mathrm{BR})_{\mathrm{SM}}$, the observed product of the Higgs boson production cross section (σ) and its branching ratio (BR) normalised to the corresponding SM values. A more detailed definition is given in Section 11.3.6 and Eq. 11.14. The signal strength overall for this channel and for specific production processes are summarised in Fig. 11.3. All results are in agreement with the SM expectation within the overall measurement precisions of approximately 9% for both experiments.

11.3.2.2 $H \to ZZ^* \to \ell^+\ell^-\ell'^+\ell'^-$

In the $H \to ZZ^* \to \ell^+\ell^-\ell'^+\ell'^-$ channel, a search is performed for a narrow mass peak over a small continuous background dominated by non-resonant ZZ^* production from $q\bar{q}$ annihilation and gg fusion processes. The contribution and the shape of this irreducible background is taken from simulation. The subdominant and reducible backgrounds stem from $Z + b\bar{b}$, $t\bar{t}$ and $Z +$ jets events. Their contribution is suppressed by requirements on lepton isolation and lepton impact parameter and their yield is estimated from control samples in data.

To distinguish the Higgs boson signal from the dominant non-resonant ZZ^* background, both ATLAS and CMS use multivariate techniques as well as a matrix element likelihood approach to construct a kinematic discriminant built for each 4ℓ event based on the ratio of complete leading-order matrix elements $|\mathcal{M}_{\mathrm{sig}}{}^2/\mathcal{M}_{\mathrm{bkg}}{}^2|$ for the signal ($gg \to H \to 4\ell$,$qq \to VH(\to 4\ell)$ and $qq \to qqH(\to 4\ell)$) and background ($q\bar{q} \to ZZ \to 4\ell$) hypotheses.

To improve the sensitivity to more exclusive production processes such as VBF, VH, and $t\bar{t}H$, the experiments divide 4ℓ events into mutually exclusive categories. Events are categorised in terms of the number of reconstructed jets, the number of additional leptons (from the decay of a vector boson in the associated production mode), number of jet tagged as containing a b-hadron, the transverse momentum of the Higgs boson (or e.g. its associated vector boson) and missing transverse momentum. Dijets with a large mass and pseudo-rapidity difference populate the VBF category. ATLAS requires the presence of an additional lepton in the VH category. In events with less than two jets, CMS uses the $p_T^{4\ell}$ to distinguish between production via the gluon fusion and the VH/VBF processes.

Since the $m_{4\ell}$ resolutions and the reducible background levels are different in the 4μ, $4e$ and $2e2\mu$ sub-channels, they are analysed separately and statistically combined to produce the final results.

The results for this channel, overall and in specific production processes are summarised in

Fig. 11.3. All results are in agreement with the SM expectation within the overall measurement precisions of approximately 9% and 12% for the ATLAS and CMS experiments respectively.

11.3.2.3 $H \to W^+W^- \to \ell^+\nu\ell^-\overline{\nu}$

In this challenging channel, experiments search for an excess of events with two leptons (electrons or muons) of opposite charge accompanied by missing energy and/or jets. A typical event selection is described below in order to give an idea of the main intricacies. Specific selections vary between experiments and between Run-1 and Run-2 analyses. Events are divided into several categories depending on the lepton flavour combination (e^+e^-, $\mu^+\mu^-$and $e^\pm\mu^\mp$) and the number of accompanying jets ($N_{\text{jet}} = 0, 1, \geq 2$). The $N_{\text{jet}} \geq 2$ category is optimised for the VBF production process by selecting two leading jets with a large pseudo-rapidity difference and with a large mass (typically $m_{jj} > 500\,\text{GeV}$).

Backgrounds contributing to this channel are numerous and depend on the category of selected events. Reducing them and accurately estimating the remainder is a major challenge in this analysis. For events with opposite-flavour leptons and no accompanying high p_T jets, the dominant background stems from non-resonant WW production. Events with same-flavour leptons suffer from large Drell–Yan contamination (note that also the opposite-flavour leptons analysis has Drell–Yan $\tau\bar{\tau}$ background in 0-jet category). The $t\bar{t}$, tW and W + jets (with the jet misidentified as a lepton) events contaminate all categories. Non-resonant WZ, ZZ and $W\gamma$ processes also contribute to the background at a sub-leading level.

A requirement of large missing transverse energy (E_T^{miss}) is used to reduce the Drell–Yan and multi-jet backgrounds. In the e^+e^- and $\mu^+\mu^-$ categories, events with $m_{\ell\ell}$ consistent with the Z mass are vetoed. The $t\bar{t}$ background is suppressed by a veto against identified b-jets and tight isolation requirements diminish the W+jets background. The scalar nature of the Higgs boson and the $V-A$ nature of the W boson decay implies that the two charged leptons in the final state are preferentially emitted at small angles with respect to each other. Therefore the dilepton invariant mass ($m_{\ell\ell}$) and the azimuthal angle difference between the leptons ($\Delta\phi_{\ell\ell}$) are used to discriminate between the signal and non-resonant WW events [143]. The transverse mass, constructed from the dilepton p_T ($p_T^{\ell\ell}$), E_T^{miss} and the azimuthal angle between E_T^{miss} and $p_T^{\ell\ell}$, is defined as $m_T = \sqrt{2p_T^{\ell\ell}E_T^{\text{miss}}(1-\cos\Delta\phi_{E_T^{\text{miss}}\ell\ell})}$ and serves as an effective discriminant against backgrounds. The transverse mass variable also tracks the Higgs boson mass but with a poor mass resolution. Background rates except for the small contributions typically from non-resonant WZ, ZZ and $W\gamma$ are evaluated from data control samples with floating normalization.

ATLAS and CMS have also searched for the associated Higgs boson production in this channel. The signal consists of up to three (WH) or four (ZH) high p_T isolated leptons with missing transverse energy and low hadronic activity. The major backgrounds stem from triboson and diboson production where each boson decays leptonically.

Measurements by ATLAS and CMS, in terms of signal strengths, for the five largest Higgs boson production modes are displayed in Fig. 11.3. All measurements are in agreement with the SM expectation within the overall measurement precisions of approximately 12% and 9% for ATLAS and CMS respectively.

11.3.3 *Measurement of the Higgs boson mass*

To measure the mass of the Higgs boson, ATLAS and CMS collaborations rely on the two high mass-resolution channels, $\gamma\gamma$ and $ZZ^*/4\ell$. The ATLAS and CMS approaches are very similar in these two analyses with small differences on the usage of categories, additional discriminating variables and per-event errors. In these two channels, the mass resolutions range from 1.4 GeV to 2 GeV for ATLAS and from 1.0 GeV to 2.8 GeV for CMS (see Ref. [144] and the reconstruction-

performance references therein). An excellent mass resolution is obtained for both experiments in the diphoton channel for central diphoton pairs (typically for events where both photons are not converted). However, the best precision in this measurement at Run 2 is obtained using the four lepton channel and in particular in the sub-channel of four muons (followed, in precision, by the two-electrons and two muons channel where the mass resolution is driven by the reconstruction of the lower mass di-lepton pair with typically lower transverse momentum leptons).

Both ATLAS and CMS have produced several Higgs boson mass measurements, including the individual and combined Run-1 measurements [144] and several Run-2 measurements by ATLAS [145, 146] and CMS [147, 148] for both the 4ℓ and the diphoton channels. The measurements performed by ATLAS include the full Run-2 dataset whereas in the case of CMS, the mass measurements were done with a fraction of the Run-2 data corresponding to the data collected in 2016. An overall combination of all available measurements has not yet been performed. The Run-1 combination including both ATLAS and CMS measurements yielded [144]:

$$m_H = 125.09 \pm 0.21\,(\text{stat.}) \pm 0.11(\text{syst.})\ \text{GeV}.$$

The current most precise di-photon channel result is obtained by ATLAS using the full Run-2 dataset and a combination with the Run-1 measurements in the $H \to \gamma\gamma$ yielding a measurement of [149]:

$$m_H = 125.22 \pm 0.11\,(\text{stat.}) \pm 0.09(\text{syst.})\ \text{GeV}.$$

The systematic uncertainty of 90 MeV is worth noting, as it results from a very challenging calibration and estimates of the amount of material upstream of the calorimeter to extrapolate the calorimeter energy response calibration from electrons in Z boson decays to photons. This result is promising for prospects in precision measurements in this channel. In Ref. [149], ATLAS has also estimated the expected effect of the interference between the signal and the gluon fusion continuum di-photon background to be of 24 MeV. This ATLAS measurement is significantly more precise than the full Run-2 measurement in the 4ℓ channel, however the latter is dominated by the statistical uncertainty of 170 MeV with a systematic uncertainty of 30 MeV [150]. The ATLAS diphoton channel measurement reached the same senstivity as the early Run-2 and Run-1 combined measurement of CMS, which uses both channels but with a much smaller amount of Run-2 data, corresponding only to the 2016 LHC run, which yielded [148]:

$$m_H = 125.38 \pm 0.11\,(\text{stat.}) \pm 0.08(\text{syst.})\ \text{GeV}.$$

ATLAS has also combined its results in the diphoton and the four-lepton channels yielding the current most precise measurement with a precision of 0.09% [151]:

$$m_H = 125.11 \pm 0.09\,(\text{stat.}) \pm 0.06(\text{syst.})\ \text{GeV}.$$

The most precise single channel result has very recently been obtained by CMS in the 4ℓ channel with the full Run 2 dataset [152]:

$$m_H = 125.08 \pm 0.12\,\text{GeV}.$$

The analysis of the entire Run-2 dataset and the LHC combination of the two experiments will be of great interest and important for the combination of all Higgs boson measurements across experiments.

11.3.4 *Higgs decays to third generation fermions ($b\bar{b}$ and $\tau^+\tau^-$)*

In the SM, fermions acquire a mass through gauge invariant interactions with the Higgs field which is also responsible for the electroweak symmetry breaking and thus for generating the masses of gauge bosons (see Section 11.2 for more details). While this minimal solution is very elegant, there is no fundamental reason for it to be the case, and probing the couplings of the Higgs boson to fermions is therefore of fundamental importance, in particular since BSM physics can largely change the SM predictions.

The discovery of the Higgs boson was made essentially through the bosonic final states. These decays probed mostly the couplings of the Higgs boson to vector bosons (the decay of the Higgs boson to photons occurring only through loops is also dominated in the SM by the coupling of the Higgs boson to W bosons). However, the predominant Higgs boson production mode is the gluon fusion, occurring only through loops dominated by the coupling of the Higgs boson to fermions. The observation of the Higgs boson in the two photons or two gluons decay modes is also an indirect evidence for the coupling of the Higgs boson to fermions (and in particular to the top quark). Nevertheless, the observation of either decays to fermions or production modes which unambiguously proceed through fermion couplings provide direct probes of the coupling of the Higgs boson to fermions and is thus of fundamental importance.

At hadron colliders, the most promising channel for probing the coupling of the Higgs field to the quarks and leptons are $H \to b\bar{b}$ and $H \to \tau^+\tau^-$, respectively. For a Higgs boson with $m_H \approx 125\,\text{GeV}$, the branching fraction to $b\bar{b}$ is about 58% and to $\tau^+\tau^-$ is about 6%. Nevertheless, the presence of very large backgrounds makes the measurement of a Higgs boson signal in these channels challenging.

One of the most prominent goals of the LHC Run-2 physics program was the direct observation of the Yukawa coupling of the Higgs boson to fermions of the third generation (bottom quarks, tau leptons and top quarks). This goal has been reached independently by both ATLAS and CMS and with only partial Run-2 datasets.

11.3.4.1 $H \to \tau^+\tau^-$

In the $H \to \tau^+\tau^-$ search, τ leptons decaying to electrons (τ_e), muons (τ_μ) and hadrons (τ_{had}) are considered. The $\tau^+\tau^-$ invariant mass ($m_{\tau\tau}$) is reconstructed from a kinematic fit of the visible products from the two τ leptons and the missing energy observed in the event. Due to the presence of missing neutrinos, the $m_{\tau\tau}$ resolution is poor ($\approx 10\% - 15\%$). As a result, a broad excess over the expected background in the $m_{\tau\tau}$ distribution is searched for. The major sources of background stem from Drell–Yan $Z \to \tau^+\tau^-$ and $Z \to e^+e^-$, W+jets, $t\bar{t}$ and multijet production. Events in all sub-channels are divided into categories based on the number and kinematic properties of additional energetic jets in the event and the transverse momentum of the reconstructed Higgs boson and the distance ΔR distance between the two τ's. The sensitivity of the search is generally higher for categories with one or more additional jets. The VBF category, consisting of a τ pair with two energetic jets separated by a large pseudo-rapidity, has the best signal-to-background ratio and search sensitivity, followed by the $\tau^+\tau^-$+1 jet category. The signal to background discrimination relies in part on the $m_{\tau\tau}$ resolution, which improves with the boost of the Higgs boson. The non-VBF categories are further subdivided according to the observed boost of the $\tau^+\tau^-$ system. ATLAS and CMS combine various kinematic properties of each event categories with multivariate techniques to build the final discriminant.

Searches for $H \to \tau^+\tau^-$ decays in the VH production mode are also performed in final states where the W or Z boson decays into leptons or jets. The irreducible background in this search arises from non-resonant WZ and ZZ diboson production. The reducible backgrounds originate from W, Z, and $t\bar{t}$ events that contain at least one fake lepton in the final state due to a misidentified jet.

The shape and yield of the major backgrounds in each category are estimated from control samples in data. Contributions from non-resonant WZ and ZZ diboson production are estimated from simulations but corrected for reconstruction efficiency using control samples formed from observed data.

The first clear evidence of direct decays of the higgs boson to taus was achieved by ATLAS and CMS in combination [153], with the observation of an excess with a significance of 5.5σ and the combined signal strength is $\mu = 1.11^{+0.24}_{-0.22}$, consistent with the SM expectation. The early Run-2 data fully corroborated these results to establish an unambiguous observation in each experiment independently. ATLAS [154] and CMS [155, 156] analysed an early Run-2 dataset to provide independent observations, with significances of 4.4σ and 4.9σ respectively.

Both ATLAS [157] and CMS [158, 159] have then completed the analyses of the full Run-2 dataset in various production channels. These results are summarised in Fig. 11.3. These results perform simultaneously measurements of the VBF production, the gluon fusion mode where the Higgs boson has a sizeable boost, and the associated production with a vector boson as well as the associated production with a pair of top quarks. It is interesting to note that the with the current measurements the gluon fusion channels have a sensitivity which is very close to the VBF production.

11.3.4.2 $H \to b\bar{b}$

To measure the decays of the Higgs boson to a pair of b-quarks, the most sensitive production modes are the associated WH and ZH processes allowing use of the leptonic W and Z decays which are helpful for triggering the events and to reject QCD backgrounds. The W bosons are reconstructed via their leptonic decay $W \to \ell\bar{\nu}_\ell$ where $\ell = e, \mu$ or τ. The Z bosons are reconstructed via their decay into $e^+e^-, \mu^+\mu^-$or $\nu\bar{\nu}$. The Higgs boson candidate mass is reconstructed from two b-tagged jets in the event. Backgrounds arise from production of W and Z bosons in association with gluon, light and heavy-flavoured jets (V+jets), $t\bar{t}$, diboson (ZZ and WZ with $Z \to b\bar{b}$) and QCD multi-jet processes. Due to the limited $m_{b\bar{b}}$ mass resolution, a SM Higgs boson signal is expected to appear as a relatively broad enhancement in the reconstructed dijet mass distribution. The crucial elements in this search are b-jet tagging with high efficiency and low fake rate, accurate estimate of b-jet momentum and estimate of backgrounds from various signal depleted control samples constructed from data.

At the Tevatron, the $H \to b\bar{b}$ channel contributed the majority of the Higgs boson search sensitivity below $m_H = 130\,\text{GeV}$. To separate signal from background, CDF and D0 used multivariate analysis (MVA) techniques that combined several discriminating variables into a single final discriminant. Each channel was divided into exclusive sub-channels according to various lepton, jet multiplicity, and b-tagging characteristics in order to group events with similar signal-to-background ratio and thus optimise the overall search sensitivity. The combined CDF and D0 data showed [44, 160] an excess of events with respect to the predicted background in the 115–140 GeV mass range in the most sensitive bins of the discriminant distributions suggesting the potential presence of a signal. At $m_H = 125\,\text{GeV}$, the observed signal strength was $\mu = 1.59^{+0.69}_{-0.72}$.

At the LHC, in order to reduce the dominant V+jets background, following Ref. [92], experiments select a region in the VH production phase space where the vector boson is significantly boosted and recoils from the $H \to b\bar{b}$ candidate with a large azimuthal angle $\Delta\phi_{VH}$. For each channel, events are categorised into different $p_T(V)$ regions with varying signal/background ratios. Events with higher $p_T(V)$ have smaller backgrounds and better $m_{b\bar{b}}$ resolution. Experiments use MVA classifiers based on kinematic, topological and quality of b-jet tagging and trained on different values of m_H to separate Higgs boson signal in each category from backgrounds. The main discriminating variables in this analysis are the transverse momentum of the vector boson and the

di-b-jet invariant mass.

The direct observation of the Higgs boson decaying to a pair of b-quarks, a major result of Run 2, was obtained by both ATLAS and CMS independently after the update of their search with similar analyses as those performed at Run 1 but with a larger dataset of approximately 80 fb^{-1} of data collected in 2015, 2016 and 2017. The increase in signal cross sections of nearly a factor of 3 at the centre-of-mass energy of 13 TeV with respect to 7 TeV, has also been instrumental in bringing the two experiments to the required sensitivity to claim an evidence for this decay mode in the VH production mode (in the high transverse momentum of the vector boson fiducial region of interest for this channel). The expected significance for a SM Higgs boson was 4.3σ for ATLAS [161] and 4.9σ for CMS [162]. Both ATLAS and CMS observed significant excesses corresponding to 4.9σ and 4.8σ respectively with Run-2 data only. When combined with results obtained in Run 1, the observed (expected) significance of the excesses were 5.4σ (5.5σ) and 5.6σ (5.5σ) respectively. These results provided direct and unambiguous observation for the $H \to b\bar{b}$ decay through the VH production mode.

Since these important observations, both experiments have completed the analysis of the full Run-2 dataset using two reconstruction techniques. The first is based on the reconstruction of the Higgs boson with two jets is referred to as *resolved*. The second is based on the reconstruction of the Higgs boson as a large radius jet and is referred to as *boosted*. These measurements expand the range of measurements of the Higgs boson decays to b-quarks in association with a vector boson at higher transverse momentum, above 400 GeV. These results are summarised in Fig. 11.3. It should be noted that the sensitivity of these analyses are already limited by systematic uncertainties.

Also, the LHCb collaboration has performed a search for the VH production with subsequent decay of the Higgs boson to a pair of b-quarks [163] with 1.98 fb^{-1} of data taken at a centre-of-mass energy of 8 TeV. The final state is required to have two reconstructed b quarks and one lepton in the LHCb acceptance of $2 < \eta < 5$. The sensitivity of this search is an expected 95% CL exclusion of 84 times the SM production rate. This analysis is also used to set a limit on the VH production with the subsequent decay of the Higgs boson in a pair of c quarks with a 95% CL limit at 6.4×10^3 times the SM production rate, while the expected sensitivity corresponds to an exclusion of 7.9×10^3 times the SM production rate.

ATLAS and CMS have also searched for $H \to b\bar{b}$ in the VBF production mode. The event topology consists of two VBF-tagging energetic light-quark jets in the forward and backward direction relative to the beam direction and two b-tagged jets in the central region of the detector. Due to the electroweak nature of the process, for the signal events, no additional energetic jet activity (excluding that from the Higgs boson) is expected in the rapidity gap between the two VBF-tagging jets. The dominant background in this search stems from QCD production of multi-jet events and the hadronic decays of vector bosons accompanied by additional jets. A contribution of Higgs boson events produced in the ggF process but with two or more associated jets is expected in the signal sample. The signal is expected as a relatively broad enhancement in the $m_{b\bar{b}}$ distribution over the smoothly falling contribution from the SM background processes. Both ATLAS [164] and CMS [165] have produced results in this channel with Run-1 data, but with limited sensitivity. Both experiments performed a similar analysis with Run-2 data [166, 167].

Two of the main difficulties for the VBF production mode are the large QCD background and the difficulty in triggering fully hadronic events. Both difficulties are addressed, by the proposal made in Ref. [168], where the requirement of an additional photon in the final state reduces the background through an interference effect and enhances the possibilities for triggering. This analysis has been carried out by ATLAS at Run 2 [169] and its result combined with the standard VBF channel. The sensitivity in this channel is smaller than in the fully hadronic mode. Through the combination of these channels ATLAS has reached a first evidence at 3 standard deviations of the

Higgs boson decaying to a pair of b quarks in the VBF production mode. The results are reported below

$$\begin{aligned} \text{ATLAS}\ \ \mu^{b\bar{b}}_{VBF(\gamma)} &= 0.99\,^{+0.30}_{-0.30}\ (\text{stat})\ ^{+0.18}_{-0.16}\ (\text{syst}), \\ \text{CMS}\ \ \mu^{b\bar{b}}_{VBF} &= 1.01 \pm 0.36\ (\text{stat})\ ^{+0.40}_{-0.27}\ (\text{syst}). \end{aligned} \tag{11.12}$$

The sensitivity in the inclusive search for the Higgs boson in the ggF production mode with $H \to b\bar{b}$ is limited by the overwhelming background from the inclusive production of $pp \to b\bar{b} + X$ via the strong interaction. With the increase in centre-of-mass energy to 13 TeV, and taking advantage of the harder transverse momentum spectrum of the $gg \to H$ production mode with respect to the QCD background, a search for high p_T Higgs boson decaying to a pair of b quarks in association with an energetic Initial State Radiation (ISR) jet. Considerable efforts have been made using state-of-the-art deep learning techniques to improve the performance of the identification of a Higgs boson decaying to b quarks and reconstructed as a large radius jet at high transverse momentum. In order to gain sensitivity in this channel and reconstruct the Higgs boson within one jet of radius 0.8 or 1.0 a lower cut at 450 GeV of transverse momentum is required. This analysis was performed by both ATLAS [170] and CMS [171] with the entire Run-2 data dataset. As in the case of VH production mode, this analysis is sensitive also to the inclusive $Z \to b\bar{b}$ production, which is an important step in the validation of the analysis chain. The $Z \to b\bar{b}$ decay is observed with a significance in excess of five standard deviations, in agreement with the expected rate from the Standard Model. . This estimate has a non negligible uncertainty from the precise estimate of the fiducial signal cross section in the specific acceptance of this analysis. CMS observes an excesses at $m_H = 125$ GeV of 1.2σ [171] with a sensitivity of 0.9σ. It should be noted that the estimates of the signal expectation in this remote region of phase space at high transverse momentum for the production are highly non-trivial and subject to fairly large theoretical and statistical uncertainties:

$$\text{ATLAS}\ \ \mu^{b\bar{b}}_{\text{inclusive}} = -0.1 \pm 3.5\ (1.0 \pm 3.4\,\text{expected}), \quad \text{CMS}\ \ \mu^{b\bar{b}}_{\text{inclusive}} = 2.1\,^{+1.9}_{-1.7}. \tag{11.13}$$

In addition to the inclusive production, in [171] CMS has also performed a search sensitive to the VBF production in the boosted Higgs regime, yielding a sensitivity of 0.9σ. In this channel a broad excess has been observed which results in an observed excess with a significance of 3.0σ. These results are particularly interesting as these measurements will bring a strong complement to the main channels in the high transverse momentum regime.

Another important production mode sensitive to the decay of the Higgs boson to bottom quarks, is the associated production with a pair of top quarks. The results of the searches for this process have been combined with the channels described above, to provide an additional constraint on the Yukawa coupling of the Higgs boson to bottom quarks. The channels corresponding to this production mode are described in Section 11.3.5.

11.3.5 *Higgs boson production in association with top quarks*

11.3.5.1 *The associated production with top quark pairs*

As discussed in Section 11.2, the coupling of the Higgs boson to top quarks plays a special role in the electroweak symmetry breaking mechanism in the SM, as well as in its possible extensions. Substantial indirect evidence of this coupling is provided by the compatibility of observed rates of the Higgs boson in the principal discovery channels, given that the main production process – gluon fusion – is dominated by a top quark loop. Direct evidence of this coupling at the LHC and the future e^+e^- colliders will be mainly available through the $t\bar{t}H$ final state and will permit a clean measurement of the top quark-Higgs boson Yukawa coupling. The $t\bar{t}H$ production cross section at the LHC is small in comparison with the ggF or even VH production modes. The production cross

section for a 125 GeV Higgs boson in pp collisions at $\sqrt{s} = 8$ TeV of about 130 fb made it challenging to measure the $t\bar{t}H$ process with the LHC Run-1 dataset. However, at Run 2, the increase in cross section at $\sqrt{s} = 13$ TeV is substantial, reaching approximately 500 fb.

The analysis channels for such complex final states can be separated in four classes according to the decays of the Higgs boson. In each of these classes, most of the decay final states of the top quarks are considered (fully hadronic, semi-leptonic and dilepton decay final states).

The first analysis is the search for $t\bar{t}H$ production in the $H \to \gamma\gamma$ channel. This analysis relies on the search for a narrow mass peak in the $m_{\gamma\gamma}$ distribution. The background is estimated from the $m_{\gamma\gamma}$ sidebands. The sensitivity in this channel is mostly limited by the available statistics.

The second analysis is the search for the Higgs boson decaying to ZZ^* and subsequently to four leptons (electrons and/or muons). This channel is currently limited by the low statistics due to the small branching fraction of the Z decays to leptons.

In the third analysis the W^+W^- , $\tau^+\tau^-$ and ZZ^* final states are searched for inclusively in multilepton event topologies (but not including the resonant $H \to 4\ell$ channel that is covered in the specific analysis described in Section 11.3.2). The corresponding $t\bar{t}H$ modes can be decomposed in terms of the decays of the Higgs boson and those of the top quarks as having two b-quarks and four W bosons (or two W and two taus, or two W and two Z) in the final state.

The fourth channel is the search in the $H \to b\bar{b}$ channel. This search is intricate due to the large backgrounds, both physical and combinatorial in resolving the $b\bar{b}$ system from the Higgs boson decay, in events with six jets and four b-tagged jets. Already with the Run-1 dataset, the sensitivity of this analysis was strongly impacted by the systematic uncertainties on the background predictions.

Prior to its start, it was unclear if this process would at all be observable at the LHC. A first milestone was reached with the completion of the Run-1 analyses by ATLAS and CMS with a complete set of results in these channels and their combination [172, 173]. These results are reported in Table 11.5. However the sensitivity remained very limited. The breakthrough in the search for this process of fundamental importance came with the Run-2 data at a higher centre-of-mass energy of 13 TeV and the increase of a factor of nearly four of the production cross section of the $t\bar{t}H$ associated production process.

Using only a partial Run-2 dataset, ATLAS and CMS were able to independently make an unambiguous observation of this process. For these results ATLAS and CMS had different strategies. ATLAS relied mostly in the $t\bar{t}(H \to \gamma\gamma)$ channel where a narrow peak over a continuous background is searched for. It is interesting to note that the rapid evolution of the sensitivity in the diphoton channel owes not only to the large increase in cross section, but also to the fact that high mass diphoton events in an environment with additonal leptons, jets and b-tagged jets the search for a pair of photon at high mass has a low background. In contrast with the inclusive search for $H \to \gamma\gamma$, the analyses in this channel reached a signal-to-background ratio in excess of unity. This channel, which is characterised by a narrow peak over a continuous background, also has the advantage of being less prone to systematic uncertainties than channels where the assessment of backgrounds cannot be made through the use of sidebands. ATLAS used up to 79.8 fb^{-1} of Run-2 data to reach an expected sensitivity of 4.9σ and an observed significance of 5.8σ with the Run-2 partial dataset alone, and 6.3σ (with 5.1σ expected) in combination with the Run-1 results [174]. CMS instead relied on a smaller dataset of 35.9 fb^{-1} and relied on all channels. The most sensitive in this case was the $ttH(bb)$ whose sensitivity was limited by systematic uncertainties. CMS reached a sensitivity of 4.2σ and observed an excess with respect to the background-only hypothesis of 5.2σ, combining the Run-1 and Run-2 results [175].

This direct observation of the Yukawa coupling of the Higgs boson to top quarks was particularly important in comparison to the indirect evidence through the gluon fusion production process

dominated by the top quark loop

Since the observation of this important process, with few exceptions, all channels have been updated with the full Run-2 dataset, by both experiments.

For the principal decays of the Higgs boson in the diphoton and four lepton channels, the measurements are done in the framework of 'Simplified Template Cross Section' discussed in Section 11.5.1.5). The diphoton channels were updated by both the ATLAS and CMS experiments in Refs. [176, 177]. The four lepton decays of the Higgs boson in the associated production with a pair of top quarks is a search for a narrow peak in the busy $t\bar{t}H$ environment. It was also performed by ATLAS [176] and CMS [177] with the full Run-2 datasets. These results are reported in Table 11.5. This channel has currently very low statistic but also very high purity, reaching signal-to-background ratios in excess of 10.

To address the WW, ZZ and $\tau\tau$ decay modes, an approach based on multiple channels with electrons, muons and taus decaying hadronically, the so-called "multi-lepton", is adopted by both experiments. This analysis excludes the $H \to 4\ell$ channel. CMS has analysed the Full Run-2 dataset [178] and ATLAS only part of it [179]. In a preliminary release of this analysis using a larger, but not full Run-2 dataset corresponding to an integrated luminosity of approximately $80\,\text{fb}^{-1}$, the ATLAS experiment found that the normalisation of the $t\bar{t}W$ background was larger than expected from SM calculations by factors ranging from 1.3 to 1.7 and modelling issues were observed in analysis regions where the $t\bar{t}W$ process is dominant [179]. The search for Higgs boson decays to tau leptons in association with a pair of top quarks was carried out by ATLAS with the full Run-2 dataset and discussed in 11.3.4.1 [180]. Using the full dataset in this channel CMS obtained an observation of the Higgs boson production in association with top quarks with an observed significance of 4.7 standard deviations (5.2σ expected). The results are reported in Table 11.5. The rate of the $t\bar{t}W$ background in this analysis is also high by a factor of approximately 1.4.

Both ATLAS and CMS have performed the analysis of Higgs bosons decaying to b-quarks in the $t\bar{t}H$ production mode with the full Run-2 dataset. In ATLAS, this analysis was performed in the semi-leptonic and di-leptonic channels [181], including a resolved mode where the Higgs boson is reconstructed as two standard jets and a boosted mode where the Higgs boson is reconstructed as a single large radius jet. CMS also performed this analysis with the full Run-2 dataset, including in addition the fully hadronic mode where both W bosons from top decays subsequently decay hadronically [182]. The results reported in Table 11.5. It should be noted that in this channel a deficit in observed Higgs boson decays is observed. This deficit is rather significant and in tension with the observation of the other $t\bar{t}H$ modes as well as the observation of the Higgs boson in the $b\bar{b}$ channels.

The discrepancies observed in both the multilepton and the $H \to b\bar{b}$ channels will require further studies.

A combination of all available channels has been performed by ATLAS [183] and CMS [184] and is reported in Fig. 11.3. It should be noted that the latest $t\bar{t}H(\to b\bar{b})$ channel from CMS with the full Run 2 data has not yet been included in the combination. A fit of individual decay modes in the ttH production is also given therein.

11.3.5.2 *The associated production with a single top quark*

An additional production mode of the Higgs boson in association with a top quark is the single top associated production mode. There is an interesting similarity between this production mode and the $H \to \gamma\gamma$ decay mode. Both processes proceed through either the top Yukawa coupling or the interaction of the Higgs boson with the W boson, with a negative interference between the two. Representative Feynman diagrams for this production process are shown in Fig. 11.1. Contrary to the diphoton decay channel, in this production mode the interference occurs at the tree level and

Table 11.5: Summary of the results of searches for a Higgs boson in association with a top quark pair by ATLAS and CMS. The results are given in terms of a measured signal strength.

$t\bar{t}H$	ATLAS Run 1	CMS Run 1	ATLAS Run 2	CMS Run 2
$H \to \gamma\gamma$	$1.3\ ^{+2.6}_{-1.7}\ ^{+2.5}_{-1.7}$	$1.2\ ^{+2.5}_{-1.7}\ ^{+2.6}_{-1.8}$	$1.38\ ^{+0.33}_{-0.31}\ ^{+0.26}_{-0.18}$	$2.27^{+0.86}_{-0.74}$
$H \to 4\ell$	—	—	$1.2\ ^{+1.4}_{-0.8}$	$0.00\ ^{+0.91}_{-0.00}$
$H \to WW/\tau\tau/ZZ$	$1.4\ \pm 0.6\ \pm 1.0$	3.3 ± 1.4	$1.56\ ^{+0.30}_{-0.29}\ ^{+0.30}_{-0.27}$	$0.92\ ^{+0.26}_{-0.23}$
$H \to b\bar{b}$	$1.4\ \pm 1.0\ \pm 0.6$	$1.6\ ^{+1.6}_{-1.5}$	$0.35\ \pm 0.20\ \pm 0.30$	$0.33 \pm 0.16 \pm 0.21$
Combination	$1.7\ \pm 0.5\ \pm 0.8$	$2.6\ ^{+1.0}_{-0.9}$	$0.97\ \pm 0.14\ ^{+0.14}_{-0.13}$	$0.94\ \pm 0.20\ ^{+0.09}_{-0.14}$

is dominant. This process can therefore be used to further discriminate a negative relative sign between the couplings of the Higgs boson to fermions and its couplings to gauge bosons [185].

ATLAS and CMS have produced specific searches for the tH production mode with the Run-1 and Run-2 data exploiting a variety of Higgs boson decay modes resulting in final states with photons, bottom quarks, and multiple charged leptons, including tau leptons. In particular, with the Run-2 data, CMS has searched for multi-leptonic decay signatures from the $H \to WW^*$, $H \to \tau^+\tau^-$ and $H \to ZZ^*$ modes [186]. This analysis restricts values of κ_t, the top-Higgs coupling normalised to its SM value, to $[-1.25, 1.60]$ at 95% CL. CMS has also performed an analysis of the 2015 dataset to search for the $H \to b\bar{b}$ mode [187], yielding much less stringent constraints.

The diphoton channel has also been used to search specifically for this production mode by ATLAS using Run-1 data, yielding the restricted range of allowed values of κ_t at the 95% CL to $[-1.3, 8]$.

The strongest constraint on the negative (relative) sign of κ_t was obtained by CMS using the recent analysis of the full dataset [178] in the multilepton ($H \to WW$, $H \to ZZ$, $H \to \tau\tau$) discussed in 11.3.5.1, negative values of κ_t are disfavoured and the only non excluded negative values of κ_t at 95% CL. range between -0.9 and -0.7.

11.3.6 *Combining the main channels*

The analysis strategy used by the LHC experiments to perform the searches for the Higgs boson has been based on the Higgs boson decay modes. It is a natural choice given that it focusses on the decay products of the object searched for. However, for each channel, exclusive sub-channels have been defined to target different production modes and kinematic regimes, and these sub-channels have been combined. The natural extension of this approach in order to probe further the production and decay modes of the Higgs boson is to combine the analysis channels together. Such a combination is also used in Section 11.5 to further measure the coupling properties of the Higgs boson.

At the LHC, the total cross section cannot be measured independently of the decay branching fractions. As a consequence, the total width of the Higgs boson cannot be directly measured. However, a combined measurement of the large number of categories described above with different sensitivities to various production and decay modes, permits a wide variety of measurements of the production, decay and coupling properties. These measurements, however, rely on assumptions.

Combining Higgs observation channels requires that measurements in all channels are done under the same Higgs boson mass hypothesis. This is always the case within experiments but is not necessarily the case across experiments. At Run 1, prior to combining the measurements of rates in ATLAS and CMS, a common and thus combined Higgs boson mass measurement was made. Only

thereafter were the ATLAS and CMS measurements combined [153]. The Run 1 full combination results were derived by the two collaborations, taking rigorously into account all correlations in the systematic uncertainties and in the large number of channels and their categories. For a review of the Run-1 combined results see former PDG reviews in [188] and references therein.

It is important to note that, between the Run-1 and the Run-2 results, the signal theoretical systematic uncertainties have improved significantly.

At Run 2, ATLAS [183] and CMS [184] have already produced combined measurements of the coupling properties and production cross section ratios of the Higgs boson.

In this section, only the results on the main Higgs boson production and decay modes will be discussed. Only a brief presentation of the combination framework is given here (a more detailed description is given in Ref. [189]). This framework will also be used in Section 11.5 to discuss the measurements of the coupling properties of the Higgs boson.

11.3.6.1 *Principles of the combination*

The combination of the Higgs boson analysis channels in each experiment and for the two experiments together was done using a fit of a signal and background model to the data. As described above, the data was made of a large number of categories, aiming at reconstructing exclusive production and decay modes. In the combination of ATLAS and CMS [153], there were approximately 600 categories. The combination was a simultaneous fit to the data across all these categories, using a reduced number of parameters of interest and the Higgs boson mass fixed to its measured value at Run 1 [144]. The much larger number of categories present in the ATLAS and CMS combination [153] is due to additional separation in terms of finer exclusive production regions, decay channels of the Z and the W bosons, and taus, control regions where little-to-no signal is present, and different center-of-mass energies.

In their Run-2 individual combinations, ATLAS and CMS have not considered the $Z\gamma$ channel. Both ATLAS and CMS experiment have included the $\mu\mu$ channel based on a partial Run-2 dataset corresponding to an integrated luminosity of $36\,\text{fb}^{-1}$ only.

The key to understanding how the combination of channels works relies on the combination master formula, which expresses for each category, indexed by c, of a given channel (typically a category covers mostly one decay mode, but possibly various production modes), the measured number of signal events n_s^c as a function of a limited number of parameters as follows:

$$n_s^c = \left(\sum_{i,f} \mu_i \, \sigma_i^{\text{SM}} \times A_{if}^c \times \varepsilon_{if}^c \times \mu_f \, \text{BR}_f^{\text{SM}} \right) \times \mathcal{L}^c. \tag{11.14}$$

The production index is defined as $i \in \{\text{ggF}, \text{VBF}, ZH, WH, t\bar{t}H, tH, \ldots\}$ (including specific modes and regions of phase space) and the decay index is defined as $f \in \{\gamma\gamma, WW, ZZ, bb, \tau\tau, \mu\mu, Z\gamma\}$, while σ_i^{SM} and BR_f^{SM} are the corresponding production cross sections and decay branching fractions, estimated as described in Section 11.2, assuming that the Higgs boson is that of the SM. A_{if}^c and ε_{if}^c are the signal acceptance and the reconstruction efficiency for the given production and decay modes in the category c. $\mathcal{L}^c$ is the integrated luminosity used for that specific category. For the purpose of this review, these parameters can be considered as fixed[2].

The parameters of interest in the master formula are the signal strength parameters μ_i and μ_f. It is important to note that the formula relies on the factorisation of the production cross section and decay branching fraction, which assumes the narrow width approximation. The width of the Higgs boson will be discussed in Section 11.4, however, for the precision needed here, the fact that the Higgs boson has been observed in decay channels with high mass resolution as a

[2] In the combination performed by ATLAS and CMS, the systematic uncertainties on these parameters are taken into account by allowing these parameters to vary within their constraints in the fit.

resonance is sufficient to validate this hypothesis. It is also manifest in the above equation that the ten parameters for the production modes (μ_i) and decay modes (μ_f) cannot be determined simultaneously. This illustrates that total cross sections or branching fractions cannot be measured without further assumptions in this fit.

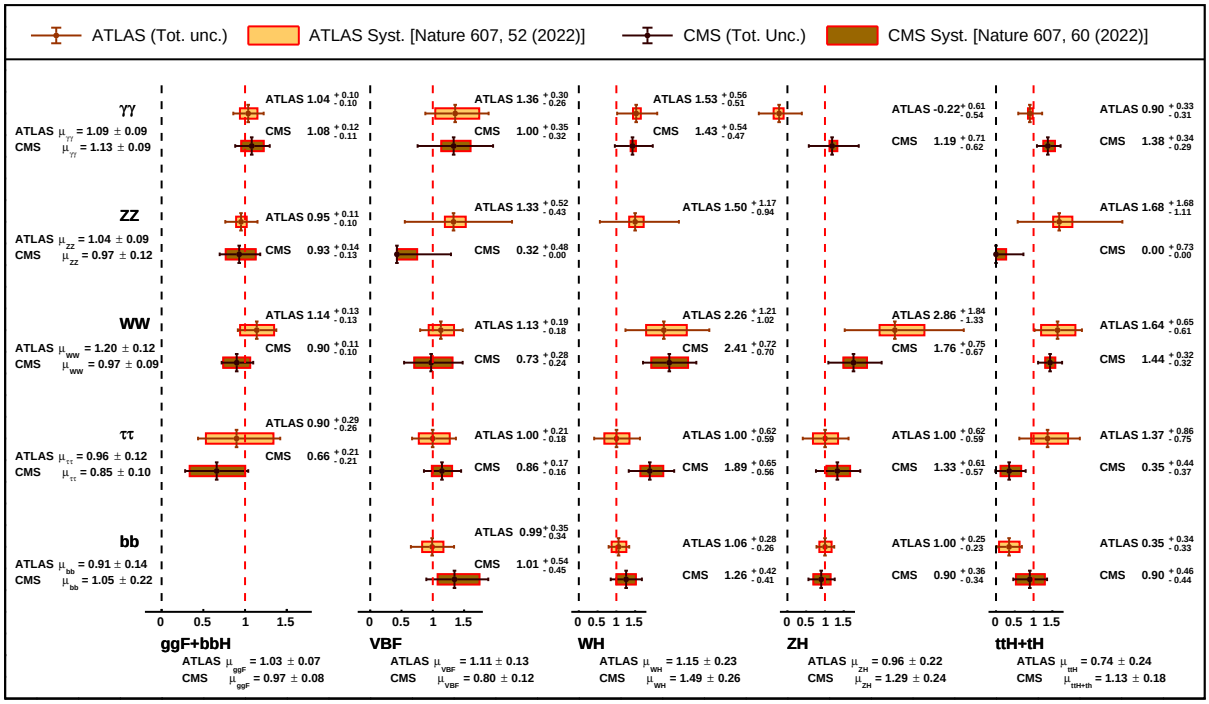

Figure 11.3: Combined measurements by ATLAS [183] and CMS [184] of the products $\sigma \cdot \mathrm{BR}$, normalised to the SM predictions, for the five main production and five main decay modes.

The master formula also illustrates an important caveat to the measurement of signal strength parameters. In case these are interpreted as scale factors of the production cross sections or branching fractions, then all the other quantities such as the acceptances and efficiencies, A_{if}^c and ε_{if}^c, need to be assumed as independent and fixed to their estimated values for the SM Higgs boson. An additional important caveat to note concerning these combined results is that only the normalisation is varied, while the discriminating variables for the signal are not modified and are still used in the fit. These caveats are of particular importance in the use of the combination to measure the coupling properties of the Higgs boson, as discussed in Section 11.5. For relatively small perturbations of the couplings of the Higgs boson from the SM values, this hypothesis is valid.

However, the products $\mu_i \times \mu_f$ can be considered as free parameters and in principle measurable (if there is sufficient sensitivity from specific categories). Measuring the products of signal strengths can be viewed as measuring the cross sections times the branching fraction, $\sigma \cdot \mathrm{BR}$. Measurements by ATLAS and CMS of $\sigma \cdot \mathrm{BR}$, normalised to the SM predictions, for the five largest Higgs boson production modes and five major Higgs decay modes are displayed in Fig. 11.3.

Other fits involving ratios of cross sections, which are less sensitive to theory uncertainties, are performed and reported in Ref. [189].

The most constrained fit in the combination allows for only one single parameter to vary, i.e., $\forall(i,f), \mu_i = \mu_f = \mu$. This global-signal-strength model provides the simplest probe of the compatibility of the signal with the SM Higgs boson. Indeed, it is sensitive to any deviation from the SM Higgs boson couplings provided that these deviations do not cancel overall. The full Run-1

combination determines the global signal strength to be

$$\mu = 1.09 \pm 0.11 = 1.09 \pm 0.07\ (\text{stat.})\ \pm 0.04\ (\text{expt.})\ \pm 0.03\ (\text{th. bkg.})\ \pm 0.07\ (\text{th. sig.}), \quad (11.15)$$

where the statistical, experimental uncertainties as well as the theoretical uncertainties on the background and on the signal are reported separately. The ATLAS Run-2 combination of the global signal strength yields [183]:

$$\mu = 1.05 \pm 0.06 = 1.05\ \pm 0.03\ (\text{stat.}) \pm 0.03\ (\text{exp.})\ \pm 0.02\ (\text{th. bkg.})\ \pm 0.04\ (\text{th. sig.}), \quad (11.16)$$

while the CMS Run-2 combination yields [184] $\mu = 1.002\ \pm 0.057$.

These overall signal strengths are fully compatible with the SM expectation, $\mu = 1$, with a precision of 6%. It is interesting to note that the main uncertainty in these measurements arises from the limited precision in the theoretical predictions for the signal production processes. The precision reached with the individual experiments combinations using partial Run-2 data sets have already exceeded the full Run-1 ATLAS and CMS combination precision.

11.3.6.2 *Main decay modes*

Despite the large number of decay channels, since the cross sections cannot be independently measured, from the measurements described in this section it is impossible to measure the decay branching fractions without a loss of generality. The simplest assumption that can be made is that the production cross sections are those of the SM, which is equivalent to assume that, for all i indices, $\mu_i = 1$. All branching fractions μ_f can then be measured in a simple 7 parameter fit. Results of these measurements are reported in Fig. 11.3.

11.3.6.3 *Main production modes*

Most analysis channels are divided into exclusive categories allowing for an increased overall sensitivity and permitting to access the various Higgs boson production modes. The cross sections of the main production modes can be measured assuming that the branching fractions are those of the SM, i.e., for all f indices $\mu_f = 1$. These assumptions lead to a 6 parameter combination.

The gluon fusion production process is the dominant production mode. Although no numerical estimate of combined significance of observation for this process has been given by the experiments, it is considered as established due to the overwhelming evidence from the three main discovery channels. At the LHC, all production modes have been unambiguously observed. The intricate VH production mode has been unambiguously observed by ATLAS and CMS independently (as discussed in Section 11.3.4) through the $V(H \to b\bar{b})$ channel. The results of these measurements are reported in Fig. 11.3.

With the Run-2 data, all the main production processes have been established, and in particular the $pp \to t\bar{t}H$ process, which provides direct evidence of the coupling of the Higgs boson to top quarks. This is another milestone in the LHC physics program.

11.3.7 *Probing the Higgs boson coupling to the second generation*

11.3.7.1 *First evidence for $H \to \mu^+\mu^-$*

The branching fraction in the $H \to \mu^+\mu^-$ channel for a 125 GeV SM Higgs boson is 2.2×10^{-4}, about ten times smaller than that for $H \to \gamma\gamma$. The major challenge in this channel is the extremely small, permil level, signal-to-background ratio. The dominant and irreducible background arises from the $Z/\gamma^* \to \mu^+\mu^-$ process which has a rate several orders of magnitude larger than that from the SM Higgs boson signal. Due to the precise muon momentum measurement achieved by ATLAS and CMS, the $m_{\mu^+\mu^-}$ mass resolution is very good ($\approx$ 2–4% for ATLAS and $\approx$ 1–3% for CMS depending on the selected categories; a better resolution is expected for CMS due its higher

magnetic field strength in the inner detector). A search is performed for a narrow peak over a large but smoothly falling background. For optimal search sensitivity, events are divided into several categories. Either taking advantage of the superior muon momentum measurement in the central region, events can be subdivided by the pseudo-rapidity of the muons, or designing selections aiming at specific production processes such in particular as the vector boson fusion.

ATLAS and CMS analyses target the main production modes such as gluon fusion, associated production with a vector boson (including in the vector boson leptonic decay modes), vector boson fusion and associated production with a top-quark pair. The analyses use multivariate and deep machine learning methods to discriminate signal from background in these Higgs production categories. The signal in both experiments is extracted from a fit to the di-muon invariant mass spectrum and the background is modeled using a suite of analytical functions, except in the case of the most sensitive channel (VBF) in the CMS analysis where the distribution of a discriminant Deep Neural Network output is used.

With the Run-2 dataset, ATLAS measured [190] a signal strengths of $\mu = 1.2 \pm 0.6$ with an observed (expected) significance of $2.0(1.7)\sigma$. The 95% CL limit on $pp \to H \to \mu^+\mu^-$ was set at 2.2 times the SM prediction while the expected limit on a $H \to \mu^+\mu^-$ signal assuming the absence (presence) of a SM signal was 1.1 (2.0). CMS reported [191] the first evidence for $H \to \mu^+\mu^-$ at 3σ level with a signal strength of $\mu = 1.19 \pm 0.40\,(\text{stat.}) \pm 0.15\,(\text{syst.})$ and an expected analysis sensitivity of 2.5σ. These measurements provide the first direct evidence for the decay $H \to \mu^+\mu^-$ and thus of the Yukawa coupling of the Higgs boson to second generation fermions.

11.3.7.2 *Constraints on Higgs boson coupling to charm quarks*

The possibility of probing the Yukawa coupling to the charm has been discussed early in Ref. [192] where indirect bounds are estimated from a combined fit to the Higgs data and the importance of using charm tagging is emphasised. A SM decay rate in standard production was long thought to be out of reach at the LHC. However recent results, in particular from CMS have shown that a different perspective might be emerging [193].

The channels which are currently foreseen to be most sensitive are similar to those aiming at the b-quark Yukawa coupling, and pertain to the VH production mode. As was discussed in [188], the typical sensitivity of these analysis using the LHC Run-2 data on the production times branching fraction was approximately a factor of 30 times the expected rate in the Standard Model.

The key aspect to bring sensitivity to the charm coupling is the ability of flavour tagging algorithms to discriminate charm quark initiated jets from both b quark and light quark jets. Significant progress was recently made in development of parton flavour taggers using state-of-the-art machine learning techniques [194] and additional information to these algorithms. Novel algorithms have also been used to identify pairs of charm quarks resulting from the decay of a Higgs boson, in particular in a regime where the Higgs boson is reconstructed as a large radius jets with a distinctive substructure. These new techniques have resulted in impressive improvements which have led to the first observation of Z boson decays to charm quarks at a hadron collider with a significance of 5.7 standard deviations [193] and an expected sensitivity to the exclusion of a Higgs boson signal decaying to a pair of charm quarks of 7.6 times the Standard Model rate. The observed limit for CMS is at 14 times the SM rate. This led CMS to set limits on the absolute value of κ_c, the Yukawa coupling of the Higgs boson to charm quarks with respect to its value in the Standard Model. The expected 95% CL interval is $|\kappa_c| < 3.4$. The observed 95% CL interval is the following:

$$1.1 < |\kappa_c| < 5.5 \tag{11.17}$$

This is the most stringent constraint today. The ATLAS analysis [195], in contrast, is still relying on traditional techniques and sets an observed (expected) limit at 26 (31) times the SM rate, using

the VH production mode where the vector boson decays to leptons.

CMS complemented this search in the VH production mode with an inclusive search for the Higgs boson produced at high transverse momentum (in excess of 450 GeV) and decaying to a pair of charm quarks [196]. The observed (expected) limit at 95% CL is 47 (39) times the SM rate, which is also an impressive result as it is almost comparable to the previous results obtained in the more sensitive VH channel.

With this striking improvement in sensitivity, CMS reappraised their prospect for the search of Higgs boson decays to charm quarks at the HL-LHC and showed that a CMS could reach a relative precision on the the production rate of approximately 80%. In combination with ATLAS and potential improvements in the analysis, this is bringing the Yukawa coupling of the Higgs boson closer to being at reach at the HL-LHC.

11.3.8 *Searches for rare decays of the Higgs boson*

11.3.8.1 *Combined evidence for $H \to Z\gamma$ and the first evidence for the Dalitz $H \to \ell^+\ell^-\gamma$ decay*

The search for $H \to Z\gamma$ is performed in the final states where the Z boson decays into opposite sign and same flavour leptons ($\ell^+\ell^-$), ℓ here refers to e or μ. While the branching fraction for $H \to Z\gamma$ is comparable to $H \to \gamma\gamma$ (about 10^{-3}) at $m_H = 125\,\text{GeV}$, the observable signal yield is brought down by the small branching ratio of $Z \to (e^+e^- + \mu^+\mu^-) = 6.7 \times 10^{-2}$. In these channels, the $m_{\ell\ell\gamma}$ mass resolution is excellent (1–3%), therefore the analyses search for a narrow mass peak over a continuous background. The major backgrounds arise from the $Z+\gamma$ final state radiation in Drell–Yan decays and from the $Z+$jets processes where a jet is misidentified as a photon. The ratio of signal over background in this channel is typically of the order of 0.5%. In a narrow window of a few GeV around 125 GeV, several hundreds of events are expected in a Run-2 dataset corresponding to approximately $36\,\text{fb}^{-1}$. Events are divided into mutually exclusive categories on the basis either of the expected $m_{Z\gamma}$ resolution or exclusive production mode categories.

With the full Run-2 dataset, ATLAS observes an excess with a significance of 2.2σ while an excess with a significance of 1.2σ is expected. CMS observes an excess with a significance of 2.6σ while 1.2σ is expected. ATLAS and CMS have jointly published a combination of these results, yielding a first evidence for the Higgs boson decay to a Z boson and a photon at the LHC with an observed significance of 3.4σ and an expected sensitivity of 1.6σ [197]. This combined result is compatible with the SM hypothesis at 1.9σ.

Both ATLAS and CMS experiments have extended the search for the so-called Dalitz Higgs boson decays $H \to \gamma^*\gamma \to \ell^+\ell^-\gamma$ in the low mass γ^* range of approximately 20-30 GeV. This decay mode has a substantially larger branching fraction compared to the $Z\gamma$ decay, as $\Gamma(H \to \gamma^*\gamma \to e^+e^-\gamma) \sim 3.5\% \times \Gamma(H \to \gamma\gamma)$ and $\Gamma(H \to \gamma^*\gamma \to \mu^+\mu^-\gamma) \sim 1.7\% \times \Gamma(H \to \gamma\gamma)$, while $\Gamma(H \to Z\gamma) = 2.3\% \times \Gamma(H \to \gamma\gamma)$ (which does not account for the subsequent decay of the Z boson to electrons or muons). With the Run-1 dataset, CMS observes an upper limit of 6.7 times the SM branching ratio [198]. With a partial Run-2 dataset, in the $\gamma^*\gamma$ CMS obtained a much more stringent limits on the cross section times the corresponding branching fractions of 1.4 (6.1) times the SM cross section [199]. CMS also performed a combination of this mode with $H \to Z\gamma$, obtaining a combined observed (expected) limit of 3.9 (2.0) times the SM branching fractions.

Using the full Run-2 dataset corresponding to $139\,\text{fb}^{-1}$, ATLAS obtained the first evidence for Higgs boson decays to a low-mass dilepton pair and a photon with a significance of 3.2 (2.1) standard deviations (expected) [200]. The invariant mass requirement on the di-lepton is $m_{\ell\ell} < 30\,\text{GeV}$. The corresponding signal strength is $\mu = 1.5 \pm 0.5$, compatible with the SM expectation.

11.3.8.2 *Higgs coupling to first generation, search for $H \to e^+e^-$*

Probing the Yukawa couplings to the first generation fermions is extremely challenging at the LHC given the overwhelming backgrounds and very small signal rates.

A search similar to the $H \to \mu^+\mu^-$ is performed in the non-VBF categories by CMS in the di-electron channel [201]. In this search, the contribution from the peaking background from Higgs boson decays to diphotons mis-identified as di-electrons (when converted photons are faking electrons) needs to be carefully assessed. The sensitivity to the SM Higgs decays is negligible given the extremely small branching fraction to e^+e^-, approximately 40,000 times smaller than the branching fraction to dimuons. It is nevertheless interesting to probe this decay channel to search for potential large anomalous couplings. Assuming a SM Higgs boson production cross section, the observed limit on the $H \to e^+e^-$ branching fraction at the 95% CL is 3.0×10^{-4}, more than five orders of magnitude larger than the expected SM prediction. ATLAS has also performed a search for the $H \to e^+e^-$ decay mode with the Run-2 dataset, placing a limit of 3.6×10^{-4} on the branching fraction [202].

It is important to note that processes not depending on the electron Yukawa coupling such as the $H \to e^+e^-\gamma$ (where the photon is soft), are sizeably larger than the direct Yukawa coupling process, but also much smaller than the current constraints, making any interpretation in terms of constraint on the electron Yukawa couplings far from straightforward.

11.3.8.3 *Invisible decays of the Higgs boson*

The discovery of the Higgs boson immediately raised the question of its couplings to DM and how it could be used to reveal at colliders the existence of a dark sector coupled to the SM via the Higgs boson portal, see Ref. [203] and references therein. If kinematically accessible and with a sufficiently large coupling to the Higgs boson, DM particles, such as, e.g., neutralinos in SUSY models, graviscalars in models with extra dimensions or heavy neutrinos in the context of four-generation fermion models, would manifest themselves as invisible decays of the Higgs boson, thus strongly motivating searches for the invisible decays of the Higgs boson.

It should be noted that in the Standard Model the branching fraction of a Higgs boson into invisible decays through the $H \to ZZ^* \to \nu\bar{\nu}\nu\bar{\nu}$ process has a branching fraction of 0.12%.

To identify an invisibly decaying Higgs boson at the LHC, it must be produced in association with other particles. Searches for invisible decays of the Higgs boson at the LHC have been carried out in the three associated production modes of the Higgs boson with the highest SM cross sections and target events with large missing energy.

The ggF production mode has the largest SM cross section but it usually results in the Higgs boson being created alone and hence leaving no characteristic signature in the detector of its invisible decay. One way to search for invisible decays in ggF production mode is to look for events with the monojet topology arising from initial state gluon radiation and containing missing energy. The major irreducible background in such searches stems from Z + jets events where the Z boson decays into a pair of neutrinos [204]. The analysis with the best sensitivity targets the VBF production topology but it suffers from large backgrounds arising from events with two jets and large missing energy. The VH mode has much smaller cross section but the presence of a W or Z boson allows a variety of final states that can be tagged with relatively low background.

ATLAS and CMS have searched for such final states at Run 1 and have observed no significant excess over the predicted backgrounds (for references, see the previous edition of this review [141]). Table 11.6 summarises the 95% CL limits on the invisible decays of the Higgs boson assuming a SM Higgs boson production cross section and the corresponding detector acceptances.

ATLAS and CMS have performed the search for invisible decays of the Higgs boson at Run 2 with the full dataset in all the aforementionned channels [205–207]. The results are summarised in Table 11.6.

These constraints can then be further used to probe Higgs portal models to DM [203], where an additional weakly interacting particle χ with mass lower than $m_H/2$ is introduced as DM candidate

Table 11.6: Summary of the channels searched for and the corresponding 95% CL limits from ATLAS and CMS on the branching fraction for the Higgs boson decay to invisible particles assuming a SM Higgs boson production cross section. The results in parentheses are the expected exclusions.

	ATLAS (Run 1)	ATLAS (Run 2)	CMS (Run 1)	CMS (Run 2)
ggF (monojet); $H \to$ inv.	–	33 (38) %	67 (71) %	49 (32)%
VBF; $H \to$ inv.	28 (31) %	14.5 (10.3) %	57 (40) %	18 (10) %
ZH; $Z \to \ell^+\ell^-$; $H \to$ inv.	75 (62)%	18.5 (18.5) %	75 (91) %	
VH; $Z, W \to jj$; $H \to$ inv.	78 (86)%	83 (58) %	–	21 (18)%
ZH; $Z \to b\bar{b}$; $H \to$ inv.	–	–	182 (189)%	
$t\bar{t}H$; $H \to$ inv.	–	38 (30)%	–	26 (30)%
Run 1 & 2 Combination	10.7 (7.7)%		15 (8)%	

and where the Higgs boson is considered as the only mediator between the SM particles and DM. In this model, it is interesting to express the limit on the invisible branching fraction in terms of strength of interaction of DM with standard matter, i.e., in terms of it interaction cross section with nucleons $\sigma_{\chi-N}$. In this model, the couplings of the Higgs boson to SM particles are assumed to be those of the SM and the interaction of the Higgs boson with the nucleon is parametrised in a Higgs-Nucleon form factor estimated using lattice QCD calculations [203]. The results for the ATLAS llimits are shown in Fig. 11.4.

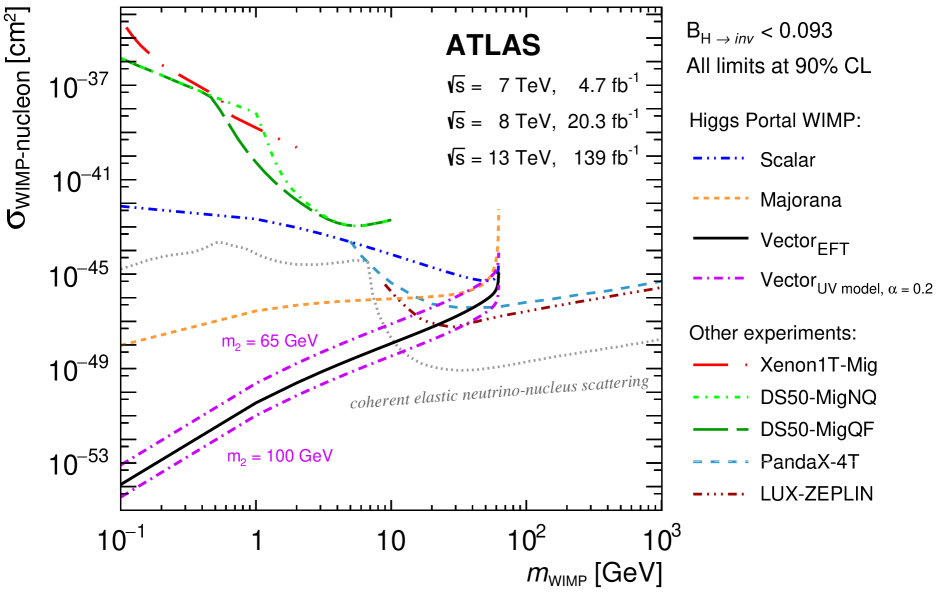

Figure 11.4: 90% CL upper limits on the spin-independent WIMP-nucleon scattering cross section as a function of the DM particle mass for direct detection experiments experiments and the interpretation of the H $\to$ invisible combination result in models where the Higgs boson is a portal between the SM matter and the Dark Sector. For the vector UV-model, m_2 are two representative values of the predicted Dark Higgs particle with mixing angle α. The regions above the limit contours are excluded in the range shown in the plot. From Ref. [205].

11.3.8.4 *Exclusive Higgs boson decays*

A possibility to access the charm Yukawa coupling has been discussed in Ref. [208]. It relies on the decays of the Higgs boson to a final state with quarkonia. Searches have been performed in several channels including $H \to \Upsilon\gamma, J/\Psi\gamma, \phi\gamma, \rho\gamma$ these processes can provide indirect constraints on the Higgs boson Yukawa coupling to b, charm, strange and light quarks. The limits obtained so far in these channels [209,210] are reported in the Higgs particle listings [188]. Limits on branching fractions range between 10^{-3}–10^{-4}.

CMS has also performed a search of the decays of the Higgs boson in the $J/\Psi J/\Psi$ and $\Upsilon\Upsilon$ final states to cover the cases where the photon in the $J/\Psi\gamma$ decay is virtual and transforms into a J/Ψ meson, These decays provide an additional channel potentially sensitive to BSM phenomena [211].

More recently a search for Higgs boson decays to mesons and a photon in the channels $H \to \omega\gamma$ and $H \to K^*\gamma$ have been carried out by the ATLAS experiment [212]. The limits on these processes are of 1.5×10^{-4} and 8.5×10^{-5} on the $\omega\gamma$ and the $K^*\gamma$ respectively.

Another class of searches for exclusive decays of the Higgs boson is $H \to ZQ$ where Q is a quarkomium state. This decay results from the interference of two contributions, one where the Higgs boson couples to a quark-anti-quark pair which forms a quarkonium and radiates a Z boson at leading order, and another one from the off-shell decay $H \to ZZ^*$ or $H \to Z\gamma^*$ and the conversion of the off-shell Z or photon into a quarkonium. A search was carried out by ATLAS in the ZJ/Ψ and Z/η_c channel in the $Z \to \ell^+\ell^-$ and a light hadronically decaying resonance signature [213] and by CMS in the ZJ/Ψ and ZJ/Υ channels in fully leptonic final states [214].

11.3.8.5 *Lepton flavour violating (LFV) Higgs boson decays*

Given the Yukawa suppression of the couplings of the Higgs boson to quarks and leptons of the first two generations and the small total width of the Higgs boson, new physics decay modes could easily have sizeable branching fractions. One very interesting possibility is the Lepton Flavour Violating (LFV) decays of the Higgs boson, in particular in the $\tau\mu$ and τe modes. These decays are suppressed in the SM but they could easily be enhanced in theories such as two-Higgs-doublet models (discussed in Section 11.6). Indirect constraints on the LFV Yukawa couplings $|Y_{\tau\mu}|$ can be obtained from channels such as the $\tau \to 3\mu$ or $\tau \to \mu\gamma$, or a re-interpretation of the search for Higgs boson decays to $\tau^+\tau^-$. A direct search at the LHC, however, complements these indirect limits.

The search for LFV decays in the $\tau\mu$, τe and μe channels were carried out with the Run-1 and early Run-2 datasets in several channels according to the subsequent decay of the τ [215–220]. The limits on LFV decays of the Higgs boson are reviewed in this volume of the particle listings [188] and reached 0.15% in the $\tau\mu$ channel and 0.22% in the τe channel.

ATLAS [221] has performed the analysis with the full Run-2 dataset, yielding limits of 0.20% and 0.18% on the $e\tau$ and $\mu\tau$ channels respectively. CMS [222] has performed analyses with the full Run-2 dataset of the $e\mu$ channel reaching a limit of 4.4×10^{-5} at 95% CL.

The CMS search in the $e\mu$ channel was done not only at the specific Higgs boson mass, but in a wider mass domain between 110 GeV and 160 GeV. A mild excess with a global significance of 2.8 standard deviations is observed for a mass hypothesis of approximately 146 GeV.

11.3.8.6 *Flavour changing neutral current decays of the top quark*

The discovery of the Higgs boson at a mass smaller than the top quark mass opened a new decay channel for the top quark. The decays of the top quark to a Higgs boson and a charm or an up quark proceed through a Flavour Changing Neutral Current (FCNC) which are forbidden in the Standard Model at tree level and suppressed at higher orders through the Glashow–Iliopoulos–Maiani (GIM) mechanism [3]. The SM prediction for these branching fractions is $\mathrm{BR}(t \to Hc) = 10^{-15}$ and two orders of magnitude less for the Hu final state. These decay channels of the top quark are, therefore,

very interesting to probe possible FCNC interactions in the Yukawa couplings to the quark sector, see Section 11.6.

ATLAS has searched for FCNC top decays specifically in channels involving a Higgs boson that subsequently decays into a pair of b quarks, two photons, a tau pair or two W bosons [223]. It has also reinterpreted a search for the $t\bar{t}H$ production in the multilepton final state (discussed in Section 11.3.5.1) [173]. The latter channel covers Higgs boson decays to a pair of W bosons and a pair of taus. No significant excess was observed in any of the specific channels (as discussed in Section 11.3.5.1, a slight excess is observed in the $t\bar{t}H$ multilepton channel) and 95% CL upper limits are set on $\mathrm{BR}(t \to Hc) < 0.46\%$ with an expected sensitivity of 0.25% and $\mathrm{BR}(t \to Hu) < 0.45\%$ with an expected sensitivity of 0.29%. CMS has performed a search for these FCNC top decays in the diphoton and multi-lepton channels [224], placing a 95% CL upper limit on $\mathrm{BR}(t \to Hc) < 0.40\%$ with an expected sensitivity of 0.43%.

From these limits on branching fractions, constraints on non-flavour-diagonal Yukawa couplings of a FCNC Lagrangian of the form:

$$\mathcal{L}_{\mathrm{FCNC}} = \lambda_{tcH}\bar{t}Hc + \lambda_{tuH}\bar{t}Hu + h.c. \tag{11.18}$$

can be derived. The 95% CL observed (expected) upper limits from ATLAS on the $|\lambda_{tcH}|$ and $|\lambda_{tuH}|$ couplings are 0.13 (0.10) and 0.13 (0.10), respectively.

The results above are derived from the combination of several channels for searches performed with Run-1 data. Both ATLAS and CMS have produced updates of individual channels with Run-2 data. ATLAS has searched for FCNC top decays with subsequent decays of the Higgs boson to a pair of photons [225], yielding a 95% CL upper limit on $\mathrm{BR}(t \to Hc) < 0.22\%$ with an expected sensitivity of 0.16%. CMS has searched for FCNC top decays with subsequent decays of the Higgs boson to a pair of b-quarks [226], yiedling a 95% CL upper limit on $\mathrm{BR}(t \to Hu) < 0.079\%$ with an expected sensitivity of 0.011% and on $\mathrm{BR}(t \to Hc) < 0.094\%$ with an expected sensitivity of 0.086%.

11.3.8.7 *Exotic Higgs boson decays*

The 125 GeV Higgs boson serves not only as a probe for potential DM candidates, but also to search for other exotic particles arising from fields associated with a low-mass hidden sector (for a review, see for instance Ref. [227]). Such hidden sectors are composed of fields that are singlet under the SM gauge group $\mathrm{SU}(3) \times \mathrm{SU}(2) \times U(1)$. These models are referred to as hidden valley models [228]. Since a light Higgs boson is a particle with a narrow width, even modest couplings to new states can give rise to a significant modification of the Higgs boson phenomenology through exotic decays. Simple hidden valley models exist in which the Higgs boson decays to an invisible fundamental particle, which has a long lifetime to decay back to SM particles through a small mixing with the SM Higgs boson, see Ref. [228] for a concrete example. The Higgs boson may also decay to a pair of hidden valley "v-quarks," which subsequently hadronise in the hidden sector, forming "v-mesons." These mesons often prefer to decay to the heaviest state kinematically available, so that a possible signature is $H \to 4b$. Some of the v-mesons may be stable, implying a mixed missing energy plus heavy flavour final state. In other cases, the v-mesons may decay to leptons, implying the presence of low mass lepton resonances in high-H_T events [229]. Other scenarios have been studied [230] in which the Higgs boson decays predominantly into light hidden sector particles, either directly, or through light SUSY states, and with subsequent cascades that increase the multiplicity of hidden sector particles. In such scenarios, the high-multiplicity hidden-sector particles, after decaying back into the SM, appear in the detector as clusters of collimated leptons known as "lepton jets".

A variety of models have been investigated searching for final states involving dark photons

and hidden valley scalars. The resulting topologies typically have leptons or light hadrons which in some cases can be prompt (i.e., originating from the hard process interaction point) or not and are in some cases collimated and reconstructed as jets [231,232], and long-lived weakly interacting particles. The latter occur not only in hidden valley scenarios, but also in gauge-mediated extensions of the minimal SUSY standard model (MSSM), the MSSM with R-parity violation, and inelastic DM scenarios [233]. Finally, CMS has performed a search for pair production of light bosons [234]. Such a scenario can occur in SUSY models with additional hidden (or dark) valleys.

11.3.9 *Higgs boson pair production and self-coupling*

Higgs boson pair production in the SM is a rare but very important mode to measure and search for. The measurement of Higgs boson pair production is essential to directly constrain the trilinear Higgs boson self coupling and the search for Higgs boson pair resonances is key in a variety of BSM models. The latter searches are discussed in Section 11.6.7.

In the SM, the main non-resonant production mode of two Higgs bosons proceeds through a loop, mainly of top quarks, see Fig. 11.1 (h). Another production mode is via the trilinear coupling of the Higgs boson, see Fig. 11.1 (i), whose amplitude is not negligible compared to the former. These diagrams interfere negatively, making the overall production rate smaller than what would be expected in the absence of a trilinear coupling.

11.3.9.1 *Searches for Higgs boson pair production*

The searches for Higgs boson pair production both resonant and non-resonant are important probes for a variety of BSM theories, and they can be done in a large number of Higgs boson decay channels. At Run 1, ATLAS and CMS have searched for both resonant and non resonant Higgs boson pair production in the following channels: (i) $HH \to b\bar{b}\gamma\gamma$; (ii) $HH \to b\bar{b}\tau^+\tau^-$; (iii) $HH \to b\bar{b}b\bar{b}$; (iv) $HH \to b\bar{b}4\ell$; (v) $HH \to WW^*\gamma\gamma$; (vi) in final states containing multiple leptons (electrons or muons) covering the WW^*WW^*, WW^*ZZ^*, ZZ^*ZZ^*, $ZZ^*\tau^+\tau^-$, $WW^*\tau^+\tau^-$, $ZZ^*b\bar{b}$, $\tau^+\tau^-\tau^+\tau^-$ channels; and (vi) $\gamma\gamma\tau^+\tau^-$ channels.

At Run 2, similarly to the $t\bar{t}H$ production process, the di-Higgs production profits from a significant increase in production cross section of a factor in excess of 3 from 8 TeV to 13 TeV, and most of these channels have been updated both by ATLAS [235] and CMS [184,236]. The detailed description of the various analyses used can be found in the references therein. All the results and their combinations are summarised in Table 11.7 and in Fig. 11.5 (left). The channels (i)-(iii) are the most sensitive to the HH production. These three channels have been updated with the full Run-2 dataset except the $HH \to b\bar{b}\tau^+\tau^-$ channel by CMS and the $HH \to b\bar{b}b\bar{b}$ channel by ATLAS which have both been analysed using a partial Run-2 dataset.

In several of these analysis channels the VBF production mode is searched for separately providing sensitivity to the coupling involving two vector bosons and two Higgs bosons HHVV which is an expected coupling in the Standard Model.

The current single channel most stringent limits obtained on the HHVV coupling modifier denoted κ_{2V} are obtained from the analysis performed by CMS [237] in the $b\bar{b}b\bar{b}$:

$$-0.1 < \kappa_{2V} < 2.2\,(\text{observed}), \quad -0.4 < \kappa_{2V} < 2.5\,(\text{expected})$$

and for the overall most stringent constraints are obtained through the combination of channels in ATLAS, yielding [235]:

$$-0.1 < \kappa_{2V} < 2.0\,(\text{observed}), \quad 0.0 < \kappa_{2V} < 2.1\,(\text{expected})$$

Table 11.7: Summary of the final states investigated in the search for Higgs boson pair production by ATLAS and CMS, the results reported in bold are based on the full Run-2 dataset. For ATLAS, the result indicated by (*) uses mostly the $b\bar{b}W^+W^-$ channel. Results are 95% CL upper limits on the observed (expected) signal strengths.

Channel	ATLAS	CMS
$b\bar{b}\gamma\gamma$	**4.2 (5.7)**	**8.4 (5.5)**
$b\bar{b}b\bar{b}$	**5.4 (8.1)**	**7.2 (4.2)**
$b\bar{b}\tau^+\tau^-$	**4.7 (3.9)**	**3.3 (5.2)**
$b\bar{b}4\ell$	-	**32 (40)**
$W^+W^-W^+W^-$	160 (120)	–
$W^+W^-\gamma\gamma$	230 (170)	**97 (52)**
$b\bar{b}VV$	305 (305)*	**14 (18)**
Multi-lepton	–	**19 (21)**
Combination	**2.4 (2.9)**	**3.4 (2.5)**

11.3.9.2 *The Higgs boson self coupling*

The Higgs boson self coupling is an extremely important direct probe of the Higgs potential with implications on our understanding of the electroweak phase transition. Constraints on the trilinear self coupling from HH processes is an outstanding long term goal of the LHC and the reach in sensitivity has been reappraised in the light of the recent HH analyses from ATLAS and CMS, shedding a different light on the achievable sensitivity [118]. Constraints from the HHH final state on the quartic Higgs boson self coupling are out of reach at the LHC due mostly to the very small production rates and intricate final states.

In the SM, the Higgs boson pair production through the trilinear Higgs boson self coupling has an on-shell component and a large off-shell component. The on-shell $H \to H^*H^*$ is strongly disfavoured, requiring two off-shell Higgs bosons in the final state. The sensitivity region to the trilinear coupling production as in Fig. 11.1 (i), is mainly in the kinematic region where the two Higgs boson in the final state are on-shell and the Higgs boson acts as a propagator (off-shell). As discussed in the introduction to this section, this process interferes negatively with the background Higgs boson pair production (Fig. 11.1 (h)). The extraction of the trilinear component of the di-Higgs production measurements is very similar to the extraction of the off-shell component of the Higgs coupling to vector bosons discussed in Section 11.4.2.

The measurement of the trilinear coupling requires separating the contributions of the diagram of Fig. 11.1 (i) from the box diagram of Fig. 11.1 (h), and therefore a precise knowledge of the top-Yukawa coupling is needed. Each diagram alone would produce a rather distinct m_{HH} distribution. And, for values of the trilinear coupling close to the SM value, an additional discriminating feature of the signal with respect to one obtained with the box contribution alone is a deficit in the number of events. With large variations of the trilinear coupling, an excess of events over the SM prediction would be observed (for a value of the trilinear coupling about 6 times larger than its SM value, the number of events is equal to the SM expectation). Additional sensitivity to the trilinear coupling is also obtained from the kinematical distributions of the signal taking in particular into account the effect of the HH mass distribution which discriminates the main contributions of Fig. 11.1.

This further discrimination is instrumental in resolving the degeneracy in the total cross section mentioned above. Bounds on the trilinear coupling are obtained from limits on the HH production as a function of the trilinear coupling factor κ_λ as illustrated in Fig. 11.5. As the sensitivity in this channel grows it will be interesting to more closely look at the combined and individual likelihoods as a function of the trilinear coupling to quantify the exclusion of the secondary minimum induced by the degeneracy between the value of κ_λ yielding the same overall HH rate as the Standard Model (*i.e.* $\kappa_\lambda = 1$). The results obtained by ATLAS [235] and CMS [184] are the following:

$$\begin{aligned} &\text{(ATLAS)} \; -0.6 < \kappa_\lambda < 6.6 \,\text{(observed)}, -2.1 < \kappa_\lambda < 7.8 \,\text{(expected)}, \\ &\text{(CMS)} \; -1.2 < \kappa_\lambda < 6.5 \,\text{(observed)}, \end{aligned} \tag{11.19}$$

where κ_λ is the ratio between the trilinear coupling value left free in the fit and its expected value in the SM ($\kappa_\lambda = 1$ corresponds to the SM). For the CMS result the expected excluded range is not specified in [184], however its illustration in the exclusion figure therin shows that it is compatible with the observation. The so-called κ formalism is discussed in more detail in Section 11.5.1.1. These results are also illustrated in Fig. 11.5.

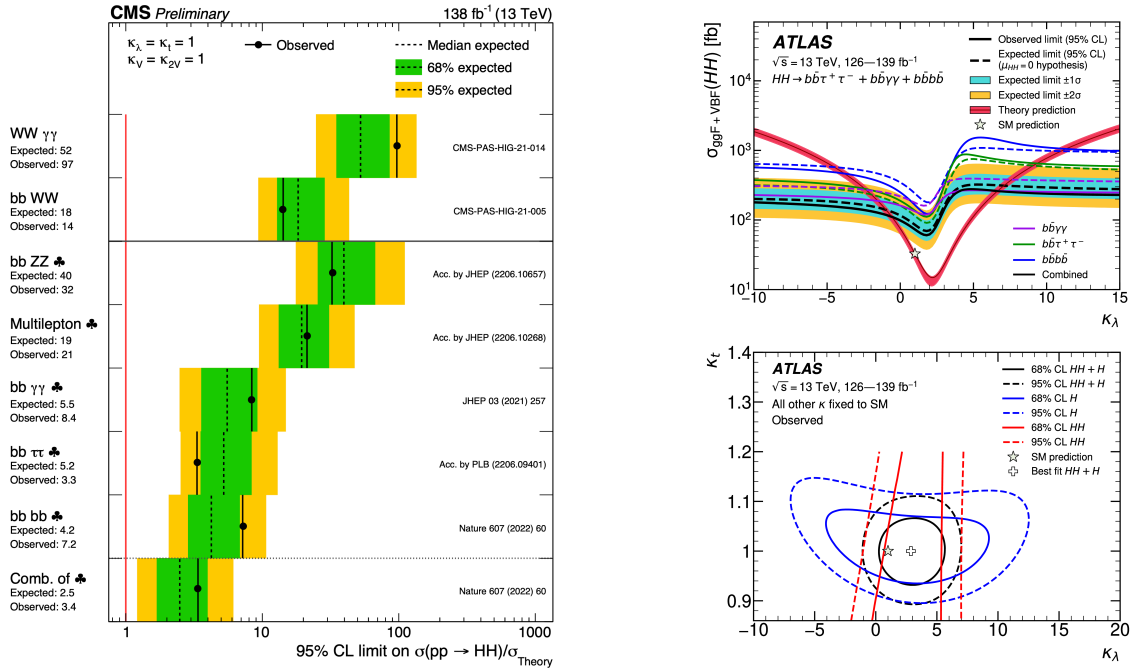

Figure 11.5: (Left) Upper limits obtained by CMS on the total $pp \to HH$ production cross section. (Top right) Upper limits obtained by ATLAS on the total $pp \to HH$ production cross section as a function of the trilinear coupling modifier κ_λ. The variation of the limit corresponds to variations in the signal acceptance. The expected total production cross section is also illustrated (red). (Bottom right) Likelihood contours for the ATLAS di-Higgs and single-Higgs combined results as a function of κ_λ and κ_t.

Single Higgs production can indirectly also be used to further constrain the trilinear coupling of the Higgs boson, both using inclusive total or differential cross sections. A combination of di-Higgs and single-Higgs boson production results has been performed by the ATLAS collaboration yielding the following limits [235]:

$$-0.4 < \kappa_\lambda < 6.3 \,\text{(observed)},$$

It is interesting to note that currently the *direct* ($-0.6 < \kappa_\lambda < 6.6$) and *indirect* constraints ($-4.0 < \kappa_\lambda < 10.3$) on the Higgs boson trilinear self-coupling are of comparable strength. However, the double Higgs boson measurements are dominated by statistical uncertainties and are expected to improve more rapidly than the precision on single Higgs boson measurements. It should also be stressed that the constraints on the trilinear self-coupling obtained via the NLO fit of single Higgs boson data are model-dependent since the NLO effects induced by a shift of the trilinear self-coupling compete with possible LO effects sourced by the deviations of the Higgs boson couplings to the other SM particles. The different effects can be disentangled by the measurements of various kinematical differential distributions in addition to the study of the inclusive rates [238], but the expected sensitivity obtained in such global fits are not as strong as when only the Higgs boson self-coupling is allowed to deviate from its SM value [119]. It should also be noted that in this fit the parameters κ_t, κ_b, κ_τ and κ_V are fit simultaneously.

The analyses performed at Run 2 bring substantial improvements from those of Run 1, and they were first used to reappraise the sensitivity of the LHC in the High Luminosity regime in the framework of the update of the European Strategy for Particle Physics [118]. The result in terms of bounds on the trilinear coupling indicated that the significance of the observation of the HH process reaches 4σ. It is also apparent that the degeneracy of secondary minimum at intermediate values of κ_λ is resolved by the use of the kinematic discriminants. This secondary minimum was expected to be excluded at 99.4% CL and at HL-LHC, the foreseen precision on κ_λ was estimated to reach approximately 50%. These studies were based on early LHC Run-2 analyses. Then in the framework of the Snowmass2021 studies [239] and more recently using the latest HH searches results, these projections have been updated. Both experiments have reappraised their studies at HL-LHC [240], to reach individually a sensitivity of approximately 3.5σ, a significant improvement compared to the sensitivities estimated between 2.5σ and 3σ in [118]. These studies indicate that a sensitivity of 5σ in combination of the two experiments should be reached at HL-LHC.

Higher precisions can be reached at pp colliders (and e^+e^- colliders) at higher centre-of-mass energies. The foreseen precision for a High-Energy (HE) LHC at a centre-of-mass energy of 27 TeV is expected to be within 10% to 20% [118]. At a very large hadron collider at a centre-of-mass energy of 100 TeV, a 5% sensitivity is expected to be reached, provided that the theoretical and parametric uncertainties are kept at the 1% level [241].

One of the main open questions in particle physics is related to the precise history of the EWSB mechanism. This in turn can be of relevance to provide a mechanism for generating the matter -antimatter asymmetry of the universe at the electroweak scale, the so called electroweak baryogenesis (EWBG) (see Refs. [242, 243] for some reviews). In the SM EWBG is ruled out, but new physics models, in particular those additional scalar particles coupled/mixed with the Higgs boson, can provide a successful alternative. Given that di-Higgs production will become an excellent probe of trilinear Higgs coupling modifications, it will provide a unique window into the history of EWSB and will become a powerful test of EWBG models.

11.3.10 *Beyond the main Higgs boson production modes*

Most of the production modes illustrated in Fig.11.1 have been investigated at the LHC so far. These processes are often referred to as the 'main production modes'. Beyond these production modes, two additional SM processes involving the Higgs boson have been investigated and are worth noting.

The first is the four top production mode which is closely related to the $t\bar{t}H$ mode. This process has recently been unambiguously observed at the LHC by both ATLAS [244] and CMS [245]. This production mode has a non trivial contribution from the exchange of a Higgs boson. A first limit on the Yukawa coupling of the Higgs boson has thus been derived using this four top process,

$|\kappa_t| < 1.8(1.6)$, under the assumption that the Yukawa coupling of the Higgs boson to top quarks in CP even [244].

Another process beyond the main production modes is the associated WH production through Vector Boson Fusion (VBF) yielding a topology of events with two jets in the forward region with a large rapidity gap, a W boson and a Higgs boson. This process is particularly interesting as it is sensitive to the relative sign of the coupling of the Higgs boson to the W and Z boson through the interference of the processes where the Higgs boson couples either to the W or the Z bosons in the vector boson fusion process. ATLAS has carried out analyses targeting at the decay of the Higgs boson to $b\bar{b}$ and W^+W^- for this process, resulting in the exclusion of the opposite sign hypothesis by 8 standard deviations and an upper limit corresponding to 11.2 times the cross section expected in the Standard Model [246].

11.3.11 *First results on the main production and decay channels at 13.6 TeV*

After a long shutdown between 2019 and 2022, devoted to the upgrades of the experiments and the machine to prepare for the High Luminosity phase , in the Spring 2022 the LHC delivered pp collisions data at an enhanced centre-of-mass energy of 13.6 TeV. During this high-energy run, ATLAS and CMS have collected datasets corresponding to integrated luminosities of approximately 60 fb^{-1} each. The first preliminary measurements of Higgs boson production at this increased centre-of-mass energy using the two high-resolution channels $H \to \gamma\gamma$ and $H \to ZZ^* \to \ell^+\ell^-\ell'^+\ell'^-$ have been carried out by ATLAS [247], see Fig. 11.6. The measurements are in good agreement within the precision with the theoretical prediction which display the expected increase of approximately 7% in inclusive cross section from the increase in centre-of-mass energy.

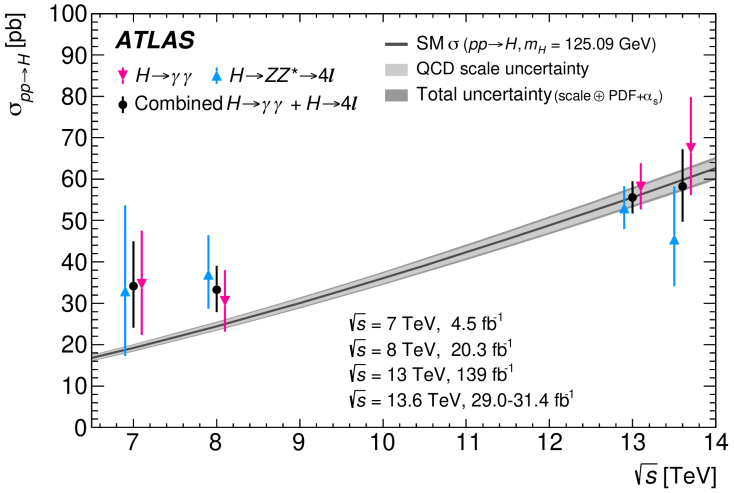

Figure 11.6: Higgs boson production cross sections as a function of the pp centre-of-mass energy. The SM predictions are shown by the shaded band.

11.4 Main quantum numbers and width of the Higgs boson

11.4.1 *Main quantum numbers* J^{PC}

Probing the Higgs boson quantum numbers is essential to further unveiling its coupling properties. The measurements of the signal event yields in all the channels discussed in Section 11.3 and their compatibility with the SM Higgs boson predictions, give a qualitative but, nonetheless, compelling indication of its nature. For the observed particle not to be of spin 0 and +1 parity would require an improbable conspiracy of effects. It is nevertheless important to test this hypoth-

esis independently, in particular since the measurements of coupling properties of the Higgs boson assume that it is a CP-even state.

This qualitative picture is further complemented by the implications of the observation of the particle in the diphoton channel. According to the Landau–Yang theorem [248], the observation made in the diphoton channel excludes the spin-1 hypothesis and restricts possibilities for the spin to 0 or 2.

The Landau–Yang theorem does not apply if the observed state is not decaying to a pair of photons but to a pair of scalars subsequently decaying to two very collimated pairs of photons (as for example in the case of $H \to a_1 a_1 \to 4\gamma$). This possibility has not been rigorously excluded but is not experimentally favoured since tight selection criteria are applied on the electromagnetic shower shapes of the reconstructed photons. A more systematic analysis of shower shapes and the fraction of conversions could be performed to further discriminate between the single prompt photon and the two overlapping photons hypotheses. There are also potential theoretical loopholes concerning the applicability of the Landau–Yang theorem, such as off-shell vector boson decays.

The spin 1 hypothesis has therefore been investigated quantitatively with the LHC Run-1 dataset and has been excluded at more than 95% CL through the analysis of the Higgs boson decays to WW^* and ZZ^* channels. These results are reported in previous versions of this review and will not be covered herein. [188].

11.4.1.1 *Charge conjugation*

The charge conjugation quantum number is multiplicative, therefore given that the Higgs-like particle is observed in the $H \to \gamma\gamma$ channel, and given that photons are C-odd eigenstates, assuming C conservation, the observed neutral particle should be C-even.

11.4.1.2 *Spin and parity*

To probe the spin and parity quantum numbers of the discovered particle, a systematic analysis of its production and decay processes is performed in several analyses. These analyses are designed to be independent of the measured event yields and they rely instead on the production and the decay angles, and on the threshold distributions as long as a significant signal is observed, i.e., in situations when an excess over the expected background can be used to further discriminate between signal hypotheses. These analyses are based on probing various alternative models of spin and parity [249]. These models can be expressed in terms of an effective Lagrangian [250] or in terms of helicity amplitudes [251]. The two approaches are equivalent.

i. *Spin-0 models*

The interaction Lagrangian relevant for the analysis of spin-0 particle interaction with a pair of W or Z bosons with either fixed or mixed SM and BSM CP-even couplings or CP-odd couplings, is the following [252]:

$$\begin{aligned}\mathcal{L}_0^{W,Z} \supset \Bigg\{ & \cos(\alpha)\kappa_{\rm SM}\left[\frac{1}{2}g_{HZZ}Z_\mu Z^\mu + g_{HWW}W^+_\mu W^{-\mu}\right] \\ & - \frac{1}{4\Lambda}\left[\cos(\alpha)\kappa_{HZZ}Z_{\mu\nu}Z^{\mu\nu} + \sin(\alpha)\kappa_{AZZ}Z_{\mu\nu}\tilde{Z}^{\mu\nu}\right] \\ & - \frac{1}{2\Lambda}\left[\cos(\alpha)\kappa_{HWW}W^+_{\mu\nu}W^{-\mu\nu} + \sin(\alpha)\kappa_{AWW}W^+_{\mu\nu}\tilde{W}^{-\mu\nu}\right]\Bigg\} H, \end{aligned} \tag{11.20}$$

where $V^\mu = Z^\mu, W^{+\mu}$ are the vector boson fields, $V^{\pm\mu\nu}$ are the reduced field tensors, $\tilde{V}^{\pm\mu\nu} = 1/2\,\varepsilon^{\mu\nu\rho\sigma}V_{\rho\sigma}$ are the dual tensor fields, and Λ defines an effective theory energy scale. The factors $\kappa_{\rm SM}, \kappa_{HZZ}, \kappa_{HWW}, \kappa_{AZZ}, \kappa_{AWW}$ denote the coupling constants corresponding to the coupling of

the SM and BSM CP-even and CP-odd components of the Higgs boson to the W and Z fields. The mixing angle α allows for the production of a CP-mixed state and the CP-symmetry is broken when $\alpha \neq 0, \pi$.

This formalism can be used to probe both CP-mixing for a spin-0 state, as discussed in Section 11.4.1.5 or specific alternative hypotheses, as discussed below, such as a pure CP-odd state ($J^P = 0^-$) corresponding to $\alpha = \pi/2$, $\kappa_{\rm SM} = \kappa_{HVV} = 0$ and $\kappa_{AVV} = 1$. A BSM CP-even state $J^P = 0^+$ corresponds to $\alpha = 0$, $\kappa_{AVV} = 0$, $\kappa_{HVV} = 1$ and $\kappa_{\rm SM}$ arbitrary. These hypotheses are compared to the SM Higgs boson hypothesis corresponding to $\alpha = 0$ and $\kappa_{HVV} = \kappa_{AVV} = 0$ and $\kappa_{\rm SM} = 1$. This formalism has been adopted by the ATLAS experiment.

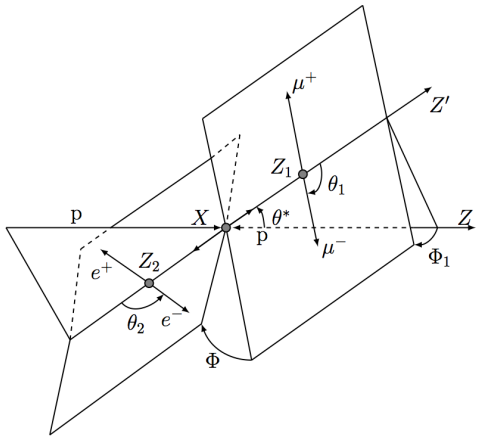

Figure 11.7: Definition of the production and decay angles defined for the $H \to ZZ^{(*)} \to 4\ell$ final state.

A different parametrisation of anomalous couplings of a spin-zero boson with two gauge bosons VV can also expressed in the general form of the scattering amplitude A:

$$A \sim \left[a_1^{VV} - \frac{\kappa_1^{VV} q_1^2 + \kappa_2^{VV} q_2^2}{(\Lambda_1^{VV})^2} - \frac{\kappa_3^{VV} (q_1+q_2)^2}{(\Lambda_Q^{VV})^2} \right] m_{V_1}^2 \varepsilon_{V_1}^* \varepsilon_{V_2}^* + a_2^{VV} f_{\mu\nu}^{*(1)} f^{*(2)\mu\nu} + a_3^{VV} f_{\mu\nu}^{*(1)} \tilde{f}^{*(2)\mu\nu} \tag{11.21}$$

where ε_i is the polarization vector of the boson V_i, $f_{\mu\nu}^{*(i)} = \varepsilon_i^\mu q^\nu - \varepsilon_i^\nu q^\mu$ is a scalar tensor constructed from the vector boson V_i polarization and four momentum, $\tilde{f}_{\mu\nu}^{*(i)} = \frac{1}{2}\varepsilon_{\mu\nu\rho\sigma} f^{*(i)\rho\sigma}$ is the corresponding pseudo-scalar tensor. Λ_1 and Λ_Q are new physics scales, $a_{1,2,3}$ are coupling strength modifiers and $|\kappa_{(1,2,3)}^{VV}| = 0$ or 1. This parametrisation can be used both for gluons, photons and electroweak vector bosons, as well as the $Z\gamma$ coupling. In the case of the W and Z bosons, the custodial symmetry would require that $a^{WW} = a^{ZZ}$ and, at tree-level, the only non-zero contributions would come from the a_1 term. It is fully equivalent to the interaction Lagrangian approach described above. This formalism has been adopted by the CMS experiment.

Finally, CP-odd interactions can also be expressed in the framework of the Standard Model Effective Field Theory (SMEFT) in various possible bases (as discussed in Section 11.5.2). This formalism is more in line with analyses of a broader ensemble of observable probing the Standard Model. In this case the effective Lagrangian is defined as a function of the $\Phi^\dagger\Phi$ gauge invariant and the gauge field tensors before the electroweak symmetry breaking $W_{\mu\nu}^I$ and $B_{\mu\nu}$ with three operators, $\Phi^\dagger\Phi\tilde{W}_{\mu\nu}^I W^{I\mu\nu}$, $\Phi^\dagger\Phi\tilde{W}_{\mu\nu}^I B^{\mu\nu}$, and $\Phi^\dagger\Phi\tilde{B}_{\mu\nu} B^{\mu\nu}$, and their corresponding Wilson coefficients $c_{H\tilde{W}}$, $c_{H\tilde{W}B}$, and $c_{H\tilde{B}}$ respectively.

It is important to note that, as is apparant in Eq. (11.20), CP-odd couplings of the Higgs boson to vector boson are not allowed at tree level and are therefore suppressed at higher order by the scale Λ. Instead, CP-odd couplings of the Higgs boson to fermions are allowed at tree level, these can be parametrised in a somewhat simpler fashion with the following Lagrangian which accounts only for an additional pseudo-scalar term:

$$\mathcal{L}_0^{\psi_f} \supset \frac{\lambda_f}{\sqrt{2}} \left(\kappa_f H \overline{\psi}_f \psi_f + i \tilde{\kappa}_f H \overline{\psi}_f \gamma_5 \psi_f \right). \tag{11.22}$$

This formulation is equivalent to a definition a CP-mixing angle $\varphi_f = \tan \frac{\tilde{\kappa}_f}{\kappa_f}$.

It is interesting to note that CP-odd Higgs couplings to fermions could have a significant impact on the very clean and precisely measured low energy observables as the electron EDM [253]. Owing to its large Yukawa couplings, the CP-odd top Yukawa is strongly constrained by the stringent electron EDM limits to better than $\tilde{\kappa}_t < 0.001$ [253]. This makes it very challenging at the LHC to surpass. However, one should keep in mind that EDM experiments provide an indirect constraint on the SM Yukawa couplings, in particular in this case they constrain the product $\kappa_e \times \tilde{\kappa}_t$, and one needs to make assumptions on the value of κ_e, a quantity that remains out of reach experimentally. The limits on the tau Yukawa coupling from the electron EDM constraints are much less stringent and at the level of $\tilde{\kappa}_\tau < 0.3$ [253]. This makes the possibility of measuring CP mixing of the fermion Higgs Yukawa couplings particularly interesting in the tau channels since these can be accessed from the Higgs decays directly using tau polarisation sensitive variable and will be discussed herein. For more details on the searches for CP-odd couplings of the Higgs boson to vector bosons please see previous versions of this review [188].

ii. *Spin-2 model*

The graviton-inspired interaction Lagrangian for a spin-2 boson $X^{\mu\nu}$ that does not carry any color, weak and electromagnetic charge and that uniquely interacts with the energy momentum tensor $\mathcal{T}^{V,f}$ of vector bosons V or fermions f, can be written as follows [252]:

$$\mathcal{L}_2 \supset \frac{1}{\Lambda} \left[\sum_V \xi_V \mathcal{T}^V_{\mu\nu} X^{\mu\nu} + \sum_f \xi_f \mathcal{T}^f_{\mu\nu} X^{\mu\nu} \right], \tag{11.23}$$

where the strength of the interaction is determined by the couplings ξ_V and ξ_f. The simplest scenarios, referred to as universal couplings (UC), correspond to $\xi_V = \xi_f$. They predict a large branching ratio to photons (of approximately 5%) and negligible couplings to massive gauge bosons (W and Z). They are therefore disfavoured, and other models are investigated where the couplings of the W, Z and γ are assumed to be independent. Universality of the couplings refers to $\xi_g = \xi_q$. Two other scenarios are considered: $\xi_q = 0$ and $\xi_q = 2\xi_g$. In these scenarios, a large enhancement of the tail of the transverse momentum of the spin-2 state is expected and requires a further selection requirement in order to probe the models within the range of validity of the effective field theory. Two requirements are considered, $p_T^X < 300\,\text{GeV}$ and $p_T^X < 125\,\text{GeV}$ [250].

11.4.1.3 *The VH production at D0*

The mass of the VH system is a powerful discriminant to distinguish a $J^P = 0^+$, with a threshold behaviour in $d\sigma/dM^2 \sim \beta, \beta^3, \beta^5$ from a 0^+, 0^- and 2^+ state, respectively [254]. The VH mass observable not only discriminates signal hypotheses, but also has an increased separation between the 0^- and 2^+ hypotheses with respect to the backgrounds, thus allowing, with a small and not yet significant signal yield, to exclude that the observed state is 0^- at 98% CL [255] and

2^+ at the 99.9% CL [256], assuming a signal produced with their best fit signal strength (which was $\mu = 1.23$).

11.4.1.4 *Probing the spin in the $\gamma\gamma$ channel at the LHC*

In the $H \to \gamma\gamma$ channel, the analysis is performed inclusively using the production angle $\cos\theta^*_{CS}$ and the transverse momentum of the diphoton pair [250]. The polar angle in the rest frame is defined with respect to the bisector axis of the momenta of the incoming protons and is referred to as the polar angle in the Collins–Soper frame [257]. The SM Higgs boson signal distribution is expected to be uniform with a cutoff due to the selection requirements on the photons transverse momentum. The $H \to \gamma\gamma$ channel is mostly sensitive to the gluon-initiated spin-2 production scenarios, which yield a $\cos\theta^*_{CS}$ distribution peaking at values close to 1. The ATLAS limits are derived from a fit of the signal in bins of $\cos\theta^*_{CS}$ and diphoton transverse momentum. The data is compatible with the SM 0^+ hypothesis and contributes strongly to the exclusion of several spin-2 scenarios. The conclusions are the same from CMS results [251].

11.4.1.5 *Probing CP-mixing and anomalous HVV couplings*

The careful study of the kinematic properties of angular distributions in events observed in the $H \to ZZ^{(*)} \to 4\ell$ and $H \to WW^{(*)} \to \ell\nu\ell\nu$ channel, as well as the analysis of production observables sensitive to anomalous HVV interactions in the VBF or VH production have been used to set limits wither on CP-mixing parameters, amplitude terms ot Wilson coefficients in the framework of SMEFT. These analysis assume that the observed particle is a spin-0 state, several results were obtained by the ATLAS [258] and CMS [251] collaborations, all show a good agreement with the Standard Model CP-even hypothesis. Recent specific examples are given here.

In the $H \to WW^{(*)} \to \ell\nu\ell\nu$ channel, the production and decay angles cannot be easily reconstructed due to the presence of neutrinos in the final state, however, sensitivity arises from the $V-A$ structure of the decay of the W bosons. A scalar state thus yields a clear spin correlation pattern that implies that the charged leptons e or μ from the decays of the W bosons are produced close to one another in the transverse plane. This feature impacts observables such as the azimuthal angle between the two leptons $\Delta\Phi_{\ell\ell}$ or their invariant mass $m_{\ell\ell}$ in addition to the threshold behaviour of the decay. It can be used to discriminate between various spin and parity hypotheses.

The $H \to ZZ^{(*)} \to 4\ell$ coupling analysis, as described in Section 11.3, also uses a discriminant based on the 0^+ nature of the Higgs boson to further separate signal and background. In this analysis, this feature is used to discriminate between signal hypotheses. The observables sensitive to the spin and parity have first been identified in Ref. [249,259,260] the masses of the two Z bosons (due to the threshold dependence of the mass of the off-shell Z boson [249, 261]), two production angles θ^* and Φ_1, and three decay angles, Φ, θ_1 and θ_2. The production and decay angles are defined as:

– θ_1 and θ_2, the angles between the negative final state lepton and the direction of flight of Z_1 and Z_2 in the rest frame.

– Φ, the angle between the decay planes of the four final state leptons expressed in the four lepton rest frame.

– Φ_1, the angle defined between the decay plane of the leading lepton pair and a plane defined by the vector of the Z_1 in the four lepton rest frame and the positive direction of the proton axis.

– θ^*, the production angle of the Z_1 defined in the four lepton rest frame with respect to the proton axis.

These angles are illustrated in Fig. 11.7 [260].

These analyses are sensitive to various J^P hypotheses and in particular discriminate the 0^+ hypothesis from the 0^-. In all scenarios investigated, and for both ATLAS and CMS, the data is compatible with the 0^+ hypothesis. ATLAS and CMS exclude a pure pseudo-scalar nature of the

observed boson at CL_S levels of 98% and 99.8% [251].

An individual ZZ^* channel measurement has also been carried out with a partial Run-2 dataset by ATLAS [258]. CMS has performed a CP-mixing analysis of a partial Run-2 dataset of 36 pb^{-1} combined with the full Run-1 data using the ZZ^* channel [262]. In this analysis the CMS experiment sets constraints on the parameters defined in the parametrisation (11.21) of the scattering amplitude.

With the full Run-2 dataset, analyses have started exploiting in combination both the production and decay modes of the Higgs boson as exemplified by the analysis carried out by ATLAS using the $H \to ZZ^* \to 4\ell$ analysis taking advantage of the production and decay angles of the process and VBF production sensitive observables [263]. Very similar analyses have been carried out in CMS as well. The analysis uses optimal observables constructed from matrix elements of the SMEFT. These optimal observables are defined from the ratio of the interference term between the Standard Model and the SMEFT matrix elements (normalised to the Standard Model) for given values of the Wilson coefficients $c_{H\tilde{W}}$, $c_{H\tilde{W}B}$, and $c_{H\tilde{B}}$ below Eq. (11.21). As illustrated in Fig. 11.8, all measurements are in agreement with the Standard Model. ATLAS has also performed a similar analysis with the Higgs boson decaying to two photons analysing the VBF production mode [264] which can then be used to constrain the $c_{H\tilde{W}}$ parameter as shown in Fig. 11.8.

An analysis of Higgs boson anomalous couplings HVV (as well as pseudo-scalar Yukawa coupling to the top) in the $H \to 4\ell$ channel was also carried out by CMS [265].

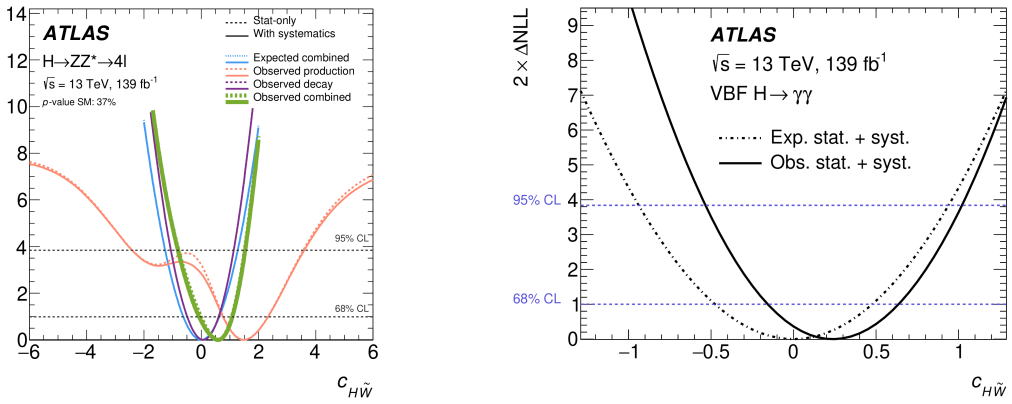

Figure 11.8: The measurement of the $c_{H\tilde{W}}$ Wilson coefficent based on the optimal observable sensitive to the Higgs boson production, its decay and their combination (left) for the ATLAS $H \to ZZ^* \to 4\ell$ analysis. The measurement of the $c_{H\tilde{W}}$ Wilson coefficent based on optimal observable sensitive to the Higgs boson production in the VBF channel (right) for the ATLAS $H \to \gamma\gamma$.

ATLAS has also performed an analysis using optimal observables [266], defined as the ratio of the interference between the CP-odd and the SM contributions normalised to the SM matrix element squared, using the Run-1 data. In this study, the CP-mixing contributions are described in the framework of an effective field theory governed by a single parameter $\tilde{d}$, found to be consistent with its SM value of $\tilde{d} = 0$ and constrained to the interval [-0.11,0.05] at the 68% CL.

CP invariance in the HVV coupling can also be probed with the VBF production process in the $H \to \tau^+\tau^-$ channel or similarly to the D0 analysis in the VH channels. CMS has performed an analysis in this channel and has combined its results with the aforementioned ZZ^* channel using the same dataset [267].

Finally two aditional specific measurements as for example in $H \to WW^*jj$ [268] by ATLAS and using the $H \to \tau^+\tau^-$ final state [269] by CMS in several production modes have also been used to set limits on both anomalous CP-even and CP-odd couplings.

These measurements show the complementarity of the study of production and decay modes, separately and in combination, and underscores the importance of a synthetic approach that combines all the available information.

11.4.1.6 *Probing $Hf\overline{f}$ coupling CP properties in $pp \to t\bar{t}H$ production*

Although EDM limits disfavour large CP-odd effects in the top Yukawa coupling of the Higgs boson, these indirect limits are model dependent. It is therefore important to further probe these effects directly. This can be achieved using the $pp \to t\bar{t}H$ process. The increased sensitivity to the this process at Run 2 in particular in the channels where the Higgs boson decays to a pair of photons provide a good sensitivity to the CP properties of the coupling through kinematics and angular distributions between the Higgs boson and the top quarks produced in the final state.

With the full Run-2 dataset, several Higgs boson decay channels have been investigated. ATLAS [270] excludes CP-mixing angles φ_t greater than 43° and smaller than −43° at 95% confidence level in the $H \to \gamma\gamma$ channel and has recently published constraints using the $H \to b\bar{b}$ channel with a measurement of $\varphi_t = 11^o\,^{+52^o}_{-73^o}$ [271].

Also using the full Run-2 dataset, CMS [272] measures the CP-odd fraction defined as follows:

$$f_{CP} = \frac{|\tilde{\kappa_t}|^2}{|\kappa_t|^2| + |\tilde{\kappa_t}|^2} \times \text{sign}(\tilde{\kappa_t}/\kappa_t)$$

in the diphoton channel to be $f_{CP} = 0.00 \pm 0.33$. CMS also derived a constraint on the CP-odd fraction using the $H \to 4\ell$ channel [265]. More recently CMS has analysed the ttH multi-lepton channel, sensitive both to the $H \to WW$ and $H \to \tau^+\tau^-$ decays, to probe the top Yukawa CP properties [273], and combined its results with the two aforementioned channels to yield the following constraint on the CP-odd fraction:

$$|f_{CP}| = 0.28^{+0.27}_{-0.28}.$$

Both the ATLAS and CMS experiments used multivariate analyses in order to maximize the sensitivity to the measurement of the CP properties of the $Hf\overline{f}$ coupling. Both experiments used leptonic and hadronic decays of the top quarks.

11.4.1.7 *Probing $Hf\overline{f}$ coupling CP properties in $H \to \tau^+\tau^-$ decays*

As discussed in Section 11.4.1, it interesting to investigate the CP properties of the $Hf\overline{f}$ coupling is the Higgs decay to taus through tau polarisation sensitive variables.

CMS performed a first analysis with the full Run-2 dataset [274] of the transverse spin correlations between the tau leptons in the final state which are sensitive to the CP mixing angle or relative component of the scalar and pseudo scalar couplings of the Higgs boson to taus. These transverse spin correlations are in turn related to the direction of the decay products of the taus.

In the case of the two-body decay of a tau to a charged pion and a neutrino, the transverse momentum component of the charged pions are typically anti-aligned for the case of a scalar decay and aligned for the pseudo-scalar case. The angle between the decay planes as illustrated in Fig. 11.9-(left) is therefore sensitive to the CP-mixing. Given that the tau direction cannot be measured directly, the impact parameter direction is used instead as a proxy, where the impact parameter direction is defined as the direction between the interaction point and the point of closest approach of the pion track. This direction in the rest frame of the Higgs boson are denoted $\lambda^{\pm}$, as shown in Fig. 11.9-(centre). In the case of three-body or more decays of the taus as for example the

decays to a intermediate rho or an $a_1(1260)$ vector mesons which subsequently decay to $\rho \to \pi^+\pi^0$ and $a_1 \to \pi^+\pi^0\pi^0$ respectively, the planes are defined as either as the (π^+, π^0) plane as as shown in Fig. 11.9-(centre) in the case of the ρ decay, or the plane formed by the cahrged pion and a combination of the two neutral pions in the case of the a_1 decay. The discrimination obtained, showing the two extreme fully scalar and pseudo-scalar cases are illustrated in Fig. 11.9-(right). ATLAS performed a similar analysis [275]. The results obtained are the following:

$$\begin{array}{lll} \text{ATLAS} & \varphi_\tau = 9^o \pm 16^o & (0^o \pm 28^o) \quad [274] \\ \text{CMS} & \varphi_\tau = -1^o \pm 19^o & (0^o \pm 21^o) \quad [275] \end{array}$$

It is interesting to note that the precision reached by both experiments is already at the level that was foreseen for HL-LHC by initial studies [276], which yielded a precision ranging between $\pm 18^o$ and $\pm 30^o$.

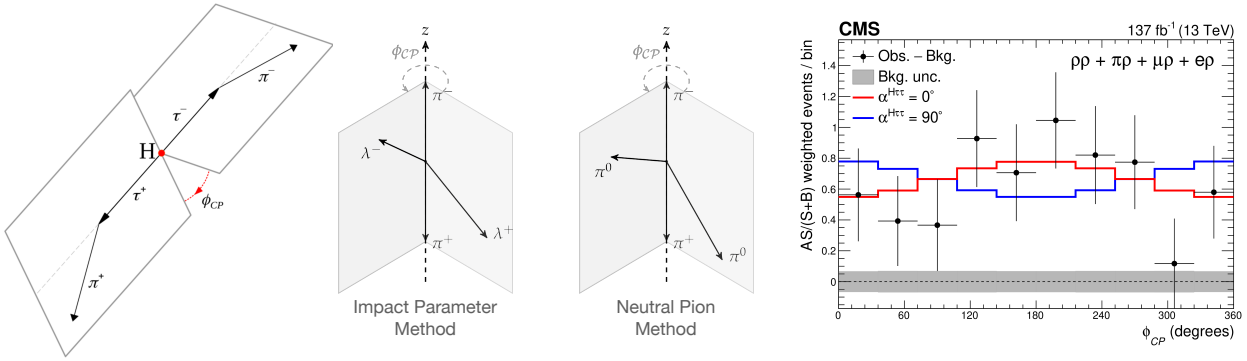

Figure 11.9: Sketch of the definition of the φ_{CP} angle for for the decays $\tau^\pm \to \pi^\pm \nu_\tau$ (left) and the definition at reconstruction level of φ_{CP} observables (center). The distribution weighted per tau decay categories of the φ_{CP} observables, including the expected distributions for the expected pure scalar or pure pseudo scalar cases.

11.4.2 *Off-shell couplings of the Higgs boson*

In the dominant ggF production mode with a subsequent decay of the Higgs boson into a pair of electroweak vector bosons, the production cross section of an off-shell Higgs boson is known to be sizeable. This follows as a consequence of the enhanced couplings of the Higgs boson to the longitudinal polarization of the massive vector bosons at high energy.

The off-shell to on-shell cross section ratio is approximately 8% in the SM [277]. This part of the 'off-shell' regime corresponding to the exchange of a Higgs boson as a propagator and not as a narrow mass state is very interesting as it is sensitive to physics beyond the SM. Still, the Higgs contribution to VV production at large invariant mass remains small compared to the background. In addition, the difficulty in the off-shell VV analysis, beyond the small signal-to-background ratio, is due to a large negative interference between the signal and the $gg \to VV$ background.

The resulting presence of a SM Higgs boson signal in the far off-shell domain results in a deficit of events with respect to the expectation from background only events. It is only when the off-shell couplings of the Higgs boson are larger than expected in the SM that the presence of a signal appears as an excess over the background expectation. One additional intricacy arises from the precision in the prediction of the rate for $gg \to VV$, a loop process at lowest order, and its interference with the signal.

Besides this 'continuum' $gg \to VV$ background with which the 'off-shell' Higgs process interferes, the largest background comes from the $qq \to VV$ production, making this analysis very challenging.

It is interesting to note that, in this regime, the Higgs boson is studied as a propagator and not as a particle. The measurement of its off-shell couplings is therefore absolute and does not rely on the knowledge of the total Higgs boson width. The off-shell coupling constraints can then be used to indirectly constrain the width of the Higgs boson, under specific assumptions detailed in Section 11.4.3.3.

This measurement has been carried out in the $H \to ZZ \to 4\ell$, $H \to ZZ \to \ell\ell\nu\nu$ and $H \to WW \to \ell\nu\ell\nu$ channels, via the ggF, VBF and VH production modes. To enhance the sensitivity of the analysis, the knowledge of the full kinematics of the events is important. In particular the signal and the background can be further distinguished by the invariant mass of the VV system, which is more accurately accessible in the $H \to ZZ \to 4\ell$ channel. Angular distributions also play an important role in this analysis. For these reasons, the $H \to ZZ^{(*)} \to 4\ell$ channel is significantly more sensitive than $H \to WW^{(*)} \to \ell\nu\ell\nu$.

Limits on the off-shell rates have been reported for the two channels by ATLAS [278] and CMS [279] with Run-1 data. The combined results, assuming that the off-shell rates in the ZZ and WW channels scale equally, are given for two different hypotheses on the VBF production rate: fixing it to its SM value or scaling it as the gluon fusion rate. The observed (expected) limits on the off-shell rate fraction with respect to its SM expectation is 6.7 (9.1) for ATLAS [278] with the VBF rate fixed to its SM value and 2.4 (6.2) for CMS [279] where no assumption is made on the relative production rates of gluon-fusion and VBF. In both cases, the custodial symmetry is assumed and the ratio of the rates in the ZZ and WW decays are fixed to those of the SM. Results without this assumption have also been reported in Ref. [279].

The situation using the Run-2 data has significantly changed. Both ATLAS [280] and CMS [281] have performed off-shell Higgs boson analyses to constrain the off-shell Higgs boson production rates with the full Run-2 datasets using the $H \to ZZ^*$ channel. The results obtained have already reached an impressive sensitivity. Both experiments have considered two independent off-shell contributions, the first corresponding to the ggF production denoted $\mu_{\mathrm{g,off-shell}}$ and the second corresponding the VBF and VH denoted $\mu_{\mathrm{V,off-shell}}$. For simplicity we will report only the results considering $\mu_{\mathrm{g,off-shell}} = \mu_{\mathrm{V,off-shell}} = \mu_{\mathrm{off-shell}}$ here.

The first striking result is that both experiments exclude the background-only hypothesis $\mu_{\mathrm{off-shell}} = 0$ with a significance of 3.2σ (2.2σ) observed (expected) for ATLAS [280] and 3.6σ for CMS [281]. This corresponds to a first evidence for the off-shell production of a Higgs boson, through the measurment of a significant deficit in the overall $gg \to VV$ production.

The measured off-shell signal strengths $\mu_{\mathrm{off-shell}}$ are the following:

$$\begin{aligned} \text{(ATLAS)}\ \ \mu_{\mathrm{off-shell}} &= 1.1^{+0.7}_{-0.6}\ \text{(obs)}\ \ [1.00^{+0.9}_{-0.9}\ \text{(exp)}], \\ \text{(CMS)}\ \ \mu_{\mathrm{off-shell}} &= 0.74^{+0.56}_{-0.38}\text{(obs)}\ \ [1.00^{+1.00}_{-0.84}\ \text{(exp)}]. \end{aligned} \tag{11.24}$$

11.4.3 *The Higgs boson width*

In the SM, the Higgs boson width is very precisely predicted once the Higgs boson mass is known. For a mass of 125 GeV, the Higgs boson has a very narrow width of 4.1 MeV [40]. It is dominated by the fermionic decays partial width at approximately 75%, while the vector boson modes are suppressed and contribute 25% only.

At the LHC or the Tevatron, in all production modes, only the cross sections times branching fractions can be measured. As a consequence, the total width of the Higgs boson cannot be directly derived form the measurements of Higgs boson rates without additional assumptions. Direct constraints on the Higgs boson width are much larger than the expected width of the SM Higgs boson.

11.4.3.1 *Direct constraints*

Analyses of the reconstructed mass line-shape in the two channels with a good mass resolution, the $H \to \gamma\gamma$ and $H \to ZZ^{(*)} \to 4\ell$ channels, allow for a direct measurement of the width of the SM Higgs boson. The intrinsic mass resolution in these channels is about 1–2 GeV, much larger than the expected width of the SM Higgs boson. As a result, only upper limits on the Higgs boson width have been set by ATLAS [282] and more recently CMS [152]. The two main challenges of direct constraints on the width through the measurement of the line-shape are: (i) the modelling of resolution uncertainties and (ii) the modelling of the interference between the signal and the continuum background which can be sizeable for large widths, in particular in the range where direct constraints are set. These challenges affect mostly the diphoton channel. Given that these interference effects are small with respect to the individual channels sensitivity, they are neglected in deriving constraints on the total width. The combined constraints, however, being more precise, could be affected by the interference. Direct lineshape measurements provide the most unambiguous access to the Higgs boson width, however constraints are still two orders of magnitude larger than the expected SM width. The current results are fully compatible with the SM hypothesis. The most stringent limit is obtained by CMS of 330 MeV at 95% CL [152].

Another direct constraint on the Higgs boson width can be obtained, in the $H \to ZZ^{(*)} \to 4\ell$ channel, from the measurement of the average lifetime of the Higgs boson calculated from the displacement of the four-lepton vertex from the beam spot. This analysis has been carried out by CMS (see references in Ref. [141]), using the measured decay length. The measured $c\tau_H$ is $2^{+25}_{-2}\,\mu$m, yielding an observed (and expected) limit at the 95% CL of $c\tau_H < 57(56)\,\mu$m. From this upper limit on the lifetime of the Higgs boson, the 95% CL lower limit on its width is $\Gamma_H > 3.5 \times 10^{-12}$ GeV.

11.4.3.2 *Indirect constraints from mass shift in the diphoton channel*

In the diphoton channel, it was noticed in Ref. [283], that the effect of the interference between the main signal $gg \to H \to \gamma\gamma$ and the continuum irreducible background $gg \to \gamma\gamma$, taking into account detector resolution effects, is responsible for a non negligible mass shift. The size of the mass shift depends on the total width of the Higgs boson and it was suggested that measuring this mass shift could provide a constraint on the width [283]. It was further noticed that the mass shift has a dependence also on the diphoton transverse momentum. The total width of the Higgs boson could therefore be constrained using the diphoton channel alone.

Further studies were performed by ATLAS to estimate the size of the expected mass shift [284]. The expected shift in mass in the diphoton channel is 35 ± 9 MeV for the SM Higgs boson. Very preliminary studies of the sensitivity of this method to estimate the width of the Higgs boson in the High-Luminosity regime have been made by ATLAS [285] and yield an expected 95% CL upper limit on the total width of approximately 200 MeV from 3 ab^{-1} of 14 TeV data.

11.4.3.3 *Indirect constraints from on-shell rate in the diphoton channel*

In the diphoton channel, it was noticed in Ref. [286], that the interference between the main signal $gg \to H \to \gamma\gamma$ amplitude and the continuum irreducible background $gg \to \gamma\gamma$ amplitude generates non-negligible change in the on-shell cross sections, as a result of the existence of a relative phase between these amplitudes. The size of this on-shell interference effect depends on the total width of the Higgs boson and it was suggested that measuring this on-shell cross section precisely could provide a constraint on the Higgs total width. This interference effect yields a reduction of around 2% for the $gg \to H \to \gamma\gamma$ cross section measurement in the SM. The current evaluation of this interference effect is performed at NLO and has a $^{+50\%}_{-30\%}$ uncertainty, due to the fact that the large relative phase is driven by the two-loop $gg \to \gamma\gamma$ background amplitude [283, 286]. This on-shell interference effect has a dependence on the p_T of the diphoton system and the photon polar angle in the diphoton rest frame, which can be further exploited to improve the measurement to

constrain the Higgs total width.

Taking the ratios of the on-shell cross section of Higgs boson to diphoton channel and the cross section of Higgs boson to four-leptons channel where the interference effect is negligible could put a bound on the Higgs boson total width. This ratio is free from many dominant sources of systematic uncertainties for cross section measurements, i.e., PDF uncertainty and luminosity uncertainty, and can be further improved by the accumulation of the LHC data. From this cross section ratio measurement alone, a preliminary estimation of the current limit from this interference effect with current 30% precision puts an upper bound of 800 MeV on the Higgs boson total width and the limit improves to 60 MeV with 3 ab^{-1} of 14 TeV data [286, 287].

11.4.3.4 *Indirect constraints from off-shell couplings*

Using simultaneously on-shell and off-shell measurements in the VV channels, it was noticed [277,288] that the total width of the Higgs boson could be constrained. This can be illustrated from the parametrisation of the signal strength measurements both on-shell ($\mu_{\text{on-shell}}$) and off-shell ($\mu_{\text{off-shell}}$) as a function of the couplings modifiers κ_g and κ_V parameterizing the main process $gg \to H \to VV$ (see Section 11.5.1 for the definition of these coupling modifiers). The on-shell and off-shell signal strengths can be written as:

$$\mu_{\text{on-shell}} = \frac{\kappa^2_{g,\,\text{on-shell}}\,\kappa^2_{V,\,\text{on-shell}}}{\Gamma_H/\Gamma_{\text{SM}}}, \quad \mu_{\text{off-shell}} = \kappa^2_{g,\,\text{off-shell}}\,\kappa^2_{V,\,\text{off-shell}}. \tag{11.25}$$

A bound on the Higgs boson width can then be obtained from the measurements of the on-shell and off-shell signal strengths. This assumes that no new physics alters the Higgs boson couplings in the off-shell regime, i.e., that the running of its couplings in this energy range does not differ from the Standard Model [289, 290].

Both ATLAS [278] and CMS [281] have used their very strong off-shell production analyses described above, with kinematic event characteristics to further gain in sensitivity to discriminate between the signal and background.

In addition, in the CMS analysis, results are also derived allowing for anomalous couplings of the Higgs boson, therefore reducing the discriminating power of the kinematic variables used in the analysis but reducing the model dependence. The sensitivity already reached at Run 2 is remarkable:

$$\text{(ATLAS)}\ \ \Gamma_H = 4.5^{+3.3}_{-2.5}\ \ [4.1^{+3.8}_{-3.8}\ \text{(exp)}]\ \text{MeV}, \tag{11.26}$$

$$\text{(CMS)}\ \ \Gamma_H = 3.2^{+2.4}_{-1.7}\ \ [4.1^{+4.0}_{-3.5}\ \text{(exp)}]\ \text{MeV}. \tag{11.27}$$

ATLAS and CMS have also performed a study of the prospects for measuring the Higgs boson width mainly in the four lepton channel. Projecting to a luminosity of 3 ab^{-1}, it was concluded that, within assumptions similar to the ones mentioned above and assuming the SM central value, the observed (expected) combined upper limit at the 95% CL on the total width of the Higgs boson would be $3.8\times\Gamma_{\text{SM}}$ ($3.4\times\Gamma_{\text{SM}}$), i.e., the width of the Higgs boson could be constrained with the following precision [118]:

$$\Gamma_H = 4.1^{+0.7}_{-0.8}\,\text{MeV}. \tag{11.28}$$

11.5 Probing the coupling properties of the Higgs boson

As discussed in Section 11.2, within the SM, all the Higgs boson couplings are fixed unambiguously once all the particle masses are known. Any deviation in the measurement of the couplings of the Higgs boson could therefore signal BSM physics.

Measuring the Higgs boson couplings without relying on the SM assumption requires a general framework treating deviations from the SM coherently at the quantum level in order to provide theoretical predictions for relevant observables to be confronted with experimental data. An attempt in that direction has been formalised in the so-called κ-formalism [291], following earlier attempts [292] and initial phenomenological studies of the first hints of the existence of the Higgs boson [293]. In this LO-inspired approach, the SM Higgs boson couplings are rescaled by arbitrary factors, κ's, keeping the same Lorentz structure of the interactions. This formalism allows for simple interpretation of the signal strengths measured in the various Higgs channels. It has been utilised to test various physics scenarios, like the existence of additional new particles contributing to the radiative Higgs boson production and decays, or to probe various symmetries of the SM itself, as for example the custodial symmetry. It only compares the experimental measurements to their best SM predictions and does not require any new BSM computations per se. And, from a more theoretical perspective, its relevance arises from the fact that it actually fully captures the leading effects in single Higgs processes of well motivated scenarios. Still, the κ-formalism has obvious limitations and certainly does not capture the most general deformations of the SM, even under the assumptions of heavy and decoupling new physics. A particularly acute shortcoming at the time Higgs physics is entering a precision era is the lack of proficiency to assert the richness of kinematical distributions beyond simple signal strength measurements. Several extensions and alternative approaches are being developed as part of the activities of the LHC Higgs Cross Section Working Group [43].

The Higgs Pseudo-Observable (HPO) approach [294] allows one to report the data in terms of a finite set of on-shell form factors parametrising amplitudes of physical processes subject to constraints from Lorentz invariance and other general requirements like analyticity, unitarity, and crossing symmetry. These form factors are expanded in powers of kinematical invariants of the process around the known poles of SM particles, assuming that poles from BSM particles are absent in the relevant energy regime. A set of HPOs have been proposed to characterise both the Higgs boson decays and the EW Higgs boson production channels, thus exploring different kinematical regimes. Prospective studies concluded that these HPOs can be measured/bounded at the percent level at the HL-LHC and could therefore be used to constrain some explicit models of new physics.

Another systematic and popular approach to characterise the possible Higgs boson coupling deviations induced by BSM physics is the use of Effective Field Theories (EFT) [295,296]. This approach assumes again that the new physics degrees of freedom are sufficiently heavy to be integrated out, and they give rise to effective interactions among the light SM particles. By construction, an EFT approach cannot systematically account for deviations in Higgs physics induced by light degrees of freedom unless they are added themselves as extra fields in the effective Lagrangians, requiring to know about these light fields beforehand. In Section 11.6, several examples of models with light degrees of freedom affecting Higgs boson production and decay rates will be presented. Like in explicit UV models and unlike the κ-approach, the main advantage of EFTs is their prowess to relate different observables in different sectors and at different energies to constrain a finite set of effective interactions among the SM degrees of freedom. In an EFT, the SM Lagrangian is extended by a set of higher-dimensional operators, and it reproduces the low-energy limit of a more fundamental UV description. It will be assumed that the Higgs boson is part of a CP-even EW doublet, Φ, and that the Lagrangian is an analytic function of the gauge invariant $\Phi^\dagger\Phi$. This scenario is commonly referred as SMEFT. Even though it is not fully established experimentally, this set-up is motivated by the measurements of the Higgs couplings to the different SM particles that show an alignement with their masses, such an alignment naturally follows under this assumption of a linear realisation of the $\mathrm{SU}(2)_L \times \mathrm{U}(1)_Y$ symmetry of the SM. General Lagrangians bypassing

this linear assumption have been explicitly written down, see for instance Ref. [297], and connections with explicit UV models made [298, 299]. They rely on a chiral expansion with a specific power-counting, effectively resumming the expansion in powers of the Higgs field, usually referred as HEFT as opposed to SMEFT.

11.5.1 *Probing coupling properties*

11.5.1.1 *From effective Lagrangians to Higgs observables*

The κ framework, described in detail in Ref. [39, 291], facilitates the characterisation of Higgs coupling properties in terms of a series of Higgs coupling strength modifier parameters κ_i, which are defined as the ratios of the couplings of the Higgs bosons to particles i to their corresponding SM values. The κ framework assumes a single narrow resonance so that the zero-width approximation can be used to decompose the cross section as a product of two factors characterising the production and the decay of the Higgs boson. The κ parameters are introduced by expressing each of the these factors as their SM expectation multiplied by the square of a coupling strength modifier for the corresponding process at leading order:

$$(\sigma \cdot \mathrm{BR})(i \to \mathrm{H} \ \to f) = \frac{\sigma_i^{SM} \kappa_i^2 \cdot \Gamma_f^{SM} \kappa_f^2}{\Gamma_H^{SM} \kappa_H^2} \quad \to \quad \mu_i^f \equiv \frac{\sigma \cdot \mathrm{BR}}{\sigma_{\mathrm{SM}} \cdot \mathrm{BR}_{\mathrm{SM}}} = \frac{\kappa_i^2 \cdot \kappa_f^2}{\kappa_H^2}, \tag{11.29}$$

where μ_i^f is the rate relative to the SM expectation and κ_H^2 is an expression that adjusts the SM Higgs width to take into account the modifications induced by the deformed Higgs boson couplings. When all κ_i are set to 1, the SM is reproduced. For loop-induced processes, e.g. $H \to \gamma\gamma$, there is a choice of either resolving the coupling strength modification in its SM expectation, i.e., $\kappa_\gamma(\kappa_t, \kappa_W)$ or keeping κ_γ as an effective coupling strength parameter.

The κ-framework is the simplest parametrisation directly related to experimental measurements of the Higgs boson production and decay modes. For this reason, it has been widely used by the community. It can also be connected to the SMEFT formalism as follows. Restricting to the EFT directions not probed outside Higgs physics [300], the Higgs boson couplings are written in the unitary gauge as:

$$\begin{aligned}\mathcal{L} = {} & \kappa_Z \frac{m_Z^2}{v} Z_\mu Z^\mu H + \kappa_W \frac{2m_W^2}{v} W_\mu^+ W^{-\mu} H + \kappa_{VV} \frac{\alpha}{2\pi v} \left(\cos^2\theta_W Z_{\mu\nu} Z^{\mu\nu} + 2\, W_{\mu\nu}^+ W^{-\mu\nu} \right) H \\ & + \kappa_g \frac{\alpha_s}{12\pi v} G_{\mu\nu}^a G^{a\mu\nu} H + \kappa_\gamma \frac{2\alpha}{9\pi v} A_{\mu\nu} A^{\mu\nu} H + \kappa_{Z\gamma} \frac{\alpha}{\pi v} A_{\mu\nu} Z^{\mu\nu} H - \sum_F \kappa_F \frac{m_F}{v} \overline{F} F H + \kappa_3 \frac{m_H^2}{2v} H^3 + \ldots .\end{aligned} \tag{11.30}$$

The exact correspondence between the effective coefficients of the dimension-6 operators and the κ's can be found for instance in Ref. [40]. In the SM, the Higgs boson does not couple to massless gauge bosons at tree level, hence $\kappa_g = \kappa_\gamma = \kappa_{Z\gamma} = 0$. Nonetheless, the contact operators are generated radiatively by SM particle loops. In particular, the top quark gives a contribution to the 3 coefficients $\kappa_g, \kappa_\gamma, \kappa_{Z\gamma}$ that does not decouple in the infinite top mass limit (for instance, in that heavy limit, the top quark contribution amounts to $\Delta\kappa_\gamma = \Delta\kappa_g = 1$ [21, 22, 301], while the $W^\pm$ also contributes to κ_γ). Depending on the nature of new physics, these effective couplings can be generated at tree level or only at the radiative/loop level, see Refs. [295, 302–304] for further discussions.

The coefficient for the contact interactions of the Higgs boson to the W and Z field strengths is not independent but obeys the relation

$$(1 - \cos^4\theta_W)\kappa_{VV} = \sin 2\theta_W \kappa_{Z\gamma} + \sin^2\theta_W \kappa_{\gamma\gamma}. \tag{11.31}$$

This relation is a general consequence of the custodial symmetry [305], which also imposes $\kappa_Z = \kappa_W$ at leading order ($\kappa_Z/\kappa_W - 1$ is a measure of custodial symmetry breaking and, as such, is already constrained by electroweak precision data and the bounds on anomalous gauge couplings). When the Higgs boson is part of an $\mathrm{SU}(2)_L$ doublet, the custodial symmetry in the bosonic sector could only be broken by the $\mathcal{O}_T = \frac{1}{2}\left(\Phi^\dagger \overleftrightarrow{D}^\mu \Phi\right)^2$ operator at the level of dimension-6 operators and it is accidentally realised among the interactions with four derivatives, like the contact interactions considered.

The coefficient κ_3 is the trilinear Higgs boson self-coupling parameter which corresponds to the more generic κ_λ self-coupling parameter discussed in Section 11.3.9.1. Before the associated production of a Higgs boson with a pair of top quarks was observed, the Higgs boson coupling to the top quark was only probed indirectly via the one-loop gluon fusion production or the radiative decay into two photons. However, these two processes are only sensitive to the combinations of couplings $(\kappa_t + \kappa_g)$ and $(\kappa_t + \kappa_\gamma)$ and not to the individual couplings. Therefore a deviation in the Higgs boson coupling to the top quark can in principle always be masked by new contact interactions to photons and gluons (and this is precisely what is happening in minimal incarnations of composite Higgs models [306]). The current and still limited sensitivity, of the order of 20%, in the $t\bar{t}H$ channel leaves elongated ellipses in the direction $\kappa_g = \kappa_\gamma = 1 - \kappa_t$.

The operators already bounded by EW precision data and the limits on anomalous gauge couplings modify in general the Lorentz structure of the Higgs couplings and hence induce some modifications of the kinematical differential distributions [307]. A promising way to have a direct access to the effective coefficients of these operators in Higgs physics is to study the VH associated production with a W or a Z at large invariant mass of the VH system [308]. These differential distributions could also be a way to test the hypothesis that the Higgs boson belongs to a $\mathrm{SU}(2)_L$ doublet together with the longitudinal components of the massive electroweak gauge bosons.

11.5.1.2 *Measurements of the Higgs boson coupling properties*

As described in Section 11.3, a framework was developed by ATLAS and CMS [153], individually and together, to combine the very large number of exclusive categories aimed at reconstructing the five main decay modes and the five main production modes of the Higgs boson. The general conclusion of this combination, illustrating the compatibility of the observation with the SM expectations, is given in Section 11.3. The same framework with its master formula, Eq. (11.14), can be used to further measure coupling properties of the Higgs boson under specific additional assumptions.

i. *Interpretations of the experimental data*

The measurements of the coupling properties of the Higgs boson are entirely based on the formalism of the effective Lagrangian described above. Measurements of coupling properties in this framework implies assessing the parameters of the model Eq. (11.30) or combinations of these parameters with different sets of assumptions.

These measurements are carried out with the combination framework described in Section 11.3.6, where the μ_i and μ_f signal strength parameters are further interpreted in terms of modifiers of the SM couplings κ_k where $k \in \{Z, W, f, g, \gamma, Z\gamma\}$ as in Eq. (11.30). The number of signal events per category for the various production modes are typically estimated at higher orders in the analyses but are scaled by these single LO-inspired factors, thus not taking into account possible intricacies and correlations of these parameters through the higher-order corrections. This approximation is valid within the level of precision of current results and their compatibility with the SM expectation.

In this formalism, further assumptions are explicitly made: (i) the signals observed in the differ-

ent search channels originate from a single narrow resonance with a mass of 125 GeV; (ii) similarly to the combination described in Section 11.3.6, the narrow width approximation is assumed (to allow the decomposition of signal yields into products of production and decay signal strengths); (iii) the tensor structure of the couplings is assumed to be the same as that of a SM Higgs boson. This means in particular that the observed state is assumed to be a CP-even scalar as in the SM.

Loop-level couplings such as the $gg \to H$, $H \to \gamma\gamma$ and $H \to Z\gamma$ can either be treated effectively, with κ_g, κ_γ and $\kappa_{Z\gamma}$ as free parameters in the fit or these parameters can be expressed in terms of the know SM field content and as a function of the SM coupling modifiers, in the following way [309] by either scaling cross sections (for κ_g given for a centre-of-mass energy of 13 TeV and a Higgs boson mass of 125 GeV) or partial widths (for κ_γ and $\kappa_{Z\gamma}$ for a Higgs boson mass of 125 GeV):

$$\begin{aligned}
\kappa_g^2(\kappa_t,\kappa_b,\kappa_c) &= 1.042\,\kappa_t^2 - 0.040\,\kappa_t\kappa_b + 0.002\,\kappa_b^2 - 0.005\kappa_t\kappa_c + 0.0005\kappa_b\kappa_c + 0.00002\kappa_c^2,\\
\kappa_\gamma^2(\kappa_t,\kappa_W) &= 1.59\,\kappa_W^2 - 0.66\,\kappa_W\kappa_t + 0.07\,\kappa_t^2,\\
\kappa_{Z\gamma}^2(\kappa_t,\kappa_W) &= 1.12\,\kappa_V^2 - 0.15\,\kappa_V\kappa_F + 0.03\,\kappa_F^2.
\end{aligned} \tag{11.32}$$

It should be noted that the parametrisation of the gluon coupling modifier could also be used to scale the $H \to gg$ partial width and would be different from the cross section parametrisation. However when considered effectively, i.e., without resolving the content of the loop in terms of SM fields, it can be assumed that the scaling behaviour of the production cross section and partial width will be very similar.

The parametrisations are given for a Higgs boson mass hypothesis of 125 GeV (and in the last two expressions, all the Higgs-fermion couplings are assumed to be rescaled by an universal multiplicative factor κ_F). It can be noted from the expression of κ_γ that the coupling of the Higgs boson to photons is dominated by the loop of W bosons, and it is affected by the top quark loop mostly through its interference with the W loop. The sensitivity of the current measurements to the relative sign of the fermion and vector boson couplings to the Higgs boson is due to this large negative interference term. The κ_g parameter is expressed in terms of the scaling of production cross sections and therefore also depends on the pp collisions centre-of-mass energy. The parametrisations of κ_γ and $\kappa_{Z\gamma}$ are obtained from the scaling of partial widths and are only dependent on the Higgs boson mass hypothesis. Experiments use a more complete parametrisation with the contributions from the b-quarks, τ-leptons in the loops [39, 291].

The global fit is then performed expressing the μ_i and μ_f parameters in terms of a limited number of κ_k parameters or their ratios, under various assumptions. The parametrisation for the main production modes are: (i) $\mu_{\text{ggF}} = \kappa_g^2$ for the gluon fusion and an effective coupling of the Higgs boson to the gluons; (ii) $\mu_{\text{VBF},VH} = \kappa_V^2$ for the VBF and VH processes when the W and Z couplings are assumed to scale equally, and $\mu_{\text{VBF}}^2(\kappa_W,\kappa_Z) = (\kappa_W^2\sigma_{WWH} + \kappa_Z^2\sigma_{ZZH})/(\sigma_{WWH} + \sigma_{ZZH})$, when the couplings to the W and Z bosons are varied independently (σ_{WWH} and σ_{ZZH} denote the VBF cross sections via the fusion of a W and a Z boson respectively, the small interference term is neglected); (iii) $\mu_{t\bar{t}H} = \kappa_t^2$ for the $t\bar{t}H$ production mode. Numerically the production modes signal strengths as a function of the coupling modifiers to the SM fields for a centre-of-mass energy of 13 TeV and and Higgs boson mass of 125 GeV are:

$$\mu_{\text{ggF}} = 1.040\kappa_t^2 + 0.002\kappa_b^2 - 0.038\kappa_t\kappa_b, \quad \text{and} \quad \mu_{\text{VBF}} = 0.73\kappa_W^2 + 0.27\kappa_Z^2. \tag{11.33}$$

The decay mode signal strengths are parametrised as $\mu_k = \kappa_k^2/\kappa_H^2$ where $k \in \{Z, W, f, g, \gamma, Z\gamma\}$ denotes the decay mode and κ_H, the overall modifier of the total width that affects all the signal yields. κ_H is a priori an independent parameter. However, when it is assumed that the Higgs boson cannot decay to new particles beyond those of the SM, κ_H can also be treated as an effective

parameter and expressed in terms of the coupling modifiers to the SM field content. Its general expression is:

$$\kappa_H^2 = 0.57\kappa_b^2 + 0.06\kappa_\tau^2 + 0.03\kappa_c^2 + 0.22\kappa_W^2 + 0.03\kappa_Z^2 + 0.09\kappa_g^2 + 0.0023\kappa_\gamma^2. \quad (11.34)$$

The general expression of the total width of the Higgs boson can be written as follows:

$$\Gamma_H = \frac{\kappa_H^2 \Gamma_H^{\rm SM}}{1 - {\rm BR}_{\rm BSM}} \quad (11.35)$$

where $\Gamma_H^{\rm SM}$ is the total width of the SM Higgs boson and ${\rm BR}_{\rm BSM}$ is the branching fraction of the Higgs boson to new particles beyond the SM.

It is worth reminding that, in the absence of a measurement of the Higgs width wich can be accessed through Off-Shell couplings measurements as discussed inSection 11.4.2, LHC requires some hypotheses in order to extract the Higgs couplings from the measured Higgs signal strengths. In particular, one can assume either (i) no BSM particles in the decay, or (ii) any BSM particles in the decay would give rise to invisble signatures and thus be detectable through invisible Higgs boson channels (or in other terms that there is no BSM undetected contribution), or (iii) $|\kappa_V| \leq 1$. These scenarios will be examined below.

Specific parametrisations will be made in order to address the following aspects of the coupling properties of the Higgs boson under different assumptions, depending essentially on two assumptions concerning either the natural width of the Higgs boson, whether it consists of partial width from Standard Model particles only or not, or the effective couplings of the Higgs boson to photons, gluons, $Z\gamma$ and $\gamma^*\gamma$, whether these contributions are parametrised as function of the Standard Model field content in the loops or whether these couplings are considered as effective.

Negative values of couplings are not excluded a priori, but would imply the existence of new physics at a light scale and would also raise questions about the validity of the perturbative treatment of the SM deformations and also about the stability of the vacuum [310]. Since the results are only sensitive to the relative sign of vector bosons with respect to fermions, by convention negative coupling values will only be considered for vector boson couplings. Among the five main Higgs boson decay channels, only the $\gamma\gamma$ is sensitive to the sign of κ_F (or κ_V) through the interference of the W and t loops as shown in Eq. (11.32). The current global fit disfavours a negative value of κ_F at more than five standard deviations. A specific analysis for the Higgs boson production in association with a single top quark has been proposed in order to more directly probe the sign of κ_F (see references in Ref. [141]). All available experimental data show a fair agreement of the SM prediction of the couplings of the Higgs boson to fermions and gauge bosons.

ii. *Coupling measurements and probing BSM physics in loops and in the decay*

Measuring Higgs boson couplings to other Standard Model fields requires either assumptions on the total Higgs boson width, or an assumption on the coupling of the Higgs boson to vector bosons, or a direct constraint on the Higgs boson width as the one obtained from the ratio of off-shell to on-shell Higgs boson couplings. These three cases will be discussed briefly. With the precision reached by analyses discussed in Section 11.3.1, strong assumptions on the BSM content of the loop-induced couplings of the Higgs boson to vector bosons as Hgg, $H\gamma\gamma$ or $HZ\gamma$ are not needed and these couplings can be considered as effective and provide a stringent probe of new fields potentially entering the loop.

Using the full Run-2 dataset and the formalism described in Section i., ATLAS [183] and CMS [184], have performed interpretations of the results presented in Section 11.3.6 to derive measurements of the Higgs boson couplings. These results are summarised in Table 11.8.

Table 11.8: Coupling modifier combined measurements assuming the absence of perceptible new physics in the decay of the Higgs boson. No assumption is made for the loop level couplings of the Higgs boson to gluons and photons which are considered as effective. The last column gives the expected precision at the HL-LHC [118].

	LHC Run 1	ATLAS Run 2	CMS Run 2	HL-LHC (expected)
κ_γ	$0.87^{+0.14}_{-0.09}$	1.01 ± 0.06	1.10 ± 0.08	1.8%
κ_W	$0.87^{+0.13}_{-0.09}$	1.05 ± 0.06	1.02 ± 0.08	1.7%
κ_Z	-0.98 ± 0.10	0.99 ± 0.06	1.04 ± 0.07	1.5%
κ_g	$0.78^{+0.13}_{-0.10}$	0.95 ± 0.07	0.92 ± 0.08	2.5%
κ_t	$1.40^{+0.24}_{-0.21}$	0.94 ± 0.11	1.01 ± 0.11	3.4%
κ_b	$0.49^{+0.27}_{-0.15}$	0.89 ± 0.11	0.99 ± 0.16	3.7%
κ_τ	$0.84^{+0.15}_{-0.11}$	0.93 ± 0.07	0.92 ± 0.08	1.9%
κ_μ	–	$1.06^{+0.25}_{-0.30}$	1.12 ± 0.21	4.3%
$\kappa_{Z\gamma}$	–	$1.38^{+0.31}_{-0.36}$	1.65 ± 0.34	9.8%

The results above are obtained under the assumption that the Higgs boson decays only to SM particles. The degeneracy that originates from the fact that at LHC only production cross sections times branching fractions are measured is embodied in the degeneracy between all κ factors and κ_H. It is interesting to note that in order to measure all couplings to be in agreement with the Standard Model model value requires that any deviation in the Higgs boson total width or κ_H be precisely compensated by all couplings to Standard Model fields in the same fashion. This is often referred to a flat direction, meaning that all the couplings are scaled by a factor α and the Higgs boson width by a factor α^2. A model realising such flat direction is given in [311]. It requires the introduction of a scalar field which decays for instance light hadrons which would not be detectable in the current experimental setups and are referred to as 'undetected'. It cannot be 'invisible' as it would otherwise be constrained by direct invisible Higgs boson constraints. The model parameters would also have to lead to couplings of the Higgs to Standard Model fields to be larger than in the Standard Model and a coupling of the Higgs boson to the scalar which will have to match the scaling of the Standard Model couplings. The former condition is exotic and the later requires a 'conspiracy'.

As we have previously discussed, the flat direction can however be removed in two ways. The first is to impose $\kappa_V \leq 1$. This will induce a constraint on κ_H which can be seen for instance from processes such as VBF Higgs production with subsequent decays to two vector bosons which are proportional to κ_V^4/κ_H^2. As was discussed, BSM scenarios yielding $\kappa_V > 1$ can be considered exotic. The measurements using this constraints from the ATLAS experiment are shown in Fig. 11.10 (left). The second is to use the Higgs boson width derived from the off-shell Higgs boson production measurements. In this specific interpretation, the flat off-shell Higgs measurement constrain the visible, invisible and undetected branching fractions. The 'visible' branching fraction corresponds to the Higgs branchings to Standard Model fields. The invisible branching fraction is constrained from 'invisible' Higgs searches. The flat direction is therefore represented by the 'undetected' branching fraction which is then constrained by the off-shell Higgs boson measurements. This constraint was used in previous Higgs boson couplings measurements (see references for example the partial Run-2 combination performed in [312]).

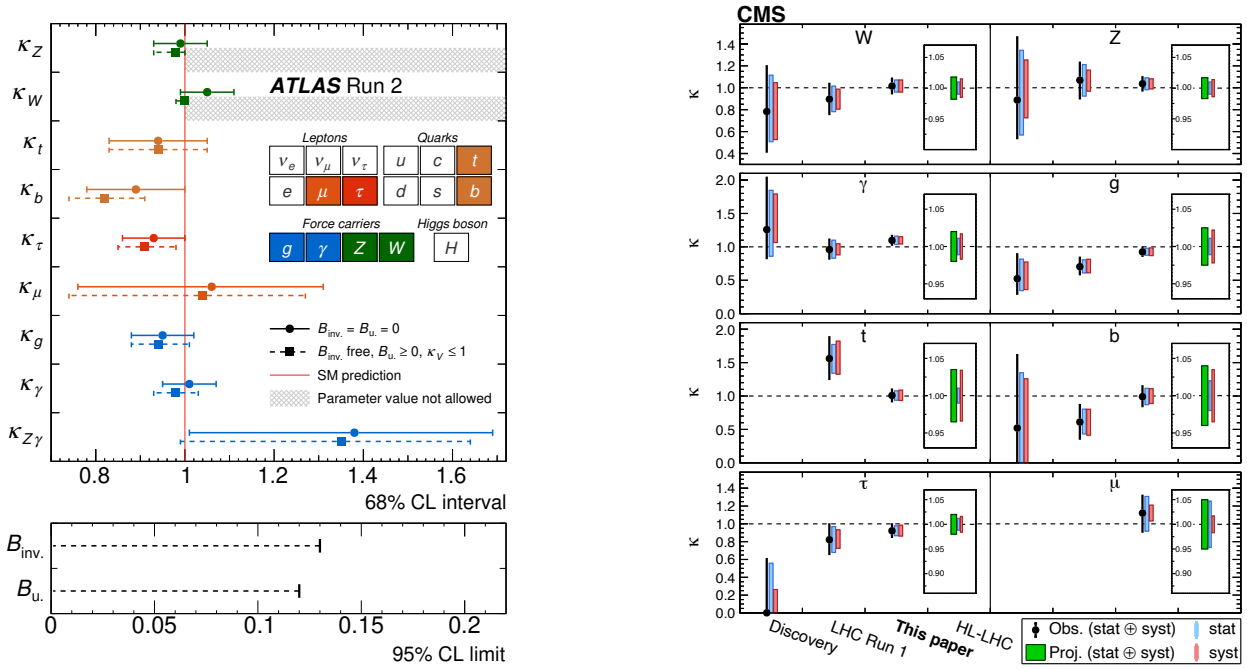

Figure 11.10: ATLAS [183] (left) and CMS [184] (right) combined measurements of coupling modifiers with various assumptions. The ATLAS measurments also use the off-shell Higgs measurements.

Interpretations which are less sensitive to modelling systematic uncertainties and require no constraints on the natural width of the Higgs bosons have been considered, either through the ratio of cross section and branching ratios (see results in Ref. [141]) or through a more generic approach to avoid the degeneracy in the measurement of the coupling modifiers, probing the coupling properties of the Higgs boson through ratio of couplings. In the latter model, the cross section times branching fraction of the $gg \to H \to ZZ$ process is parametrised as a function of a single coupling modifier:

$$\kappa_{gZ} = \kappa_g \times \frac{\kappa_Z}{\kappa_H}. \tag{11.36}$$

Then all combination signals can be parametrised with the following ratios of coupling modifiers: (i) the $\lambda_{Zg} = \kappa_Z/\kappa_g$ ratio which is mainly probed by the measurements of the VBF and ZH production; (ii) the $\lambda_{tg} = \kappa_t/\kappa_g$ ratio constrained by the $t\bar{t}H$ production process; (iii) the $\lambda_{WZ} = \kappa_W/\kappa_Z$ ratio mainly probed by the WW and ZZ decay modes; (iv) the $\lambda_{\tau Z} = \kappa_\tau/\kappa_Z$ ratio constrained by the $\tau^+\tau^-$ channel; (v) the $\lambda_{bZ} = \kappa_b/\kappa_Z$ ratio probed mainly by the $VH(b\bar{b})$ channels; and (vi) the $\lambda_{\gamma Z} = \kappa_\gamma/\kappa_Z$ ratio constrained by the diphoton channel. In this parametrisation, the ZZ channel plays an important normalisation role (the results are discussed in detail in the previous edition of this review [141]).

11.5.1.3 *Differential cross sections*

To further characterise the production and decay properties of the Higgs boson, with the increase in size of the LHC datasets, measurements of fiducial and differential cross sections are being carried out by ATLAS and CMS both at Run 1 (the references can be found in the previous edition of this review [141]) and Run 2 and in several channels [313–316]: the diphoton, the four leptons, the WW, $b\bar{b}$ and $\tau^+\tau^-$ channels.

The definition of a fiducial volume as close as possible to the reconstruction level selection

criteria is very important, as it will minimise the model dependence from possible variations in the signal reconstruction efficiencies. Minimising model dependence of unfolded fiducial differential cross section measurements is also key to ensure their usefulness to further probe and tune more accurate models in the future.

While strict fiducial requirements are key to minimise model dependence, if the decay products are part of the fiducial volume definition, these make combinations of decay channels impossible. To gain precision in the measurement of the production properties of the Higgs boson, the fiducial volume can be defined in terms of the Higgs boson distributions, while its decay channels and properties are fully integrated. This has been used to combine differential cross section for instance in the transverse momentum of the Higgs boson. Such hybrid approaches are also discussed in Section 11.5.1.5.

A large number of observables have been studied aiming at probing the accuracy of the modelling of the Higgs boson production simulations as well as measuring the properties of the Higgs boson.

The measured differential cross section in the Higgs boson transverse momentum by ATLAS and CMS using the full Run-2 datasets are illustrated in Fig. 11.11 [314, 315, 317].

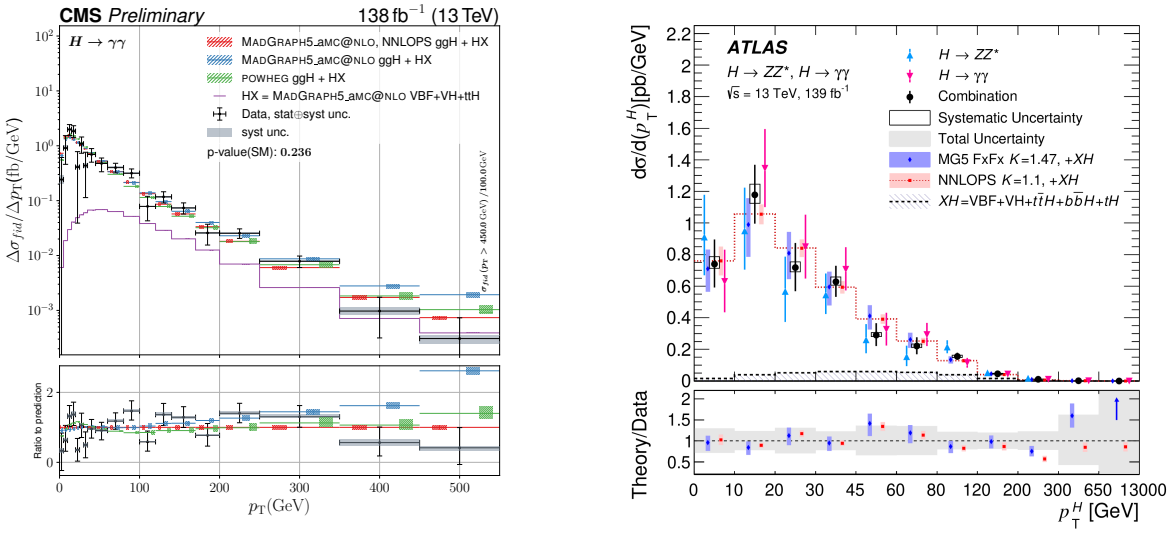

Figure 11.11: (Left) Fiducial differential cross sections in Higgs boson transverse momentum in the $H \to \gamma\gamma$ channel from the CMS experiment [315]. (Right) Partially fiducial combined cross sections using the $H \to \gamma\gamma$ and $H \to 4\ell$ channels from the ATLAS experiment [314].

The Higgs boson transverse momentum distribution is of particular importance to probe new physics in the Higgs production. An example of interpretations that can be made using these measurements is the constraints on the b and charm quark Yukawa couplings through their impact on the production, both via the loop-level gluon fusion contribution or the $gg \to b\bar{b}H, c\bar{c}H$ processes. These results are also combined with the direct search for the $VH(b\bar{b})$ process and shown in Fig. 11.12. It is interesting to compare the constraint, $|\kappa_c| < 8.5$, from the $VH(c\bar{c})$ production analysis alone and the limit obtained using only the differential distribution which is approximately the double of the direct search limit as well as the limit that also uses the normalisation which yields $|\kappa_c| < 2.3$. The latter indirect limits assume that $\kappa_b = 1$. This shows the already good strength of the shape analysis as well as the limit coming from the parametrisation of the normalisation in the $H \to \gamma\gamma, 4\ell$ decay channels. The constraint coming from the normalisation is due to the

modification of the total width from from the charm and b quark couplings [314].

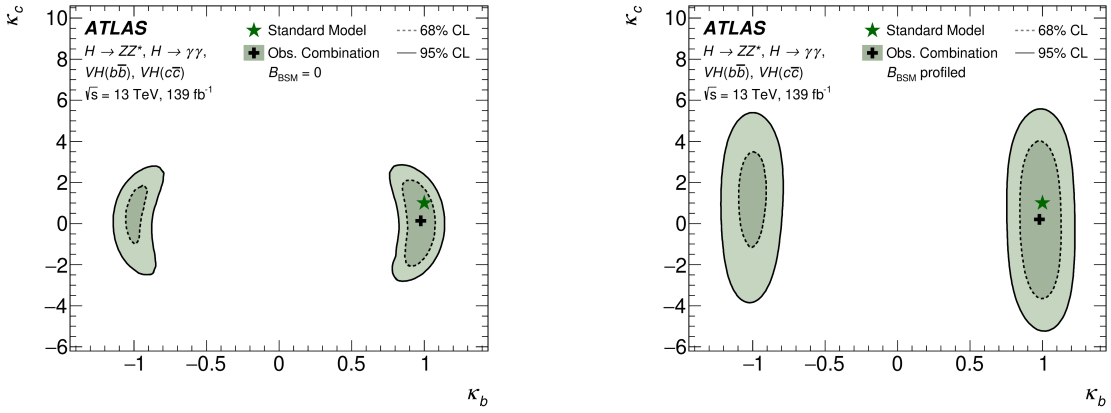

Figure 11.12: Measured likelihood contours for the κ_b and κ_c parameters from a simultaneous fit of the direct search for $VH(b\bar{b}, c\bar{c})$ analyses and the measurement of the differential cross section in transverse momentum in the $H \to \gamma\gamma, 4\ell$ channels, using the overall normalisation of the cross sections parametrised as a function of the κ_b and κ_c couplings and assuming no non-Standard Model contributions to the total width of the Higgs boson (left) and using only the differential shape in transverse momentum [314].

11.5.1.4 *Constraints on non-SM Higgs boson interactions in an effective Lagrangian*

An example of the possible use of differential cross sections in constraining non-SM Higgs boson couplings in an EFT is given by ATLAS [318]. In this analysis, differential cross section measured in the diphoton channel are used to constrain an effective Lagrangian where the SM is supplemented by dimension six CP-even operators of the Strongly Interacting Light Higgs (SILH) formulation [295] and corresponding CP-odd operators. The diphoton differential cross sections are mainly sensitive to the operators that affect the Higgs boson interactions with gauge bosons. CMS has also recently analysed [313] the Higgs boson transverse momentum distribution to constrain the Higgs boson couplings to top, bottom, and charm quarks as well as the effective coupling to gluons. This analysis is, however, not performed in an EFT framework.

The differential distributions used in this combination are: (i) the transverse momentum of the Higgs boson, (ii) the number of reconstructed jets produced in association with the diphoton pair, (iii) the invariant mass of the diphoton system and (iv) the difference in azimuthal angle of the leading and sub-leading jets in events with two or more jets. This analysis shows how differential information significantly improves the sensitivity to dimension-6 operators.

11.5.1.5 *Simplified Template Cross Sections (STXS)*

An overarching subject of discussion between the theory and experimental communities in the field of Higgs physics has been how experimentalists could best communicate their results to be most efficiently used by others for further interpretation. The commonly used practice is that results are given at particle level within a well-defined fiducial volume of phase space. The fiducial volume is usually defined close enough to the experimental reconstruction to minimise the possible variations of the reconstruction efficiency within the particle level fiducial volume. In this way, results minimise their dependence on theoretical uncertainties.

ATLAS and CMS have produced fiducial and unfolded cross sections based on all objects re-

constructed in the events. These measurements could be used for further interpretation. However, performing a proper combination of channels taking into account all experimental systematic uncertainties is non trivial and given the number of channels, combinations are very involved. A proposal [40, 319] was made by the LHC Higgs Working Group to produce results in each decay channel with a well defined fiducial phase space of the Higgs boson (and not its decay products) and for other associated objects pertaining to all channels, such as jets and missing transverse momentum (MET). The definition of the fiducial regions is motivated by maximising the experimental sensitivity, isolating possible BSM effects, and minimising the dependence on theoretical uncertainties. The number of regions is also minimised to avoid the loss of experimental sensitivity. The observables that are measured in this approach are still the standard production cross sections (the gluon fusion, the vector boson fusion, the VH and $t\bar{t}H$ associated production modes) within the defined fiducial volumes.

This approach is hybrid. It is fiducial on specific objects to reduce the theory dependence and inclusive in the Higgs kinematics in order to allow for a more straightforward combination. This approach also allows the use of multivariate techniques to enhance the sensitivity within given fiducial regions, at the expense of a greater extrapolation and therefore increased model dependence.

The currently used Simplified Template Cross Sections (STXS) scheme covers, with a limited number of bins, the ggF process in four categories in number of jets (0, 1, 2 and 2 VBF-like jets, where VBF-like means a selection of two high invariant mass jets with large pseudo rapidity difference) further subdivided in four transverse momentum categories covering the full spectrum with the last bin being inclusive for $p_T > 200\,\text{GeV}$. The VH process is subdivided in two categories depending on the number of reconstructed charged leptons corresponding to the decays of either a W boson or a Z boson, and two bins in transverse momentum. VBF and hadronic VH categories are defined using jet cuts and two bins in transverse momentum.

Measurements in this framework have been made in various decay channels. The first measurements have been performed in the main Higgs boson discovery channels. ATLAS and CMS have produced measurements of the diphoton and the 4ℓ channels with Run-2 data [258, 314, 320–325].

The ATLAS and CMS collaborations have also performed measurements of the STXS in the $H \to W^+W^-$ decay channel [326, 327].

CMS has also carried out a measurement of the STXS in the $H \to \tau^+\tau^-$ decay channel targeting the high transverse momentum of the Higgs boson [156], in particular in the channel where the Higgs boson is produced with one jet of transverse energy in excess of 200 GeV.

ATLAS [328] has made a measurement of the STXS aiming at the VH production mode in the $H \to b\bar{b}$ decay mode at high transverse momentum of the vector boson above 250 GeV, where the discrimination of the background further increases.

A combination of STXS across decay channels has also been carried out by ATLAS with the full Run-2 dataset [183, 329, 330].

11.5.2 *Effective Lagrangian framework*

The SMEFT has the same field content and it respects the same linearly-realised $\text{SU}(3)_C \times \text{SU}(2)_L \times \text{U}(1)_Y$ local symmetry as the SM. The difference is the presence of operators with canonical mass-dimension d larger than 4. These are organised in a systematic expansion in d, where each consecutive term is suppressed by a larger power of a high mass scale. Assuming baryon and lepton number conservation, the most general Lagrangian takes the form

$$\mathcal{L}_{\text{eff}} = \mathcal{L}_{\text{SM}} + \sum_i c_i^{(6)} \mathcal{O}_i^{(6)} + \sum_j c_j^{(8)} \mathcal{O}_j^{(8)} + \cdots . \tag{11.37}$$

The contribution of the higher order operators of dimension d to physical amplitudes is suppressed by $(E/\Lambda)^{d-4}$, where E is the relevant energy scale of the process and Λ is the energy scale sup-

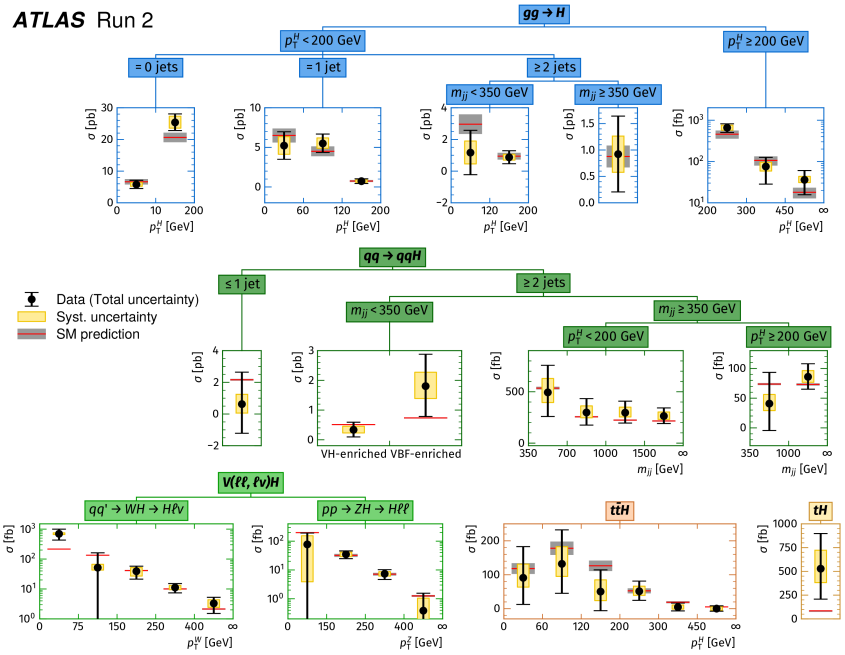

Figure 11.13: Simultaneous combined measurement of simplified template cross sections assuming SM branching fractions of the Higgs boson [183].

pressing the higher-dimensional operators. The Wilson coefficients $c_i^{(d)}$ encode the virtual effects of the heavy new physics in low-energy observables. Their precise forms in terms of masses and couplings of the new particles can be obtained via matching with the ultraviolet (UV) completion of the SM [331–334], or inferred using specific power-counting rules [295, 335].

The list of dimension-6 operators was first classified in a systematic way in Ref. [336] after the works of Ref. [337]. Subsequent analyses pointed out the presence of redundant operators, and a minimal and complete list of operators was finally provided in Ref. [338][3]. For a single family of fermions, there are 76 real ways to deform the SM generated by 59 independent operators. With the 3 families of fermions of the SM, flavour indices can be added to these 59 operators, and furthermore, new operator structures, that have been dismissed by means of Fierz transformations in the single family case, have to be considered, for a total of 2499 real deformations [341].

The numbers of operators to constrain can be reduced by imposing suitable flavour assumptions. Inspired by flavour physics, a $\mathrm{U}(2)_q \times \mathrm{U}(2)_u \times \mathrm{U}(2)_d \times \mathrm{U}(3)_l \times \mathrm{U}(3)_e$ symmetry can be enforced to impose a flavour symmetry in the first two quark generations and all three lepton generations. ATLAS performed a detailed analysis of Higgs and EW data from LEP/SLD and LHC. Under the previous flavour assumption, 22 operators are affecting Higgs observables alone, 22 operators are affecting EW precision observables alone and 11 operators are affecting both sets of observables simultaneously. Dedicated samples representing SM, linear, and quadratic effects of dimension-six operators are generated at leading order using `MadGraph5_aMC@NLO` and `SMEFTsim`. Events are interfaced to `Pythia 8` to simulate parton shower and hadronization. The decays of bottom and charm hadrons are performed by `EvtGen`. For the loop-induced processes, calculations are performed with `SMEFTatNLO`, which allows for the calculation of NLO QCD corrections, instead of `SMEFTsim`. Effects of dimension-six operators on background processes are usually not taken into account except in the analysis of VBF Z measurement and of WW production. The results

[3] Complete enumerations of d=8 operators have been obtained [339] and some preliminary constraints on peculiar subsets of these operators have been derived from experimental measurements [340]. Still, in this review, the EFT Lagrangians will be truncated at the level of dimension-6 operators.

are displayed in Fig. 11.14 [342]. The current measurements cannot currently constrain simultaneously all SMEFT Wilson coefficients as numerous degrees of freedom are not contrained by the data. One option is to fit a limited (typically one) coefficient while fixing the others. Another approach as shown in Fig. 11.14 is to perform a Principal Component Analysis (PCA) which

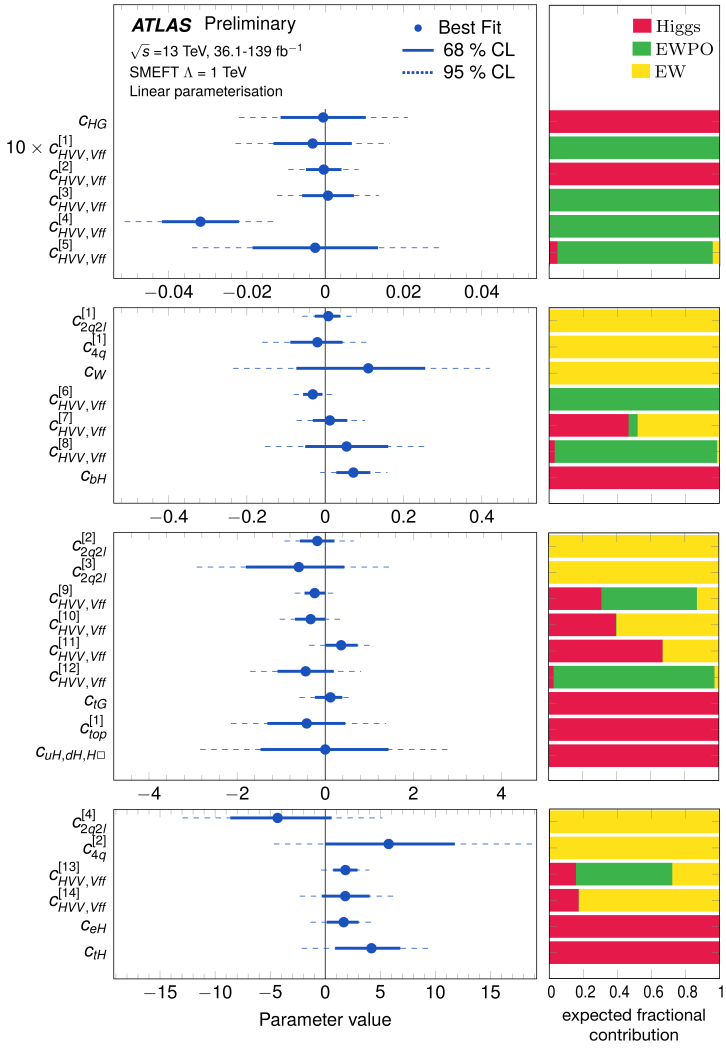

Figure 11.14: Constraints on Wilson coefficients from the combined LHC+EWPO analysis, presented in four blocks with different x-axis ranges. Right-hand side panel shows the contribution of each input measurement group to the eigenvector constraint in the Gaussian approximation.

will identify the sensitive and the flat directions of the likelihood and compute a modified basis corresponding to a linear combination of the SMEFT coefficients [342]. For this reason the results displayed in Fig. 11.14 illustrate coefficients with several indices, which correspond to the main Wilson coefficients represented in a given direction of the PCA analysis. The superscript represent a numbering of different linear combinations with similar coefficients. These results show the excellent agreement between measurements and the Standard Model expectations projected onto SMEFT sensitive directions. The largest discrepancy is observed for the $c^{[4]}_{HVV,Vff}$ coefficient which is driven by the longstanding discrepancy in the $A^{0,b}_{FB}$ measurements at LEP. In this paper [342], ATLAS has performed both fits in the linear and quadratic parametrisations of SMEFT effects

corresponding to taking into account the interference between SM and SMEFT only or the entire SMEFT effect (including the quadratic SMEFT contributions) respectively.

Phenomenological studies [343, 344] have also combined Higgs, diboson, and top quark production and decay measurements from the LHC and LEP to produce global fit of SMEFT at the dimension-6 order. Automated codes like or `Matchete` [334] or `Matchmakereft` [333] allows one to match explicit UV models onto SMEFT and hence to interpret the global EFT fit to directly constrain these UV models.

11.6 New physics models of EWSB in the light of the Higgs boson discovery

The discovery of a light scalar with couplings to gauge bosons and fermions that are consistent with SM predictions, together with the slow running of the Higgs boson self-coupling at high energies allow one to consider the SM as a valid perturbative description of nature all the way to the Planck scale. This picture is admittedly very attractive, but it posits that the Higgs boson is an elementary scalar field, whose mass has quantum sensitivity to possible new physics scales. This EW/Higgs naturalness problem [6] has become much more definite after the Higgs boson discovery.

There are two broad classes of models addressing the naturalness problem[4]. One is based on SUSY [7] (for recent reviews, see Refs. [8, 9]). This is a weakly coupled approach to EWSB, maintaining the perturbativity of the SM, and, the Higgs boson remains elementary and the corrections to its mass are screened at the scale at which SUSY is broken so the value of the weak scale remains insensitive to the details of the physics at higher scales. These theories predict at least three neutral Higgs particles and a pair of charged Higgs particles [23]. One of the neutral Higgs bosons, most often the lightest CP-even one, has properties that can resemble those of the SM Higgs boson (at least in some regions of the parameter space referred to as the alignment limit [346, 347], which in the case of sufficiently heavy additional Higgs bosons is dubbed the decoupling limit [348, 349]). Such scalar is referred to as a SM-like Higgs boson, meaning that its couplings are close to the ones predicted in the SM. The other approach invokes the existence of strong interactions at a scale of the order of one TeV or above and these new interactions induce the breaking of the electroweak symmetry [350]. In the original incarnation, dubbed technicolor, the strong interactions themselves trigger EWSB without the need of a Higgs boson. Another possibility, more compatible with the ATLAS and CMS discovery, is that the strong interactions produce four light resonances identified with the Higgs doublet and EWSB proceeds through vacuum misalignment [10] (see Refs. [11, 12] for recent reviews). In that case, the Higgs boson itself has a finite size and thus never feels the UV degrees of freedom that would otherwise have dragged its mass to much higher scales. The Higgs boson could also correspond to the Goldstone boson associated with the spontaneous breaking of scale invariance, see Ref. [351] and references therein. However, this dilaton/radion scenario now requires a jumbled model-building to be consistent with the constraints from the coupling measurements. All these BSM scenarios can have important effects on the phenomenology of the Higgs boson. Also, in each case, the role of the Higgs boson in the unitarisation of scattering amplitudes is shared by other particles which remain targets of experimental searches.

The realisation of SUSY at low energies has many good qualities that render it attractive as a model of new physics. First of all since, for every SM degree of freedom, there is a superpartner of different spin but of equal mass and effective coupling to the SM-like Higgs boson, in the case of exact SUSY, an automatic cancellation of quantum corrections to the Higgs mass parameter holds. In practice, it is known that SUSY must be broken since no superpartners of the SM particles have been observed so far. The mass difference between the precise value of the mass of any particle and that of its corresponding superpartner is proportional to the correlated soft SUSY breaking parameter, generically called $M_{\rm SUSY}$. The quantum corrections to the Higgs boson mass parameter

[4] Another solution to the naturalness problem is to lower the fundamental scale of quantum gravity, like for instance in models with large extra-dimensions, see Ref. [345].

are proportional to $M^2_{\rm SUSY}$, and provided $M_{\rm SUSY}$ is of order of a few TeV, the low energy mass parameters of the Higgs sector become insensitive to physics at the GUT or Planck scale. Another interesting feature of SUSY theories is related to the dynamical generation of EWSB [352]. In the SM, a negative Higgs mass parameter, m^2, needs to be inserted by hand to induce EWSB, see Eq. (11.1). In SUSY, instead, even if the relevant Higgs mass parameter is positive in the ultraviolet, it may become negative and induce EWSB radiatively through the strong effect of the top quark-Higgs boson coupling in its renormalisation group evolution [352].

In the following, the Higgs sector will be explored in specific SUSY models. In all of them, it is often possible to find regions of the parameter space that accommodate one neutral Higgs boson with properties that resemble those of the SM Higgs boson, whereas additional neutral and charged Higgs bosons are also predicted and are intensively being sought for at the LHC (see Section 11.6.7). In the simplest SUSY model, accommodating a SM-like Higgs boson mass of about 125 GeV results in constraints on the stop sector, with at least one stop mass in the few TeV mass range. In non-minimal SUSY extensions of the SM (details and related references can be found in the 2018 edition of this review [141]), a SM-like Higgs boson with mass of 125 GeV can be accommodated with less restrictions on the stop sector. While naturalness dictates relatively light stops and - at the two loop level - also gluinos, the first and second generation of squarks and sleptons couple weakly to the Higgs sector and may be heavy. Moreover, small values of the μ parameter and therefore light Higgsinos, the fermionic superpartners of the Higgs bosons, would be a signature of a natural realization of electroweak symmetry breaking [353]. Such SUSY spectra, consisting of TeV range stop masses and light Higgsinos, continue to be under intense scrutiny by the experimental collaborations [354], in order to understand if such natural SUSY scenarios endure and can explain why the Higgs boson remains light.

In the context of weakly coupled models of EWSB, one can also consider multiple Higgs $\mathrm{SU}(2)_L$ doublets as well as additional Higgs singlets, triplets or even more complicated multiplet structures, with or without low energy SUSY. In general, for such models, one needs to take into account experimental constraints from precision measurements and flavour changing neutral currents. The LHC signatures of such extended Higgs sectors are largely shaped by the role of the exotic scalar fields in EWSB.

The idea that the Higgs boson itself could be a composite bound state emerging from a new strongly-coupled sector has been reconsidered thanks to the insights gained from the AdS/CFT duality. The composite Higgs boson idea is an incarnation of EWSB via strong dynamics that smoothly interpolates between the standard technicolor approach and the true SM limit. To avoid the usual conflict with EW data, it is sufficient, if not necessary, that a mass gap separates the Higgs resonance from the other resonances of the strong sector. Such a mass gap can naturally follow from dynamics if the strongly-interacting sector exhibits a global symmetry, G, broken dynamically to a subgroup H at the scale f, such that, in addition to the three Nambu–Goldstone bosons of $\mathrm{SO}(4)/\mathrm{SO}(3)$ that describe the longitudinal components of the massive W and Z, the coset G/H contains a fourth Nambu–Goldstone boson that can be identified with the physical Higgs boson. Simple examples of such a coset are $\mathrm{SU}(3)/\mathrm{SU}(2)$ or $\mathrm{SO}(5)/\mathrm{SO}(4)$, the latter being favoured since it is invariant under the custodial symmetry. It is also possible to have non-minimal custodial cosets with extra Goldstone bosons leading to additional Higgs bosons in the spectrum, see for instance Ref. [355]. Modern incarnations of composite Higgs models have been recently investigated in the framework of 5D warped models where, according to the principles of the AdS/CFT correspondence, the holographic composite Higgs boson then originates from a component of a gauge field along the 5th dimension with appropriate boundary conditions.

A last crucial ingredient in the construction of viable composite Higgs boson models is the concept of partial compositeness [356], i.e., the idea that there are only linear mass mixings between

elementary fields and composite states. After diagonalisation of the mass matrices, the SM particles, fermions and gauge bosons, are admixtures of elementary and composite states and thus they interact with the strong sector, and in particular with the Higgs boson, through their composite component. This setup has important consequences on the flavour properties, chiefly the suppression of large flavour changing neutral currents involving light fermions. It also plays an important role in dynamically generating a potential for the would-be Goldstone bosons. Partial compositeness also links the properties of the Higgs boson to the spectrum of the fermionic resonances, i.e., the partners of the top quark. As in the MSSM, these top partners are really the agents that trigger the EWSB and also generate the mass of the Higgs boson that otherwise would remain an exact Goldstone boson and hence massless. The bounds from the direct searches for the top partners, in addition to the usual constraints from EW precision data, force the minimal composite Higgs models into some unnatural corners of their parameter spaces [357].

11.6.1 *Higgs bosons in the minimal supersymmetric standard model (MSSM)*

The particle masses and interactions in a SUSY theory are uniquely defined as a function of the superpotential and the Kähler potential [9]. A fundamental theory of SUSY breaking, however, is unknown at this time. Nevertheless, one can parametrise the low-energy theory in terms of the most general set of soft SUSY-breaking operators [9]. The simplest realistic model of low-energy SUSY is the minimal SUSY extension of the SM (MSSM) [9,358], that associates a SUSY partner to each gauge boson and chiral fermion of the SM, and provides a realistic model of physics at the weak scale. However, in this minimal model, with the most general set of soft SUSY-breaking terms, more than 100 new parameters are introduced. Nevertheless, only a subset of these parameters impact the Higgs boson phenomenology either directly at tree-level or through quantum effects.

The MSSM contains the particle spectrum of a two-Higgs-doublet model (2HDM) extension of the SM and the corresponding SUSY partners. Two Higgs doublets, Φ_1 and Φ_2, with hypercharge $Y = -1$ and $Y = 1$, respectively, are required to ensure an anomaly-free SUSY extension of the SM and to generate mass for down-type quarks/charged leptons (Φ_1) and up-type quarks (Φ_2) [23]. The Higgs potential reads

$$\begin{aligned} V =& m_1^2 \Phi_1^\dagger \Phi_1 + m_2^2 \Phi_2^\dagger \Phi_2 - m_3^2 (\Phi_1^T i\sigma_2 \Phi_2 + \text{h.c.}) \\ &+ \frac{1}{2}\lambda_1 (\Phi_1^\dagger \Phi_1)^2 + \frac{1}{2}\lambda_2 (\Phi_2^\dagger \Phi_2)^2 + \lambda_3 (\Phi_1^\dagger \Phi_1)(\Phi_2^\dagger \Phi_2) + \lambda_4 |\Phi_1^T i\sigma_2 \Phi_2|^2 \\ &+ \frac{1}{2}\lambda_5 \left[(\Phi_1^T i\sigma_2 \Phi_2)^2 + \text{h.c.} \right] + \left[[\lambda_6 (\Phi_1^\dagger \Phi_1) + \lambda_7 (\Phi_2^\dagger \Phi_2)] \Phi_1^T i\sigma_2 \Phi_2 + \text{h.c.} \right], \end{aligned} \tag{11.38}$$

where $m_i^2 = \mu^2 + m_{H_i}^2$ $(i = 1, 2)$, with μ being the supersymmetric Higgsino mass parameter and m_{H_i} the soft supersymmetric breaking mass parameters of the two Higgs doublets; $m_3^2 \equiv B\mu$ is associated to the B-term soft SUSY breaking parameter; and λ_i, for $i = 1$ to 7, are all the Higgs quartic couplings.

After the spontaneous breaking of the electroweak symmetry, five physical Higgs particles are left in the MSSM spectrum: one charged Higgs pair, $H^\pm$, one CP-odd neutral scalar, A, and two CP-even neutral states, H and h, with h being the lightest.[5] The Higgs sector at tree level depends on the electroweak gauge coupling constants and the vacuum expectation value v – or equivalently the Z gauge boson mass – and is determined by only two free parameters: $\tan\beta$ - the ratio of the two Higgs doublets' vacuum expectation values v_2/v_1 - and one Higgs boson mass, conventionally chosen to be the CP-odd Higgs boson mass, m_A. The other tree-level Higgs boson masses are then

[5] Observe that in the SM sections of this review, H denotes the SM Higgs boson, whereas in the sections about SUSY, or extensions of the SM with two Higgs doublets, H is used for the heaviest CP-even Higgs boson, since this is the standard notation in the literature, and the 125 GeV SM-like light Higgs boson will be denoted by h. Generically, in the MSSM, the lightest CP-even Higgs boson is indeed SM-like and thus it is naturally identified with the 125 GeV Higgs boson discovered by ATLAS and CMS, while in general 2HDM extensions, with or without SUSY, there could still be lighter scalar states below 125 GeV.

Figure 11.15: Values of the SUSY mass scale $M_{\rm SUSY} = M_S$ versus the stop mixing parameter normalised by the SUSY mass scale $X_t/M_{\rm SUSY}$, for fixed $\tan\beta = 20$, $\mu = 200\,\text{GeV}$ and $A_t = A_b = A_\tau$. The solid black line corresponds to $m_h = 125\,\text{GeV}$ while in the grey band m_h varies by $\pm 1\,\text{GeV}$. The red dotted lines are iso-values of the stop mass in GeV. This figure is based on Ref. [360].

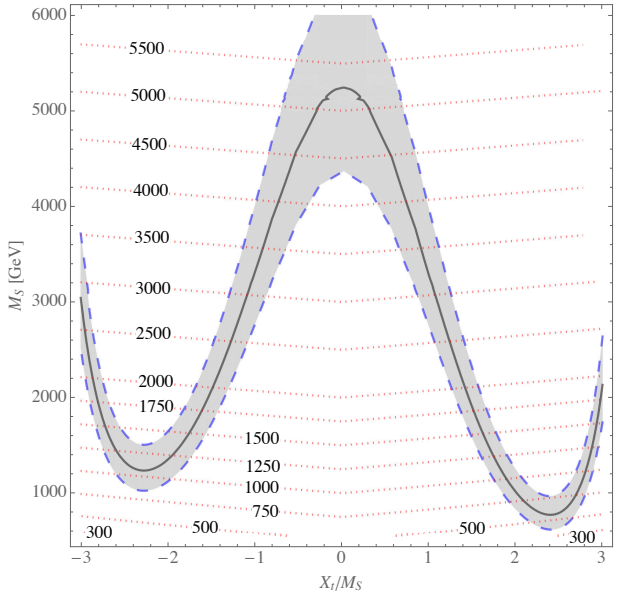

given in terms of these parameters. The tree level value of m_h is maximised not only for $m_A \gg m_Z$ but also for $\tan\beta \gg 1$. For $m_A \gg m_Z$ it acquires a maximum value $m_h = m_Z \cos 2\beta$.

Radiative corrections have a significant impact on the values of Higgs boson masses and couplings in the MSSM. The dominant radiative effects to the SM-like Higgs boson mass arise from the incomplete cancellation between top and scalar-top (stop) loops and at large $\tan\beta$ also from sbottom and stau loops. The stop, sbottom and stau masses and mixing angles depend on the SUSY Higgsino mass parameter μ and on the soft-SUSY-breaking parameters [9, 358]: M_Q, M_U, M_D, M_L, M_E, and A_t, A_b A_τ. The first three of these are the left-chiral and the right-chiral top and bottom scalar quark mass parameters. The next two are the left-chiral stau/sneutrino and the right-chiral stau mass parameters, and the last three are the trilinear parameters that enter in the off-diagonal squark/slepton mixing elements: $X_t \equiv A_t - \mu\cot\beta$ and $X_{b,\tau} \equiv A_{b,\tau} - \mu\tan\beta$. At one-loop, the electroweak gauginos yield a small contribution to the Higgs boson mass, and at the two-loop level, the masses of the gluinos also enter in the calculations. Radiative corrections to the Higgs boson masses have been computed using a number of techniques, with a variety of approximations, see Ref. [359] for a recent review.

The discovered SM-like Higgs boson, if interpreted as the lightest MSSM Higgs boson with a mass of about 125 GeV, provides information on the possible MSSM parameter space, see Fig. 11.15.

The phenomenology of the Higgs sector depends on the couplings of the Higgs bosons to gauge bosons and fermions. At tree-level, the couplings of the two CP-even Higgs bosons to W and Z bosons are given in terms of the angles α, that diagonalises the CP-even Higgs boson squared-mass matrix, and β

$$g_{hVV} = g_V m_V \sin(\beta-\alpha), \quad g_{HVV} = g_V m_V \cos(\beta-\alpha), \tag{11.39}$$

where $g_V \equiv 2m_V/v$, for $V = W$ or Z ($g_V m_V$ is the SM hVV coupling). Observe that in the limit

$\cos(\beta-\alpha)\to 0$, the lightest CP-even Higgs boson h behaves as the SM Higgs boson. This situation is called alignment and is achieved in specific regions of parameter space for $m_A \geq m_Z$ [348] or in the large $m_A \gg m_Z$ limit, in which alignment is achieved through decoupling [348, 349]. There are no tree-level couplings of A or $H^\pm$ to VV. The couplings of the Z boson to two neutral Higgs bosons are given by $g_{\phi AZ}(p_\phi - p_A)$, where $\phi = H$ or h, the momenta p_ϕ and p_A point into the vertex, and

$$g_{hAZ} = g_Z \cos(\beta-\alpha)/2, \quad g_{HAZ} = -g_Z \sin(\beta-\alpha)/2\,. \tag{11.40}$$

The expressions of the couplings between a charged Higgs boson, a neutral Higgs boson and the W boson as well as the expressions of the four-point couplings of vector bosons and Higgs bosons can be found in Ref. [23].

The tree-level Higgs boson couplings to fermions obey the following property: the neutral components of one Higgs doublet, Φ_1, couple exclusively to down-type fermion pairs while the neutral components of the other doublet, Φ_2, couple exclusively to up-type fermion pairs [23]. This Higgs-fermion coupling structure defines the Type-II 2HDM. In the MSSM, fermion masses are generated when both neutral Higgs components acquire a vacuum expectation value, and the relations between Yukawa couplings and fermion masses are (in third-generation notation)

$$h_{b,\tau} = \sqrt{2}\, m_{b,\tau}/(v\cos\beta), \quad h_t = \sqrt{2}\, m_t/(v\sin\beta)\,. \tag{11.41}$$

The couplings of the neutral Higgs bosons to $f\bar{f}$, relative to their SM values, $g\, m_f/(2m_W)$, are therefore given by

$$\begin{array}{ll} h b\bar{b}: \ -\sin\alpha/\cos\beta, & h t\bar{t}: \cos\alpha/\sin\beta\,, \\ H b\bar{b}: \ \cos\alpha/\cos\beta, & H t\bar{t}: \sin\alpha/\sin\beta\,, \\ A b\bar{b}: \ \gamma_5\tan\beta, & A t\bar{t}: \gamma_5\cot\beta\,. \end{array} \tag{11.42}$$

In each relation above, the factor listed for $b\bar{b}$ also pertains to $\tau^+\tau^-$. The charged Higgs boson couplings to fermion pairs, normalised to $g/(\sqrt{2}m_W)$, are given by

$$g_{H^-t\bar{b}}: m_t\cot\beta\frac{1+\gamma_5}{2} + m_b\tan\beta\frac{1-\gamma_5}{2}, \quad g_{H^-\tau^+\nu}: m_\tau\tan\beta\frac{1-\gamma_5}{2}\,. \tag{11.43}$$

The non-standard neutral Higgs bosons have significantly enhanced couplings to down-type fermions at sizeable $\tan\beta$. Radiative corrections can modify significantly the values of the Higgs boson couplings to fermion pairs and to vector boson pairs, through a radiatively-corrected value for $\cos(\beta-\alpha)$ as well as from the one-loop vertex corrections to tree-level Higgs-fermion Yukawa couplings, see Ref. [9] and references therein, for a detailed discussion.

11.6.1.1 *MSSM Higgs boson phenomenology*

The MSSM parameters have to be arranged such that the mass, the CP properties, the decay and production properties of one of the neutral Higgs bosons agree with the LHC Higgs data. Given that present data allows only for moderate departures from the SM predictions, it implies that some degree of alignment is necessary.

The SM-like branching ratios of h can be modified if decays into SUSY particles are kinematically allowed, and, in particular, decays into a pair of the lightest SUSY particles – i.e., the lightest neutralinos, $\tilde{\chi}_1^0$ – can become dominant and would be invisible if R-parity is conserved [361]. Moreover, if light superpartners exist and couple to photons and/or gluons, the h loop-induced coupling to gg and $\gamma\gamma$ could deviate sizeably from the corresponding SM predictions (see for instance the review [362]), and would be in conflict with present data (see Section 11.3). For the heavier Higgs states, there are two possibilities to be considered[6]:

[6] In very special regions of the parameter space, there is still the possibility that the heavier CP-even Higgs state is identified with the 125 GeV Higgs boson discovered by ATLAS and CMS, see for instance the discussion in Ref. [363] and the benchmark M_H^{125} defined in Ref. [364].

i) Alignment triggered by decoupling, hence $m_A \geq$ several hundred GeV: The HWW and HZZ couplings are very small. The dominant H, A decay branching ratios strongly depend on $\tan\beta$. The decay modes $H, A \to b\bar{b}$, $\tau^+\tau^-$ dominate when $\tan\beta$ is large (this holds even away from decoupling). For small $\tan\beta$, the $t\bar{t}$ decay mode dominates above its kinematic threshold. For the charged Higgs boson, $H^+ \to t\bar{b}$ dominates.

ii) Some degree of alignment without decoupling, hence $m_A \leq$ a few hundred GeV: The main difference with the previous case is that, in the low $\tan\beta$ regime ($\tan\beta \leq 5$), additional decay channels may be allowed which involve decays into the lightest SM-like Higgs boson; $A \to Zh$, $H \to hh$ as well as $H \to WW/ZZ$ decay modes are available (they are suppressed in the strict alignment limit). When kinematically open, the decays $A/H \to t\bar{t}$ become relevant or even dominant for sufficiently small $\tan\beta$. For the charged Higgs boson, $H^+ \to \tau^+\nu_\tau$ dominates below the $t\bar{b}$ threshold, and also $H^\pm \to W^\pm h$ may be searched for.

In both cases i) and ii), the heavier Higgs states, H, A and $H^\pm$, are roughly mass degenerate (with masses $\pm$ 20 GeV or less apart). If kinematically allowed, the heavy Higgs boson decays into charginos, neutralinos and third-generation squarks and sleptons can be important [365].

At hadron colliders, the dominant neutral Higgs boson production mechanism at moderate values of $\tan\beta$ is gluon fusion, mediated by loops containing heavy top and bottom quarks and the corresponding SUSY partners. The effect of light stops that may contribute to the gluon fusion production can be partially cancelled by mixing effects. Higgs boson radiation off bottom quarks becomes important for large $\tan\beta$, where at least two of the three neutral Higgs bosons have enhanced couplings to bottom-type fermions [366, 367]. Detailed discussions of the impact of radiative corrections in these search modes are presented for instance in Ref. [368]. The vector boson fusion and Higgs-strahlung production of the CP-even Higgs bosons as well as the associated production of neutral Higgs bosons with top quark pairs have lower production cross sections by at least an order of magnitude with respect to the dominant ones, depending on the precise region of MSSM parameter space [37–40]. Higgs boson pair production of non-standard MSSM Higgs bosons has been studied in Ref. [369]. For a discussion of charged Higgs boson production at LHC, see Refs. [38, 39, 370].

Strong production of a heavy neutral Higgs boson followed by its decay into top-quark pairs is a challenging channel, only most recently being searched for by ATLAS and CMS. Interference effects between the signal and the SM $t\bar{t}$ background need to be carefully taken into account [371, 372].

Summarising, the additional Higgs bosons are sought for mainly via the channels:

$$\begin{aligned}
&pp \to A/H \to \tau^+\tau^- \text{ (inclusive)},\\
&b\bar{b}A/H, A/H \to \tau^+\tau^- \text{ (with } b\text{-tag)},\\
&b\bar{b}A/H, A/H \to b\bar{b} \text{ (with } b\text{-tag)},\\
&pp \to t\bar{t} \to H^\pm W^\mp\, b\bar{b},\ H^\pm \to \tau^+\nu_\tau(\tau^-\bar{\nu}_\tau) \text{ or } t\bar{b}\,(b\bar{t})\,,\\
&gb \to H^- t \ \text{ or } \ g\bar{b} \to H^+\bar{t},\ H^\pm \to \tau^+\nu_\tau(\tau^-\bar{\nu}_\tau) \text{ or } t\bar{b}\,(b\bar{t})\ . \qquad (11.44)
\end{aligned}$$

After the Higgs boson discovery, updated MSSM benchmarks scenarios have been defined to highlight interesting conditions for the MSSM Higgs boson searches [39, 364] and are scrutinised by the LHC Higgs Working Group [373]. The latest benchmark scenarios update [364], partly based in MSSM parameter space discussions in Ref. [374], considers six benchmarks to illustrate different aspects of Higgs phenomenology in the MSSM. They include one case with complex parameters, but they all assume R-parity conservation and no flavour mixing. Each scenario contains one CP-even scalar with mass around 125 GeV and SM-like couplings. These scenarios include a M_h^{125} scenario with relatively heavy superparticles, so the Higgs phenomenology at the LHC resembles that of a

2HDM with MSSM-inspired Higgs boson couplings. Other two scenarios are characterised by some of the superparticles – staus or electroweakinos – being relatively light, that in turn is of relevance for heavy neutral Higgs boson searches. In particular, the traditional $A/H \to \tau^+\tau^-$ search channel varies depending on the values of μ and M_2, that may enable the A/H decays into electroweakinos. Another two scenarios are characterised by the phenomenon of alignment without decoupling, in which one of the two neutral CP-even scalars has SM-like couplings independently of the mass spectrum of the remaining Higgs bosons, hence allowing for all the Higgs bosons to have relatively low mass values (about few hundred GeV). Finally, there is one scenario which incorporates CP violation in the Higgs sector and gives rise to a strong admixture of the two heavier neutral states. All the above scenarios assume all parameters in the mass range from 1 to a few TeV, hence they are not applicable for values of $\tan\beta$ of order a few, for which a Higgs boson mass value of 125 GeV is out of reach. An additional study [375], relying on an EFT approach in the MSSM, focusses on two scenarios specifically designed for the low $\tan\beta$ region and ensures a 125 GeV Higgs boson mass in almost the entire parameter space by employing a flexible supersymmetric mass scale, reaching values of up to 10^{16} GeV.

An alternative approach to reduce the large number of parameters relevant to the Higgs sector is to consider that, in the Higgs basis, the only important radiative corrections are those affecting the Higgs boson mass [376]. This approximation is called hMSSM and works well in large regions of parameter space but it breaks down for sizeable values of μ and A_t, and moderate values of $\tan\beta$, for which the radiative corrections to the mixing between the two CP even eigenstates become relevant. The effect of such radiative corrections is to allow for alignment for small to intermediate values of $\tan\beta$, independent of the specific value of m_A [346]. In addition, the hMSSM assumption that the right value of the Higgs boson mass may be obtained for all values of m_A and $\tan\beta$ is in conflict with the MSSM predictions for the Higgs boson mass for small values of m_A and $\tan\beta \simeq \mathcal{O}(1)$. The recent M_h^{125} [364] and EFTMSSM benchmarks [375], are designed to address the limitations of the hMSSM, in particular the low $\tan\beta$ region for the EFTMSSM.

The compatibility between the predicted and measured Higgs boson mass sets stringent constraints on the parameter space of BSM models. The predictions are illustrated in Fig. 11.16 for two concrete scenarios. Note that to use the predicted Higgs boson mass as a constraint (exclusion at nearly constant $\tan\beta$ at high M_A in the (M_A,$\tan\beta$) plane), it is important to account for the theoretical uncertainty on the prediction which is in excess of an order of magnitude larger than the experimental uncertainty on the measured mass of the Higgs boson. The theoretical uncertainty depends itself on the specific SUSY spectrum for a given MSSM parameter set and should be estimated accordingly, however, a more generic estimate of ± 3 GeV is made and found to be a conservative choice [359].

Reviews of the properties and phenomenology of the Higgs bosons of the MSSM can be found for example in Refs. [9, 362, 378]. Future precision measurements of the Higgs boson couplings to fermions and gauge bosons together with information on heavy Higgs boson searches will provide powerful information on the SUSY parameter space [379].

Improvements in our understanding of B-physics observables put indirect constraints on additional Higgs bosons in mass ranges that would be accessible in direct LHC searches. In particular, $\mathrm{BR}(B_s \to \mu^+\mu^-)$, $\mathrm{BR}(b \to s\gamma)$, and $\mathrm{BR}(B_u \to \tau\nu)$ play an important role within minimal flavour-violating (MFV) models [380], in which flavour effects proportional to the CKM matrix elements are induced as in the SM [381].

11.6.2 *Supersymmetry with singlet extensions*

The Higgs mass parameter μ is a SUSY parameter, and as such, it should naturally be of order M_{GUT} or M_{Planck}. The fact that phenomenologically it is required that μ be at the electroweak/TeV

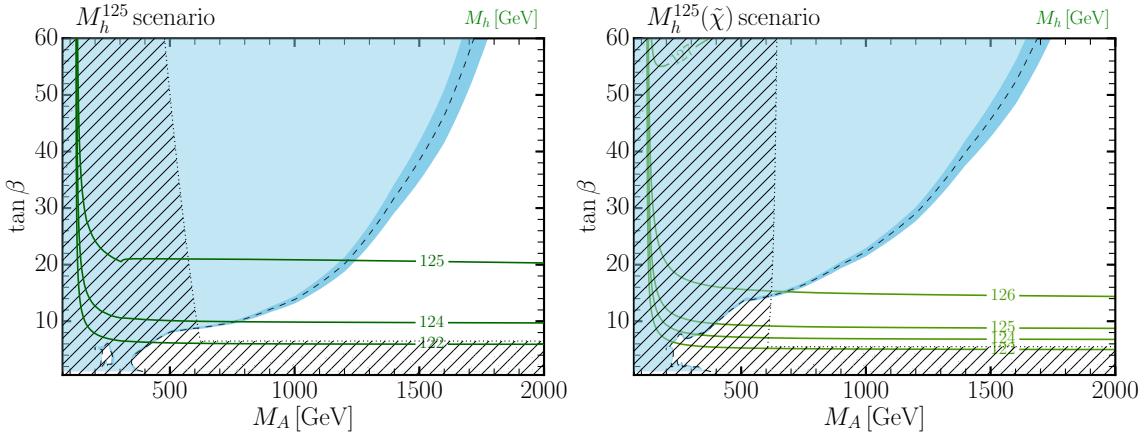

Figure 11.16: The 95% CL exclusion contours in the $(M_A, \tan\beta)$ parameter space for the M_h^{125} (right) and $M_h^{125}(\tilde{\chi})$(left) benchmark scenarios [377]. The M_h^{125} benchmark assumes that super partners are heavy, so that the phenomenology of the observed Higgs boson is not altered except in its couplings due to the existence of another doublet. The $M_h^{125}(\tilde{\chi})$ scenario on the other hand considers light electroweakinos and therefore the heavy Higgs bosons H and A can have sizeable decay rates to charginos and neutralinos, consequently suppressing the $\tau^+\tau^-$ decay rate. The nearly vertical dotted line illustrates the lower limit on the mass of the A boson from precision measurements of the Higgs boson couplings and the close-to horizontal dotted line represents the limit on $\tan\beta$ from the compatibility of the measured mass of the observed Higgs boson and the prediction using radiative corrections (mostly from the stop sector).

scale is known as the μ problem [382]. SUSY models with additional singlets can provide a solution to the μ problem, by promoting the μ parameter to a dynamical singlet superfield S that only interacts with the MSSM Higgs doublets through a coupling λ_S at the level of the superpotential. An effective μ is generated when the real scalar component of S acquires a vacuum expectation value v_S, yielding $\mu_{eff} = \lambda_S v_S$. After the minimization of the Higgs potential, the vacuum state relates the vacuum expectation values of the three CP-even neutral scalars, v_1, v_2 and v_S, to the scalar doublet and singlet soft SUSY breaking masses, hence, one expects that these VEVs should all be of order $M_{\rm SUSY}$ and therefore the μ problem is solved.

The addition of a singlet superfield to the MSSM may come along with additional symmetries imposed to the theory. Depending on such symmetries, different models with singlet extensions of the MSSM (xMSSM) have been proposed, see Ref. [383] for a general review. Among the most studied examples are the NMSSM with an additional discrete Z_3 symmetry (first introduced in Ref. [384]), the Nearly-Minimal SUSY SM (nMSSM), with additional discrete Z_5^R, and Z_7^R symmetries [385], and the U(1)′-extended MSSM (UMSSM) [386]. A Secluded U(1)′-extended MSSM (sMSSM) [387] contains three singlets in addition to the standard UMSSM Higgs boson singlet; this model is equivalent to the nMSSM in the limit that the additional singlet VEV's are large, and the trilinear singlet coupling, λ_S, is small [388]. The non-zero neutrino masses provide also a motivation for a particular extension of the MSSM, $\mu\nu$SSM [389], which also happens to address the mu problem. The computation of the Higgs boson spectrum in these various models has been reviewed in Ref. [359].

A singlet extended SUSY Higgs sector opens new avenues for discovery. Since the singlet pseudoscalar particle may be identified as the pseudo-Goldstone boson of a spontaneously broken Peccei–Quinn symmetry, it may become naturally light [390]. Generally, there is mixing of the

singlet sector with the MSSM Higgs sector, and for a sufficiently light, singlet-dominated scalar or pseudoscalar, h_S or A_S, respectively, the SM-like Higgs boson h may decay to pairs of h_S or A_S. The light scalar and/or pseudoscalar may subsequently decay to $\tau\tau$ or $b\bar{b}$ pairs. Such cascade decays are more difficult to detect than in standard searches due to the potentially soft decay products. There is also a rich phenomenology for the decays of the heavy CP-even and CP-odd doublets, H and A into two lighter Higgs bosons such as $H \to hh_S$, hh, h_Sh_S or $A \to A_Sh_S$, A_Sh as well as into a light Higgs boson and a gauge boson: $H \to A_SZ$; $A \to h_SZ$, hZ. If kinematically allowed, the heavy Higgs bosons decay into $t\bar{t}$. If the singlet-dominated scalar or pseudoscalar are somewhat heavier, the decays $h_S \to WW$ or $A_S \to h_SZ$ will be allowed.

In addition, the light singlet scenario in the NMSSM or nMSSM is typically associated with a light singlino-dominated neutralino. The 125 GeV SM-like Higgs boson can then decay to pairs of this neutralino [391], opening an invisible decay mode that is not excluded by present data. All of the Higgs bosons can decay into electroweakinos depending on kinematics and on the singlino or Higgsino composition of the electroweakinos.

In models with extended singlets, at low $\tan\beta$, it is possible to trade the requirement of a large stop mixing by a sizeable trilinear Higgs-singlet Higgs coupling λ_S, rendering more freedom on the requirements for gluon fusion production. As in the MSSM, mixing in the Higgs sector – additionally triggered by the extra new parameter λ_S – can produce variations in the Higgs–$b\bar{b}$ and Higgs–$\tau^-\tau^+$ couplings that can alter the Higgs to ZZ/WW and to diphoton rates. Light charginos at low $\tan\beta$ can independently contribute to enhance the di-photon rate, without altering any other of the Higgs boson decay rates, see for instance Ref. [392].

There is much activity in exploring the NMSSM phenomenology in the light of the 125 GeV Higgs boson as well as in defining benchmark scenarios with new topologies including Higgs decay chains, see Refs. [40, 393] and references therein. An analytic understanding of the alignment condition in the NMSSM is presented in Ref. [347]. The NMSSM with a Higgs boson of mass 125 GeV can be compatible with stop masses of order of the electroweak/TeV scale, thereby reducing the degree of fine-tuning necessary to achieve electroweak symmetry breaking. Interestingly, the alignment conditions point toward a more natural region of parameter space for electroweak symmetry breaking, while allowing for perturbativity of the theory up to the Planck scale and yielding a rich and interesting Higgs boson phenomenology at the LHC.

11.6.3 *Supersymmetry with extended gauge sectors*

In the MSSM, the tree-level value of the lightest CP-even Higgs boson mass originates from the D-term dependence of the scalar potential that comes from the SUSY kinetic terms in the Kähler potential. The D-terms lead to tree-level quartic couplings which are governed by the squares of the gauge couplings of the weak interactions, under which the Higgs boson has non-trivial charges. Hence, the lightest Higgs mass is bounded to be smaller than M_Z. In the presence of new gauge interactions at the TeV scale, and if the Higgs fields had non-trivial charges under them, new D-term contributions would lead to an enhancement of the tree-level Higgs boson mass value. Since the low energy gauge interactions reduce to the known $\mathrm{SU}(3)_c \times \mathrm{SU}(2)_L \times \mathrm{U}(1)_Y$ ones, in order for this mechanism to work, the extended gauge and Higgs sectors should be integrated out in a non-SUSY way. This means that there must be SUSY breaking terms that are of the order of, or larger than, the new gauge boson masses. The tree-level quartic couplings would then be enhanced through their dependence on the square of the gauge couplings of the extended Higgs sector. This effect will be suppressed when the heavy gauge boson masses are larger than the SUSY breaking scale and will acquire its full potential only for large values of this scale.

One of the simplest possibilities is to extend the weak interactions to a $\mathrm{SU}(2)_1 \times \mathrm{SU}(2)_2$ sector, such that the known weak interactions are obtained after the spontaneous breaking of these groups

to $\mathrm{SU}(2)_L$ [394]. This example is briefly summarised in the previous editions of this review [141]. Assuming SUSY breaking terms of the order of the new gauge boson masses, enhancements of order 50% of the MSSM D-term contribution to the Higgs boson mass may be obtained. Such enhancements are sufficient to obtain the measured Higgs mass value without the need for very heavy stops or large stop mixing parameters. This gauge extension leads to new, heavy gauge and Higgs bosons, as well as new neutralinos and charginos, that depending on the region of parameter space can induce novel phenomenology at the LHC. Gauge extensions including new Abelian gauge groups have also been considered.

Gauge extensions of the MSSM can also lead to an enhancement of the Higgs boson mass value by modifying the renormalisation group evolution of the Higgs quartic coupling to low energies. In the MSSM, the evolution of the quartic coupling is governed by the top-quark Yukawa interactions and depends on the fourth power of the top-quark Yukawa coupling. The neutralino and chargino contributions, which depend on the fourth power of the weak gauge couplings, are small due to the smallness of these couplings. Depending on the values of the soft SUSY breaking parameters in the gaugino and Higgsino sectors, the $\mathrm{SU}(2)_1$ gauginos may become light, with masses of the order of the weak scale. Since the $\mathrm{SU}(2)_1$ coupling may be significantly larger than the $\mathrm{SU}(2)_L$ one, for small values of the Higgsino mass parameter μ, the associated charginos and neutralinos may modify the evolution of the quartic coupling in a significant way [395]. This may lead to a significant increase of the lightest CP-even Higgs boson mass, even for small values of $\tan\beta \simeq 1$ for which the D-term contributions become small. Radiative corrections should be properly taken into account in this scenario as they might modify the tree-level result.

11.6.4 *Effects of CP violation*

SUSY scenarios with CP-violation (CPV) phases are theoretically appealing, since additional CPV beyond that observed in the K, D, and B meson systems is required to explain the observed cosmic matter-antimatter asymmetry. In the MSSM, CP-violation effects in the Higgs sector appear at the quantum level, while in singlet extensions of the MSSM CP-violation effects can already be effective at tree level. In general, CP-violation effects in the Higgs sector have significant constraints from electric dipole moments data [396].

In the MSSM, the gaugino mass parameters ($M_{1,2,3}$), the Higgsino mass parameter, μ, the bilinear Higgs squared-mass parameter, m_{12}^2, and the trilinear couplings of the squark and slepton fields to the Higgs fields, A_f, may carry non-trivial phases. The two parameter combinations $\arg[\mu A_f (m_{12}^2)^*]$ and $\arg[\mu M_i (m_{12}^2)^*]$ are invariant under phase redefinitions of the MSSM fields [397, 398]. Therefore, if one of these quantities is non-zero, there would be new sources of CP-violation affecting the Higgs sector through radiative corrections, see Ref. [399] and references therein. The mixing of the neutral CP-odd and CP-even Higgs boson states is no longer forbidden. Hence, m_A is no longer a physical parameter. However, the charged Higgs boson mass $m_{H^\pm}$ is still physical and can be used as an input for the computation of the neutral Higgs boson spectrum of the theory. For large values of $m_{H^\pm}$, corresponding to the decoupling limit, the properties of the lightest neutral Higgs boson state approach those of the SM Higgs boson. In particular, the upper bound on the lightest neutral Higgs boson mass takes the same value as in the CP-conserving case [398]. Nevertheless, there still can be significant mixing between the two heavier neutral mass eigenstates. For a detailed study of the Higgs boson mass spectrum and parametric dependence of the associated radiative corrections, see Ref. [399] and references therein.

Major variations to the Higgs boson phenomenology occur in the presence of explicit CPV phases. In the CPV case, vector boson pairs couple to all three neutral Higgs boson mass eigen-

states, H_i $(i = 1, 2, 3)$, with couplings

$$\begin{aligned} g_{H_iVV} &= \cos\beta\,\mathcal{O}_{1i} + \sin\beta\,\mathcal{O}_{2i}\,, \\ g_{H_iH_jZ} &= \mathcal{O}_{3i}\,(\cos\beta\,\mathcal{O}_{2j} - \sin\beta\,\mathcal{O}_{1j}) - \mathcal{O}_{3j}\,(\cos\beta\,\mathcal{O}_{2i} - \sin\beta\,\mathcal{O}_{1i})\,, \end{aligned} \tag{11.45}$$

where the g_{H_iVV} couplings are normalised to the analogous SM coupling and the $g_{H_iH_jZ}$ have been normalised to $g_Z^{\rm SM}/2$. The orthogonal matrix $\mathcal{O}_{ij}$, only defined in the $p^2 \to 0$ limit, is relating the weak eigenstates to the mass eigenstates. It has non-zero off-diagonal entries mixing the CP-even and CP-odd components of the weak eigenstates. Moreover, CPV phases imply that all neutral Higgs bosons can couple to both scalar and pseudoscalar fermion bilinear densities. The couplings of the mass eigenstates H_i to fermions depend on the loop-corrected fermion Yukawa couplings (similarly to the CP conserving (CPC) case), on $\tan\beta$ and on $\mathcal{O}_{ji}$ [400].

The production processes of neutral MSSM Higgs bosons in the CPV scenario are similar to those in the CPC scenario. Regarding the decay properties, the lightest mass eigenstate, H_1, predominantly decays to $b\bar{b}$ if kinematically allowed, with a smaller fraction decaying to $\tau^+\tau^-$. If kinematically allowed, a SM-like neutral Higgs boson, H_2 or H_3 can decay predominantly to H_1H_1 leading to many new interesting signals both at lepton and hadron colliders; otherwise it will decay preferentially to $b\bar{b}$.

The discovery of a 125 GeV Higgs boson has put strong constraints on the realisation of the CPV scenario within the MSSM. This is partly due to the fact that the observed Higgs boson rates are close to the SM values, and a large CP-violating component would necessarily induce a large variation in the rate of the SM-like Higgs boson decays into the weak gauge bosons $W^\pm$ and Z. The measured Higgs mass imposes additional constraints on the realisation of this scenario. Once all effects are considered, the CP-odd Higgs boson A component of the lightest Higgs boson tends to be smaller than about 10% [401]. This restriction can be alleviated in the NMSSM or more general two Higgs doublet models. CP-violating effects can still be significant in the heavy Higgs sector. For instance, the Higgs bosons H_2 and H_3 may be admixtures of CP-even and CP-odd scalars, and therefore both may be able to decay into pairs of weak gauge bosons. The observation of such decays would be a clear signal of CP-violation. In the MSSM, the proximity of the masses of H_2 and H_3 makes the measurement of such effect quite challenging, but in generic two Higgs doublet models, the mass splitting between the two heavy mass eigenstates may become larger, facilitating the detection of CP-violating effects at collider experiments [402].

11.6.5 *Non-supersymmetric extensions of the Higgs sector*

There are many ways to extend the minimal Higgs sector of the SM. In the preceding sections the phenomenology of SUSY Higgs sectors is considered, which at tree level implies a constrained type-II 2HDM (with restrictions on the Higgs boson masses and couplings). In the following discussion, more generic 2HDM's are presented (for some comprehensive reviews, see the reviews [403]). These models are theoretically less compelling since they do not provide an explanation for the SM Higgs naturalness problem, but can lead to different patterns of Higgs-fermion couplings, hence, to different phenomenology. It is also possible to consider models with a SM Higgs boson and one or more additional scalar SU(2) doublets that acquire no VEV and hence play no role in the EWSB mechanism. Such models are dubbed Inert Higgs Doublet Models (IHD) [404]. Without a VEV associated to it, a Higgs boson from an inert doublet has no tree-level coupling to gauge bosons and hence cannot decay into a pair of them. Moreover, imposing a Z_2 symmetry that prevents them from coupling to the fermions, it follows that, if the lightest inert Higgs boson is neutral, it becomes a good DM candidate with interesting associated collider signals. Various studies of IHD models in the light of a 125 GeV Higgs boson have been performed, see for instance Ref. [405], showing an interesting interplay between collider and direct DM detection signals.

An interesting type of 2HDMs are those in which an Abelian flavour symmetry broken at the electroweak scales creates the fermion mass hierarchies and mixing angles [406]. This idea is based on the Froggatt–Nielsen model [407], where a flavon field couples differently to the SM fermions of different flavour charges. Such flavon acquires a vacuum expectation value, breaking the flavour symmetry but leaving both the flavour breaking and the new physics scales undetermined. In Refs. [408], it was proposed to relate the flavour breaking scale to the electroweak scale by identifying the flavon with the modulus square of the Higgs field. A 2HDM, however, provides a more compelling realisation of the electroweak scale flavour breaking idea. In the most ambitious constructions of two Higgs doublet flavour models (2HDFM), the textures of the Yukawa couplings are a result of an Abelian flavour symmetry that only allows renormalisable Yukawa couplings of the top quark to the Higgs bosons. All other Yukawa couplings are generated by higher dimensional operators that produce hierarchical entries of the Yukawa matrices, explaining the observed quark masses and mixing angles. Flavour observables, LHC Higgs signal strength measurements, electroweak precision measurements, unitarity and perturbativity bounds, as well as collider searches for new scalar resonances result in precise predictions for the parameters of these 2HDFMs. In particular, correlated departures from SM Higgs boson couplings, as well as additional Higgs bosons with masses $< 700\,\text{GeV}$ must be observed at the LHC. Other incarnations of 2HDFMs can aim at only partially explaining the fermion mass hierarchies but are therefore less restrictive.

Other extensions of the Higgs sector can include multiple copies of $\text{SU}(2)_L$ doublets [409], additional Higgs singlets [410], triplets or more complicated combinations of Higgs multiplets. It is also possible to enlarge the gauge symmetry beyond $\text{SU}(2)_L \times \text{U}(1)_Y$ along with the necessary Higgs field structure to generate gauge boson and fermion masses. There are two main experimental constraints on these extensions: (i) precision measurements which constrain $\rho = m_W^2/(m_Z^2 \cos^2\theta_W)$ to be very close to 1 and (ii) flavour changing neutral current (FCNC) effects. In electroweak models based on the SM gauge group, the tree-level value of ρ is determined by the Higgs multiplet structure. By suitable choices for the hypercharges, and in some cases the mass splitting between the charged and neutral Higgs sector or the vacuum expectation values of the Higgs fields, it is possible to obtain a richer combination of singlets, doublets, triplets and higher multiplets compatible with precision measurements. Concerning the constraints coming from FCNC effects, the Glashow–Weinberg (GW) criterion [411] states that, in the presence of multiple Higgs doublets, the tree-level FCNC's mediated by neutral Higgs bosons will be absent if all fermions of a given electric charge couple to no more than one Higgs doublet. An alternative way of suppressing FCNC in a two Higgs doublet model has been considered in Ref. [412], where it is shown that it is possible to have tree level FCNC completely fixed by the CKM matrix, as a result of an Abelian symmetry.

There is a lot of activity on the study of non-supersymmetric models with an extended Higgs sector with an intense collaboration between theorists and experimentalists, in particular inside the LHC Higgs Working Group [373].

11.6.5.1 *Two-Higgs-doublet models*

General two Higgs doublet models [403] can have a more diverse Higgs-fermion coupling structure than in SUSY, and can be viewed as a simple extension of the SM to realise the spontaneous breakdown of $\text{SU}(2)_L \times \text{U}(1)_Y$ to $\text{U}(1)_{\text{em}}$. Quite generally, if the two Higgs doublets contain opposite hypercharges, the scalar potential will contain mixing mass parameters of the kind $m_{12}^2 \Phi_1^T i\sigma_2 \Phi_2 + h.c.$. In the presence of such terms, both Higgs doublets will acquire vacuum expectation values, $v_1/\sqrt{2}$ and $v_2/\sqrt{2}$, respectively, and the gauge boson masses will keep their SM expressions with the Higgs VEV v replaced by $\sqrt{v_1^2 + v_2^2}$. Apart from the mass terms, the most generic renormalisable and gauge invariant scalar potential for two Higgs doublets with opposite hypercharges contains seven quartic couplings, as presented in Eq. (11.38).

Just as in the MSSM case, after electroweak symmetry breaking and in the absence of CP-violation, the physical spectrum contains a pair of charged Higgs bosons $H^{\pm}$, a CP-odd Higgs boson A and two neutral CP-even Higgs bosons, h and H. The angles α and β diagonalise the CP-even, and the CP-odd and charged Higgs sectors, respectively. The complete 2HDM is defined only after considering the interactions of the Higgs fields to fermions. Yukawa couplings of the generic form

$$- h^a_{ij} \bar{\Psi}^i_L H_a \Psi^j_R + h.c. \tag{11.46}$$

may be added to the renormalisable Lagrangian of the theory. Contrary to the SM, the two Higgs doublet structure does not ensure the alignment of the fermion mass terms $m_{ij} = h^a_{ij} v_a/\sqrt{2}$ with the Yukawa couplings h^a_{ij}. This implies that quite generally the neutral Higgs boson will mediate flavour changing interactions between the different mass eigenstates of the fermion fields. Such flavour changing interactions should be suppressed in order to describe properly the Kaon, D and B meson phenomenology. Based on the Glashow–Weinberg criterion, it is clear that the simplest way of avoiding such transitions is to assume the existence of a symmetry that ensures the couplings of the fermions of each given quantum number (up-type and down-type quarks, charged and neutral leptons) to only one of the two Higgs doublets. Different models may be defined depending on which of these fermion fields couple to a given Higgs boson, see Table 11.9. Models of type-I are those in which all SM fermions couple to a single Higgs field. In type-II models, down-type quarks and charged leptons couple to a common Higgs field, while the up-type quarks and neutral leptons couple to the other. In models of type-III (lepton-specific), quarks couple to one of the Higgs bosons, while leptons couple to the other. Finally, in models of type-IV (flipped), up-type quarks and charged leptons couple to one of the Higgs fields while down-quarks and neutral leptons couple to the other.

Table 11.9: Higgs boson couplings to up, down and charged lepton-type $SU(2)_L$ singlet fermions in the four discrete types of 2HDM models that satisfy the Glashow–Weinberg criterion.

Model	2HDM I	2HDM II	2HDM III	2HDM IV
u	Φ_2	Φ_2	Φ_2	Φ_2
d	Φ_2	Φ_1	Φ_2	Φ_1
e	Φ_2	Φ_1	Φ_1	Φ_2

The two Higgs doublet model phenomenology depends strongly on the size of the mixing angle α and therefore on the quartic couplings. For large values of m_A, $\sin\alpha \to -\cos\beta$, $\cos\alpha \to \sin\beta$, $\cos(\beta-\alpha) \to 0$, and the lightest CP-even Higgs boson h behaves as the SM Higgs boson. The same behaviour is obtained if the quartic couplings are such that $\mathcal{M}^2_{12}\sin\beta = -(\mathcal{M}^2_{11} - m^2_h)\cos\beta$. The latter condition represents a situation in which the couplings of h to fermions and weak gauge bosons become the same as in the SM, without decoupling the rest of the non-standard scalars and it is of particular interest due to the fact that the discovered Higgs boson has SM-like properties. This situation will be referred to as alignment, as in the MSSM case.

In analogy to the effects of CP violation in the SUSY 2HDM, some parameters of the Higgs potential can be complex and one has a model that is explicitly CP violating. The three neutral mass eigenstates mixed with each other and the Higgs phenomenology is analogous to the one described for the SUSY case above, with the caveat that when considering the neutral Higgs boson couplings to the scalar and pseudoscalar fermion bilinear densities, the proper weight should be considered for the respective 2HDM's.

In type-II Higgs doublet models, at large values of $\tan\beta$ and moderate values of m_A, the non-standard Higgs bosons H, A and $H^\pm$ couple strongly to bottom quarks and τ leptons. Hence, the decay modes of the non-standard Higgs bosons tend to be dominated by the b-quark and τ-lepton modes, including top quarks or neutrinos in the case of the charged Higgs boson. However, for large and negative values of λ_4, the charged Higgs boson mass may be sufficiently heavy to allow on-shell decays $H^\pm \to W^\pm + (H, A)$, via a trilinear coupling

$$g_{H^\pm W^\mp H,A} \simeq \frac{M_W}{v} \sin(\beta-\alpha)(p_{H^+} - p_{H,A})\,, \tag{11.47}$$

where p_{H^+} and $p_{H,A}$ are the charged and neutral scalar Higgs boson momenta pointing into the vertex. On the other hand, for large and positive values of λ_5, the above charged Higgs boson decay into a $W^\pm$ and the CP-odd Higgs boson may be allowed, but the heavy Higgs boson H may be sufficiently heavy to decay into a CP-odd Higgs boson and an on-shell Z, $H \to Z + A$, via

$$g_{HZA} \simeq \frac{M_Z}{v} \sin(\beta-\alpha)(p_H - p_A). \tag{11.48}$$

The decay $H^\pm \to W^\pm + H$, on the other hand may be allowed only if $\lambda_4 < -\lambda_5$. The couplings controlling all the above decay modes are proportional to $\sin(\beta-\alpha)$ and therefore they are unsuppressed in the alignment limit. Moreover, these could still be the dominant decay modes at moderate values of $\tan\beta$, offering a way to evade the current bounds obtained assuming a dominant decay into b-quarks or τ-leptons.

The quartic couplings are restricted by the condition of stability of the effective potential as well as by the restriction of obtaining the proper value of the lightest CP-even Higgs boson mass. Close to the alignment limit, the lightest CP-even Higgs boson mass becomes

$$m_h^2 \simeq v^2(\lambda_1 \cos^4\beta + \lambda_2 \sin^4\beta + 2\tilde{\lambda}_3 v^2 \cos^2\beta \sin^2\beta + 4\lambda_6 \cos^3\beta \sin\beta + 4\lambda_7 \sin^3\beta \cos\beta)\,, \tag{11.49}$$

where $\tilde{\lambda}_3 = \lambda_3 + \lambda_4 + \lambda_5$.

The stability conditions imply the positiveness of all masses, as well as the avoidance of run-away solutions to large negative values of the fields in the scalar potential. These conditions imply

$$\lambda_1 \geq 0,\;\; \lambda_2 \geq 0,\;\; \lambda_3 + \lambda_4 - |\lambda_5| \geq -\sqrt{\lambda_1\lambda_2},\;\; \lambda_3 \geq -\sqrt{\lambda_1\lambda_2},\;\; 2|\lambda_6 + \lambda_7| < \frac{\lambda_1+\lambda_2}{2} + \tilde{\lambda}_3, \tag{11.50}$$

where the first four conditions are necessary and sufficient conditions in the case of $\lambda_6 = \lambda_7 = 0$, while the last one is a necessary condition in the case all couplings are non-zero. Therefore, to obtain the conditions that allow the decays $H^\pm \to W^\pm H, A$ and $H \to ZA$, λ_3 should take large positive values in order to compensate for the effects of λ_4 and λ_5. For more detailed discussions about 2HDM phenomenology, see for example Refs. [40, 403].

11.6.5.2 *Higgs triplets*

Electroweak triplet scalars are the simplest non-doublet extension of the SM that can participate in the spontaneous breakdown of $\mathrm{SU}(2)_L \times \mathrm{U}(1)_Y$ to $\mathrm{U}(1)_{\mathrm{em}}$. Two types of model have been developed in enough detail to make a meaningful comparison to LHC data: the Higgs triplet model (HTM) [413] and the Georgi–Machacek model (GM) [414].

The Higgs triplet model extends the SM by the addition of a complex $\mathrm{SU}(2)_L$ triplet scalar field Δ with hypercharge $Y = 2$, and a general gauge-invariant renormalisable potential $V(\Phi, \Delta)$ for Δ and the SM Higgs doublet Φ. The components of the triplet field can be parameterised as

$$\Delta = \frac{1}{\sqrt{2}} \begin{pmatrix} \Delta^+ & \sqrt{2}\Delta^{++} \\ v_\Delta + \delta + i\xi & -\Delta^+ \end{pmatrix}. \tag{11.51}$$

where Δ^+ is a singly-charged field, Δ^{++} is a doubly-charged field, δ is a neutral CP-even scalar, ξ is a neutral CP-odd scalar, and v_Δ is the triplet VEV. The general scalar potential mixes the doublet and triplet components. After electroweak symmetry breaking there are seven physical mass eigenstates, denoted $H^{\pm\pm}$, $H^\pm$, A, H, and h.

A distinguishing feature of the HTM is that it violates the custodial symmetry of the SM; thus the ρ parameter deviates from 1 even at tree level. Letting x denote the ratio of triplet and doublet VEVs, the tree level expression is

$$\rho = \frac{1+2x^2}{1+4x^2} \,. \tag{11.52}$$

The measured value of the ρ parameter then limits the triplet VEV to be quite small, $x \lesssim 0.03$, or $v_\Delta < 8\,\text{GeV}$. This constraint severely limits the role of the triplet scalar in the EWSB mechanism.

The small VEV of the Higgs triplet in the HTM is a virtue from the point of view of generating neutrino masses without the necessity for introducing right-handed neutrino fields. The gauge invariant dimension four interaction

$$h_{\nu_{ij}}\, \ell_i^T C^{-1} i\sigma_2\, \Delta\, \ell_j \,, \tag{11.53}$$

where ℓ_i are the lepton doublets, C is the charge conjugation matrix, and $h_{\nu_{ij}}$ is a complex symmetric coupling matrix, generates a Majorana mass matrix for the neutrinos:

$$m_{\nu_{ij}} = \sqrt{2} h_{\nu_{ij}} v_\Delta \,. \tag{11.54}$$

This can be combined with the usual neutrino seesaw to produce what is known as the type-II seesaw [415].

The HTM suggests the exciting possibility of measuring parameters of the neutrino mass matrix at the LHC. If the doubly-charged Higgs boson is light enough and/or its couplings to W^+W^+ are sufficiently suppressed, then its primary decay is into same-sign lepton pairs: $H^{++} \to \ell_i^+ \ell_j^+$; from Eq. (11.53) and Eq. (11.54), it is apparent that these decays are in general lepton-flavour violating with branchings proportional to elements of the neutrino mass matrix [416].

Precision electroweak data constrain the mass spectrum as well as the triplet VEV of the HTM [417]. These constraints favour a spectrum where H^{++} is the lightest of the exotic bosons, and where the mass difference between H^+ and H^{++} is a few hundred GeV. The favoured triplet VEV is a few GeV, which also favours H^{++} decays into W^+W^+ over same-sign dileptons.

The GM model addresses the ρ parameter constraint directly by building in a custodial symmetry (it was however argued that large corrections to $\rho = 1$ are generated at one-loop [418], requiring some fine-tuning to preserves agreement with EW precision data). Writing the complex scalar doublet of the SM as a $(2,2)$ under $\text{SU}(2)_L \times \text{SU}(2)_R$, it is obvious that the next simplest construction respecting custodial symmetry is a scalar transforming like a $(3,3)$ [419]. These nine real degrees of freedom correspond to a complex electroweak triplet combined with a real triplet, with the scalar potential required to be invariant under $\text{SU}(2)_R$. Under the custodial $\text{SU}(2)_{L+R}$, they transform as $1 \oplus 3 \oplus 5$, with a CP-even neutral scalar as the custodial singlet (thus matching the SM Higgs boson), a CP-odd neutral scalar in the custodial triplet, and another CP-even neutral scalar in the custodial 5-plet.

The scalar components can be decomposed as

$$\Xi = \begin{pmatrix} \chi_3^* & \xi_1 & \chi_1 \\ -\chi_2^* & \xi_2 & \chi_2 \\ \chi_1^* & -\xi_1^* & \chi_3 \end{pmatrix}, \tag{11.55}$$

where ξ_2 is a real scalar and the others are complex scalars. Linear combinations of these scalars account for the neutral custodial singlet, a neutral and singly-charged field making up the custodial triplet, and neutral, singly-charged, and doubly-charged fields making up the custodial 5-plet.

When combined with the usual SM doublet field Φ, the electroweak scale v is now related to the doublet and triplet VEVs by

$$v^2 = v_\Phi^2 + 8v_\Xi^2 \,. \tag{11.56}$$

Note that the GM triplets by themselves are sufficient to explain electroweak symmetry breaking and the existence of a 125 GeV neutral boson along with a custodial triplet of Goldstone bosons; the complex doublet field in the GM model is required to generate fermion masses via the usual dimension four Yukawa couplings. This raises the question of whether one can rule out the possibility that the 125 GeV boson is the neutral member of a custodial 5-plet rather than a custodial singlet, without invoking decays to fermions. A conclusive answer is given by observing that the ratio of the branching fractions to W versus Z bosons is completely determined by the custodial symmetry properties of the boson. For a custodial 5-plet, the ratio of the signal strength to WW over that to ZZ is predicted to be 1/4 that of a SM Higgs boson [419], and thus already ruled out by the experimental results presented in Section 11.5.

Another interesting general feature of Higgs triplet models is that, after mixing, the SM-like neutral boson can have stronger couplings to WW and ZZ than predicted by the SM [420]; this is in contrast to mixing with additional doublets and singlet, which can only reduce the WW and ZZ couplings versus the SM. This emphasises that LHC Higgs data cannot extract model independent coupling strengths for the Higgs boson [291].

Because of the built-in custodial symmetry, the triplet VEV in the GM model can be large compared to the doublet VEV. The custodial singlet neutral boson from the triplets mixes with the neutral boson from the doublet. Two interesting special cases are (i) the triplet VEV is small and the 125 GeV boson is SM-like except for small deviations, and (ii) the 125 GeV boson is mostly the custodial singlet neutral boson from the electroweak triplets. The phenomenology of the doubly-charged and singly-charged bosons is similar to that of the HTM. The constraints on the GM model from precision electroweak data, LEP data, and current LHC data are summarised in Ref. [40].

11.6.6 *Composite Higgs models*

Within the SM, EWSB is posited but has no dynamical origin. Furthermore, the Higgs boson appears to be unnaturally light. A scenario that remedies these two catches is to consider the Higgs boson as a bound state of new dynamics becoming strong around the weak scale. The Higgs boson can be made significantly lighter than the other resonances of the strong sector if it appears as a pseudo-Nambu–Goldstone boson, see Refs. [11] for reviews.

11.6.6.1 *Little Higgs models*

The idea behind the Little Higgs boson models [421] is to identify the Higgs doublet as a (pseudo) Nambu–Goldstone boson while keeping some sizeable non-derivative interactions, in particular a largish Higgs quartic interaction. By analogy with QCD where the pions $\pi^{\pm,0}$ appear as Nambu–Goldstone bosons associated to the breaking of the chiral symmetry $\mathrm{SU}(2)_\mathrm{L} \times \mathrm{SU}(2)_\mathrm{R}/\mathrm{SU}(2)$, switching on some interactions that break explicitly the global symmetry will generate masses for the would-be massless Nambu–Goldstone bosons of the order of $g\Lambda_{G/H}/(4\pi)$, where g is the coupling of the symmetry breaking interaction and $\Lambda_{G/H} = 4\pi f_{G/H}$ is the dynamical scale of the global symmetry breaking G/H. In the case of the Higgs boson, the top Yukawa interaction or the gauge interactions themselves will certainly break explicitly (part of) the global symmetry since they act non-linearly on the Higgs boson. Therefore, obtaining a Higgs boson mass around 125 GeV would demand a dynamical scale $\Lambda_{G/H}$ of the order of 1 TeV, which is known to lead to too large

oblique corrections. Raising the strong dynamical scale by at least one order of magnitude requires an additional selection rule to ensure that a Higgs boson mass is generated at the 2-loop level only

$$m_H^2 = \frac{g^2}{16\pi^2}\Lambda_{G/H}^2 \to m_H^2 = \frac{g_1^2 g_2^2}{(16\pi^2)^2}\Lambda_{G/H}^2. \tag{11.57}$$

The way to enforce this selection rule is through a "collective breaking" of the global symmetry:

$$\mathcal{L} = \mathcal{L}_{G/H} + g_1\mathcal{L}_1 + g_2\mathcal{L}_2. \tag{11.58}$$

Each interaction $\mathcal{L}_1$ or $\mathcal{L}_2$ individually preserves a subset of the global symmetry such that the Higgs boson remains an exact Nambu–Goldstone boson whenever either g_1 or g_2 is vanishing. A mass term for the Higgs boson can be generated only by diagrams involving simultaneously both interactions. At one-loop, such diagrams are not quadratically divergent, so the Higgs boson mass is not UV sensitive. Explicitly, the cancellation of the SM quadratic divergences is achieved by a set of new particles around the Fermi scale: gauge bosons, vector-like quarks, and extra massive scalars, which are related, by the original global symmetry, to the SM particles with the same spin. Contrary to SUSY, the cancellation of the quadratic divergences is achieved by same-spin particles. These new particles, with definite couplings to SM particles as dictated by the global symmetries of the theory, are perfect goals for the LHC.

The simplest incarnation of the collective breaking idea, the so-called littlest Higgs boson model, is based on a non-linear σ-model describing the spontaneous breaking SU(5) down to SO(5). A subgroup $\mathrm{SU}(2)_1 \times \mathrm{U}(1)_1 \times \mathrm{SU}(2)_2 \times \mathrm{U}(1)_2$ is weakly gauged. This model contains a weak doublet, that is identified with the Higgs doublet, and a complex weak triplet whose mass is not protected by collective breaking. Other popular little Higgs models are based on different coset spaces: minimal moose $(\mathrm{SU}(3)^2/\mathrm{SU}(3))$, the simplest little Higgs $(\mathrm{SU}(3)^2/\mathrm{SU}(2)^2)$, the bestest little Higgs $(\mathrm{SO}(6)^2/\mathrm{SO}(6))$. For comprehensive reviews, see Ref. [422].

Generically, oblique corrections in Little Higgs models are reduced either by increasing the coupling of one of the gauge groups (in the case of product group models) or by increasing the masses of the W and Z partners, leading ultimately to a fine-tuning of the order of a few percents (see for instance Ref. [423] and references therein). The compatibility of Little Higgs models with experimental data is significantly improved when the global symmetry involves a custodial symmetry as well as a T-parity [424] under which, in analogy with R-parity in SUSY models, the SM particles are even and their partners are odd. Such Little Higgs models would therefore appear in colliders as jet(s) with missing transverse energy [425] and the ATLAS and CMS searches for squarks and gluinos can be recast to obtain limits on the masses of the heavy vector-like quarks. The T-even top partner, with an expected mass below 1 TeV to cancel the top loop quadratic divergence without too much fine-tuning, would decay dominantly into a $t+Z$ pair or into a $b+W$ pair or even into $t+H$. The latest CMS and ATLAS direct searches [426] for vector-like top partners put a lower bound around 1.1–1.3 TeV (for various branching fraction combinations), excluding the most natural region of the parameter space of these models, i.e., imposing a fine-tuning below the percent level.

The motivation for Little Higgs models is to solve the little hierarchy problem, i.e., to push the need for new physics (responsible for the stability of the weak scale) up to around 10 TeV. Per se, Little Higgs models are effective theories valid up to their cutoff scale $\Lambda_{G/H}$. Their UV completions could either be weakly or strongly coupled.

11.6.6.2 *Models of partial compositeness*

Even in composite models, the Higgs boson cannot appear as a regular resonance of the strong sector without endangering the viability of the setup when confronted to data. The way out is that

the Higgs boson appears as a pseudo Nambu–Goldstone boson: the new strongly coupled sector is supposed to be invariant under a global symmetry G spontaneously broken to a subgroup H at the scale f (the typical mass scale of the resonances of the strong sector is $m_\rho \sim g_\rho f$ with g_ρ the characteristic coupling of the strong sector). To avoid conflict with EW precision measurements, the strong interactions themselves should better not break the EW symmetry. Hence the SM gauge symmetry itself should be contained in H. See Table 11.10 for a few examples of coset spaces.

Table 11.10: Global symmetry breaking patterns and the corresponding Goldstone boson contents of the SM, the minimal composite Higgs model, the next to minimal composite Higgs model, and the minimal composite two Higgs doublet model. Note that the SU(3) model does not have a custodial invariance. a denotes a CP-odd scalar while h and H are CP-even scalars.

Model	Symmetry Pattern	Goldstones
SM	SO(4)/SO(3)	W_L, Z_L
–	SU(3)/SU(2)×U(1)	W_L, Z_L, H
MCHM	SO(5)/SO(4)	W_L, Z_L, H
NMCHM	SO(6)/SO(5)	W_L, Z_L, H, a
MC2HM	SO(6)/SO(4)×SO(2)	$W_L, Z_L, h, H, H^\pm, a$

The SM (light) fermions and gauge bosons cannot be part of the strong sector itself since LEP data have already put stringent bounds on the compositeness scale of these particles far above the TeV scale. The gauge bosons couple to the strong sector by a weak gauging of a SU(2)×U(1) subgroup of the global symmetry G. Inspiration for the construction of such models comes from the AdS/CFT correspondence: the components of a gauge field along an extra warped space dimension can be interpreted as the Goldstone bosons resulting from the breaking of global symmetry of the strong sector. The couplings of the SM fermions to the strong sector could a priori take two different forms:

(i) a bilinear coupling of two SM fermions to a composite scalar operator, $\mathcal{O}$, of the form $\mathcal{L} = y\,\bar{q}_L u_R \mathcal{O} + h.c.$, in simple analogy with the SM Yukawa interactions. This is the way fermion masses were introduced in technicolor theories and it generically comes with severe flavour problems and calls for extended model-building gymnastics [12] to circumvent them;

(ii) a linear mass mixing with fermionic vector-like operators: $\mathcal{L} = \lambda_L\,\bar{q}_L \mathcal{Q}_R + \lambda_R \bar{\mathcal{U}}_L u_R$. $\mathcal{Q}$ and $\mathcal{U}$ are two fermionic composite operators of mass M_Q and M_U.

Being part of the composite sector, the composite fermionic operators can have a direct coupling of generic order Y_* to the Higgs boson. In analogy with the photon-ρ mixing in QCD, once the linear mixings are diagonalised, the physical states are a linear combination of elementary and composite fields. Effective Yukawa couplings are generated and read for instance for the up-type quark

$$y = Y_* \sin\theta_L \sin\theta_R \tag{11.59}$$

where $\sin\theta_i = \lambda_i/\sqrt{M^2_{Q,U} + \lambda_i^2}$, $i = L, R$, measure the amount of compositeness of the SM left- and right-handed up-type quark. If the strong sector is flavour-anarchic, i.e., if the couplings of the Higgs boson to the composite fermions does not exhibit any particular flavour structure, the relation Eq. (11.59) implies that the light fermions are mostly elementary states ($\sin\theta_i \ll 1$), while the third generation quarks need to have a sizable degree of compositeness. The partial

compositeness paradigm offers an appealing dynamical explanation of the hierarchies in the fermion masses. In fact, assuming the strong sector to be almost conformal above the confinement scale, the low-energy values of the mass-mixing parameters $\lambda_{L,R}$ are determined by the (constant) anomalous dimension of the composite operator they mix with. If the UV scale at which the linear mixings are generated is large, then $\mathcal{O}(1)$ differences in the anomalous dimensions can generate naturally large hierarchies in the fermion masses via renormalisation group running [427]. While the introduction of partial compositeness greatly ameliorated the flavour problem of the original composite Higgs models, nevertheless, it did not solve the issue completely, at least in the case where the strong sector is assumed to be flavour-anarchic [428]. While the partial compositeness set-up naturally emerges in models built in space-times with extra dimensions, no fully realistic microscopic realisation of partial compositeness has been proposed in the literature.

Another nice aspect of the partial compositeness structure is the dynamical generation of the Higgs potential that is not arbitrary like in the SM. The Higgs boson being a pseudo-Nambu–Goldstone boson, its mass does not receive any contribution from the strong sector itself but it is generated at the one-loop level via the couplings of the SM particles to the strong sector since these interactions are breaking the global symmetries under which the Higgs doublet transforms non-linearly. Obtaining $v \ll f$, as required phenomenologically, requires some degree of tuning, which scales like $\xi \equiv v^2/f^2$. A mild tuning of the order of 10% ($\xi \approx 0.1$) is typically enough to comply with electroweak precision constraints. This is an important point: in partial compositeness models, the entire Higgs potential is generated at one loop, therefore the separation between v and f can only be obtained at a price of a tuning. This marks a difference with respect to the Little Higgs models which realise a parametric hierarchy between the quartic and mass terms through the collective symmetry breaking mechanism. In fact in Little Higgs models, the quartic coupling is a tree-level effect, leading to a potential

$$V(H) \approx \frac{g_{\rm SM}^2}{16\pi^2} m_\rho^2 H^2 + g_{\rm SM}^2 H^4, \tag{11.60}$$

where $g_{\rm SM}$ generically denotes the SM couplings. The minimisation condition reads $v^2/f^2 \sim g_\rho^2/(16\pi^2)$, therefore v is formally loop suppressed with respect to f. This is the major achievement of the Little Higgs constructions, which however comes at the price of the presence of sub-TeV vectors carrying EW quantum numbers and therefore giving rise generically to large oblique corrections to the propagators of the W and the Z gauge bosons.

After minimisation, the dynamically generated potential leads to an estimate of the Higgs boson mass as

$$m_H^2 \approx g_\rho^3\, y_t 2\pi^2 v^2. \tag{11.61}$$

It follows that the limit $f \to \infty$, i.e., $\xi \to 0$, is a true decoupling limit: all the resonances of the strong sector become heavy but the Higgs boson whose mass is protected by the symmetries of the coset G/H. When compared to the experimentally measured Higgs boson mass, this estimate puts an upper bound on the strength of the strong interactions: $g_\rho \lesssim 2$. In this limit of not so large coupling, the Higgs potential receives additional contributions. In particular, the fermionic resonances in the top sector which follow from the global symmetry structure of the new physics sector can help raising the Higgs boson mass. Using some dispersion relation techniques, the mass of the Higgs is connected to the resonance masses. In the minimal SO(5)/SO(4) model, it was shown [429] that a 125 GeV mass can be obtained if at least one of the fermionic resonances is lighter than $\sim 1.4\, f$. As in SUSY scenarios, the top sector is playing a crucial role in the dynamics of EWSB and can provide the first direct signs of new physics. The direct searches for these top partners, in particular the ones with exotic electric charges 5/3, are already exploring the natural parameter spaces of these models [430].

The main physics properties of a pseudo Nambu–Goldstone Higgs boson can be captured in a model-independent way by a small number of higher-dimensional operators. Indeed, the strong dynamics at the origin of the composite Higgs boson singles out a few operators among the complete list discussed earlier in Section 11.5: these are the operators that involve extra powers of the Higgs doublets, and they are therefore generically suppressed by a factor $1/f^2$ as opposed to the operators that involve extra derivatives or gauge bosons that are suppressed by a factor $1/(g_\rho^2 f^2)$. The relevant effective Lagrangian describing a strongly interacting light Higgs boson is:

$$\mathcal{L}_{\rm SILH} = \frac{c_H}{2f^2}\left(\partial_\mu\left(\Phi^\dagger\Phi\right)\right)^2 + \frac{c_T}{2f^2}\left(\Phi^\dagger \overleftrightarrow{D}^\mu \Phi\right)^2 - \frac{c_6\lambda}{f^2}\left(\Phi^\dagger\Phi\right)^3 + \left(\sum_f \frac{c_f\, y_f}{f^2}\Phi^\dagger\Phi\bar{f}_L\Phi f_R + \text{h.c.}\right). \tag{11.62}$$

Typically, these new interactions induce deviations in the Higgs boson couplings that scale like $\mathcal{O}(v^2/f^2)$. Hence, the measurements of the Higgs boson couplings can be translated into some constraints on the compositeness scale, $4\pi f$, of the Higgs boson. The peculiarity of these composite models is that, due to the Goldstone nature of the Higgs boson, the direct couplings to photons and gluons are further suppressed and generically the coupling modifiers scale like

$$\kappa_{W,Z,f} \sim 1 + \mathcal{O}\left(\frac{v^2}{f^2}\right), \quad \kappa_{Z\gamma} \sim \mathcal{O}\left(\frac{v^2}{f^2}\right), \quad \kappa_{\gamma,g} \sim \mathcal{O}\left(\frac{v^2}{f^2}\times\frac{y_t^2}{g_\rho^2}\right), \tag{11.63}$$

where g_ρ denotes the typical coupling strength among the states of the strongly coupled sector and y_t is the top Yukawa coupling, the largest interaction that breaks the Goldstone symmetry. The $\kappa_{Z\gamma,\gamma,g}$ coupling modifiers are not generated by the strong coupling operators of Eq. (11.62) but by some subleading form-factor operator generated by loops of heavy resonances of the strong sector. The coupling modifiers also receive additional contributions from the other resonances of the strong sector, in particular the fermionic resonances of the top sector that are required to be light to generate a 125 GeV Higgs boson mass. Some indirect information on the resonance spectrum could thus be inferred by a precise measurement of the Higgs boson coupling deviations. However, it was realised, see in particular Ref. [306], that the task is actually complicated by the fact that, in the minimal models, these top partners give a contribution to both κ_t (resulting from a modification of the top Yukawa coupling) and κ_γ and κ_g (resulting from new heavy particles running into the loops) and the structure of interactions is such that the net effect vanishes for inclusive quantities like $\sigma(gg \to H)$ or $\Gamma(H \to \gamma\gamma)$ as a consequence of the Higgs low energy theorem [21, 22, 301]. So, one would need to rely on differential distribution, like the Higgs boson p_T distribution discussed in Section 11.2.4.1, to *see* the top partner effects in Higgs data [431]. The off-shell channel $gg \to H^* \to 4\ell$ [290] and the double Higgs boson production $gg \to HH$ [432] can also help to resolve the gluon loop and separate the top and top-partner contributions.

11.6.6.3 *Minimal composite Higgs models*

The minimal composite Higgs models (MCHM) are concrete examples of the partial compositeness paradigm. The Higgs doublet is described by the coset space SO(5)/SO(4) where a subgroup $\mathrm{SU}(2)_L\times\mathrm{U}(1)_Y$ is weakly gauged and under which the four Goldstone bosons transform as a doublet of hypercharge 1. There is some freedom on how the global symmetry is acting on the SM fermions: in MCHM4 the quarks and leptons are embedded into spinorial representations of SO(5), while in MHCM5 they are part of fundamental representations (it might also be interesting phenomenologically to consider larger representations like MCHM14 [433] with the SM fermions inside a representation of dimension 14). It is also possible to consider that fermions of different chirality and flavour are in different representations of SO(5), leading to a more varied phenomenology [434].

The non-linearly realised symmetry acting on the Goldstone bosons leads to general predictions of the coupling of the Higgs boson to the EW gauge bosons. For instance, it can be shown that the quadratic terms in the W and Z bosons read

$$m_W^2(H)\left(W_\mu W^\mu + \frac{1}{2\cos^2\theta_W} Z_\mu Z^\mu\right), \tag{11.64}$$

with $m_W(H) = \frac{gf}{2}\sin\frac{H}{f}$. Expanding around the EW vacuum, the expression of the weak scale is $v = f\sin(\langle H\rangle/f)$. And the values of the modified Higgs boson couplings to the W and Z become:

$$g_{HVV} = \frac{2m_V^2}{v}\sqrt{1-v^2/f^2}\,, \quad g_{HHVV} = \frac{2m_V^2}{v^2}(1-2v^2/f^2)\,. \tag{11.65}$$

Note that the Higgs boson couplings to gauge bosons is always suppressed compared to the SM prediction. This is a general result [435] that holds as long as the coset space is compact.

The Higgs boson couplings to the fermions depend on the representation which the SM fermions are embedded into. The most commonly used embeddings consider all fermion doublets and singlets in the same representations. While, in MCHM4 and MCHM5, the modifications of the couplings depend only on the Higgs boson compositeness scale, in MCHM14 the leading corrections depend also on the mass spectrum of the resonances [433]. This is due to the fact that more than one SO(5) invariant gives rise to SM fermion masses. The (κ_V, κ_f) experimental fit of the Higgs boson couplings can be used to derive a lower bound on the Higgs boson compositeness scale $4\pi f \gtrsim 9\,\text{TeV}$, which is less stringent than the indirect bound obtained from EW precision data, $4\pi f \gtrsim 15\,\text{TeV}$ [436] but more robust and less subject on assumptions [437].

11.6.6.4 *Twin Higgs models*

In all composite models presented above, the particles responsible for canceling the quadratic divergences in the Higgs boson mass are charged under the SM gauge symmetries. In particular, the top partner carries color charge, implying a reasonably large minimal production cross section at the LHC. An alternative scenario, which is experimentally quite challenging and might explain the null result in various new physics searches, is the case nowadays referred to as "neutral naturalness" [13, 14], where the particles canceling the 1-loop quadratic divergences are neutral under the SM. The canonical example for such theories is the Twin Higgs model of Ref. [13]. This is an example of a pseudo-Goldstone boson model with an approximate global SU(4) symmetry broken to SU(3). The Twin Higgs model is obtained by gauging the $\text{SU}(2)_A\times\text{SU}(2)_B$ subgroup of SU(4), where $\text{SU}(2)_A$ is identified with the SM $\text{SU}(2)_L$, while $\text{SU}(2)_B$ is the twin SU(2) group. Gauging this subgroup breaks the SU(4) symmetry explicitly, but quadratically divergent corrections do not involve the Higgs boson when the gauge couplings of the two SU(2) subgroups are equal, $g_A = g_B$. The SU(4)→ SU(3) breaking will also result in the breaking of the twin $\text{SU}(2)_B$ group and, as a result, three of the seven Goldstone bosons will be eaten, leaving 4 Goldstone bosons corresponding to the SM Higgs doublet. In fact, imposing the Z_2 symmetry on the full model will ensure the cancellation of all 1-loop quadratic divergences to the Higgs boson mass. Logarithmically divergent terms can, however, arise for example from gauge loops, leading to a Higgs boson mass of order $g^2 f/4\pi$, which is of the order of the physical Higgs boson mass for $f \sim 1\,\text{TeV}$. The quadratic divergences from the top sector can be eliminated if the Z_2 protecting the Higgs boson mass remains unbroken by the couplings that result in the top Yukawa coupling. This can be achieved by introducing top partners charged under a twin $\text{SU}(3)_C$. In this case, the quadratic divergences are cancelled by top partners that are neutral under the SM gauge symmetries.

Twin Higgs models are low-energy effective theories valid up to a cutoff scale of order $\Lambda \sim 4\pi f \sim 5$–$10\,\text{TeV}$, beyond which a UV completion has to be specified. The simplest such possibility

is to also make the Higgs boson composite, and to UV complete the twin Higgs model via gauge and top partners at masses of the order of a few TeV. A concrete implementation is the holographic twin Higgs model [438], which also incorporates a custodial symmetry to protect the T-parameter from large corrections. It is based on a warped extra dimensional theory with a bulk SO(8) gauge group, which incorporates the SU(4) global symmetry discussed above enlarged to contain the $SU(2)_L \times SU(2)_R$ custodial symmetry. In addition, the bulk contains either a full SU(7) group or an $SU(3) \times SU(3) \times U(1) \times U(1) \times Z_2$ subgroup of it to incorporate the QCD, its twin, and the hypercharge local symmetries. The breaking on the UV brane is to the SM symmetries and their twin symmetries, while on the IR brane $SO(8) \to SO(7)$, giving rise to the 7 Goldstone bosons, three of which will be again eaten by the twin W, Z. The main difference compared to ordinary composite Higgs models is that, in composite twin Higgs models, the cancellation of the one-loop quadratic divergences is achieved by the twin partners. They have a mass of order 700 GeV–1 TeV and they are uncharged under the SM gauge group. This allows the IR scale of the warped extra dimension to be raised to the multi-TeV range without reintroducing the hierarchy problem. The role of the composite partners is to UV complete the theory, rather than to cancel the one-loop quadratic divergences. For more details about the composite twin Higgs models, see Refs. [439].

11.6.7 *Searches for signatures of extended Higgs sectors*

The measurements described in Sections 11.3 to 11.5 have established the existence of one state of the electroweak symmetry breaking sector, compatible with a SM Higgs boson, but not that it is the only one. As was discussed above, several classes of models beyond the SM require extended Higgs sectors. The searches are typically designed to be as model-independent as possible[7] and can be categorised in the classes summarised as follows:

(i) the search for an additional CP-even state mostly in the high mass domain decaying to vector bosons, which would correspond either to the heavy CP-even state in a generic 2HDM where the light state would be the discovered Higgs boson at 125 GeV or to a generic additional singlet;

(ii) the search for a state in the high mass domain decaying to pairs of fermions, which would correspond to the CP-odd A or the heavy CP-even state H in a generic 2HDM;

(iii) the search for charged Higgs bosons, which also appear in generic 2HDMs;

(iv) the search for a CP-odd state a in the low mass region which appears in the NMSSM in a variety of final states, e.g., with one or two a bosons decaying to pairs of photons, muons, taus, and b-quarks;

(v) the search for doubly charged Higgs bosons which are expected in extensions of the Higgs sector with triplets.

Below is a concise description of the most recent searches performed at the LHC and elsewhere. A summary of these searches in terms of final states is given in Table 11.11 where the corresponding references are given for more details.

11.6.7.1 *Searches for an additional CP-even state*

(a) Exclusion limits from LEP

The searches for the SM Higgs boson at LEP provided an absolute lower limit of 114 GeV on its mass. These searches are also relevant for non-SM Higgs bosons. These searches were interpreted as 95% CL upper bounds on the ratio of the coupling g_{HZZ} to its SM prediction as a function of the Higgs boson mass [139, 523]. These results have an impact on MSSM benchmarks such as

[7] Still, most non-SUSY models are likely to include further states and dynamics above the weak scale to stabilise the scalar sector and this new and unknown physics may influence the searches described in this section in a way difficult to estimate.

Table 11.11: Summary of references to the searches for additional states from extended Higgs sectors. (BBr) denotes the BaBar experiment and (TeV), the Tevatron experiments. V denotes either the W or the Z boson. Only Run-2 searches references are indicated except when searches have been carried out using Run-1 data only. References for Run-1 searches are available in Ref. [141].

	ATLAS	CMS	Other experiments
CP-even H			
$H \to \gamma\gamma$	[440, 441]	[442, 443]	—
$H \to \gamma\gamma$ (low mass)	[444]	[445]	—
$H \to Z\gamma$	[446, 447]	[448]	—
$H \to ZZ \to 4\ell$	[449]	[450]	—
$H \to ZZ \to \ell\ell\nu\nu$	[449]	[451]	—
$H \to WZ \to \ell\ell\ell\nu$	—	[452]	—
$H \to ZZ \to \ell\ell q\bar{q}$	[453]	[454, 455]	—
$H \to ZZ \to \nu\nu q\bar{q}$	[456]	—	—
$H \to WW \to \ell\nu\ell\nu$	[457]	[458]	—
$H \to WW \to \ell\nu q\overline{q'}$	[459]	[458]	—
$H \to VV \to q\overline{q'}q\overline{q'}(JJ)$	[460, 461]	—	—
$H \to VV$ combination	[462]	—	—
$H \to hh \to b\bar{b}\tau\tau, b\bar{b}\gamma\gamma, 4b,$ $\gamma\gamma WW^*, bbWW^*, WW^*WW^*, bbZZ^*$	[463–465]	[455, 466, 467]	—
CP-odd A (and/or CP-even H)			
$H, A \to \tau^+\tau^-$	[468]	[469, 470]	[471, 472] (TeV) [473] (LHCb)
$A \to \tau^+\tau^-$ (low mass)	—	[474]	—
$H, A \to \mu^+\mu^-$	[475]	[476]	—
$H \to \mu\tau, e\tau$ LFV		[477]	—
$bj\mu^+\mu^-$ (low $\mu^+\mu^-$ mass)	[478]	[479]	—
$H, A \to t\bar{t}$	[461, 480]	[481]	—
$H, A \to b\bar{b}$	[482]	[483]	[484, 485] (TeV)
$A \to hV \to b\bar{b}q\overline{q'}, b\bar{b}\ell\nu, b\bar{b}\ell\ell, \ell\ell\tau\tau, \nu\bar{\nu}b\bar{b}$	[486, 487]	[488, 489]	—
$A \to ZH$	[490]	[491]	—
$H \to ZA \to b\bar{b}\ell^+\ell^-$	[213]	[492]	—
Charged $H^\pm$			
$H^\pm \to \tau^\pm\nu$	[493, 494]	[495]	—
$H^\pm \to cs$	[496]	[497]	—
$H^\pm \to tb$	[498]	[499]	—
$H^\pm \to W^\pm Z$	[500]	[501, 502]	—
$H^\pm \to W^\pm A$	—	[503]	—
$H^\pm \to HW^\pm$	—	[504]	—
$H^\pm \to cb$	—	[505]	—
CP-odd a			
$a \to \mu^+\mu^-$	[506]	[507]	—
$h \to aa \to 4\mu, 4\tau, 2\mu2\tau, 4\gamma$	[508]	[509–512]	[513] (LEP)
[514] (TeV) $h \to aa \to bb\mu\mu, bb\tau\tau, 4b$	[515, 516]	[517, 518]	—
$\Upsilon_{1s,3s} \to a\gamma$	—	—	[519, 520] (BBr)
Doubly charged $H^{\pm\pm}$	[521]	[502, 522]	—

the low-m_H scenario where the heavy CP-even Higgs boson is the discovered 125 GeV boson [374], which is also nearly ruled out by current direct constraints and charged Higgs boson limits from LHC. These results also impact scenarios of light CP-even Higgs boson of the NMSSM which are constrained to project predominantly onto the EW singlet component. Additional interest for these scenarios is due to the slight excess observed at LEP [139] at a Higgs boson mass hypothesis of approximately 98 GeV, bolstered by a possible excess in the diphoton channel at 96 GeV in Run-2 data of CMS [445].

(b) Searches at the LHC

At the LHC, the searches for the SM Higgs boson before the 2012 discovery covered a wide range of mass hypotheses up to approximately 1 TeV. After the discovery, the SM Higgs boson searches have been reappraised to search for a heavy CP-even state, extending progressively the search mass range beyond 1 TeV. This state could be the heavy CP-even Higgs boson of a 2HDM, or a generic additional singlet. In both cases, the natural width of the additional H state can be very different from that of the SM Higgs boson. To preserve unitarity of the longitudinal vector boson scattering and the longitudinal vector boson scattering into fermion pairs, the couplings of the additional CP-even Higgs boson to gauge bosons and fermions should not be too large and should constrain the natural width to be smaller than that of a unique Higgs boson at high mass with couplings to fermions and gauge bosons as predicted by the SM (and provided that trilinear and quartic couplings are not too large and that no new state affects the heavy state total width). It is therefore reasonable to consider total widths for the high mass CP-even state smaller than the equivalent SM width. Two specific cases have been considered: (i) the SM width using the complex pole scheme (CPS), and (ii) the narrow width approximation. For the sake of generality, these searches are now done as a function of the Higgs boson mass and total width.

Searches for the Higgs boson in the channels $H \to \gamma\gamma$, $H \to Z\gamma$, $H \to WW^{(*)}$ leptonic and semi-leptonic, and in the $H \to ZZ^{(*)}$ searches in the 4ℓ, $\ell\ell q\bar{q}$ and $\ell\ell\nu\nu$ channels have also been done, but some of them are simple reinterpretations of the SM Higgs boson search in the CPS scheme. References for these searches are summarised in Table 11.11.

(c) Searches for an additional resonance decaying to a pair of Higgs bosons

In addition to the rare and expected Higgs boson pair production mode, high mass CP-even Higgs bosons can be searched for in the resonant double Higgs boson mode. Searches for such processes, where the Higgs boson is used as a tool for searches for BSM phenomena, have been carried out in a variety of distinct modes depending on the subsequent decays of each Higgs bosons. ATLAS and CMS have searched for the $H \to hh \to b\bar{b}\tau\tau$, $b\bar{b}\gamma\gamma$, $H \to hh \to 4b$, $H \to hh \to \gamma\gamma WW^*$, $H \to hh \to bbWW^*$, $H \to hh \to WW^*WW^*$ and $H \to hh \to bbZZ^*$ final states. For mass hypotheses of an additional Higgs boson below 500 GeV, the two dominant search channels are the $b\bar{b}\gamma\gamma$ and the $b\bar{b}\tau\tau$ channels. For masses above 500 GeV, the most powerful search is with the $4b$ final state. As illustrated in Fig. 11.17, these searches provide useful limits in the low $\tan\beta$ and high mass domain. The list of references for these searches is given in Table 11.11.

(d) Searches for an additional state with the presence of the Higgs boson

In the post-discovery era, analyses searching for additional Higgs bosons need to take into account the presence of the 125 GeV Higgs boson. For searches with sufficiently high mass resolution to disentangle the additional states which are not degenerate in mass, the strength of the observed state and limits on the signal strength of a potential additional state can be set independently, as discussed in the next section. However, in some cases where channels do not have a sufficiently fine mass resolution to resolve states nearly degenerate in mass, specific analyses need to be designed. There are two examples of such analyses: (i) the search for an additional state in the

$H \to WW^{(*)} \to \ell\nu\ell\nu$ channel in ATLAS, and (ii) the search for nearly degenerate states in the $H \to \gamma\gamma$ channel with the CMS detector.

In the $H \to WW^{(*)} \to \ell\nu\ell\nu$ channel, the search for an additional state is done using a boosted decision tree combining several discriminating kinematic characteristics to separate both the signal from the background and a high mass signal H from the lower mass state h [524]. A simultaneous fit of the two states h and H is then made to test the presence of an additional state. In this case, the usual null hypothesis of background includes the SM signal.

The CMS search for nearly degenerate mass states decaying to a pair of photons [525] is more generic and could for instance apply to CP-odd Higgs bosons as well. It consists of a fit to the diphoton mass spectrum using two nearly degenerate mass templates.

(e) Type I 2HDM and fermiophobia

The measurements of coupling properties of the 125 GeV Higgs boson directly establish its couplings to fermions. However, the presence of an additional fermiophobic state, as predicted by Type I 2HDMs, is not excluded. Prior to the discovery, ATLAS and CMS have performed searches for a fermiophobic Higgs boson, i.e., produced through couplings with vector bosons only (VBF and VH) and decaying in two photons. CMS has further combined these results with searches in the W^+W^- and ZZ channels, assuming fermiophobic production and decay. This way, CMS excluded a fermiophobic Higgs boson in the range $110\,\text{GeV} < m_H < 188\,\text{GeV}$ at the 95% CL. References for these Run-1 measurements can be found in Ref. [141]

11.6.7.2 *Searches for additional neutral states ($\phi \equiv h$, H, A) decaying to fermions*

(a) Exclusion limits from LEP

In e^+e^- collisions, around the centre-of-mass energies reached by LEP, the main production mechanisms of the neutral MSSM Higgs bosons were the Higgs-strahlung processes $e^+e^- \to hZ$, HZ and the pair production processes $e^+e^- \to hA$, HA, while the vector boson fusion processes played a marginal role. Higgs boson decays to $b\bar{b}$ and $\tau^+\tau^-$ were used in these searches.

The searches and limits from the four LEP experiments are described in Refs. [526]. The combined LEP data did not contain any excess of events which would imply the production of a Higgs boson. Combined limits were derived [523]. For $m_A \gg M_Z$, the limit on m_h is nearly that of the SM searches, as $\sin^2(\beta-\alpha) \approx 1$. For high values of $\tan\beta$ and low m_A ($m_A \leq m_h^{max}$), the $e^+e^- \to hA$ searches become the most important, and the lightest Higgs boson h is non SM-like. In this region, the 95% CL mass bounds are $m_h > 92.8\,\text{GeV}$ and $m_A > 93.4\,\text{GeV}$. In the m_h^{max} scenario [527], values of $\tan\beta$ from 0.7 to 2.0 are excluded taking $m_t = 174.3\,\text{GeV}$, while a much larger $\tan\beta$ region is excluded for other benchmark scenarios such as the no-mixing one.

A flavour-independent limit for Higgs bosons in the Higgs-strahlung process at LEP has also been set at 112 GeV [528].

Neutral Higgs bosons may also be produced by Yukawa processes $e^+e^- \to f\bar{f}\phi$, where the Higgs particle $\phi \equiv h$, H, A, is radiated off a massive fermion ($f \equiv b$ or $\tau^\pm$). These processes can be dominant at low masses, and whenever the $e^+e^- \to hZ$ and hA processes are suppressed. The corresponding ratios of the $f\bar{f}h$ and $f\bar{f}A$ couplings to the SM coupling are $-\sin\alpha/\cos\beta$ and $\tan\beta$, respectively. The LEP data have been used to search for $b\bar{b}\,b\bar{b}$, $b\bar{b}\tau^+\tau^-$, and $\tau^+\tau^-\,\tau^+\tau^-$ final states [529]. Regions of low mass and high enhancement factors are excluded by these searches.

The searches for the Higgs boson at LEP also included the case where it does not predominantly decay to a pair of b quarks. All four collaborations conducted dedicated searches for the Higgs boson with reduced model dependence, assuming it is produced via the Higgs-strahlung process, and not addressing its flavour of decay, a lower limit on the Higgs boson mass of 112.9 GeV is set by combining the data of all four experiments [528].

Using an effective Lagrangian approach and combining results sensitive to the $h\gamma\gamma$, $hZ\gamma$ and hZZ couplings, an interpretation of several searches for the Higgs boson was made and set a lower limit of 106.7 GeV on the mass of a Higgs boson that can couple anomalously to photons [528].

(b) Searches at the Tevatron and the LHC

The best sensitivity is in the regime with low to moderate m_A and with large $\tan\beta$ which enhances the couplings of the Higgs bosons to down-type fermions. The corresponding limits on the Higgs boson production cross section times the branching ratio of the Higgs boson into down-type fermions can be interpreted in MSSM benchmark scenarios [530]. The most promising channels at the Tevatron are the inclusive $p\bar{p} \to \phi \to \tau^+\tau^-$ process ($\phi = A, H, h$), with contributions from both $gg \to \phi$ and $b\bar{b}\phi$ production, and $b\bar{b}\phi, \phi \to \tau^+\tau^-$ or $\phi \to b\bar{b}$, with $b\tau\tau$ or three tagged b-jets in the final state, respectively. Although the Higgs boson production via gluon fusion has a higher cross section in general than via associated production, it cannot be used to study the $\phi \to b\bar{b}$ decay mode since the signal is overwhelmed by the QCD background.

CDF and D0 have searched for neutral Higgs bosons produced in association with bottom quarks and which decay into $b\bar{b}$ [484,485], or into $\tau^+\tau^-$ [471,472]. The most recent searches in the $b\bar{b}\phi$ channel with $\phi \to b\bar{b}$ analyse approximately 2.6 fb^{-1} (CDF) and 5.2 fb^{-1} (D0) of data, seeking events with at least three b-tagged jets. The cross section is defined such that at least one b quark not from ϕ decay is required to have $p_T > 20$ GeV and $|\eta| < 5$. The invariant mass of the two leading jets as well as b-tagging variables are used to discriminate the signal from the backgrounds. The QCD background rates and shapes are inferred from data control samples, in particular, the sample with two b-tagged jets and a third, untagged jet. Separate-signal hypotheses are tested and limits are placed on $\sigma(p\bar{p} \to b\bar{b}\phi) \times \text{BR}(\phi \to b\bar{b})$. A local excess of approximately 2.5σ significance has been observed in the mass range of 130–160 GeV, but D0's search is more sensitive and sets stronger limits. The D0 result had a $\mathcal{O}(2\sigma)$ local upward fluctuation in the 110 to 125 GeV mass range. These results have been superseded by the LHC searches and the excess seen by D0 has not been confirmed elsewhere.

A substantially larger sensitivity in the search for the $\phi \to \tau^+\tau^-$ is obtained with the ATLAS and CMS analyses. The higher centre-of-mass energy reached at the Run 2 brings a substantial, though not excessively large, increase in sensitivity due to the intermediate masses probed. Both ATLAS and CMS have reported the result of their searches in this important channel with the full 2016 dataset. The searches are performed in categories of the decays of the two tau leptons: $e\tau_{\text{had}}$, $\mu\tau_{\text{had}}$, $e\mu$, and $\mu\mu$, where τ_{had} denotes a tau lepton which decays to one or more hadrons plus a tau neutrino, e denotes $\tau \to e\nu\nu$, and μ denotes $\tau \to \mu\nu\nu$. The dominant background comes from $Z \to \tau^+\tau^-$ decays, although $t\bar{t}$, W+jets and Z+jets events contribute as well. Separating events into categories based on the number of b-tagged jets improves the sensitivity in the MSSM. The $b\bar{b}$ annihilation process and radiation of a Higgs boson from a b quark gives rise to events in which the Higgs boson is accompanied by a $b\bar{b}$ pair in the final state. Requiring the presence of one or more b-jets reduces the background from Z+jets. Data control samples are used to constrain background rates. The rates for jets to be identified as a hadronically decaying tau lepton are measured in dijet samples, and W+jets samples provide a measurement of the rate of events that, with a fake hadronic tau, can pass the signal selection requirements. Lepton fake rates are measured using samples of isolated lepton candidates and same-sign lepton candidates. Constraints from the ATLAS searches are shown in Fig. 11.17 (left) in the hMSSM approximation defined in Ref. [376]. The neutral Higgs boson searches consider the contributions of both the CP-odd and CP-even neutral Higgs bosons with enhanced couplings to bottom quarks, similarly to was done for the Tevatron results. In Fig. 11.17, decays of the charged Higgs boson into $\tau\nu$ and decays of the heavy Higgs boson into a pair of SM-like Higgs bosons or gauge bosons, or decays of A into hZ are also

being constrained. In addition, decays of the neutral Higgs bosons into muon pairs are also being explored. In the $m_h^{\text{mod+}}$ scenario, the region of $\tan\beta$ lower than 5 does not allow for a Higgs boson mass m_h close to 125 GeV. For the hMSSM scenario, instead, the SM-like Higgs boson mass is fixed as an input and hence the requirement that it is close to 125 GeV is always fulfilled, although this may imply other limitations as discussed in Section 11.6.1.1.

A search for $\phi \to \mu^+\mu^-$ has also been performed by ATLAS [475] and CMS [476] and no significant deviations from the SM expectation were observed, allowing to set model-independent limit on the product of the branching fraction for the decay into a muon pair and the cross section for the production of a scalar neutral boson, either via gluon fusion, or in association with b quarks, in the mass range from 130 to 1000 GeV.

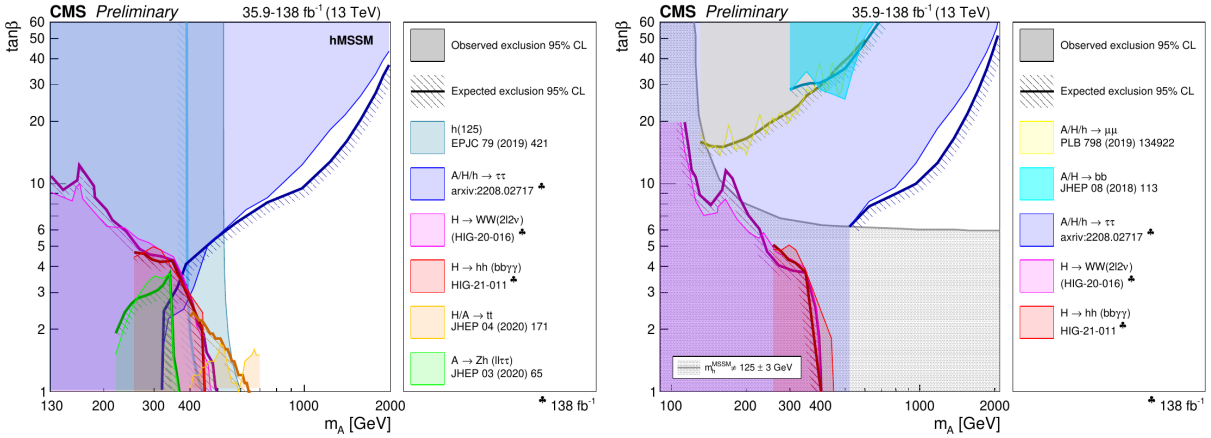

Figure 11.17: The 95% CL exclusion contours in the $(M_A, \tan\beta)$ parameter space for: (left) a summary of CMS Run-2 searches in the hMSSM and (right) in the M_h^{125} scenario.

Finally, searches for a resonance decaying to a top quark pair were done by ATLAS [480,531] and CMS [481,532]. These searches were interpreted as searches for scalar resonances by ATLAS [480], however, an important component of these searches is an accurate treatment of the interference effects between the signal and the continuum background. These effects can yield a dip and peak structure instead of a simple peak [372]. ATLAS has performed a search for a high mass state decaying to a pair of top quarks taking into account the deformation in mass shape of the signal in the presence of the continuum background [533].

The LHC has the potential to explore a broad range of SUSY parameter space through the search for non-SM-like Higgs bosons. As illustrated in Fig. 11.17, the parameter space corresponding to large $\tan\beta$ values and large masses of the A boson are covered mostly by the searches in the $A, H \to \tau^+\tau^-$ channel. A projection of the combined sensitivity of ATLAS and CMS at the HL-LHC has been performed in Ref. [118], showing that, compared to the current sensitivity, the full HL-LHC luminosity can expand the exclusion domain by nearly 1 TeV. In the low $\tan\beta$ limit, the parameter space spanning large A boson masses is best excluded indirectly from the observed Higgs boson measurements. This is illustrated in the M_h^{125} scenario by the nearly horizontal exclusion which is due to the compatibility of the Higgs boson mass measurement with its prediction from radiative corrections (mostly from the stop sector). Nevertheless, Fig. 11.17 (right) shows a broad region with intermediate $\tan\beta$ and large values of m_A that is not accessed by current searches, and in which the most promising channel is the very difficult search for $t\bar{t}$ decays with its aforementioned intricacies [379]. In this region of parameter space, it is possible that only the SM-like Higgs boson

can be within the LHC's reach. If no other state of the EWSB sector than the 125 GeV state is discovered, it may be challenging to determine only from the Higgs sector whether there is a SUSY extension of the SM in nature.

11.6.7.3 *Searches for a CP-odd state decaying to hZ*

Similarly, to the search for a CP-even high mass Higgs boson decaying to a pair of Higgs bosons, the search for a CP-odd states decaying to hZ was carried out at the LHC by ATLAS and CMS in various channels: (i) $(Z \to \ell\ell)(h \to b\bar{b})$, (ii) $(Z \to \nu\nu)(h \to b\bar{b})$, (iii) $(Z \to \ell\ell)(h \to \tau\tau)$, and (iv) $(Z \to \ell\ell)(h \to \tau\tau)$. The searches where the A boson decays to a pair of b quarks have been performed both in the regime where both b-jets are resolved and in the boosted regime where the two b-jets are merged in a single larger radius jet. These searches have been used to constrain the parameter space of 2HDMs. In the MSSM, these searches place limits on small values of $\tan\beta$ for masses of A between 220 GeV and 360 GeV.

11.6.7.4 *Searches for low mass states*

Searches for pseudo-scalar Higgs boson at intermediate to low masses, below the Z mass (in the 25 GeV to 80 GeV mass range) have been performed by CMS both in the $\tau^+\tau^-$ [534] and the $\mu^+\mu^-$ [535] decay channels. A light pseudo-scalar in this mass range is excluded by current direct constraints in the MSSM but not in general 2HDMs [536]. These searches are done in the decay channels where the pseudo-scalar Higgs boson is produced in association with a pair of b-quarks and decays into a pair of taus or muons.

CMS has also reported an anomaly observed in the search for $\mu^+\mu^-$ resonances produced with one jet tagged as containing a b-hadron and a forward jet in the Run-1 data. A mild excess appeared in the di-muon mass distribution at approximately 28 GeV. Another very mild excess was then also found in the 2016 Run-2 data [479]. ATLAS then performed a similar analysis with the full Run-2 dataset corresponding to an integrated luminosity of approximately 139 fb^{-1}, and no significant excess was found [478].

Searches for low mass Higgs bosons were also performed in the diphoton channel by both ATLAS and CMS [537, 538] at Run 1. ATLAS and CMS have updated the results of this search with Run-2 data [440, 442]. A modest excess has been observed by CMS at a mass of 95.4 GeV with a local significance of 2.9σ (the corresponding global significance is 1.3σ). A slight excess was also seen by ATLAS at the same mass of 95.4 GeV with a local significance of 1.7σ. No significant excess has been observed in this region by ATLAS at Run 1. This mildly significant excess also coincides in mass with the excess observed at LEP and discussed in Section 11.6.7.1. It is interesting to note that the sensitivity of searches at masses very near that of the Z boson, require a very strong rejection of events where electrons are misidentified as photons. Dedicated experimental methods have been developped to reduce the vulnerability of the analysis in this specific mass region to this background. It has therefore raised interest and speculations on its possible nature, see for instance Ref. [539] and references therein.

11.6.7.5 *Searches for charged Higgs bosons $H^\pm$*

At e^+e^- colliders, charged Higgs bosons can be pair produced in the s-channel via γ or Z boson exchange. This process is dominant in the LEP centre-of-mass energies range, i.e., up to 209 GeV. At higher centre-of-mass energies, other processes can play an important role such as the production in top quark decays via $t \to b + H^+$ if $m_{H^\pm} < m_t - m_b$ or via the one-loop process $e^+e^- \to W^\pm H^\mp$ [540, 541], which allows the production of a charged Higgs boson with $m_{H^\pm} > \sqrt{s}/2$, even when H^+H^- production is kinematically forbidden. Other single charged Higgs boson production mechanisms include $t\bar{b}H^-/\bar{t}bH^+$ production [123], $\tau^+\nu H^-/\tau^-\bar{\nu}H^+$ production [542], and a variety of processes in which $H^\pm$ is produced in association with a one or two other gauge

and/or Higgs bosons [543].

At hadron colliders, charged Higgs bosons can be produced in several different modes depending on the value of its mass with respect to the top-quark mass. For light values of the charged Higgs boson mass, defined by Higgs boson masses smaller than the mass of the top quark (with experimental analyses typically considering masses up to $m_{H^\pm} \leq 160\,\text{GeV}$), the top-quark decay $t \to Hb$ is allowed and the charged Higgs boson is light enough so that top-quark off-shell effects can be neglected. The cross section for the production of a light charged Higgs boson is simply given by the product of the top-pair production cross section and the branching ratio of a top quark into a charged Higgs boson. The top-pair production cross section is known up to NNLO in perturbative QCD [544], and relevant QCD and SUSY-QCD including NLO corrections to the branching ratio for $t \to H^+b$ have been computed in the literature, see Refs. [545–547] and references therein. At present, the theoretical accuracy for the production of a light charged Higgs boson is at the few percent level. For the intermediate mass range, values of $m_{H^\pm}$ near m_t, the finite top-width effects as well as the interplay between top-quark resonant and non-resonant diagrams cannot be neglected. Hence, the full process $pp \to H^\pm W^\mp b\bar{b}$ (with massive b-quarks) must be considered to perform a reliable perturbative calculation of the charged Higgs boson production cross section [547]. For heavy charged Higgs boson scenarios, with charged Higgs boson masses larger than the top-quark mass (typically above 180 GeV), the dominant charged Higgs boson production channel is the associated production with a top quark/antiquark and a (possibly low transverse momentum) bottom antiquark/quark. Theoretical calculation at NLO have been computed both at the inclusive and fully-differential level in the five-flavour scheme and in the four-flavour scheme, see Ref. [40] and references therein. Charged Higgs bosons can also be produced via associated production with $W^\pm$ bosons through $b\bar{b}$ annihilation and gg-fusion annihilation [548].

For charged Higgs boson production cross section predictions for the Tevatron and the LHC, see Refs. [38, 39, 370].

(a) Exclusion limits from LEP

Charged Higgs bosons have been searched for at LEP, where the combined data of the four experiments, ALEPH, DELPHI, L3, and OPAL, were sensitive to masses of up to about 90 GeV [523] in two decay channels, $\tau\nu$ and $c\bar{s}$. The combined LEP data exclude, at 95% CL, charged Higgs bosons with mass below 80 GeV (Type II scenario) or 72.5 GeV (Type I scenario) [549].

(b) Exclusion limits from Tevatron

Compared to the mass domain covered by LEP searches, the Tevatron covered a complementary range of charged Higgs boson masses. CDF and D0 have also searched for charged Higgs bosons in top quark decays with subsequent decays to $\tau\nu$ or to $c\bar{s}$ [550]. For the $H^+ \to c\bar{s}$ channel, the limits on $\text{BR}(t \to H^+b)$ from CDF and D0 are $\approx 20\%$ in the mass range $90\,\text{GeV} < m_{H^+} < 160\,\text{GeV}$ and assuming a branching fraction of 100% in this specific final state. $H^+ \to \tau^+\nu_\tau$ channel, D0's limits on $\text{BR}(t \to H^+b)$ are also $\approx 20\%$ in the same mass range and assuming a branching fraction of 100% in this final state. These limits are valid in general 2HDMs, and they have also been interpreted in terms of the MSSM [550].

(c) Exclusion limits from LHC

Similarly, to the Tevatron, at the LHC, light charged Higgs bosons can be searched for in the decays of top quarks. The main initial production mode for light charged Higgs bosons ($m_{H^\pm} < m_t - m_b$) is top pair production. The subsequent decay modes of the charged Higgs boson for these searches are $\tau\nu$ and $c\bar{s}$. More recently, ATLAS and CMS have also searched for higher mass charged Higgs bosons ($m_{H^\pm} > m_t + m_b$) in $H^+ \to t\bar{b}$. The main production modes are the associated production of a charged Higgs boson in association with a top and a bottom quark or

in association with a top quark only.

The decay $H^+ \to \tau^+\nu_\tau$ is searched typically in three final state topologies:

(i) lepton+jets: with $t\bar{t} \to \bar{b}WH^+ \to b\bar{b}(q\bar{q}')(\tau_{\rm lep}\nu)$, i.e., the W boson decays hadronically and the tau decays into an electron or a muon, with two neutrinos;

(ii) τ +lepton: with $t\bar{t} \to \bar{b}WH^+ \to b\bar{b}(l\nu)(\tau_{\rm had}\nu)$, i.e., the W boson decays leptonically (with $\ell = e,\, \mu$) and the tau decays hadronically;

(iii) τ+jets: $t\bar{t} \to \bar{b}WH^+ \to b\bar{b}(q\bar{q}')(\tau_{\rm had}\nu)$, i.e., both the W boson and the τ decay hadronically.

CMS has also searched for the charged Higgs boson in the decay products of top quark pairs: $t\bar{t} \to H^\pm W^\mp b\bar{b}$ and $t\bar{t} \to H^+H^- b\bar{b}$ as well. Three types of final states with large missing transverse energy and jets originating from b-quark hadronisation have been analysed: the fully-hadronic channel with a hadronically decaying tau in association with jets, the dilepton channel with a hadronically decaying tau in association with an electron or muon and the dilepton channel with an electron-muon pair. The results of the searches at the LHC are illustrated in Figure 11.17.

Both ATLAS and CMS have also searched for high mass charged Higgs bosons decaying to a top and bottom quarks. The main production mode for this search is the associated production with one top quark (5-flavour scheme) or a top quark and and bottom quark (4-flavour scheme) in the final state. The s-channel production mode where the charged Higgs boson is produced alone in the final state at tree level is also considered. This search is particularly intricate and it is sensitive to the modelling of the top pair production background produced in association with additional partons and in particular b-quarks. No excess was found and the results are expressed in terms of exclusion limits of cross section times branching fractions.

ATLAS and CMS have also searched for charged Higgs bosons in top quark decays assuming $\mathrm{BR}(H^+ \to c\bar{s}) = 100\%$ [496, 551], and sets limits of $\approx 20\%$ on $\mathrm{BR}(t \to H^+b)$ in the $90\,\mathrm{GeV} < m_{H^+} < 160\,\mathrm{GeV}$ mass range.

In 2HDMs, the decay of the charged Higgs boson to a W and a Z boson is allowed only at loop level and is therefore suppressed. However the $H^\pm \to W^\pm Z$ decay channel is allowed in Higgs triplet models. ATLAS [500] has searched for such decays, requiring that the charged Higgs boson is produced through the fusion of vector bosons. No excess with respect to the SM backgrounds has been observed in this channel, and the results are interpreted in the Georgi–Machacek model [414] discussed in Section 11.6.5.2.

At the LHC, various other channels still remain to be explored, in particular searches involving additional neutral scalars in particular in the WH, WA channels (A is the pseudo-scalar MSSM Higgs boson), and in the Wa channel (a is the light CP-odd scalars of the NMSSM).

11.6.7.6 *Interpretation of the measurements of the coupling properties of the Higgs boson*

The 125 GeV Higgs boson being part of any hypothetically extended EWSB sector, it can be used through the compatibility of its measured couplings and mass with those predicted in specific models to provide constraints on these specific models parameters.

As discussed in Section 11.6.1.1, the mass of the Higgs boson limits drastically the MSSM parameter space and can be used to set limits on specific MSSM benchmarks. This is the case for the Mh125 scenario as illustrated in Fig. 11.16 and in Fig. 11.17, corresponding approximately to a lower limit on $\tan\beta$ in this model [118].

The measurements of the Higgs boson couplings, discussed in Section 11.5, can be interpreted in the framework of a constrained model where the couplings of the Higgs boson to vector bosons, up-type quarks, down-type quarks and leptons, are varied. In 2HDMs, these couplings are functions of the mixing angle α between the observed Higgs boson and the heavy CP-even neutral scalar, and of the ratio of the vacuum expectation values of the two doublets, $\tan\beta$. In the case of the

MSSM, the two parameters are the A boson mass and $\tan\beta$ (the sole two parameters needed to describe the MSSM Higgs sector at tree level). The coupling measurements have been interpreted both by ATLAS [312] and CMS [552] in specific MSSM benchmarks and in 2HDMs. The exclusion contour in the hMSSM for the ATLAS combination [312] is illustrated in Fig. 11.17.

11.6.7.7 *Searches for a light CP-odd Higgs boson*

A light pseudo-scalar boson a is present in any two Higgs doublet model enhanced with an additional singlet field. A prominent example is the NMSSM. The theoretical motivations for singlet extensions of the MSSM are discussed in Section 11.6.2. There is also a variety of other models with light additional spin-0 bosons such as two Higgs doublet models with a scalar, Little Higgs models or light scalar mediator to a dark sector.

In the framework of the NMSSM, the searches now focus on the low a mass region for several reasons:

(i) in the NMSSM, the light pseudo-scalar a boson can, as a pseudo-Goldstone boson, be a natural candidate for an axion;

(ii) scenarios where $m_a > 2m_b$ and a CP-even state h decaying to a pair of a ($m_h > 2m_a$) are excluded by direct searches at LEP in the four b's channel [514, 523, 553];

(iii) in the pre-discovery era, LEP limits on a CP-even Higgs boson resulted in fine-tuning MSSM constraints [554] which could be evaded through non standard decays of the Higgs boson to aa;

(iv) in the NMSSM, a CP-odd a boson with a mass in the range 9.2–12 GeV can also account for the difference observed between the measured anomalous muon magnetic moment and its prediction [555].

The benchmark scenarios have also changed in the light of the Higgs boson discovery. The 125 GeV state could be the lightest or the next-to-lightest of the three CP-even states of the NMSSM. Light pseudo-scalar scenarios are still very interesting in particular for the potential axion candidate. There are three main types of direct searches for the light a boson:

(i) for masses below the Υ resonance, the search is for radiative decays $\Upsilon \to a\gamma$ at B-factories;

(ii) the inclusive search in high energy pp collisions at the LHC;

(iii) the search for decays of the observed CP-even Higgs h boson into a pair of a bosons;

Radiative decays $\Upsilon \to a\gamma$ have been searched for in various colliders, the most recent results are searches for radiative decays of the $\Upsilon(1s)$ to $a\gamma$ with a subsequent decay of the a boson to a pair of taus at CLEO [556], and the radiative decays of the $\Upsilon(1s, 2s, 3s)$ to $a\gamma$ with subsequent decays to a pair of muons or taus by BaBar [519, 520].

Direct inclusive searches for the light pseudo scalar a boson were performed in the $a \to \mu\mu$ channel at the Tevatron by D0 [514] and by ATLAS [506], CMS [507], and LHCb [164] at the LHC.

Finally, searches for the decays of the Higgs boson to a pair of a bosons were performed with subsequent decays to four photons, in the four muons final state, in the two muons and two taus final state, and in the four taus final state.

No significant excess in the searches for a light CP-odd a boson was found and limits on the production times branching fractions of the a boson have been set.

References for all these searches are summarised in Table 11.11.

11.6.7.8 *Searches in Higgs decays*

Dark-photons or axion-like particles searches can also be carried out within the decays of the Higgs boson to four leptons through dilepton pair resonances. Such search has been carried out by

ATLAS and CMS [557]. Alternatively signatures of dark photons escaping detection with mising transverse momentum signatures have also been searched for by ATLAS [558].

11.6.7.9 *Searches for doubly charged Higgs bosons* $H^{\pm\pm}$

As discussed in Section 11.6.5, the generation of small neutrino masses via the standard EWSB mechanism described in Section 11.2 requires unnaturally small Yukawa couplings, provided that neutrinos are Dirac-type fermions. A Majorana mass term with a see-saw mechanism for neutrinos, would allow for naturally small masses and would also yield a framework for the appealing scenario of leptogenesis. However, within the SM, Majorana mass terms correspond to (non-renomalizable) dimension-5 operators. Such effective interactions can be generated via renormalisable interactions with an electroweak triplet of complex scalar fields (corresponding to a type-II see-saw mechanism). Other models such as the Zee–Babu model, with the introduction of two $\mathrm{SU}(2)_L$ singlets, also generate Majorana mass terms. The signature of such models would be the presence of doubly charged Higgs bosons $H^{\pm\pm}$.

The main production mechanisms of $H^{\pm\pm}$ bosons at hadron colliders are the pair production in the s-channel through the exchange of a Z boson or a photon and the associated production with a charged Higgs boson through the exchange of a W boson. Various searches for doubly charged Higgs bosons have been performed by ATLAS and CMS at Run 1 [559] and Run 2 [521, 522]. Typically, these searches aim at low values of the Higgs triplet vacuum expectation for which the doubly charged Higgs boson will decay mostly to leptons (for high values, the decay to W bosons will become predominant). These searches assume that the coupling to W bosons is negligible and that the main production mode is through the Drell–Yan process.

11.6.7.10 *Searches for non-standard production processes of the Higgs boson*

The discovery of the Higgs boson has also allowed for searches of BSM processes involving standard decays of the Higgs boson. One example directly pertaining to the search for additional states of the EWSB sector is the search for Higgs bosons in the cascade decay of a heavy CP-even Higgs boson decaying to charged Higgs boson and a W boson, and the charged Higgs boson subsequently decaying to H and another W boson. This search has been performed by ATLAS in $b\bar{b}$ decays of the 125 GeV Higgs boson [560].

11.6.7.11 *Outlook on searches for additional states*

The LHC program of searches for additional states covers a large variety of decay and production channels. Since the Higgs boson discovery, many new channels have been explored at the LHC, e.g., the searches for additional states decaying into hh or Vh or ZA. The search for charged Higgs bosons has been extended to include the WZ, WA and the very difficult $t\bar{b}$ decay channel.

11.7 Summary and outlook

Summary– The discovery of the Higgs boson is a major milestone in the history of particle physics as well as an extraordinary achievement of the LHC machine and the ATLAS and CMS experiments. Eleven years after the discovery, substantial progress in the field of Higgs boson physics has been accomplished and a significant number of measurements probing the nature of this unique particle have been made. They are revealing an increasingly precise profile of the Higgs boson.

The LHC has concluded its Run 2 in 2018, delivering a dataset of 13 TeV pp collisions corresponding to an integrated luminosity of more than $150\,\mathrm{fb}^{-1}$ of data collected by ATLAS and CMS. The Run 3 started in 2022 at 13.6 TeV and more than $70\,\mathrm{fb}^{-1}$ of additional data were delivered. First cross section measurements at this new centre-of-mass energy have been presented and are reported herein. With the substantial increase in production rates at the higher center-of-mass energy (mostly from Run 1 to Run 2) and the larger datasets, new landmark results in Higgs

physics have been achieved. They are highlighted in the 10th anniversary papers of the Higgs boson discovery [183, 184].

Three new results of fundamental importance have been achieved with Run-2 datasets by ATLAS and CMS independently: (i) the clear and unambiguous observation of the Higgs boson decay to taus; (ii) the clear and unambiguous observation of the Higgs boson decay to a pair of b quarks; (iii) the clear and unambiguous observation of the production of the Higgs boson through the $t\bar{t}H$ process. These results provide direct evidence for the Yukawa coupling of the Higgs boson to fermions of the third generation: taus, bottom quarks and top quarks, at rates compatible with those expected in the SM. In addition, the evidence for the decay of the Higgs boson to muons is being consolidated. These, and all other experimental measurements, are consistent with the EWSB mechanism of the SM.

New theoretical calculations and developments in Monte-Carlo simulations pertaining to Higgs physics are still occurring at a rapid pace. For example, the theoretical prediction for the dominant gluon fusion production mode now includes the latest N3LO result at the inclusive and differential levels, which is twice as precise as previous N2LO calculations. With these improvements in the state-of-the-art theory predictions and the increase in luminosity and center-of-mass energy, Higgs physics has definitively entered a precision era. Its impact can already be seen on the latest Run-2 combined measurements of the Higgs boson couplings (see Section 11.5).

Since the discovery of the Higgs boson, new ideas have emerged to probe its rare decays and production modes, as well as to indirectly measure the Higgs boson width through the study of its off-shell couplings, or via on-shell interference effects. The Higgs boson has now become part of the standard toolkit in searches for new physics, with Higgs measurements being used in SMEFT global fits.

Many extensions of the SM at higher energies call for an enlargement of the EWSB sector. Hence, direct searches for additional scalar states can provide valuable insights on the dynamics of the EWSB mechanism. The ATLAS and CMS experiments have searched for additional Higgs bosons in the Run-2 data, and have imposed constraints in broad ranges of mass and couplings for various scenarios with an extended Higgs sector.

The landscape of Higgs physics has been scrutinized extensively since its discovery. The current precisions on the measurements of the couplings of the Higgs boson to gauge bosons and third generation fermions are typically of the order of 10–20%. The uncertainty on the Higgs boson coupling to the muon shrank below 50%, and the upper limits on the branching fraction to new invisible particles are approximately 10%. Sensitivity to the Higgs boson self-coupling has not reached the SM value yet, and there is no information on how the Higgs field acquired its VEV in the early times of the Universe. However, significant progress in being made through exploration of di-Higgs production, including new analyses based on machine learning algorithms. This situation allows for new challenges to ultimately increase further the reach in precision and it also widens the possibilities of unveiling the true nature and the dynamics of the electroweak symmetry breaking mechanism.

Outlook– The unitarisation of the vector boson scattering (VBS) amplitudes, dominated at high energies by their longitudinal polarisation, has been the basis of the *no lose* theorem at the LHC, and was a determining consideration in the building of the accelerator and detectors. It motivated the existence of a Higgs boson or the observability of manifestations of strong dynamics at the TeV scale. Now that a Higgs boson has been found and its couplings to gauge bosons are - within current accuracy - consistent with the SM predictions, perturbative unitarity is preserved to a large extent with the sole exchange of the Higgs boson, and without the need for any additional states. VBS remains still an important channel to further investigate in order to better understand the nature of the Higgs sector and the possible completion of the SM at the TeV scale. In association

with the double Higgs boson production channel by vector boson fusion, VBS could, for instance, confirm that the Higgs boson is part of a weak doublet and also establish whether it is an elementary object or a composite state that could emerge as a pseudo-Nambu–Goldstone boson from a new underlying broken symmetry.

The fermion-Higgs boson couplings are not governed by local gauge symmetry. Thus, in addition to a new particle, the LHC has also discovered a new force, different in nature from the other fundamental interactions since it is non-universal and distinguishes between the three families of quarks and leptons. The existence of the Higgs boson embodies the problem of an unnatural cancellation among the quantum corrections to its mass if new physics is present at scales significantly higher than the EW scale. The non-observation of additional states which could stabilise the Higgs boson mass is a challenge for natural scenarios like Supersymmetry or models with a new strong interaction in which the Higgs boson is not a fundamental particle. This increasingly pressing paradox starts questioning the principle of naturalness and it also inspires new solutions tied to the cosmological evolution of the Universe.

The search for the Higgs boson has occupied the particle physics community for the last 50 years. Its discovery has shaped and sharpened the physics programs of the LHC and of prospective future accelerators [126, 561]. With respect to current data, at the HL-LHC the precision will improve by a factor of approximately 5–10 depending on the observables considered. Table 11.8 displays the expected sensitivities in the characterization of the Higgs boson at HL-LHC: in this table, the parameters κ_i specify by how much the coupling of the Higgs boson to a given particle i deviates from the SM expectation. The only channels which are expected to be limited by data statistics are the rare decays to muons and $Z\gamma$. In all other cases, the experimental systematic uncertainties are similar to the statistical uncertainties, but the dominant source of uncertainty arises from theory, and this remains the case even after assuming that, by the end of the HL-LHC run, the theory uncertainties can be reduced by a factor two compared to the current uncertainties, a hypothesis that appears realistic but still requires dedicated and concerted work [118]. For both hadron and lepton colliders, some theoretical progress is crucial to fully exploit and capitalise on the experimental data. In particular, the expected HL-LHC data together with rapid ongoing progress in theoretical calculations are defining a new era of precision Higgs boson measurements.

Acknowledgements

We would like to thank many of our colleagues for proofreading this review, for useful criticism and for their input in general: W. Altmannshofer, J. de Blas, G. Branco, G. Buchalla, J. Campbell, F. Caola, F. Cerutti, C. Csáki, R. Contino, J. Conway, N. Craig, A. David, S. Dawson, J.B. De Vivie, J. D'Hondt, G. Durieux, C. Englert, J.R. Espinosa, A. Falkowski, L. Fayard, W. Fischer, S. Forte, S. Gori, M. Grazzini, J. Gu, H. Haber, B. Heinemann, S. Heinemeyer, J. Hubisz, A. Korytov, B. Jäger, H. Ji, T. Junk, P. Langacker, J. Lykken, F. Maltoni, M.L. Mangano, B. Mansoulié, M. McCullough, R. Mishra, M. Mühlleitner, B. Murray, M. Neubert, A. Nisati, Y. Paul, G. Perez, G. Petrucciani, A. Pomarol, E. Pontón, R. Rattazzi, D. Rebuzzi, L. Reina, F. Riva, R. Salerno, J. Santiago, E. Salvioni, N. Shah, G. Shaughnessy, M. Spira, A. Strumia, K. Tackmann, R. Tanaka, J. Terning, A. Vartak, C. Wagner, N. Wardle, A. Weiler, A. Wulzer, and G. Zanderighi. We are also most grateful to the ATLAS, CDF, CMS and D0 collaborations for their help with this review.

M.C. is supported by Fermilab, that is operated by Fermi Research Alliance, LLC under Contract No. DE–AC02–07CH11359 with the United States Department of Energy. C.G. is supported by the Helmholtz Association and by the Deutsche Forschungsgemeinschaft under Germany's Excellence Strategy – EXC 2121 "Quantum Universe" – 390833306. V.S. is supported by the grant DE–SC0009919 of the United States Department of Energy.

References

[1] G. Aad *et al.* (ATLAS), Phys. Lett. **B716**, 1 (2012), [arXiv:1207.7214].

[2] S. Chatrchyan *et al.* (CMS), Phys. Lett. **B716**, 30 (2012), [arXiv:1207.7235].

[3] S.L. Glashow, Nucl. Phys. **20**, 579 (1961); S. Weinberg, Phys. Rev. Lett. **19**, 1264 (1967); A. Salam, *Elementary Particle Theory*, eds.: Svartholm, Almquist and Wiksells, Stockholm, 1968; S. L. Glashow, J. Iliopoulos and L. Maiani, Phys. Rev. **D2**, 1285 (1970).

[4] F. Englert and R. Brout, Phys. Rev. Lett. **13**, 321 (1964), [,157(1964)]; P. W. Higgs, Phys. Rev. **145**, 1156 (1966); G. S. Guralnik, C. R. Hagen and T. W. B. Kibble, Phys. Rev. Lett. **13**, 585 (1964), [,162(1964)].

[5] J. M. Cornwall, D. N. Levin and G. Tiktopoulos, Phys. Rev. Lett. **30**, 1268 (1973), [Erratum: Phys. Rev. Lett. **31**, 572 (1973)]; J. M. Cornwall, D. N. Levin and G. Tiktopoulos, Phys. Rev. **D10**, 1145 (1974), [Erratum: Phys. Rev. **D11**, 972 (1975)]; C. H. Llewellyn Smith, Phys. Lett. **46B**, 233 (1973); B. W. Lee, C. Quigg and H. B. Thacker, Phys. Rev. **D16**, 1519 (1977).

[6] K. G. Wilson, Phys. Rev. **D3**, 1818 (1971); G. 't Hooft, in *Proc. of 1979 Cargèse Institute on Recent Developments in Gauge Theories,* p. 135 Press, New York 1980; For a modern discussion, see the GGI Tea Break's Seminar by G.F. Giudice and R. Rattazzi, https://is.gd/nUnjAr (2021).

[7] J. Wess and B. Zumino, Phys. Lett. **49B**, 52 (1974).

[8] S. P. Martin, Adv. Ser. Direct. High Energy Phys. 1–98 (1998), [hep-ph/9709356].

[9] B.C. Allanach and H.E. Haber, *Supersymmetry, Part I (Theory)*, in this volume.

[10] D. B. Kaplan and H. Georgi, Phys. Lett. **136B**, 183 (1984).

[11] B. Bellazzini, C. Csaki and J. Serra, Eur. Phys. J. **C74**, 5, 2766 (2014), [arXiv:1401.2457]; G. Panico and A. Wulzer, Lect. Notes Phys. **913**, pp.1 (2016), [arXiv:1506.01961]; C. Csaki, C. Grojean and J. Terning, Rev. Mod. Phys. **88**, 4, 045001 (2016), [arXiv:1512.00468].

[12] K.M. Black, R.S. Chivukula and M. Narain, *Dynamical Electroweak Symmetry Breaking: Implications of the H0*, in this volume.

[13] Z. Chacko, H.-S. Goh and R. Harnik, Phys. Rev. Lett. **96**, 231802 (2006), [hep-ph/0506256]; Z. Chacko, H.-S. Goh and R. Harnik, JHEP **01**, 108 (2006), [hep-ph/0512088].

[14] N. Craig *et al.*, JHEP **07**, 105 (2015), [arXiv:1501.05310]; N. Craig, S. Knapen and P. Longhi, Phys. Rev. Lett. **114**, 6, 061803 (2015), [arXiv:1410.6808].

[15] P. W. Graham, D. E. Kaplan and S. Rajendran, Phys. Rev. Lett. **115**, 22, 221801 (2015), [arXiv:1504.07551]; J. R. Espinosa *et al.*, Phys. Rev. Lett. **115**, 25, 251803 (2015), [arXiv:1506.09217]; G. Dvali (2019), [arXiv:1908.05984].

[16] C. Csaki *et al.*, Phys. Rev. Lett. **126**, 091801 (2021), [arXiv:2007.14396]; N. Arkani-Hamed, R. Tito D'agnolo and H. D. Kim (2020), [arXiv:2012.04652]; R. Tito D'Agnolo and D. Teresi (2021), [arXiv:2106.04591].

[17] T. Flacke *et al.*, JHEP **06**, 050 (2017), [arXiv:1610.02025].

[18] J. Khoury and O. Parrikar, JCAP **12**, 014 (2019), [arXiv:1907.07693]; G. F. Giudice, M. McCullough and T. You (2021), [arXiv:2105.08617].

[19] S. Weinberg, Phys. Rev. Lett. **43**, 1566 (1979).

[20] See the particle listing section at `http://pdg.lbl.gov`.

[21] J. R. Ellis, M. K. Gaillard and D. V. Nanopoulos, Nucl. Phys. **B106**, 292 (1976).

[22] M. A. Shifman *et al.*, Sov. J. Nucl. Phys. **30**, 711 (1979), [Yad. Fiz.30,1368(1979)].

[23] J. F. Gunion *et al.*, *The Higgs Hunter's Guide*, Addison-Wesley (1990).

[24] P. Sikivie *et al.*, Nucl. Phys. **B173**, 189 (1980); H. Georgi, Ann. Rev. Nucl. Part. Sci. **43**, 209 (1993).

[25] M. J. G. Veltman, Nucl. Phys. **B123**, 89 (1977).

[26] M. Luscher and P. Weisz, Nucl. Phys. **B290**, 25 (1987); M. Luscher and P. Weisz, Nucl. Phys. **B295**, 65 (1988).

[27] G. Degrassi *et al.*, JHEP **08**, 098 (2012), [arXiv:1205.6497]; S. Alekhin, A. Djouadi and S. Moch, Phys. Lett. **B716**, 214 (2012), [arXiv:1207.0980]; D. Buttazzo *et al.*, JHEP **12**, 089 (2013), [arXiv:1307.3536].

[28] V. Branchina, E. Messina and M. Sher, Phys. Rev. **D91**, 013003 (2015), [arXiv:1408.5302].

[29] A. Hook *et al.*, JHEP **01**, 061 (2015), [arXiv:1404.5953]; J. Kearney, H. Yoo and K. M. Zurek, Phys. Rev. **D91**, 12, 123537 (2015), [arXiv:1503.05193].

[30] J. R. Espinosa, D. Racco and A. Riotto, Phys. Rev. Lett. **120**, 12, 121301 (2018), [arXiv:1710.11196].

[31] J. R. Espinosa, D. Racco and A. Riotto, JCAP **1809**, 09, 012 (2018), [arXiv:1804.07732].

[32] A. Andreassen, W. Frost and M. D. Schwartz, Phys. Rev. **D97**, 5, 056006 (2018), [arXiv:1707.08124]; S. Chigusa, T. Moroi and Y. Shoji, Phys. Rev. Lett. **119**, 21, 211801 (2017), [arXiv:1707.09301].

[33] M. Shaposhnikov and C. Wetterich, Phys. Lett. **B683**, 196 (2010), [arXiv:0912.0208]; M. Holthausen, K. S. Lim and M. Lindner, JHEP **02**, 037 (2012), [arXiv:1112.2415].

[34] F. L. Bezrukov and M. Shaposhnikov, Phys. Lett. **B659**, 703 (2008), [arXiv:0710.3755]; F. L. Bezrukov, A. Magnin and M. Shaposhnikov, Phys. Lett. **B675**, 88 (2009), [arXiv:0812.4950].

[35] C. P. Burgess, H. M. Lee and M. Trott, JHEP **09**, 103 (2009), [arXiv:0902.4465]; J. L. F. Barbon and J. R. Espinosa, Phys. Rev. **D79**, 081302 (2009), [arXiv:0903.0355]; M. P. Hertzberg, JHEP **11**, 023 (2010), [arXiv:1002.2995].

[36] A. Djouadi, Phys. Rept. **457**, 1 (2008), [hep-ph/0503172].

[37] S. Dittmaier *et al.* (LHC Higgs Cross Section Working Group), CERN Report **2011-002** (2011), [arXiv:1101.0593].

[38] S. Dittmaier *et al.* (LHC Higgs Cross Section Working Group), CERN Report **2012-002** (2012), [arXiv:1201.3084].

[39] S. Heinemeyer *et al.* (LHC Higgs Cross Section Working Group), CERN Report **2013-004** (2013), [arXiv:1307.1347].

[40] D. de Florian *et al.* (LHC Higgs Cross Section Working Group), CERN Report **2017-002** (2016), [arXiv:1610.07922].

[41] S. Catani *et al.*, Phys. Rev. Lett. **130**, 11, 111902 (2023), [arXiv:2210.07846].

[42] M. Grazzini, S. Kallweit and M. Wiesemann, Eur. Phys. J. C **78**, 7, 537 (2018), [arXiv:1711.06631].

[43] LHC Higgs Working Group, `https://twiki.cern.ch/twiki/bin/view/LHCPhysics/LHCHWG`.

[44] T. Aaltonen *et al.* (CDF, D0), Phys. Rev. **D88**, 5, 052014 (2013), [arXiv:1303.6346].

[45] H. M. Georgi *et al.*, Phys. Rev. Lett. **40**, 692 (1978).

[46] D. Graudenz, M. Spira and P. M. Zerwas, Phys. Rev. Lett. **70**, 1372 (1993).

[47] M. Spira *et al.*, Nucl. Phys. **B453**, 17 (1995), [hep-ph/9504378].

[48] C. Anastasiou *et al.*, Phys. Rev. Lett. **114**, 212001 (2015), [arXiv:1503.06056]; C. Anastasiou *et al.*, JHEP **05**, 058 (2016), [arXiv:1602.00695].

[49] R. V. Harlander and K. J. Ozeren, JHEP **11**, 088 (2009), [arXiv:0909.3420]; A. Pak, M. Rogal and M. Steinhauser, JHEP **02**, 025 (2010), [arXiv:0911.4662].

[50] J. Davies *et al.*, Phys. Rev. **D100**, 3, 034017 (2019), [arXiv:1906.00982]; M. Czakon *et al.* (2021), [arXiv:2105.04436].

[51] F. Caola *et al.*, JHEP **09**, 035 (2018), [arXiv:1804.07632].

[52] K. Melnikov and A. Penin, JHEP **05**, 172 (2016), [arXiv:1602.09020].

[53] C. Anastasiou and A. Penin, JHEP **07**, 195 (2020), [Erratum: JHEP 01, 164 (2021)], [arXiv:2004.03602].

[54] S. Dawson, Nucl. Phys. **B359**, 283 (1991); A. Djouadi, M. Spira and P. M. Zerwas, Phys. Lett. **B264**, 440 (1991).

[55] R. V. Harlander and W. B. Kilgore, Phys. Rev. Lett. **88**, 201801 (2002), [hep-ph/0201206]; C. Anastasiou and K. Melnikov, Nucl. Phys. **B646**, 220 (2002), [hep-ph/0207004]; V. Ravindran, J. Smith and W. L. van Neerven, Nucl. Phys. **B665**, 325 (2003), [hep-ph/0302135].

[56] A. Djouadi and P. Gambino, Phys. Rev. Lett. **73**, 2528 (1994), [hep-ph/9406432]; S. Actis *et al.*, Phys. Lett. **B670**, 12 (2008), [arXiv:0809.1301]; U. Aglietti *et al.*, Phys. Lett. **B595**, 432 (2004), [hep-ph/0404071]; G. Degrassi and F. Maltoni, Phys. Lett. **B600**, 255 (2004), [hep-ph/0407249].

[57] M. Bonetti, K. Melnikov and L. Tancredi, Phys. Rev. **D97**, 5, 056017 (2018), [Erratum: Phys. Rev. **D97**, 9, 099906 (2018)], [arXiv:1801.10403]; M. Bonetti *et al.*, JHEP **11**, 045 (2020), [arXiv:2007.09813]; M. Becchetti *et al.*, Phys. Rev. D **103**, 5, 054037 (2021), [arXiv:2010.09451].

[58] C. Anastasiou, R. Boughezal and F. Petriello, JHEP **04**, 003 (2009), [arXiv:0811.3458].

[59] C. Anastasiou *et al.*, JHEP **03**, 162 (2019), [arXiv:1811.11211].

[60] M. Bonvini *et al.*, JHEP **08**, 105 (2016), [arXiv:1603.08000].

[61] B. Mistlberger, JHEP **05**, 028 (2018), [arXiv:1802.00833].

[62] J. McGowan *et al.*, Eur. Phys. J. C **83**, 3, 185 (2023), [Erratum: Eur.Phys.J.C 83, 302 (2023)], [arXiv:2207.04739].

[63] F. Dulat, B. Mistlberger and A. Pelloni, Phys. Rev. D **99**, 3, 034004 (2019), [arXiv:1810.09462].

[64] X. Chen *et al.*, Phys. Rev. Lett. **127**, 7, 072002 (2021), [arXiv:2102.07607].

[65] G. Billis *et al.*, Phys. Rev. Lett. **127**, 7, 072001 (2021), [arXiv:2102.08039].

[66] A. Banfi, G. P. Salam and G. Zanderighi, JHEP **06**, 159 (2012), [arXiv:1203.5773]; T. Becher, M. Neubert and D. Wilhelm, JHEP **05**, 110 (2013), [arXiv:1212.2621]; A. Banfi *et al.*, JHEP **04**, 049 (2016), [arXiv:1511.02886]; J. K. L. Michel, P. Pietrulewicz and F. J. Tackmann, JHEP **04**, 142 (2019), [arXiv:1810.12911]; P. F. Monni, L. Rottoli and P. Torrielli, Phys. Rev. Lett. **124**, 25, 252001 (2020), [arXiv:1909.04704].

[67] I. Moult and I. W. Stewart, JHEP **09**, 129 (2014), [arXiv:1405.5534].

[68] V. D. Barger *et al.*, Phys. Rev. **D44**, 1426 (1991).

[69] F. A. Dreyer and A. Karlberg, Phys. Rev. Lett. **117**, 7, 072001 (2016), [arXiv:1606.00840].

[70] M. Cacciari *et al.*, Phys. Rev. Lett. **115**, 8, 082002 (2015), [Erratum: Phys. Rev. Lett. **120**, 13,139901 (2018)], [arXiv:1506.02660]; J. Cruz-Martinez *et al.*, Phys. Lett. **B781**, 672 (2018), [arXiv:1802.02445].

[71] T. Han, G. Valencia and S. Willenbrock, Phys. Rev. Lett. **69**, 3274 (1992), [hep-ph/9206246].

[72] T. Liu, K. Melnikov and A. A. Penin, Phys. Rev. Lett. **123**, 12, 122002 (2019), [arXiv:1906.10899].

[73] F. A. Dreyer, A. Karlberg and L. Tancredi, JHEP **10**, 131 (2020), [arXiv:2005.11334].

[74] M. Rauch and D. Zeppenfeld, Phys. Rev. **D95**, 11, 114015 (2017), [arXiv:1703.05676].

[75] A. Buckley *et al.* (2021), [arXiv:2105.11399].

[76] A. Denner *et al.*, JHEP **03**, 075 (2012), [arXiv:1112.5142].

[77] A. Denner *et al.*, Comput. Phys. Commun. **195**, 161 (2015), [arXiv:1412.5390].

[78] S. L. Glashow, D. V. Nanopoulos and A. Yildiz, Phys. Rev. **D18**, 1724 (1978); T. Han and S. Willenbrock, Phys. Lett. **B273**, 167 (1991); T. Han, G. Valencia, and S. Willenbrock, Phys. Rev. Lett. **69**, 3274 (1992); H. Baer, B. Bailey and J. F. Owens, Phys. Rev. **D47**, 2730 (1993); J. Ohnemus and W. J. Stirling, Phys. Rev. **D47**, 2722 (1993).

[79] A. Stange, W. J. Marciano and S. Willenbrock, Phys. Rev. **D49**, 1354 (1994), [hep-ph/9309294]; A. Stange, W. J. Marciano and S. Willenbrock, Phys. Rev. **D50**, 4491 (1994), [hep-ph/9404247].

[80] M. L. Ciccolini, S. Dittmaier and M. Krämer, Phys. Rev. **D68**, 073003 (2003), [hep-ph/0306234].

[81] R. Hamberg, W. L. van Neerven and T. Matsuura, Nucl. Phys. **B359**, 343 (1991), [Erratum: Nucl. Phys. **B644**, 403 (2002)].

[82] O. Brein, A. Djouadi and R. Harlander, Phys. Lett. **B579**, 149 (2004), [hep-ph/0307206]; L. Altenkamp *et al.*, JHEP **02**, 078 (2013), [arXiv:1211.5015].

[83] J. Davies, G. Mishima and M. Steinhauser, JHEP **03**, 034 (2021), [arXiv:2011.12314]; L. Chen *et al.*, JHEP **03**, 125 (2021), [arXiv:2011.12325].

[84] O. Brein *et al.*, Eur. Phys. J. **C72**, 1868 (2012), [arXiv:1111.0761].

[85] O. Brein, R. V. Harlander and T. J. E. Zirke, Comput. Phys. Commun. **184**, 998 (2013), [arXiv:1210.5347]; R. V. Harlander *et al.*, JHEP **05**, 089 (2018), [arXiv:1802.04817].

[86] R. Gauld *et al.*, Phys. Lett. B **817**, 136335 (2021), [arXiv:2009.14209].

[87] A. Denner *et al.*, JHEP **03**, 075 (2012), [arXiv:1112.5142].

[88] G. Ferrera, M. Grazzini, and F. Tramontano, Phys. Rev. Lett. **107**, 152003 (2011).

[89] G. Ferrera, M. Grazzini and F. Tramontano, Phys. Lett. **B740**, 51 (2015), [arXiv:1407.4747]; J. M. Campbell, R. K. Ellis and C. Williams, JHEP **06**, 179 (2016), [arXiv:1601.00658].

[90] W. Astill *et al.*, JHEP **06**, 154 (2016), [arXiv:1603.01620].

[91] F. Caola *et al.*, Phys. Rev. **D97**, 7, 074022 (2018), [arXiv:1712.06954]; R. Gauld *et al.*, JHEP **10**, 002 (2019), [arXiv:1907.05836].

[92] J. M. Butterworth *et al.*, Phys. Rev. Lett. **100**, 242001 (2008), [arXiv:0802.2470].

[93] A. Behring *et al.*, Phys. Rev. D **101**, 11, 114012 (2020), [arXiv:2003.08321].

[94] W. Bizon *et al.* (2021), [arXiv:2106.06328].

[95] J. Baglio *et al.*, JHEP **12**, 066 (2022), [arXiv:2209.06138].

[96] R. Raitio and W. W. Wada, Phys. Rev. **D19**, 941 (1979); Z. Kunszt, Nucl. Phys. **B247**, 339 (1984); J. N. Ng and P. Zakarauskas, Phys. Rev. D **29**, 876 (1984); J. F. Gunion, Phys. Lett. **B261**, 510 (1991); W. J. Marciano and F. E. Paige, Phys. Rev. Lett. **66**, 2433 (1991).

[97] W. Beenakker *et al.*, Phys. Rev. Lett. **87**, 201805 (2001), [hep-ph/0107081]; L. Reina and S. Dawson, Phys. Rev. Lett. **87**, 201804 (2001), [hep-ph/0107101]; L. Reina, S. Dawson and D. Wackeroth, Phys. Rev. D **65**, 053017 (2002), [hep-ph/0109066]; S. Dawson *et al.*, Phys. Rev. **D67**, 071503 (2003), [hep-ph/0211438]; W. Beenakker *et al.*, Nucl. Phys. **B653**, 151 (2003), [hep-ph/0211352]; S. Dawson *et al.*, Phys. Rev. **D68**, 034022 (2003), [hep-ph/0305087].

[98] Y. Zhang *et al.*, Phys. Lett. **B738**, 1 (2014), [arXiv:1407.1110]; S. Frixione *et al.*, JHEP **09**, 065 (2014), [arXiv:1407.0823]; S. Frixione *et al.*, JHEP **06**, 184 (2015), [arXiv:1504.03446].

[99] T. Plehn, G. P. Salam and M. Spannowsky, Phys. Rev. Lett. **104**, 111801 (2010), [arXiv:0910.5472].

[100] A. Kulesza *et al.*, JHEP **03**, 065 (2016), [arXiv:1509.02780]; A. Broggio *et al.*, JHEP **03**, 124 (2016), [arXiv:1510.01914]; A. Broggio *et al.*, JHEP **02**, 126 (2017), [arXiv:1611.00049]; A. Kulesza *et al.*, Phys. Rev. D **97**, 11, 114007 (2018), [arXiv:1704.03363]; A. Broggio *et al.*, JHEP **08**, 039 (2019), [arXiv:1907.04343]; A. Kulesza *et al.*, Eur. Phys. J. C **80**, 5, 428 (2020), [arXiv:2001.03031].

[101] A. Denner and R. Feger, JHEP **11**, 209 (2015), [arXiv:1506.07448].

[102] A. Denner *et al.*, JHEP **02**, 053 (2017), [arXiv:1612.07138].

[103] R. Frederix *et al.*, Phys. Lett. **B701**, 427 (2011), [arXiv:1104.5613]; H. B. Hartanto *et al.*, Phys. Rev. D **91**, 9, 094003 (2015), [arXiv:1501.04498].

[104] S. Catani *et al.*, Eur. Phys. J. C **81**, 6, 491 (2021), [arXiv:2102.03256].

[105] C. Brancaccio *et al.*, JHEP **08**, 145 (2021), [arXiv:2106.06516].

[106] F. Demartin *et al.*, Eur. Phys. J. **C75**, 6, 267 (2015), [arXiv:1504.00611].

[107] D. Pagani, I. Tsinikos and E. Vryonidou, JHEP **08**, 082 (2020), [arXiv:2006.10086].

[108] C. Duhr *et al.*, JHEP **08**, 08, 017 (2020), [arXiv:2004.04752].

[109] K.A. Assamagan *et al.*, [Higgs Working Group, "Physics at TeV Colliders" workshop, Les Houches, 2003], `arXiv:hep-ph/0406152` (2004).

[110] R. V. Harlander and W. B. Kilgore, Phys. Rev. **D68**, 013001 (2003), [hep-ph/0304035]; J. M. Campbell *et al.*, Phys. Rev. **D67**, 095002 (2003), [hep-ph/0204093]; S. Dawson *et al.*, Phys. Rev. Lett. **94**, 031802 (2005), [hep-ph/0408077]; S. Dittmaier, M. Krämer and M. Spira, Phys. Rev. **D70**, 074010 (2004), [hep-ph/0309204]; S. Dawson *et al.*, Phys. Rev. **D69**, 074027 (2004), [hep-ph/0311067].

[111] W. J. Stirling and D. J. Summers, Phys. Lett. **B283**, 411 (1992); F. Maltoni *et al.*, Phys. Rev. **D64**, 094023 (2001), [hep-ph/0106293].

[112] D. Pagani, H.-S. Shao and M. Zaro, JHEP **11**, 036 (2020), [arXiv:2005.10277].

[113] C. Grojean, A. Paul and Z. Qian, JHEP **04**, 139 (2021), [arXiv:2011.13945].

[114] S. Dawson, S. Dittmaier and M. Spira, Phys. Rev. **D58**, 115012 (1998), [hep-ph/9805244].

[115] D. de Florian and J. Mazzitelli, Phys. Rev. Lett. **111**, 201801 (2013), [arXiv:1309.6594].

[116] L.-B. Chen *et al.*, Phys. Lett. B **803**, 135292 (2020), [arXiv:1909.06808].

[117] S. Borowka *et al.*, Phys. Rev. Lett. **117**, 1, 012001 (2016), [Erratum: Phys. Rev. Lett. **117**, 7, 079901 (2016)], [arXiv:1604.06447]; J. Baglio *et al.*, Eur. Phys. J. **C79**, 6, 459 (2019), [arXiv:1811.05692]; J. Davies *et al.*, JHEP **11**, 024 (2019), [arXiv:1907.06408].

[118] M. Cepeda *et al.* (HL/HE-LHC WG2 group) (2019), [arXiv:1902.00134].

[119] J. Alison *et al.*, Rev. Phys. **5**, 100045 (2020), [arXiv:1910.00012].

[120] B.L. Ioffe and V.A. Khoze, Sov. J. Nucl. Phys. **9**, 50 (1978).

[121] D. R. T. Jones and S. T. Petcov, Phys. Lett. **84B**, 440 (1979); R. N. Cahn and S. Dawson, Phys. Lett. **136B**, 196 (1984), [Erratum: Phys. Lett. **138B**, 464 (1984)]; G. L. Kane, W. W. Repko and W. B. Rolnick, Phys. Lett. **148B**, 367 (1984); G. Altarelli, B. Mele and F. Pitolli, Nucl. Phys. **B287**, 205 (1987); W. Kilian, M. Krämer and P. M. Zerwas, Phys. Lett. **B373**, 135 (1996), [hep-ph/9512355].

[122] B. A. Kniehl, Z. Phys. **C55**, 605 (1992); J. Fleischer and F. Jegerlehner, Nucl. Phys. **B216**, 469 (1983); A. Denner *et al.*, Z. Phys. **C56**, 261 (1992); B. A. Kniehl, Int. J. Mod. Phys. **A17**, 1457 (2002), [hep-ph/0112023].

[123] K. J. F. Gaemers and G. J. Gounaris, Phys. Lett. **77B**, 379 (1978); A. Djouadi, J. Kalinowski and P. M. Zerwas, Z. Phys. **C54**, 255 (1992); B. A. Kniehl, F. Madricardo and M. Steinhauser, Phys. Rev. **D66**, 054016 (2002), [hep-ph/0205312]; S. Dittmaier *et al.*, Phys. Lett. **B441**, 383 (1998), [hep-ph/9808433]; S. Dittmaier *et al.*, Phys. Lett. **B478**, 247 (2000), [hep-ph/0002035]; S. Dawson and L. Reina, Phys. Rev. **D59**, 054012 (1999), [hep-ph/9808443].

[124] A. Arbey *et al.*, Eur. Phys. J. **C75**, 8, 371 (2015), [arXiv:1504.01726]; A. Freitas *et al.* (2019), [arXiv:1906.05379].

[125] S. Frixione *et al.* (2021), [arXiv:2108.10261].

[126] J. de Blas *et al.*, JHEP **01**, 139 (2020), [arXiv:1905.03764].

[127] A. Denner *et al.*, Eur. Phys. J. **C71**, 1753 (2011), [arXiv:1107.5909].

[128] A. Djouadi, J. Kalinowski, and M. Spira, Comp. Phys. Comm. **108**, 56 (1998); A. Djouadi *et al.*, `arXiv:1003.1643 [hep-ph]` (2010).

[129] S. G. Gorishnii *et al.*, Mod. Phys. Lett. **A5**, 2703 (1990); S. G. Gorishnii *et al.*, Phys. Rev. **D43**, 1633 (1991); A. L. Kataev and V. T. Kim, Mod. Phys. Lett. **A9**, 1309 (1994); L. R. Surguladze, Phys. Lett. **B341**, 60 (1994), [hep-ph/9405325]; S. A. Larin, T. van Ritbergen and J. A. M. Vermaseren, Phys. Lett. **B362**, 134 (1995), [hep-ph/9506465]; K. G. Chetyrkin and A. Kwiatkowski, Nucl. Phys. **B461**, 3 (1996), [hep-ph/9505358]; K. G. Chetyrkin, Phys. Lett. **B390**, 309 (1997), [hep-ph/9608318]; P. A. Baikov, K. G. Chetyrkin and J. H. Kuhn, Phys. Rev. Lett. **96**, 012003 (2006), [hep-ph/0511063].

[130] J. Fleischer and F. Jegerlehner, Phys. Rev. **D23**, 2001 (1981); D. Yu. Bardin, B. M. Vilensky and P. K. Khristova, Sov. J. Nucl. Phys. **53**, 152 (1991), [Yad. Fiz.53,240(1991)]; A. Dabelstein and W. Hollik, Z. Phys. **C53**, 507 (1992); B. A. Kniehl, Nucl. Phys. **B376**, 3 (1992); A. Djouadi *et al.*, in "In *Munich/Annecy/Hamburg 1991, Proceedings, e+ e- collisions at 500 GeV, pt. A* 11-30," (1991).

[131] T. Inami, T. Kubota and Y. Okada, Z. Phys. **C18**, 69 (1983); K. G. Chetyrkin, B. A. Kniehl and M. Steinhauser, Phys. Rev. Lett. **79**, 353 (1997), [hep-ph/9705240]; P. A. Baikov and K. G. Chetyrkin, Phys. Rev. Lett. **97**, 061803 (2006), [hep-ph/0604194].

[132] H.-Q. Zheng and D.-D. Wu, Phys. Rev. **D42**, 3760 (1990); A. Djouadi *et al.*, Phys. Lett. **B257**, 187 (1991); S. Dawson and R. P. Kauffman, Phys. Rev. **D47**, 1264 (1993); A. Djouadi, M. Spira and P. M. Zerwas, Phys. Lett. **B311**, 255 (1993), [hep-ph/9305335]; K. Melnikov and O. I. Yakovlev, Phys. Lett. **B312**, 179 (1993), [hep-ph/9302281]; M. Inoue *et al.*, Mod. Phys. Lett. **A9**, 1189 (1994).

[133] P. Maierhöfer and P. Marquard, Phys. Lett. **B721**, 131 (2013), [arXiv:1212.6233].

[134] U. Aglietti *et al.*, Phys. Lett. **B595**, 432 (2004), [hep-ph/0404071]; G. Degrassi and F. Maltoni, Phys. Lett. **B600**, 255 (2004), [hep-ph/0407249]; S. Actis *et al.*, Phys. Lett. **B670**, 12 (2008), [arXiv:0809.1301]; U. Aglietti *et al.*, Phys. Lett. **B600**, 57 (2004), [hep-ph/0407162]; G. Degrassi and F. Maltoni, Nucl. Phys. **B724**, 183 (2005), [hep-ph/0504137]; U. Aglietti *et al.*, FERMILAB-CONF (2006), [hep-ph/0612172].

[135] A. Abbasabadi *et al.*, Phys. Rev. **D55**, 5647 (1997), [hep-ph/9611209]; A. Abbasabadi and W. W. Repko, Phys. Rev. **D71**, 017304 (2005), [hep-ph/0411152]; A. Abbasabadi and W. W. Repko, JHEP **08**, 048 (2006), [hep-ph/0602087]; D. A. Dicus and W. W. Repko, Phys. Rev. **D87**, 7, 077301 (2013), [arXiv:1302.2159]; L.-B. Chen, C.-F. Qiao and R.-L. Zhu, Phys. Lett. **B726**, 306 (2013), [arXiv:1211.6058]; Y. Sun, H.-R. Chang and D.-N. Gao, JHEP **05**, 061 (2013), [arXiv:1303.2230]; G. Passarino, Phys. Lett. **B727**, 424 (2013), [arXiv:1308.0422].

[136] M. Spira, A. Djouadi and P. M. Zerwas, Phys. Lett. **B276**, 350 (1992).

[137] A. Bredenstein *et al.*, Phys. Rev. **D74**, 013004 (2006), [hep-ph/0604011]; A. Bredenstein *et al.*, JHEP **02**, 080 (2007), [hep-ph/0611234]; A. Bredenstein *et al.*, `Prophecy4f`: A Monte Carlo generator for a proper description of the Higgs decay into 4 fermions, `http://omnibus.uni-freiburg.de/~sd565/programs/prophecy4f/prophecy4f.html`.

[138] A. Ghinculov, Phys. Lett. **B337**, 137 (1994), [Erratum: Phys. Lett. **B346**, 426 (1995)], [hep-ph/9405394]; L. Durand, B. A. Kniehl and K. Riesselmann, Phys. Rev. **D51**, 5007 (1995), [hep-ph/9412311]; L. Durand, K. Riesselmann and B. A. Kniehl, Phys. Rev. Lett. **72**, 2534 (1994), [Erratum: Phys. Rev. Lett. **74**, 1699 (1995)].

[139] R. Barate *et al.* (LEP Working Group for Higgs boson searches, ALEPH, DELPHI, L3, OPAL), Phys. Lett. **B565**, 61 (2003), [hep-ex/0306033].

[140] LHC Programme Coordination, "LHC Delivered Luminosities", `https://lpc.web.cern.ch`.

[141] M. Tanabashi *et al.* (Particle Data Group), Phys. Rev. **D98**, 3, 030001 (2018).

[142] Y. L. Dokshitzer, S. I. Troian and V. A. Khoze, Sov. J. Nucl. Phys. **46**, 712 (1987), [Yad. Fiz.46,1220(1987)].

[143] M. Dittmar and H. K. Dreiner, Phys. Rev. **D55**, 167 (1997), [hep-ph/9608317].

[144] G. Aad *et al.* (ATLAS, CMS), Phys. Rev. Lett. **114**, 191803 (2015), [arXiv:1503.07589].

[145] M. Aaboud *et al.* (ATLAS), Phys. Lett. **B784**, 345 (2018), [arXiv:1806.00242].

[146] ATLAS Collaboration, ATLAS-CONF-2020-005 (2020).

[147] A. M. Sirunyan *et al.* (CMS), JHEP **11**, 047 (2017), [arXiv:1706.09936].

[148] A. M. Sirunyan *et al.* (CMS), Phys. Lett. B **805**, 135425 (2020), [arXiv:2002.06398].

[149] G. Aad *et al.* (ATLAS) (2023), [arXiv:2308.07216].

[150] G. Aad *et al.* (ATLAS), Phys. Lett. B **843**, 137880 (2023), [arXiv:2207.00320].

[151] G. Aad *et al.* (ATLAS) (2023), [arXiv:2308.04775].

[152] CMS Collaboration, CMS-PAS-HIG-21-019 (2023).

[153] G. Aad *et al.* (ATLAS, CMS), JHEP **08**, 045 (2016), [arXiv:1606.02266].

[154] M. Aaboud *et al.* (ATLAS), Phys. Rev. **D99**, 072001 (2019), [arXiv:1811.08856].

[155] A. M. Sirunyan *et al.* (CMS), Phys. Lett. **B779**, 283 (2018), [arXiv:1708.00373].

[156] CMS Collaboration, CMS-PAS-HIG-18-032 (2019).

[157] G. Aad *et al.* (ATLAS), JHEP **08**, 175 (2022), [arXiv:2201.08269].

[158] A. Tumasyan *et al.* (CMS), Eur. Phys. J. C **83**, 7, 562 (2023), [arXiv:2204.12957].

[159] A. Tumasyan *et al.* (CMS), Phys. Rev. Lett. **128**, 8, 081805 (2022), [arXiv:2107.11486].
[160] T. Aaltonen *et al.* (CDF, D0), Phys. Rev. Lett. **109**, 071804 (2012), [arXiv:1207.6436].
[161] M. Aaboud *et al.* (ATLAS), Phys. Lett. **B786**, 59 (2018), [arXiv:1808.08238].
[162] A. M. Sirunyan *et al.* (CMS), Phys. Rev. Lett. **121**, 12, 121801 (2018), [arXiv:1808.08242].
[163] LHCb-CONF-2016-006, CERN-LHCb-CONF-2016-006.
[164] M. Aaboud *et al.* (ATLAS), JHEP **11**, 112 (2016), [arXiv:1606.02181].
[165] V. Khachatryan *et al.* (CMS), Phys. Rev. **D92**, 3, 032008 (2015), [arXiv:1506.01010].
[166] G. Aad *et al.* (ATLAS), Eur. Phys. J. C **81**, 6, 537 (2021), [arXiv:2011.08280].
[167] A. Hayrapetyan *et al.* (CMS) (2023), [arXiv:2308.01253].
[168] E. Gabrielli *et al.*, Nucl. Phys. **B781**, 64 (2007), [hep-ph/0702119].
[169] G. Aad *et al.* (ATLAS), JHEP **03**, 268 (2021), [arXiv:2010.13651].
[170] G. Aad *et al.* (ATLAS), Phys. Rev. D **105**, 9, 092003 (2022), [arXiv:2111.08340].
[171] CMS Collaboration, CMS-PAS-HIG-21-020 (2023).
[172] V. Khachatryan *et al.* (CMS), Eur. Phys. J. **C75**, 6, 251 (2015), [arXiv:1502.02485].
[173] G. Aad *et al.* (ATLAS), Phys. Lett. **B749**, 519 (2015), [arXiv:1506.05988].
[174] M. Aaboud *et al.* (ATLAS), Phys. Lett. B **784**, 173 (2018), [arXiv:1806.00425].
[175] A. M. Sirunyan *et al.* (CMS), Phys. Rev. Lett. **120**, 23, 231801 (2018), [arXiv:1804.02610].
[176] G. Aad *et al.* (ATLAS), Eur. Phys. J. C **80**, 10, 957 (2020), [Erratum: Eur.Phys.J.C 81, 29 (2021), Erratum: Eur.Phys.J.C 81, 398 (2021)], [arXiv:2004.03447].
[177] A. M. Sirunyan *et al.* (CMS), Eur. Phys. J. C **81**, 6, 488 (2021), [arXiv:2103.04956].
[178] A. M. Sirunyan *et al.* (CMS), Eur. Phys. J. C **81**, 4, 378 (2021), [arXiv:2011.03652].
[179] ATLAS Collaboration, ATLAS-CONF-2019-045 (2019).
[180] ATLAS Collaboration, ATLAS-CONF-2021-044 (2021).
[181] G. Aad *et al.* (ATLAS), JHEP **06**, 097 (2022), [arXiv:2111.06712].
[182] CMS Collaboration, CMS-PAS-HIG-19-011 (2023).
[183] Nature **607**, 7917, 52 (2022), [Erratum: Nature 612, E24 (2022)], [arXiv:2207.00092].
[184] A. Tumasyan *et al.* (CMS), Nature **607**, 7917, 60 (2022), [arXiv:2207.00043].
[185] M. Farina *et al.*, JHEP **05**, 022 (2013), [arXiv:1211.3736].
[186] CMS Collaboration, CMS-PAS-HIG-17-005 (2017).
[187] CMS Collaboration, CMS-PAS-HIG-16-019 (2016).
[188] R. L. Workman *et al.* (Particle Data Group), PTEP **2022**, 083C01 (2022).
[189] C. Patrignani *et al.* (Particle Data Group), Chin. Phys. **C40**, 10, 100001 (2016).
[190] G. Aad *et al.*, Physics Letters B **812**, 135980 (2021), ISSN 0370-2693, URL https://www.sciencedirect.com/science/article/pii/S0370269320307838.
[191] A. M. Sirunyan *et al.* (CMS), JHEP **01**, 148 (2021), [arXiv:2009.04363].
[192] C. Delaunay *et al.*, Phys. Rev. **D89**, 3, 033014 (2014), [arXiv:1310.7029].
[193] (2022), [arXiv:2205.05550].
[194] H. Qu and L. Gouskos, Phys. Rev. D **101**, 056019 (2020), URL https://link.aps.org/doi/10.1103/PhysRevD.101.056019.
[195] G. Aad *et al.* (ATLAS), Eur. Phys. J. C **82**, 717 (2022), [arXiv:2201.11428].

[196] A. Tumasyan *et al.* (CMS), Phys. Rev. Lett. **131**, 4, 041801 (2023), [arXiv:2211.14181].
[197] G. Aad *et al.* (CMS, ATLAS) (2023), [arXiv:2309.03501].
[198] V. Khachatryan *et al.* (CMS), Phys. Lett. **B753**, 341 (2016), [arXiv:1507.03031].
[199] A. M. Sirunyan *et al.* (CMS), JHEP **11**, 152 (2018), [arXiv:1806.05996].
[200] G. Aad *et al.* (ATLAS), Phys. Lett. B **819**, 136412 (2021), [arXiv:2103.10322].
[201] A. M. Sirunyan *et al.* (CMS) (2022), [arXiv:2208.00265].
[202] G. Aad *et al.* (ATLAS), Phys. Lett. B **801**, 135148 (2020), [arXiv:1909.10235].
[203] A. Djouadi *et al.*, Eur. Phys. J. **C73**, 6, 2455 (2013), [arXiv:1205.3169].
[204] O. J. P. Eboli and D. Zeppenfeld, Phys. Lett. **B495**, 147 (2000), [hep-ph/0009158].
[205] Phys. Lett. B **842**, 137963 (2023), [arXiv:2301.10731].
[206] (2023), [arXiv:2303.01214].
[207] A. Tumasyan *et al.* (CMS), Phys. Rev. D **105**, 9, 092007 (2022), [arXiv:2201.11585].
[208] G. Isidori, A. V. Manohar and M. Trott, Phys. Lett. **B728**, 131 (2014), [arXiv:1305.0663]; G. T. Bodwin *et al.*, Phys. Rev. **D88**, 5, 053003 (2013), [arXiv:1306.5770]; M. König and M. Neubert, JHEP **08**, 012 (2015), [arXiv:1505.03870].
[209] G. Aad *et al.* (ATLAS), Phys. Rev. Lett. **114**, 12, 121801 (2015), [arXiv:1501.03276].
[210] G. Aad *et al.* (ATLAS), Eur. Phys. J. C **83**, 9, 781 (2023), [arXiv:2208.03122].
[211] A. M. Sirunyan *et al.* (CMS), Phys. Lett. **B797**, 134811 (2019), [arXiv:1905.10408].
[212] (2023), [arXiv:2301.09938].
[213] G. Aad *et al.* (ATLAS), Phys. Rev. Lett. **125**, 22, 221802 (2020), [arXiv:2004.01678].
[214] CMS Collaboration, CMS-PAS-HIG-20-008 (2022).
[215] A. M. Sirunyan *et al.* (CMS), Phys. Rev. D **104**, 3, 032013 (2021), [arXiv:2105.03007].
[216] G. Aad *et al.* (ATLAS), JHEP **11**, 211 (2015), [arXiv:1508.03372].
[217] G. Aad *et al.* (ATLAS), Eur. Phys. J. **C77**, 2, 70 (2017), [arXiv:1604.07730].
[218] V. Khachatryan *et al.* (CMS), Phys. Lett. **B763**, 472 (2016), [arXiv:1607.03561].
[219] G. Aad *et al.* (ATLAS) (2019), [arXiv:1907.06131].
[220] A. M. Sirunyan *et al.* (CMS), JHEP **06**, 001 (2018), [arXiv:1712.07173].
[221] G. Aad *et al.* (ATLAS), JHEP **07**, 166 (2023), [arXiv:2302.05225].
[222] A. Hayrapetyan *et al.* (CMS) (2023), [arXiv:2305.18106].
[223] G. Aad *et al.* (ATLAS), JHEP **12**, 061 (2015), [arXiv:1509.06047].
[224] V. Khachatryan *et al.* (CMS), JHEP **02**, 079 (2017), [arXiv:1610.04857].
[225] ATLAS Collaboration, JHEP **129**, 010 (2017).
[226] A. Tumasyan *et al.* (CMS), JHEP **02**, 169 (2022), [arXiv:2112.09734].
[227] D. Curtin *et al.*, Phys. Rev. D **90**, 7, 075004 (2014), [arXiv:1312.4992].
[228] M. J. Strassler and K. M. Zurek, Phys. Lett. **B651**, 374 (2007), [hep-ph/0604261]; M. J. Strassler and K. M. Zurek, Phys. Lett. **B661**, 263 (2008), [hep-ph/0605193].
[229] T. Han *et al.*, JHEP **07**, 008 (2008), [arXiv:0712.2041].
[230] A. Falkowski *et al.*, Phys. Rev. Lett. **105**, 241801 (2010), [arXiv:1007.3496].
[231] G. Aad *et al.* (ATLAS), Eur. Phys. J. C **80**, 5, 450 (2020), [arXiv:1909.01246].
[232] CMS Collaboration, CMS-PAS-EXO-19-007 (2019).

[233] D. Tucker-Smith and N. Weiner, Phys. Rev. **D64**, 043502 (2001), [hep-ph/0101138].

[234] S. Chatrchyan *et al.* (CMS), Phys. Lett. **B726**, 564 (2013), [arXiv:1210.7619].

[235] G. Aad *et al.* (ATLAS), Phys. Lett. B **843**, 137745 (2023), [arXiv:2211.01216].

[236] A. Tumasyan *et al.* (CMS), Phys. Lett. B **842**, 137531 (2023), [arXiv:2206.09401].

[237] A. Tumasyan *et al.* (CMS), Phys. Rev. Lett. **129**, 8, 081802 (2022), [arXiv:2202.09617].

[238] S. Di Vita *et al.*, JHEP **09**, 069 (2017), [arXiv:1704.01953]; F. Maltoni *et al.*, Eur. Phys. J. **C77**, 12, 887 (2017), [arXiv:1709.08649].

[239] S. Dawson *et al.*, in "Snowmass 2021," (2022), [arXiv:2209.07510].

[240] ATLAS Collaboration, ATLAS-PHYS-PUB-2022-005 (2022).

[241] M. L. Mangano, G. Ortona and M. Selvaggi, Eur. Phys. J. C **80**, 11, 1030 (2020), [arXiv:2004.03505].

[242] A. Riotto and M. Trodden, Ann. Rev. Nucl. Part. Sci. **49**, 35 (1999), [hep-ph/9901362].

[243] D. E. Morrissey and M. J. Ramsey-Musolf, New J. Phys. **14**, 125003 (2012), [arXiv:1206.2942].

[244] G. Aad *et al.* (ATLAS), Eur. Phys. J. C **83**, 6, 496 (2023), [arXiv:2303.15061].

[245] A. Hayrapetyan *et al.* (CMS) (2023), [arXiv:2305.13439].

[246] ATLAS Collaboration, ATLAS-CONF-2023-057 (2023).

[247] ATLAS Collaboration, ATLAS-CONF-2022-012 (2023).

[248] L. D. Landau, Dokl. Akad. Nauk Ser. Fiz. **60**, 2, 207 (1948); C.-N. Yang, Phys. Rev. **77**, 242 (1950).

[249] S. Bolognesi *et al.*, Phys. Rev. **D86**, 095031 (2012), [arXiv:1208.4018].

[250] G. Aad *et al.* (ATLAS), Eur. Phys. J. **C75**, 10, 476 (2015), [Erratum: Eur. Phys. J. **C76**, 3, 152 (2016)], [arXiv:1506.05669].

[251] V. Khachatryan *et al.* (CMS), Phys. Rev. **D92**, 1, 012004 (2015), [arXiv:1411.3441]; G. Aad *et al.* (ATLAS), Phys. Lett. **B726**, 120 (2013), [arXiv:1307.1432].

[252] P. Artoisenet *et al.*, JHEP **11**, 043 (2013), [arXiv:1306.6464].

[253] J. Brod, U. Haisch and J. Zupan, JHEP **11**, 180 (2013), [arXiv:1310.1385].

[254] J. Ellis *et al.*, JHEP **11**, 134 (2012), [arXiv:1208.6002].

[255] D0 Collaboration, Note 6387-CONF (2013).

[256] D0 Collaboration, Note 6406-CONF (2013).

[257] J. C. Collins and D. E. Soper, Phys. Rev. **D16**, 2219 (1977).

[258] ATLAS Collaboration, ATLAS-CONF-2017-043 (2017).

[259] S. Y. Choi *et al.*, Phys. Lett. B **553**, 61 (2003), [hep-ph/0210077].

[260] Y. Gao *et al.*, Phys. Rev. D **81**, 075022 (2010), [arXiv:1001.3396].

[261] A. De Rujula *et al.*, Phys. Rev. **D82**, 013003 (2010), [arXiv:1001.5300].

[262] A. M. Sirunyan *et al.* (CMS), Phys. Rev. **D99**, 11, 112003 (2019), [arXiv:1901.00174].

[263] G. Aad *et al.* (ATLAS) (2023), [arXiv:2304.09612].

[264] G. Aad *et al.* (ATLAS), Phys. Rev. Lett. **131**, 6, 061802 (2023), [arXiv:2208.02338].

[265] A. M. Sirunyan *et al.* (CMS), Phys. Rev. D **104**, 5, 052004 (2021), [arXiv:2104.12152].

[266] G. Aad *et al.* (ATLAS), Eur. Phys. J. **C76**, 12, 658 (2016), [arXiv:1602.04516].

[267] A. M. Sirunyan *et al.* (CMS), Submitted to: Phys. Rev. (2019), [arXiv:1903.06973].

[268] G. Aad *et al.* (ATLAS), Eur. Phys. J. C **82**, 7, 622 (2022), [arXiv:2109.13808].

[269] A. Tumasyan *et al.* (CMS), Phys. Rev. D **108**, 3, 032013 (2023), [arXiv:2205.05120].

[270] G. Aad *et al.* (ATLAS), Phys. Rev. Lett. **125**, 6, 061802 (2020), [arXiv:2004.04545].

[271] (2023), [arXiv:2303.05974].

[272] A. M. Sirunyan *et al.* (CMS), Phys. Rev. Lett. **125**, 6, 061801 (2020), [arXiv:2003.10866].

[273] A. Tumasyan *et al.* (CMS), JHEP **07**, 092 (2023), [arXiv:2208.02686].

[274] A. Tumasyan *et al.* (CMS), JHEP **06**, 012 (2022), [arXiv:2110.04836].

[275] G. Aad *et al.* (ATLAS), Eur. Phys. J. C **83**, 7, 563 (2023), [arXiv:2212.05833].

[276] ATLAS Collaboration, ATL-PHYS-PUB-2019-008 (2019).

[277] N. Kauer and G. Passarino, JHEP **08**, 116 (2012), [arXiv:1206.4803].

[278] G. Aad *et al.* (ATLAS), Eur. Phys. J. **C75**, 7, 335 (2015), [arXiv:1503.01060].

[279] V. Khachatryan *et al.* (CMS), JHEP **09**, 051 (2016), [arXiv:1605.02329].

[280] G. Aad *et al.* (ATLAS) (2023), [arXiv:2304.01532].

[281] A. Tumasyan *et al.* (CMS), Nature Phys. **18**, 11, 1329 (2022), [arXiv:2202.06923].

[282] G. Aad *et al.* (ATLAS), Phys. Rev. **D90**, 5, 052004 (2014), [arXiv:1406.3827].

[283] L. J. Dixon and M. S. Siu, Phys. Rev. Lett. **90**, 252001 (2003), [hep-ph/0302233]; S. P. Martin, Phys. Rev. **D86**, 073016 (2012), [arXiv:1208.1533]; L. J. Dixon and Y. Li, Phys. Rev. Lett. **111**, 111802 (2013), [arXiv:1305.3854].

[284] ATLAS Collaboration, ATL-PHYS-PUB-2016-009 (2016).

[285] ATLAS Collaboration, ATL-PHYS-PUB-2013-014 (2013).

[286] J. Campbell *et al.*, Phys. Rev. Lett. **119**, 18, 181801 (2017), [Addendum: Phys. Rev. Lett.119,19,199901(2017)], [arXiv:1704.08259].

[287] ATLAS Collaboration, ATL-PHYS-PUB-2014-016 (2014).

[288] F. Caola and K. Melnikov, Phys. Rev. **D88**, 054024 (2013), [arXiv:1307.4935]; J. M. Campbell, R. K. Ellis and C. Williams, JHEP **04**, 060 (2014), [arXiv:1311.3589]; J. M. Campbell, R. K. Ellis and C. Williams, Phys. Rev. **D89**, 5, 053011 (2014), [arXiv:1312.1628].

[289] C. Englert and M. Spannowsky, Phys. Rev. **D90**, 053003 (2014), [arXiv:1405.0285].

[290] A. Azatov *et al.*, Zh. Eksp. Teor. Fiz. **147**, 410 (2015), [J. Exp. Theor. Phys.120,354(2015)], [arXiv:1406.6338]; A. Azatov *et al.*, JHEP **09**, 123 (2016), [arXiv:1608.00977].

[291] A. David *et al.* (LHC Higgs Cross Section Working Group), "LHC HXSWG interim recommendations to explore the coupling structure of a Higgs-like particle," (2012), [arXiv:1209.0040].

[292] M. Dührssen, "Prospects for the measurement of Higgs boson coupling parameters in the mass range from 110–190 GeV," (2003); M. Duhrssen *et al.*, Phys. Rev. **D70**, 113009 (2004), [hep-ph/0406323]; R. Lafaye *et al.*, JHEP **08**, 009 (2009), [arXiv:0904.3866].

[293] J. R. Espinosa *et al.*, JHEP **05**, 097 (2012), [arXiv:1202.3697]; A. Azatov, R. Contino and J. Galloway, JHEP **04**, 127 (2012), [Erratum: JHEP **04**, 140 (2013)], [arXiv:1202.3415]; D. Carmi *et al.*, JHEP **07**, 136 (2012), [arXiv:1202.3144]; J. R. Espinosa *et al.*, JHEP **12**, 045 (2012), [arXiv:1207.1717].

[294] M. Gonzalez-Alonso *et al.*, Eur. Phys. J. **C75**, 128 (2015), [arXiv:1412.6038]; A. Greljo *et al.*, Eur. Phys. J. **C76**, 3, 158 (2016), [arXiv:1512.06135].

[295] G. F. Giudice *et al.*, JHEP **06**, 045 (2007), [hep-ph/0703164].

[296] S. Willenbrock and C. Zhang, Ann. Rev. Nucl. Part. Sci. **64**, 83 (2014), [arXiv:1401.0470]; I. Brivio and M. Trott, Phys. Rept. **793**, 1 (2019), [arXiv:1706.08945]; S. Dawson, C. Englert and T. Plehn, Phys. Rept. **816**, 1 (2019), [arXiv:1808.01324]; T. Cohen, PoS **TASI2018**, 011 (2019), [arXiv:1903.03622].

[297] F. Feruglio, Int. J. Mod. Phys. **A8**, 4937 (1993), [hep-ph/9301281]; G. Buchalla, O. Catà and C. Krause, Nucl. Phys. **B880**, 552 (2014), [Erratum: Nucl. Phys. **B913**, 475 (2016)], [arXiv:1307.5017]; A. V. Manohar, in "Les Houches summer school: EFT in Particle Physics and Cosmology Les Houches, Chamonix Valley, France, July 3-28, 2017," (2018), [arXiv:1804.05863]; I. Brivio *et al.*, JHEP **03**, 024 (2014), [arXiv:1311.1823].

[298] T. Cohen *et al.*, JHEP **03**, 237 (2021), [arXiv:2008.08597].

[299] I. Banta *et al.*, JHEP **02**, 029 (2022), [arXiv:2110.02967].

[300] R. S. Gupta, A. Pomarol and F. Riva, Phys. Rev. **D91**, 3, 035001 (2015), [arXiv:1405.0181].

[301] B. A. Kniehl and M. Spira, Z. Phys. **C69**, 77 (1995), [hep-ph/9505225].

[302] J. Elias-Miró *et al.*, JHEP **08**, 033 (2013), [arXiv:1302.5661].

[303] G. Buchalla *et al.*, Phys. Lett. B **750**, 298 (2015), [arXiv:1504.01707].

[304] N. Craig *et al.*, JHEP **08**, 086 (2020), [arXiv:2001.00017].

[305] R. Contino *et al.*, JHEP **07**, 035 (2013), [arXiv:1303.3876].

[306] A. Azatov and J. Galloway, Phys. Rev. **D85**, 055013 (2012), [arXiv:1110.5646].

[307] G. Isidori and M. Trott, JHEP **02**, 082 (2014), [arXiv:1307.4051]; A. Pomarol and F. Riva, JHEP **01**, 151 (2014), [arXiv:1308.2803].

[308] J. Ellis, V. Sanz and T. You, JHEP **07**, 036 (2014), [arXiv:1404.3667]; A. Biekötter *et al.*, Phys. Rev. **D91**, 055029 (2015), [arXiv:1406.7320].

[309] LHC Higgs Cross Section Working Group, `https://twiki.cern.ch/twiki/bin/view/LHCPhysics/LHCHWG2KAPPA`.

[310] M. Reece, New J. Phys. **15**, 043003 (2013), [arXiv:1208.1765].

[311] A. Azatov *et al.* (2022), [arXiv:2203.02418].

[312] G. Aad *et al.* (ATLAS), Phys. Rev. D **101**, 1, 012002 (2020), [arXiv:1909.02845].

[313] A. M. Sirunyan *et al.* (CMS), Phys. Lett. **B792**, 369 (2019), [arXiv:1812.06504].

[314] G. Aad *et al.* (ATLAS), JHEP **05**, 028 (2023), [arXiv:2207.08615].

[315] A. Hayrapetyan *et al.* (CMS) (2023), [arXiv:2305.07532].

[316] A. Tumasyan *et al.* (CMS) (2021), [arXiv:2107.11486].

[317] (2022), [arXiv:2208.12279].

[318] G. Aad *et al.* (ATLAS), Phys. Lett. **B753**, 69 (2016), [arXiv:1508.02507].

[319] N. Berger *et al.* (2019), [arXiv:1906.02754].

[320] ATLAS Collaboration, ATLAS-CONF-2017-045 (2017).

[321] CMS Collaboration, CMS-PAS-HIG-16-040 (2017).

[322] CMS Collaboration, CMS-PAS-HIG-16-041 (2017).

[323] ATLAS Collaboration, ATLAS-CONF-2018-028 (2018).

[324] A. M. Sirunyan *et al.* (CMS), JHEP **07**, 027 (2021), [arXiv:2103.06956].

[325] CMS Collaboration, CMS-PAS-HIG-19-001 (2019).

[326] G. Aad *et al.* (ATLAS), Phys. Rev. D **108**, 032005 (2023), [arXiv:2207.00338].

[327] A. Tumasyan *et al.* (CMS), Eur. Phys. J. C **83**, 7, 667 (2023), [arXiv:2206.09466].

[328] M. Aaboud *et al.* (ATLAS), JHEP **05**, 141 (2019), [arXiv:1903.04618].

[329] ATLAS Collaboration, ATLAS-CONF-2020-027 (2020).

[330] ATLAS Collaboration, ATLAS-CONF-2020-053 (2020).

[331] J. de Blas *et al.*, JHEP **03**, 109 (2018), [arXiv:1711.10391].

[332] I. Brivio *et al.*, SciPost Phys. **12**, 1, 036 (2022), [arXiv:2108.01094].

[333] A. Carmona *et al.*, SciPost Phys. **12**, 6, 198 (2022), [arXiv:2112.10787].

[334] J. Fuentes-Martín *et al.*, Eur. Phys. J. C **83**, 7, 662 (2023), [arXiv:2212.04510].

[335] A. Manohar and H. Georgi, Nucl. Phys. **B234**, 189 (1984); M. A. Luty, Phys. Rev. **D57**, 1531 (1998), [hep-ph/9706235]; D. Liu *et al.*, JHEP **11**, 141 (2016), [arXiv:1603.03064].

[336] W. Buchmuller and D. Wyler, Nucl. Phys. **B268**, 621 (1986).

[337] C. J. C. Burges and H. J. Schnitzer, Nucl. Phys. **B228**, 464 (1983); C. N. Leung, S. T. Love and S. Rao, Z. Phys. **C31**, 433 (1986).

[338] B. Grzadkowski *et al.*, JHEP **10**, 085 (2010), [arXiv:1008.4884].

[339] L. Lehman and A. Martin, JHEP **02**, 081 (2016), [arXiv:1510.00372]; B. Henning *et al.*, JHEP **08**, 016 (2017), [arXiv:1512.03433].

[340] C. Hays *et al.*, JHEP **02**, 123 (2019), [arXiv:1808.00442].

[341] R. Alonso *et al.*, JHEP **04**, 159 (2014), [arXiv:1312.2014].

[342] ATLAS Collaboration, ATL-PHYS-PUB-2022-037 (2022).

[343] J. Ellis *et al.*, JHEP **04**, 279 (2021), [arXiv:2012.02779].

[344] J. J. Ethier *et al.* (SMEFiT), JHEP **11**, 089 (2021), [arXiv:2105.00006].

[345] Y. Gershtein, and A. Pomarol, *Extra Dimenions*, in this volume.

[346] M. Carena *et al.*, Phys. Rev. **D91**, 3, 035003 (2015), [arXiv:1410.4969].

[347] M. Carena *et al.*, Phys. Rev. **D93**, 3, 035013 (2016), [arXiv:1510.09137].

[348] J. F. Gunion and H. E. Haber, Phys. Rev. **D67**, 075019 (2003), [hep-ph/0207010].

[349] H. E. Haber and Y. Nir, Nucl. Phys. **B335**, 363 (1990).

[350] S. Weinberg, Phys. Rev. **D13**, 974 (1976), [Addendum: Phys. Rev.D19,1277(1979)]; L. Susskind, Phys. Rev. **D20**, 2619 (1979); For a review, see C. T. Hill and E. H. Simmons, Phys. Reports **381**, 235 (2003) [Erratum: 390, 553 (2004)], [arXiv:hep-ph/0203079].

[351] Z. Chacko, R. Franceschini and R. K. Mishra, JHEP **04**, 015 (2013), [arXiv:1209.3259].

[352] L. E. Ibanez and G. G. Ross, Phys. Lett. **110B**, 215 (1982); L. E. Ibanez, Phys. Lett. **118B**, 73 (1982); J. R. Ellis, D. V. Nanopoulos and K. Tamvakis, Phys. Lett. **121B**, 123 (1983); L. Alvarez-Gaume, J. Polchinski and M. B. Wise, Nucl. Phys. **B221**, 495 (1983).

[353] S. Dimopoulos and G. F. Giudice, Phys. Lett. **B357**, 573 (1995), [hep-ph/9507282]; M. Papucci, J. T. Ruderman and A. Weiler, JHEP **09**, 035 (2012), [arXiv:1110.6926].

[354] ATLAS Collaboration, `https://twiki.cern.ch/twiki/bin/view/AtlasPublic/Publications`; CMS Collaboration, `http://cms-results.web.cern.ch/cms-results/public-results/publications/SUS/STOP.html`.

[355] J. Mrazek *et al.*, Nucl. Phys. **B853**, 1 (2011), [arXiv:1105.5403].

[356] D. B. Kaplan, Nucl. Phys. **B365**, 259 (1991).

[357] G. Panico *et al.*, JHEP **03**, 051 (2013), [arXiv:1210.7114].

[358] H. E. Haber and G. L. Kane, Phys. Rept. **117**, 75 (1985).

[359] P. Slavich *et al.*, Eur. Phys. J. C **81**, 5, 450 (2021), [arXiv:2012.15629].

[360] P. Draper, G. Lee and C. E. M. Wagner, Phys. Rev. **D89**, 5, 055023 (2014), [arXiv:1312.5743].

[361] E. L. Berger *et al.*, Phys. Rev. **D66**, 095001 (2002), [hep-ph/0205342].

[362] A. Djouadi, Phys. Rept. **459**, 1 (2008), [hep-ph/0503173].

[363] P. Bechtle *et al.*, Eur. Phys. J. **C77**, 2, 67 (2017), [arXiv:1608.00638].

[364] E. Bagnaschi *et al.*, Eur. Phys. J. **C79**, 7, 617 (2019), [arXiv:1808.07542].

[365] A. Djouadi, J. Kalinowski and P. M. Zerwas, Z. Phys. **C57**, 569 (1993).

[366] G. Lee and C. E. M. Wagner, Phys. Rev. **D92**, 7, 075032 (2015), [arXiv:1508.00576].

[367] D. Dicus *et al.*, Phys. Rev. **D59**, 094016 (1999), [hep-ph/9811492].

[368] M. Carena *et al.*, JHEP **07**, 091 (2012), [arXiv:1203.1041].

[369] A. A. Barrientos Bendezu and B. A. Kniehl, Phys. Rev. **D64**, 035006 (2001), [hep-ph/0103018].

[370] LHC Higgs Working Group, `https://twiki.cern.ch/twiki/bin/view/LHCPhysics/LHCHWGMSSMCharged`.

[371] D. Dicus, A. Stange and S. Willenbrock, Phys. Lett. B **333**, 126 (1994), [hep-ph/9404359]; N. Craig *et al.*, JHEP **06**, 137 (2015), [arXiv:1504.04630]; S. Gori *et al.*, Phys. Rev. D **93**, 7, 075038 (2016), [arXiv:1602.02782].

[372] A. Djouadi, J. Ellis and J. Quevillon, JHEP **07**, 105 (2016), [arXiv:1605.00542]; M. Carena and Z. Liu, JHEP **11**, 159 (2016), [arXiv:1608.07282].

[373] LHC Higgs Working Group for BSM Higgs, `https://twiki.cern.ch/twiki/bin/view/LHCPhysics/LHCHWG3`.

[374] M. Carena *et al.*, Eur. Phys. J. **C73**, 9, 2552 (2013), [arXiv:1302.7033].

[375] H. Bahl, S. Liebler and T. Stefaniak, Eur. Phys. J. **C79**, 3, 279 (2019), [arXiv:1901.05933].

[376] L. Maiani, A. D. Polosa and V. Riquer, Phys. Lett. **B718**, 465 (2012), [arXiv:1209.4816]; A. Djouadi and J. Quevillon, JHEP **10**, 028 (2013), [arXiv:1304.1787]; A. Djouadi *et al.*, Eur. Phys. J. **C73**, 2650 (2013), [arXiv:1307.5205].

[377] E. Bagnaschi *et al.*, Eur. Phys. J. C **79**, 7, 617 (2019), [arXiv:1808.07542].

[378] M. Carena and H. E. Haber, Prog. Part. Nucl. Phys. **50**, 63 (2003), [hep-ph/0208209].

[379] H. Bahl *et al.*, Eur. Phys. J. C **80**, 10, 916 (2020), [arXiv:2005.14536].

[380] R. S. Chivukula and H. Georgi, Phys. Lett. **B188**, 99 (1987); L. J. Hall and L. Randall, Phys. Rev. Lett. **65**, 2939 (1990); A. J. Buras *et al.*, Phys. Lett. **B500**, 161 (2001), [hep-ph/0007085]; G. D'Ambrosio *et al.*, Nucl. Phys. **B645**, 155 (2002), [hep-ph/0207036].

[381] M. Misiak and M. Steinhauser, Eur. Phys. J. C **77**, 3, 201 (2017), [arXiv:1702.04571].

[382] L. J. Hall, J. D. Lykken and S. Weinberg, Phys. Rev. **D27**, 2359 (1983); J. E. Kim and H. P. Nilles, Phys. Lett. **138B**, 150 (1984); G. F. Giudice and A. Masiero, Phys. Lett. **B206**, 480 (1988).

[383] U. Ellwanger, C. Hugonie and A. M. Teixeira, Phys. Rept. **496**, 1 (2010), [arXiv:0910.1785].

[384] P. Fayet, Nucl. Phys. **B90**, 104 (1975).

[385] C. Panagiotakopoulos and K. Tamvakis, Phys. Lett. **B469**, 145 (1999), [hep-ph/9908351]; A. Dedes *et al.*, Phys. Rev. **D63**, 055009 (2001), [hep-ph/0009125]; A. Menon, D. E. Morrissey and C. E. M. Wagner, Phys. Rev. **D70**, 035005 (2004), [hep-ph/0404184].

[386] M. Cvetic *et al.*, Phys. Rev. **D56**, 2861 (1997), [Erratum: Phys. Rev. **D58**, 119905 (1998)], [hep-ph/9703317]; P. Langacker and J. Wang, Phys. Rev. **D58**, 115010 (1998), [hep-ph/9804428].

[387] J. Erler, P. Langacker and T.-j. Li, Phys. Rev. **D66**, 015002 (2002), [hep-ph/0205001]; T. Han, P. Langacker and B. McElrath, Phys. Rev. **D70**, 115006 (2004), [hep-ph/0405244]; V. Barger *et al.*, Phys. Rev. **D73**, 115010 (2006), [hep-ph/0603247].

[388] V. Barger, P. Langacker and G. Shaughnessy, Phys. Rev. **D75**, 055013 (2007), [hep-ph/0611239].

[389] D. E. Lopez-Fogliani and C. Munoz, Phys. Rev. Lett. **97**, 041801 (2006), [hep-ph/0508297].

[390] B. A. Dobrescu, G. L. Landsberg and K. T. Matchev, Phys. Rev. **D63**, 075003 (2001), [hep-ph/0005308]; R. Dermisek and J. F. Gunion, Phys. Rev. Lett. **95**, 041801 (2005), [hep-ph/0502105].

[391] O. J. P. Eboli and D. Zeppenfeld, Phys. Lett. **B495**, 147 (2000), [hep-ph/0009158]; H. Davoudiasl, T. Han and H. E. Logan, Phys. Rev. **D71**, 115007 (2005), [hep-ph/0412269].

[392] J.-J. Cao *et al.*, JHEP **03**, 086 (2012), [arXiv:1202.5821].

[393] LHC Higgs Working Group, Beyond the Standard Model Higgs – NMSSM, `https://twiki.cern.ch/twiki/bin/view/LHCPhysics/LHCHWGNMSSM`.

[394] P. Batra *et al.*, JHEP **02**, 043 (2004), [hep-ph/0309149].

[395] R. Huo *et al.*, Phys. Rev. **D87**, 5, 055011 (2013), [arXiv:1212.0560].

[396] J. Engel, M. J. Ramsey-Musolf and U. van Kolck, Prog. Part. Nucl. Phys. **71**, 21 (2013), [arXiv:1303.2371].

[397] S. Dimopoulos and S. D. Thomas, Nucl. Phys. **B465**, 23 (1996), [hep-ph/9510220]; S. D. Thomas, Int. J. Mod. Phys. **A13**, 2307 (1998), [hep-ph/9803420].

[398] A. Pilaftsis and C. E. M. Wagner, Nucl. Phys. **B553**, 3 (1999), [hep-ph/9902371].

[399] M. Frank *et al.*, JHEP **02**, 047 (2007), [hep-ph/0611326].

[400] M. Carena *et al.*, Nucl. Phys. **B586**, 92 (2000), [hep-ph/0003180].

[401] B. Li and C. E. M. Wagner, Phys. Rev. **D91**, 095019 (2015), [arXiv:1502.02210].

[402] M. D. Goodsell and F. Staub, Eur. Phys. J. **C77**, 1, 46 (2017), [arXiv:1604.05335]; A. Chakraborty *et al.*, Phys. Rev. **D90**, 5, 055005 (2014), [arXiv:1301.2745]; M. Carena *et al.*, JHEP **02**, 123 (2016), [arXiv:1512.00437].

[403] J. F. Gunion and H. E. Haber, Phys. Rev. **D67**, 075019 (2003), [hep-ph/0207010]; G. C. Branco *et al.*, Phys. Rept. **516**, 1 (2012), [arXiv:1106.0034].

[404] N. G. Deshpande and E. Ma, Phys. Rev. **D18**, 2574 (1978).

[405] A. Goudelis, B. Herrmann and S. O., JHEP **09**, 106 (2013), [arXiv:1303.3010].

[406] M. Bauer, M. Carena and K. Gemmler, JHEP **11**, 016 (2015), [arXiv:1506.01719]; M. Bauer, M. Carena and K. Gemmler, Phys. Rev. **D94**, 11, 115030 (2016), [arXiv:1512.03458].

[407] C. D. Froggatt and H. B. Nielsen, Nucl. Phys. **B147**, 277 (1979).

[408] K. S. Babu and S. Nandi, Phys. Rev. **D62**, 033002 (2000), [hep-ph/9907213]; G. F. Giudice and O. Lebedev, Phys. Lett. **B665**, 79 (2008), [arXiv:0804.1753].

[409] E. Accomando *et al.*, CERN Report **2006-009** (2006), [hep-ph/0608079].

[410] T. Robens and T. Stefaniak, Eur. Phys. J. **C75**, 104 (2015), [arXiv:1501.02234].

[411] S. L. Glashow and S. Weinberg, Phys. Rev. **D15**, 1958 (1977); E. A. Paschos, Phys. Rev. **D15**, 1966 (1977).

[412] G. C. Branco, W. Grimus and L. Lavoura, Phys. Lett. **B380**, 119 (1996), [hep-ph/9601383]; F. J. Botella, G. C. Branco and M. N. Rebelo, Phys. Lett. **B687**, 194 (2010), [arXiv:0911.1753].

[413] J. Schechter and J. W. F. Valle, Phys. Rev. **D22**, 2227 (1980); T. P. Cheng and L.-F. Li, Phys. Rev. **D22**, 2860 (1980).

[414] H. Georgi and M. Machacek, Nucl. Phys. **B262**, 463 (1985); M. S. Chanowitz and M. Golden, Phys. Lett. **165B**, 105 (1985); J. F. Gunion, R. Vega and J. Wudka, Phys. Rev. **D42**, 1673 (1990).

[415] P. Nath *et al.*, Nucl. Phys. Proc. Suppl. **200-202**, 185 (2010), [arXiv:1001.2693].

[416] J. Garayoa and T. Schwetz, JHEP **03**, 009 (2008), [arXiv:0712.1453].

[417] H. E. Haber and H. E. Logan, Phys. Rev. **D62**, 015011 (2000), [hep-ph/9909335]; S. Kanemura and K. Yagyu, Phys. Rev. **D85**, 115009 (2012), [arXiv:1201.6287].

[418] J. F. Gunion, R. Vega and J. Wudka, Phys. Rev. **D43**, 2322 (1991).

[419] I. Low and J. Lykken, JHEP **10**, 053 (2010), [arXiv:1005.0872]; I. Low, J. Lykken and G. Shaughnessy, Phys. Rev. **D86**, 093012 (2012), [arXiv:1207.1093].

[420] H. E. Logan and M.-A. Roy, Phys. Rev. **D82**, 115011 (2010), [arXiv:1008.4869]; A. Falkowski, S. Rychkov and A. Urbano, JHEP **04**, 073 (2012), [arXiv:1202.1532].

[421] N. Arkani-Hamed *et al.*, JHEP **07**, 034 (2002), [hep-ph/0206021]; N. Arkani-Hamed, A. G. Cohen and H. Georgi, Phys. Lett. **B513**, 232 (2001), [hep-ph/0105239].

[422] M. Perelstein, Prog. Part. Nucl. Phys. **58**, 247 (2007), [hep-ph/0512128]; M. Schmaltz and D. Tucker-Smith, Ann. Rev. Nucl. Part. Sci. **55**, 229 (2005), [hep-ph/0502182].

[423] J. A. Casas, J. R. Espinosa and I. Hidalgo, JHEP **03**, 038 (2005), [hep-ph/0502066].

[424] H.-C. Cheng and I. Low, JHEP **09**, 051 (2003), [hep-ph/0308199].

[425] M. Carena *et al.*, Phys. Rev. **D75**, 091701 (2007), [hep-ph/0610156].

[426] M. Aaboud *et al.* (ATLAS), Phys. Rev. Lett. **121**, 21, 211801 (2018), [arXiv:1808.02343]; A. M. Sirunyan *et al.* (CMS), Eur. Phys. J. **C79**, 4, 364 (2019), [arXiv:1812.09768].

[427] H. Georgi, A. E. Nelson and A. Manohar, Phys. Lett. **126B**, 169 (1983); A. E. Nelson and M. J. Strassler, JHEP **09**, 030 (2000), [hep-ph/0006251]; S. Davidson, G. Isidori and S. Uhlig, Phys. Lett. **B663**, 73 (2008), [arXiv:0711.3376].

[428] C. Csaki, A. Falkowski and A. Weiler, JHEP **09**, 008 (2008), [arXiv:0804.1954]; B. Keren-Zur *et al.*, Nucl. Phys. **B867**, 394 (2013), [arXiv:1205.5803].

[429] O. Matsedonskyi, G. Panico and A. Wulzer, JHEP **01**, 164 (2013), [arXiv:1204.6333]; M. Redi and A. Tesi, JHEP **10**, 166 (2012), [arXiv:1205.0232]; D. Marzocca, M. Serone and J. Shu, JHEP **08**, 013 (2012), [arXiv:1205.0770]; A. Pomarol and F. Riva, JHEP **08**, 135 (2012), [arXiv:1205.6434].

[430] R. Contino and G. Servant, JHEP **06**, 026 (2008), [arXiv:0801.1679]; J. Mrazek and A. Wulzer, Phys. Rev. **D81**, 075006 (2010), [arXiv:0909.3977]; A. De Simone *et al.*, JHEP **04**, 004 (2013), [arXiv:1211.5663]; A. Azatov *et al.*, Phys. Rev. **D89**, 7, 075001 (2014), [arXiv:1308.6601].

[431] A. Banfi, A. Martin and V. Sanz, JHEP **08**, 053 (2014), [arXiv:1308.4771]; A. Azatov and A. Paul, JHEP **01**, 014 (2014), [arXiv:1309.5273]; C. Grojean *et al.*, JHEP **05**, 022 (2014), [arXiv:1312.3317].

[432] A. Azatov *et al.*, Phys. Rev. **D92**, 3, 035001 (2015), [arXiv:1502.00539].

[433] K. Agashe, R. Contino and A. Pomarol, Nucl. Phys. **B719**, 165 (2005), [hep-ph/0412089]; R. Contino, L. Da Rold and A. Pomarol, Phys. Rev. **D75**, 055014 (2007), [hep-ph/0612048]; D. Pappadopulo, A. Thamm and R. Torre, JHEP **07**, 058 (2013), [arXiv:1303.3062]; M. Montull *et al.*, Phys. Rev. **D88**, 095006 (2013), [arXiv:1308.0559].

[434] M. Carena, L. Da Rold and E. Pontón, JHEP **06**, 159 (2014), [arXiv:1402.2987]; D. Liu, I. Low and C. E. M. Wagner, Phys. Rev. **D96**, 3, 035013 (2017), [arXiv:1703.07791].

[435] I. Low, R. Rattazzi and A. Vichi, JHEP **04**, 126 (2010), [arXiv:0907.5413].

[436] M. Ciuchini *et al.*, JHEP **08**, 106 (2013), [arXiv:1306.4644].

[437] C. Grojean, O. Matsedonskyi and G. Panico, JHEP **10**, 160 (2013), [arXiv:1306.4655].

[438] M. Geller and O. Telem, Phys. Rev. Lett. **114**, 191801 (2015), [arXiv:1411.2974].

[439] P. Batra and Z. Chacko, Phys. Rev. **D79**, 095012 (2009), [arXiv:0811.0394]; R. Barbieri *et al.*, JHEP **08**, 161 (2015), [arXiv:1501.07803]; M. Low, A. Tesi and L.-T. Wang, Phys. Rev. **D91**, 095012 (2015), [arXiv:1501.07890].

[440] ATLAS Collaboration, ATLAS-CONF-2023-035 (2023).

[441] G. Aad *et al.* (ATLAS), JHEP **07**, 155 (2023), [arXiv:2211.04172].

[442] CMS Collaboration, CMS-PAS-HIG-20-002 (2023).

[443] CMS Collaboration, CMS-PAS-HIG-17-13 (2017).

[444] M. Aaboud *et al.* (ATLAS), Phys. Lett. **B775**, 105 (2017), [arXiv:1707.04147].

[445] A. M. Sirunyan *et al.* (CMS), Phys. Lett. B **793**, 320 (2019), [arXiv:1811.08459].

[446] ATLAS Collaboration, ATLAS-CONF-2023-030 (2023).

[447] M. Aaboud *et al.* (ATLAS), JHEP **10**, 112 (2017), [arXiv:1708.00212].

[448] CMS Collaboration, CMS-PAS-HIG-16-014 (2016).

[449] G. Aad *et al.* (ATLAS), Eur. Phys. J. C **81**, 4, 332 (2021), [arXiv:2009.14791].

[450] CMS Collaboration, CMS-PAS-HIG-16-033 (2016).

[451] CMS Collaboration, CMS-PAS-HIG-16-023 (2016).

[452] G. Aad *et al.* (ATLAS), Eur. Phys. J. C **83**, 7, 633 (2023), [arXiv:2207.03925].

[453] G. Aad *et al.* (ATLAS), Eur. Phys. J. C **80**, 12, 1165 (2020), [arXiv:2004.14636].

[454] CMS Collaboration, CMS-PAS-HIG-16-034 (2017).

[455] A. M. Sirunyan *et al.* (CMS), Phys. Rev. D **102**, 3, 032003 (2020), [arXiv:2006.06391].

[456] ATLAS Collaboration, ATLAS-CONF-2016-082 (2016).

[457] ATLAS Collaboration, ATLAS-CONF-2013-067 (2013).

[458] A. M. Sirunyan *et al.* (CMS), JHEP **03**, 034 (2020), [arXiv:1912.01594].

[459] ATLAS Collaboration, ATLAS-CONF-2012-018 (2012).

[460] M. Aaboud *et al.* (ATLAS), Phys. Lett. **B777**, 91 (2018), [arXiv:1708.04445].

[461] G. Aad *et al.* (ATLAS), JHEP **09**, 091 (2019), [arXiv:1906.08589].

[462] M. Aaboud *et al.* (ATLAS), Phys. Rev. **D98**, 5, 052008 (2018), [arXiv:1808.02380].

[463] G. Aad *et al.* (ATLAS), Phys. Rev. D **106**, 5, 052001 (2022), [arXiv:2112.11876].

[464] ATLAS Collaboration, ATLAS-CONF-2016-004 (2016); M. Aaboud *et al.* (ATLAS), JHEP **05**, 124 (2019), [arXiv:1811.11028]; M. Aaboud *et al.* (ATLAS), Eur. Phys. J. **C78**, 12, 1007 (2018), [arXiv:1807.08567].

[465] ATLAS Collaboration, ATLAS-CONF-2019-030 (2019); M. Aaboud *et al.* (ATLAS), Phys. Rev. Lett. **121**, 19, 191801 (2018), [Erratum: Phys. Rev. Lett. **122**, 089901 (2019)], [arXiv:1808.00336]; G. Aad *et al.* (ATLAS) (2019), [arXiv:1908.06765].

[466] A. M. Sirunyan *et al.* (CMS), Phys. Lett. B **788**, 7 (2019), [arXiv:1806.00408].

[467] V. Khachatryan *et al.* (CMS), Phys. Lett. **B755**, 217 (2016), [arXiv:1510.01181].

[468] G. Aad *et al.* (ATLAS), Phys. Rev. Lett. **125**, 5, 051801 (2020), [arXiv:2002.12223].

[469] A. Tumasyan *et al.* (CMS), JHEP **07**, 073 (2023), [arXiv:2208.02717].

[470] A. M. Sirunyan *et al.* (CMS), JHEP **09**, 007 (2018), [arXiv:1803.06553].

[471] V. M. Abazov *et al.* (D0), Phys. Rev. Lett. **104**, 151801 (2010), [arXiv:0912.0968].

[472] D0 Collaboration, D0Note 5974-CONF (2011).

[473] R. Aaij *et al.* (LHCb), JHEP **05**, 132 (2013), [arXiv:1304.2591].

[474] A. M. Sirunyan *et al.* (CMS), JHEP **05**, 210 (2019), [arXiv:1903.10228].

[475] M. Aaboud *et al.* (ATLAS), JHEP **07**, 117 (2019), [arXiv:1901.08144].

[476] A. M. Sirunyan *et al.* (CMS) (2019), [arXiv:1907.03152].

[477] A. M. Sirunyan *et al.* (CMS), JHEP **03**, 103 (2020), [arXiv:1911.10267].

[478] ATLAS Collaboration, ATLAS-CONF-2019-036 (2019).

[479] A. M. Sirunyan *et al.* (CMS), JHEP **11**, 161 (2018), [arXiv:1808.01890].

[480] G. Aad *et al.* (ATLAS), JHEP **08**, 148 (2015), [arXiv:1505.07018].

[481] A. M. Sirunyan *et al.* (CMS), JHEP **04**, 171 (2020), [arXiv:1908.01115].

[482] G. Aad *et al.* (ATLAS), Phys. Rev. D **102**, 3, 032004 (2020), [arXiv:1907.02749].

[483] S. Chatrchyan *et al.* (CMS), Phys. Lett. **B722**, 207 (2013), [arXiv:1302.2892]; CMS Collaboration, CMS-PAS-HIG-16-025 (2016); A. M. Sirunyan *et al.* (CMS), JHEP **08**, 113 (2018), [arXiv:1805.12191].

[484] V. M. Abazov *et al.* (D0), Phys. Lett. **B698**, 97 (2011), [arXiv:1011.1931].

[485] T. Aaltonen *et al.* (CDF), Phys. Rev. **D85**, 032005 (2012), [arXiv:1106.4782].

[486] ATLAS Collaboration, ATLAS-CONF-2017-055 (2017).

[487] G. Aad *et al.* (ATLAS), Phys. Rev. D **102**, 11, 112008 (2020), [arXiv:2007.05293]; G. Aad *et al.* (ATLAS), Phys. Lett. **B744**, 163 (2015), [arXiv:1502.04478].

[488] A. M. Sirunyan *et al.* (CMS), JHEP **03**, 065 (2020), [arXiv:1910.11634].

[489] A. M. Sirunyan *et al.* (CMS), Eur. Phys. J. **C79**, 7, 564 (2019), [arXiv:1903.00941].

[490] M. Aaboud *et al.* (ATLAS), Phys. Lett. B **783**, 392 (2018), [arXiv:1804.01126].

[491] V. Khachatryan *et al.* (CMS), Phys. Lett. B **759**, 369 (2016), [arXiv:1603.02991].

[492] A. M. Sirunyan *et al.* (CMS), JHEP **03**, 055 (2020), [arXiv:1911.03781].

[493] M. Aaboud *et al.* (ATLAS), Phys. Lett. **B759**, 555 (2016), [arXiv:1603.09203].

[494] M. Aaboud *et al.* (ATLAS), JHEP **09**, 139 (2018), [arXiv:1807.07915].

[495] CMS Collaboration, CMS-PAS-HIG-16-031 (2016); A. M. Sirunyan *et al.* (CMS), JHEP **07**, 142 (2019), [arXiv:1903.04560].

[496] ATLAS Collaboration, ATLAS-CONF-2012-010 (2012).

[497] A. M. Sirunyan *et al.* (CMS), Phys. Rev. D **102**, 7, 072001 (2020), [arXiv:2005.08900].

[498] G. Aad *et al.* (ATLAS), JHEP **06**, 145 (2021), [arXiv:2102.10076].

[499] A. M. Sirunyan *et al.* (CMS), JHEP **07**, 126 (2020), [arXiv:2001.07763]; V. Khachatryan *et al.* (CMS), JHEP **11**, 018 (2015), [arXiv:1508.07774]; A. M. Sirunyan *et al.* (CMS) (2019), [arXiv:1908.09206].

[500] G. Aad *et al.* (ATLAS), Phys. Rev. Lett. **114**, 23, 231801 (2015), [arXiv:1503.04233].

[501] A. M. Sirunyan *et al.* (CMS), Phys. Rev. Lett. **119**, 14, 141802 (2017), [arXiv:1705.02942].

[502] A. M. Sirunyan *et al.* (CMS), Eur. Phys. J. C **81**, 8, 723 (2021), [arXiv:2104.04762].

[503] A. M. Sirunyan *et al.* (CMS), Phys. Rev. Lett. **123**, 13, 131802 (2019), [arXiv:1905.07453].

[504] A. Tumasyan *et al.* (CMS), JHEP **09**, 032 (2023), [arXiv:2207.01046].

[505] A. M. Sirunyan *et al.* (CMS), JHEP **11**, 115 (2018), [arXiv:1808.06575].

[506] ATLAS Collaboration, ATLAS-CONF-2011-020 (2011).

[507] A. M. Sirunyan *et al.* (CMS), JHEP **11**, 010 (2017), [arXiv:1707.07283].

[508] G. Aad *et al.* (ATLAS), Phys. Rev. **D92**, 5, 052002 (2015), [arXiv:1505.01609]; ATLAS Collaboration, ATLAS-CONF-2012-079 (2012).

[509] A. Tumasyan *et al.* (CMS), JHEP **07**, 148 (2023), [arXiv:2208.01469].

[510] A. Tumasyan *et al.* (CMS), Phys. Rev. Lett. **131**, 101801 (2023), [arXiv:2209.06197].

[511] A. Tumasyan *et al.* (CMS), JHEP **11**, 057 (2021), [arXiv:2106.10361].

[512] A. M. Sirunyan *et al.* (CMS), JHEP **08**, 139 (2020), [arXiv:2005.08694]; V. Khachatryan *et al.* (CMS), JHEP **10**, 076 (2017), [arXiv:1701.02032]; A. M. Sirunyan *et al.* (CMS), Phys. Lett. **B795**, 398 (2019), [arXiv:1812.06359]; A. M. Sirunyan *et al.* (CMS), Phys. Lett. **B796**, 131 (2019), [arXiv:1812.00380]; A. M. Sirunyan *et al.* (CMS) (2019), [arXiv:1907.07235]; A. M. Sirunyan *et al.* (CMS), Phys. Lett. **B785**, 462 (2018), [arXiv:1805.10191]; A. M. Sirunyan *et al.* (CMS), JHEP **11**, 018 (2018), [arXiv:1805.04865]; CMS Collaboration, CMS-PAS-HIG-18-015 (2019).

[513] S. Schael *et al.* (ALEPH), JHEP **05**, 049 (2010), [arXiv:1003.0705].

[514] V. M. Abazov *et al.* (D0), Phys. Rev. Lett. **103**, 061801 (2009), [arXiv:0905.3381].

[515] G. Aad *et al.* (ATLAS), Phys. Rev. D **105**, 1, 012006 (2022), [arXiv:2110.00313].

[516] M. Aaboud *et al.* (ATLAS), JHEP **10**, 031 (2018), [arXiv:1806.07355].

[517] A. M. Sirunyan *et al.* (CMS), Phys. Lett. B **795**, 398 (2019), [arXiv:1812.06359].

[518] A. M. Sirunyan *et al.* (CMS), Phys. Lett. B **785**, 462 (2018), [arXiv:1805.10191].

[519] B. Aubert *et al.* (BaBar), Phys. Rev. Lett. **103**, 081803 (2009), [arXiv:0905.4539].

[520] B. Aubert *et al.* (BaBar), Phys. Rev. Lett. **103**, 181801 (2009), [arXiv:0906.2219].

[521] ATLAS Collaboration, ATLAS-CONF-2016-051 (2016); ATLAS Collaboration, ATLAS-CONF-2017-053 (2017); M. Aaboud *et al.* (ATLAS), Eur. Phys. J. **C79**, 1, 58 (2019), [arXiv:1808.01899].

[522] CMS Collaboration, CMS-PAS-HIG-16-036 (2017).

[523] S. Schael *et al.* (ALEPH, DELPHI, L3, OPAL, LEP Working Group for Higgs Boson Searches), Eur. Phys. J. **C47**, 547 (2006), [hep-ex/0602042].

[524] ATLAS Collaboration, ATLAS-CONF-2013-027 (2013).

[525] CMS Collaboration, CMS-PAS-HIG-13-016 (2013).

[526] A. Heister *et al.* (ALEPH), Phys. Lett. **B526**, 191 (2002), [hep-ex/0201014]; P. Achard *et al.* (L3), Phys. Lett. **B545**, 30 (2002), [hep-ex/0208042].

[527] M. Carena *et al.* (1999), [hep-ph/9912223].

[528] M. M. Kado and C. G. Tully, Ann. Rev. Nucl. Part. Sci. **52**, 65 (2002).

[529] G. Abbiendi *et al.* (OPAL), Eur. Phys. J. **C23**, 397 (2002), [hep-ex/0111010]; J. Abdallah *et al.* (DELPHI), Eur. Phys. J. **C38**, 1 (2004), [hep-ex/0410017].

[530] M. Carena *et al.*, Eur. Phys. J. **C45**, 797 (2006), [hep-ph/0511023].

[531] ATLAS Collaboration, ATLAS-CONF-2016-104 (2016).

[532] S. Chatrchyan *et al.* (CMS), JHEP **09**, 029 (2012), [Erratum: JHEP **03**, 132 (2014)], [arXiv:1204.2488].

[533] M. Aaboud *et al.* (ATLAS), Phys. Rev. Lett. **119**, 19, 191803 (2017), [arXiv:1707.06025].

[534] V. Khachatryan *et al.* (CMS), Phys. Lett. **B758**, 296 (2016), [arXiv:1511.03610].

[535] A. M. Sirunyan *et al.* (CMS), JHEP **11**, 010 (2017), [arXiv:1707.07283].

[536] J. Bernon *et al.*, Phys. Rev. **D91**, 7, 075019 (2015), [arXiv:1412.3385].

[537] G. Aad *et al.* (ATLAS), Phys. Rev. Lett. **113**, 17, 171801 (2014), [arXiv:1407.6583].

[538] CMS Collaboration, CMS-PAS-HIG-14-037 (2015).

[539] T. Biekötter, S. Heinemeyer and G. Weiglein (2023), [arXiv:2306.03889].

[540] S. H. Zhu, arXiv preprint (1999), [hep-ph/9901221].

[541] H. E. Logan and S.-f. Su, Phys. Rev. **D66**, 035001 (2002), [hep-ph/0203270].

[542] A. Gutierrez-Rodriguez and O. A. Sampayo, Phys. Rev. **D62**, 055004 (2000).

[543] S. Kanemura, S. Moretti and K. Odagiri, JHEP **02**, 011 (2001), [hep-ph/0012030].

[544] M. Czakon, P. Fiedler and A. Mitov, Phys. Rev. Lett. **110**, 252004 (2013), [arXiv:1303.6254].

[545] M. Carena *et al.*, Nucl. Phys. **B577**, 88 (2000), [hep-ph/9912516].

[546] J. M. Campbell, R. K. Ellis and F. Tramontano, Phys. Rev. **D70**, 094012 (2004), [hep-ph/0408158].

[547] C. Degrande *et al.*, Phys. Lett. **B772**, 87 (2017), [arXiv:1607.05291].

[548] A. A. Barrientos Bendezu and B. A. Kniehl, Phys. Rev. **D63**, 015009 (2001), [hep-ph/0007336]; A. A. Barrientos Bendezu and B. A. Kniehl, Nucl. Phys. **B568**, 305 (2000), [hep-ph/9908385].

[549] G. Abbiendi *et al.* (ALEPH, DELPHI, L3, OPAL, LEP), Eur. Phys. J. **C73**, 2463 (2013), [arXiv:1301.6065].

[550] B. Abbott *et al.* (D0), Phys. Rev. Lett. **82**, 4975 (1999), [hep-ex/9902028]; A. Abulencia *et al.* (CDF), Phys. Rev. Lett. **96**, 042003 (2006), [hep-ex/0510065]; V. M. Abazov *et al.* (D0), Phys. Lett. **B682**, 278 (2009), [arXiv:0908.1811].

[551] V. Khachatryan *et al.* (CMS), JHEP **12**, 178 (2015), [arXiv:1510.04252].

[552] A. M. Sirunyan *et al.* (CMS), Eur. Phys. J. **C79**, 5, 421 (2019), [arXiv:1809.10733].

[553] J. Abdallah *et al.* (DELPHI), Eur. Phys. J. **C54**, 1 (2008), [Erratum: Eur. Phys. J. **C56**, 165 (2008)], [arXiv:0801.3586].

[554] R. Dermisek, Mod. Phys. Lett. **A24**, 1631 (2009), [arXiv:0907.0297].

[555] J. F. Gunion, JHEP **08**, 032 (2009), [arXiv:0808.2509].

[556] W. Love *et al.* (CLEO), Phys. Rev. Lett. **101**, 151802 (2008), [arXiv:0807.1427].

[557] G. Aad *et al.* (ATLAS), JHEP **03**, 041 (2022), [arXiv:2110.13673]; A. Tumasyan *et al.* (CMS), Eur. Phys. J. C **82**, 4, 290 (2022), [arXiv:2111.01299].

[558] G. Aad *et al.* (ATLAS), JHEP **07**, 133 (2023), [arXiv:2212.09649].

[559] G. Aad *et al.* (ATLAS), Eur. Phys. J. **C72**, 2244 (2012), [arXiv:1210.5070]; S. Chatrchyan *et al.* (CMS), Eur. Phys. J. **C72**, 2189 (2012), [arXiv:1207.2666].

[560] G. Aad *et al.* (ATLAS), Phys. Rev. **D89**, 3, 032002 (2014), [arXiv:1312.1956].

[561] J. de Blas *et al.*, in "Snowmass 2021," (2022), [arXiv:2206.08326].